

# **Selective targeting to glioma with nucleic acid aptamers**

**by**

**Shraddha Aptekar**

A thesis submitted in partial fulfilment for the requirements for the degree of  
Doctor of Philosophy at the University of Central Lancashire

February 2015

## DECLARATION

### Concurrent registration for two or more academic awards

I declare that while registered as a candidate for the research degree, I have not been a registered candidate or enrolled student for another award of the University or other academic or professional institution

---

### Material submitted for another award

I declare that no material contained in the thesis has been used in any other submission for an academic award and is solely my own work

---

### Collaboration

Where a candidate's research programme is part of a collaborative project, the thesis must indicate in addition clearly the candidate's individual contribution and the extent of the collaboration. Please state below:

**Signature of Candidate** \_\_\_\_\_

**Type of Award** \_\_\_\_\_

**School** \_\_\_\_\_

## ABSTRACT

The term glioma encompasses brain tumours arising from the glial cells. Malignant glioma are characterised by a rapid growth rate and high capacity for invasive infiltration to surrounding brain tissue, hence diagnosis and treatment is difficult, and patient survival is poor. Aptamers are small molecular ligands composed of short oligonucleotides that bind to a target with high specificity and affinity. They are produced *in vitro* through a method called systematic evolution of ligands by exponential enrichment (SELEX).

The aim of the study was to examine the binding selectivity of DNA aptamers on commercial glial cell lines and primary glioma tissues. RNA aptamers and their DNA homologues (SA44, SA43, SA56) were selected for study which showed strong binding affinity to the target U87MG cells as measured by flow cytometry. SA44 and SA43 showed higher uptake and cytoplasmic localisation in U87MG and 1321N1 glioma cell lines compared to non-cancerous SVGP12 cells and non-glioma MCF-7 and T24 cells as measured by confocal microscopy. The data was confirmed quantitatively by flow cytometry analysis, which showed that the aptamers were able to actively internalise in U87MG and 1321N1 tumorigenic cells compared to the non-cancerous and non-glioma cell types. Histochemistry staining on paraffin embedded, formalin fixed patient tissues revealed that the binding selectivity was found to be significantly higher for only SA43 aptamer ( $p < 0.05$ ) in glioma tissues (grade I, II, III and IV) compared to the non-cancerous and tissues. Aptamer SA43 also showed cell type selectivity within the tissue.

The results indicate that SA43 aptamer can differentiate between glioma and non-cancerous cells and tissues and therefore, show promise for histological diagnosis of glioma and targeted delivery. In the future, targeting tumour cells and tissues through the use of SA43 aptamer will help develop molecular imaging, targeted delivery by reduction of the non-specific toxicity of chemotherapy and selectively directing anti-cancer drugs to tumour cells.

## TABLE OF CONTENTS

<b>DECLARATION</b> .....	2
<b>ABSTRACT</b> .....	3
<b>LIST OF TABLES</b> .....	7
<b>LIST OF FIGURES</b> .....	8
<b>ACKNOWLEDGEMENTS</b> .....	12
<b>ABBREVIATIONS</b> .....	13
<b>CHAPTER 1 INTRODUCTION</b> .....	16
1.1 Introduction to CNS tumours.....	16
1.2 Glioma.....	17
1.3 Risk factors.....	17
1.4 Diagnostic imaging of glioma.....	19
1.5 The WHO based classification of glioma.....	21
1.5.1 Limitations with current histological diagnosis.....	23
1.6 Advances in diagnosis of glioma.....	24
1.7 Establishment of tumour cell models.....	28
1.7.1 Applications of glioma cell lines to model human gliomas.....	28
1.7.2 Applications of pathological tissues to model human glioma.....	29
1.8 Current treatment strategies for malignant glioma.....	30
1.8.1 Surgery.....	30
1.8.2 Radiotherapy.....	31
1.8.3 Chemotherapy.....	32
1.9 Novel chemotherapeutics and issues identified while targeting and treating glioma.....	33
1.10 Future approaches towards targeting and treating glioma.....	38
1.11 Historical review of aptamer.....	40
1.12 Secondary and tertiary structure of aptamer.....	41
1.13 Generation of aptamers.....	43
1.14 Aptamers versus antibodies.....	45
1.15 Modification of oligonucleotide aptamers to improve their function.....	47
1.16 Applications of aptamers.....	49
1.16.1 Aptamers based molecular imaging.....	50
1.16.2 Aptamers for target identification.....	53
1.16.3 Aptamer as therapeutics - clinical trials of aptamers in medicine.....	54
1.16.4 Aptamer conjugates for targeted drug delivery.....	57
1.17 Aptamers and glioma.....	59
1.18 Scope for the present study.....	60
1.19 Aims and Objectives.....	61
1.19.1 Main Aim.....	61
1.19.2 Objectives.....	61
<b>CHAPTER 2 MATERIALS AND METHODS</b> .....	63
2.1 Cell lines.....	63
2.1.1 Materials.....	63
2.1.2 Media and supplements.....	64
2.1.3 Routine cell culture and maintenance.....	64

2.2 Growth and biological characteristics of cells lines used in the study.....	65
2.2.1 Growth kinetics of cell lines .....	65
2.2.2 Data analysis .....	65
2.3 Characterisation of cell lines using Immunocytochemistry assay .....	66
2.3.1 Cell fixation .....	67
2.3.2 Cell staining and visualisation .....	68
2.4 Oligonucleotide synthesis and labelling.....	68
2.5 Determining the binding affinity of the aptamers to the target U87MG cells by flow cytometry .....	69
2.6 Cellular uptake and localisation of aptamers by confocal microscopy.....	71
2.6.1 Determining the optimum standard concentration for each Cy3-labelled aptamer using the target U87MG cells .....	71
2.6.2 Assessing the uptake of the aptamers on live glial and non-glial cells.....	72
2.7 Cellular uptake and internalisation of aptamers by flow cytometry .....	73
2.7.1 Assessing the aptamer uptake on live glial and non-glial cells .....	73
2.7.2 Effect of temperature on aptamer binding to the cells.....	74
2.7.3 Effect of protease trypsin on aptamer binding to the cells .....	75
2.8 Effect of aptamers on cell viability .....	76
2.9 Aptamer binding on fixed cells .....	76
2.9.1 Fixation and permeabilisation.....	76
2.9.2 Aptamer labelling and imaging.....	77
2.10 Aptamer binding selectivity to patient tissue samples .....	77
2.10.1 Dewaxing of paraffin embedded sections.....	78
2.10.2 Antigen retrieval .....	78
2.10.3 Aptamer labelling and imaging.....	78
2.10.4 Schematic explanation of the protocol for immuno-scoring .....	79
2.10.5 Data analysis .....	81

### **CHAPTER 3 GROWTH AND BIOLOGICAL CHARACTERISTICS OF CELL CULTURE MODELS .....**

3.1 Introduction .....	82
3.2 Results .....	82
3.2.1 Growth curves.....	82
3.2.2 Immuno-cytochemical characterisation of various cell lines using specific markers.....	85
3.3 Discussion .....	89

### **CHAPTER 4 BINDING ANALYSIS OF SHORTENED RNA AND DNA APTAMERS.....**

4.1 Introduction .....	92
4.2 Results .....	94
4.2.1 Characterisation of published and shortened RNA aptamers .....	94
4.2.2 Concentration dependent binding study of shortened aptamers in live U87MG cells.....	99
4.2.3 Selective uptake of shortened RNA aptamers in live cell lines .....	107
4.2.4 Comparison of binding affinity of the shortened RNA aptamers with the DNA homologs. ....	121
4.2.5 Selective uptake of the lead DNA aptamers on various cell types .....	123
4.2.6 Summary of results for the binding selectivity of DNA and RNA aptamers ...	134

4.3 Discussion .....	135
<b>CHAPTER 5 GLIOMA SPECIFIC INTERNALISATION STUDY OF THE DNA APTAMERS</b> .....	141
5.1 Introduction .....	141
5.2 Results .....	143
5.2.1 Effect of temperature on aptamer binding to cells.....	143
5.2.2 Effect of trypsin protease digestion on aptamers binding to cells .....	147
5.2.3 Effect of aptamers on cell viability.....	150
5.3 Discussion .....	153
<b>CHAPTER 6 HISTOCHEMICAL ANALYSIS OF DNA APTAMERS</b> .....	158
6.1 Introduction .....	158
6.2 Results .....	158
6.2.1 Binding analysis of aptamers on fixed cells. ....	158
6.2.2 Binding analysis of aptamers on fixed clinical tissues .....	161
6.3 Discussion .....	177
<b>CHAPTER 7 DETERMINING THE FATE OF SA43 DNA APTAMER IN TUMOUR CELLS</b> .....	183
7.1 Introduction .....	183
7.2 Results .....	183
7.3 Discussion .....	186
<b>CHAPTER 8 GENERAL DISCUSSIONS AND FUTURE WORK</b> .....	188
8.1 Challenges for glioma targeted therapy and overall summary.....	188
8.2 Internalisation property of SA43 DNA aptamer and its implication on targeted drug delivery .....	189
8.3 Putative target for SA43 DNA aptamer (in relation to parallel study) .....	191
8.4 Predicting the mechanism of the uptake of SA43 DNA aptamer .....	193
8.5 Aptamer and its entry through BBB.....	196
8.6 The bigger picture: Future perspectives of combined strategies for cancer therapy using aptamer–nanoparticle–drug conjugate model for controlled drug release .....	197
8.6 Summary .....	203
<b>APPENDICES</b> .....	204
<b>REFERENCES</b> .....	210

## LIST OF TABLES

Table 1.1 List of environmental risk factors for brain tumours investigated in epidemiological studies.....	18
Table 1.2 Histological classification of diffuse gliomas and their overall survival.....	22
Table 1.3 Selected agents tested in recurrent GBM.....	34
Table 1.4 Properties of aptamers versus antibodies.....	47
Table 1.5 Promising aptamers involved in diagnostic imaging and treatment of various diseases.....	53
Table 1.6 Current therapeutic aptamers in various stages of clinical development.....	56
Table 2.1 Surface-area and plating volume in each culture dish used in the study .....	66
Table 2.2 Antibodies used in the study and their working concentrations. ....	67
Table 2.3 Primary sequences of aptamers used in the study.....	69
Table 4.1 Summary of uptake and binding selectivity of aptamers on various cell types.....	134
Table 6.1 Comparison of each DNA aptamer binding on non-cancerous tissues against various glioma grade and meningioma tissues using Fishers exact test.....	171
Table 8.1 Strengths and weaknesses of drugs, aptamers and nanoparticles during targeted tumour therapy. ....	199

## LIST OF FIGURES

1.1	Brain imaging of GBM	20
1.2	IDH1 immunohistochemistry using IMab-1 antibody (x 100)	25
1.3	Molecular and genetic characterization and pathways to primary and secondary GBMs at population level.	27
1.4	Brain MRI image (FLAIR, axial plane) of a 44 years old man with recurrent GBM.	37
1.5	The secondary and tertiary structure depictions of aptamers.	42
1.6	General scheme of cell-SELEX procedure	44
1.7	Size comparison of an antibody and an aptamer.	46
1.8	Modifications employed to improve the function and pharmacokinetic profile of aptamers.	48
1.9	Pegaptanib structure and target binding	55
2.1	Representative images from tumour tissues showing differential staining intensities with the studied DNA aptamers	80
3.1	The growth kinetics of cultured glial and non-glial cell lines used for the study.	84
3.2	Expression of HLA-I, GFAP and VEGF antigens (green) in cultured 1321N1 and U87MG cells	86
3.3	Expression of HLA-I, GFAP and VEGF antigens (green) in cultured SVGP12 and T98G cells	87
3.4	Expression of HLA, VEGF, and GFAP antigens (green) in cultured MCF-7, T24, and C2C12 cells.	88
4.1	Primary sequence and secondary structure of the selected published aptamers with high binding affinity for U87MG cells and lowest free energies	96
4.2	Primary sequences and predicted secondary structures of shortened aptamers SA44 RNA, SA43 RNA, and SA56 with lowest free energies	97
4.3	Determination of binding affinity ( $K_d$ ) of the shortened aptamers SA44 RNA, SA43 RNA, and SA56 RNA to the	98

	target U87MG cells.	
4.4	Concentration dependent uptake and cellular localisation of SA44 RNA aptamer	101/102
4.5	Concentration dependent uptake and cellular localisation of SA43 RNA aptamer	103/104
4.6	Concentration dependent uptake and cellular localisation of SA56 RNA aptamer.	105/106
4.7	Selective uptake of SA44 RNA on various cell types using confocal microscopy.	109/110
4.8	Selective uptake of SA43 RNA on various cell types using confocal microscopy.	111/112
4.9	Selective uptake of SA56 RNA on various cell types using confocal microscopy	113/114
4.10	Representative flow cytometry profiles and quantitative analysis of the uptake of SA44 RNA on various cell types.	117
4.11	Representative flow cytometry profiles and quantitative analysis of the uptake of SA43 RNA on various cell types	118
4.12	Representative flow cytometry profiles and quantitative analysis of the uptake of SA56 RNA on various cell types	119
4.13	Comparative binding selectivity of aptamers SA44 RNA and SA43 RNA across various cell types	120
4.14	Comparative binding selectivity of aptamer SA56 RNA across various cell types	120
4.15	Determination of binding affinity ( $K_d$ ) of aptamers SA44 DNA and SA43 DNA towards the target U87MG cells	122
4.16	Uptake of random aptamers SAN1 and SAN2 DNA on various cell lines by confocal microscopy	125/126
4.17	Selective uptake of SA44 DNA on various cell types using confocal microscopy	127/128
4.18	Selective uptake of SA43 DNA on various cell types using confocal microscopy	129/130
4.19	Representative flow cytometry profiles of the uptake of SA44	131

	DNA on various cell types	
4.20	Representative flow cytometry profiles of the uptake of SA43 DNA on various cell types	132
4.21	Comparative binding selectivity of aptamer SA44 DNA and SA43 DNA across various cell types	133
5.1	Representative flow cytometry profiles showing temperature dependent uptake of SA44 DNA and SA43 DNA.	144/145
5.2	Temperature dependent uptake of aptamer SA43 DNA and SA44 DNA	146
5.3	Representative flow cytometry profiles showing the effect of trypsin protease digestion on aptamers binding to cells	148
5.4	Comparative effect of trypsin treatment on internalisation potential of SA44 DNA and SA43 DNA on U87MG, 1321N1, and SVGP12 cells	149
5.5	Effect of SA44 DNA on cell viability using Presto blue assay	151
5.6	Effect of SA43 DNA on cell viability using Presto blue assay	152
5.7	Internalisation property of the aptamer SA43 DNA in glioma cells	155
6.1	Binding analysis of DNA aptamers on fixed cells	160
6.2	Representative images of tissue sections from non-cancerous (BTNW no. 596) and different pathological grade glioma (BTNW no 814, grade I; 726, grade II; 738, grade III; and 1077, grade IV) patients stained with a biotinylated random sequence aptamer	164/165
6.3	Representative images of tissue sections from non-cancerous (BTNW no. 596) and different pathological grade glioma (BTNW no 814, grade I; 726, grade II; 738, grade III; and 1077, grade IV) patients stained with biotinylated SA44, SA43 and SA56 DNA aptamers	166/167
6.4	Representative images of tissue sections from different pathological grade meningioma grade I (BTNW no. 759), and meningioma grade II (BTNW no. 760) patients stained with	168/169

	biotinylated random aptamer, SA44, SA43 and SA56 DNA aptamers.	
6.5	Scatter plot showing the mean and the distribution of average scores for each aptamer on patient's tissue sections	170
6.6	SA43 DNA aptamer showing moderate staining in three non-cancerous tissues	173
6.7	SA43 DNA selectivity within the cells of the cerebellar tissue	174
6.8	SA43 DNA aptamer showing weak to no staining in three high-grade glioma tissues	175
6.9	Representative images from various glioma pathological grades including meningiomas showing negligible binding to endothelial cells with SA43 DNA aptamer	176
7.1	Time dependent uptake and cellular localisation of SA43 DNA on U87MG, 1321N1 and SVGP12 cells	184/185
8.1	Predicted mechanisms for targeted drug release through the use of aptamer-nanoparticle-drug conjugate	202

## ACKNOWLEDGEMENTS

### **“Guru Brahma Guru Vishnu Guru Devo Maheshwara Guru Sakshat Param Brahma Tasmai Shri Gurave Namah”**

Chanting the above Sanskrit mantra, which stands for salutation to the noble Guru (teacher) and places the Guru above everyone else on the planet, I would like to firstly thank my supervisors, Dr Lisa Shaw, Dr. Jane Alder and Prof. Robert Lea for their immense support and guidance throughout the study. They have been my main inspiration and encouraged me to not just grow as an experientialist but also think out of the box and be an independent researcher. A big thanks to Dr. Clare Lawrence for her immense contribution and support throughout the study. I would also like to take an opportunity to thank Prof. Jai Paul Singh for his advice and input related to the study.

The project was challenging and completely novel to start in UCLAN and would not have been possible without BTNW and university funding, and therefore, a huge thanks to the team involved for trusting me to work on this project and providing the funds. I would also like to thank Kate Ashton and Dr. Tim Dawson from Royal Preston Hospital for their contribution in supplying brain tissues for the study. A special thanks to my colleague Dr. Mohit Arora, who is working on finding the targets for the aptamers related to the study. I totally appreciate his extreme hard work in finding the targets, without which we could not have reached to clearer conclusions. I would also like to thank Dr. Gail Welsby, Dr. Phil Welsby, Dr. Julie Shorrocks and Dr. Vicky Jones for their input in discussions related to the study.

Last two years have been a bit tough staying away from parents considering my mothers health, as she was diagnosed with bone metastases. But, with Gods grace and my family blessings, accomplishment of PhD will be a dream come true for my family and myself. Studying PhD in cancer research and considering mother’s health has changed the overall aim of my life to a different path of doing something valuable for human kind in relation to cancer.

Last but not the least, I would like to thank my beloved mum, dad, sister Shreya, my life partner Shashank, and my friends Deeba, Dilip, Krunal, Viviana, Minaj, Shruti, Gauri, and Magic (our little dog) for encouraging and supporting me during my weak and happy moments.

**ABBREVIATIONS**

5- ALA	5- aminolevulinic acid
A	Adenine
ABC	Avidin-biotin complex
AG	Arabinogalactan
ANOVA	Analysis of variance
AP	Aptoprecipitation
APC	Adenomatous polyposis coli
ATCC	American Type Culture Collection
BBB	Blood brain barrier
BBB	Blood brain barrier
BCNU	bis-chloroethylnitrosourea
BRCA1	Breast cancer 1
BTNW	Brain Tumour North West
C	Cytosine
CCL2	Chemokine ligand 12
Cdr2	Cerebellar degeneration-related protein 2
CNS	Central nervous system
CSCs	Cancer stem cells
CSF	Cerebrospinal fluid
CT	Computed tomography
CTr	Clinical trails
CUR	Curcumin
DAB	3,3-Diaminobenzidine
DAPI	4', 6-diamidino-2-phenylindole
DMEM	Dulbecco's modified eagle medium
DNA	Deoxyribonucleic acid
Dox	Doxorubicin
ECACC	European Collection of Cell Cultures
EGFR	Epidermal growth factor receptor
ELISA	Enzyme-linked immunosorbent assay
EMEM	Eagle's minimum essential medium

EpCAM	Epithelial cell adhesion molecule
EPR	Enhanced permeability and retention effect
ER	Estrogen receptor
FBS	Fetal bovine serum
FDA	Food and Drug administration
FLAIR	Fluid attenuation inversion recovery
FRET	Fluorescence resonant energy transfer
G	Guanine
GBM	Glioblastoma multiforme
GFAP	Glial fibrillary acidic protein
GSCs	Glioma stem-like cells
HC	Histochemistry
HDAC	Histone deacetylase
HER	Human epidermal growth factor
HIV	Human immunodeficiency virus
HLA	Human leukocyte antigen
HPLC	High performance liquid chromatography
HSP	Heat shock protein
IDH	Isocitrate dehydrogenase
IHC	Immunohistochemistry
IL	Interleukin
IP	Immunoprecipitation
kDa	kilo Dalton
LSM	Laser scanning microscopy
MDI	Multiple document interface
MFI	Mean fluorescence intensity
MGMT	O6-methylguanine-DNA methyltransferase
mi-RNA	Micro-RNAs
MRI	Magnetic resonance imaging
MS	Mass-spectrometry
NAEE	Non-essential amino acid
NF	Neurofibromatosis
NHEJ	Non-homologous end joining
NICE	National Institute of Clinical health Excellence

NP	Nanoparticle
PBS	Phosphate buffer saline
PBS	Phosphate buffer saline
PCD	Paraneoplastic cerebellar degeneration
PDGFR	Platelet derived growth factor receptor
PE	Phycoerythrin
PEG	Polyethylene glycol
PET	Positron emission tomography
PFA	Paraformaldehyde
PFS	Progression free survival
PHMNP	Pegylated porous hollow magnetic nanoparticles
PI	Propyidium iodide
PKC	Protein kinase C
PNS	Peripheral nervous system
PR	Progesterone receptors
PSMA	Prostrate specific membrane antigen
PTEN	Phosphate and tensin homolog
QD	Quantum dot
RNA	Ribonucleic acid
SA	Shortened aptamer
SELEX	Systemic Evolution of Ligands by Exponential enrichment
SLS	Scientific laboratory supplies
SPECT	Single photon emission computed tomography
T	Thymine
T-ALL	T-cell acute lymphoblastic leukaemia
TCA	Tri-carboxylic cycle
TCL-SPION	Thermally cross-linked supramagnetic iron oxide nanoparticle
TP53	Tumour protein p53
U	Uracil
UK NEQAS	United Kingdom National External Quality Assessment Service
VEGF	Vascular endothelial growth factor
VEGFR	Vascular growth factor receptor
WHO	World Health Organisation
$\alpha$ KG	$\alpha$ -ketoglutarate

## CHAPTER 1 INTRODUCTION

### 1.1 Introduction to CNS tumours

Oncogenesis, the development of tumour cells, involves breakdown of the control of normal cell growth, somatic mutations such as activation and over-expression of proto-oncogenes (Tyagi *et al.*, 2002), inactivation and decreased expression of tumour-suppression genes (Maslon and Hupp, 2010; Rivlin *et al.*, 2011) and alteration in mutator genes. These factors have been associated with oncogenesis of all tissues including those within the central nervous system (CNS). Primary CNS tumours consist of a varied group of neoplasms, which are derived from several different cell lineages. Despite major advances in surgical and clinical neuro-oncology, there are still 7000 people in the UK diagnosed with brain cancer per year and it remains the 10<sup>th</sup> most common cancer in men and 13<sup>th</sup> in women (Ohgaki and Kleihues, 2005). Brain tumours derived from the intracranial tissues and meninges vary in malignancy ranging from benign to aggressive (Mckinney, 2004). The benign tumour can infiltrate and spread locally and give rise to a malignant tumour. Malignant tumours of the brain are of rare occurrence and account for approximately 2 % of all cancers in adults (Mckinney, 2004; Sehmer *et al.*, 2014).

During the past two decades, tremendous efforts in diagnosis and treatment have been made in the field of brain tumour biology with a main focus on malignant glioma and medulloblastoma, which are the most common CNS cancers of adults and children, respectively (Huse and Holland, 2010). It has been reported that, glial cells (mature astrocytes or oligodendrocytes) may differentiate in response to genetic mutations (refer to section 1.6) and undergo neoplastic transformation leading to gliomagenesis

(Hambardzumyan *et al.*, 2008).

## 1.2 Glioma

The term glioma encompasses all tumours that are thought to be of glial cell origin, and are the most frequent brain tumour observed (Schwartzbaum *et al.*, 2006; Ricard *et al.*, 2012; Sehmer *et al.*, 2014). Glioma account for more than 80 % of the primary malignant brain tumours out of which, glioblastoma multiforme (GBM) is the most frequent type with the poorest survival rate of all the groups (Ohgaki and Kleihues, 2005; Ricard *et al.*, 2012). As an aggressive malignant type of cancer, glioma often results in deaths of the affected patients within one to two years following diagnosis (Ricard *et al.*, 2012; Sehmer *et al.*, 2014).

Gliomas can arise from neural stem cells or de-differentiated mature neural cells (Ignatova *et al.*, 2002; Singh *et al.*, 2004; Hambardzumyan *et al.*, 2008), or from progenitor cells (Persson *et al.*, 2010), which transform into cancer stem cells. These cancer stem cells (CSCs) constitute a heterogenous group of undifferentiated neoplastic cells with properties such as pluripotency, tumorigenicity at low cell numbers, and recapitulation of phenotypic and histological characteristics of the original tumour (Lee *et al.*, 2006; Hatiboglu *et al.*, 2010). It has been postulated that glioma CSCs (gCSCs) play an essential role in tumour initiation, proliferation, progression, metastasis, recurrence and resistance to therapy (Hatiboglu *et al.*, 2010).

## 1.3 Risk factors

The incidence of malignant brain tumour in the UK averaged for 8.1 per 100,000 males and 5.3 per 100,100 females every year. The overall annual incidence rate of brain tumours in the UK population is 6.5 per 100,000 (Mckinney, 2004; Ricard *et al.*, 2012;

Sehmer *et al.*, 2014). These statistics have remained almost constant in the past 10 years. Eighty-six percent of these tumours have been accounted for glioma. The risk factors for the cause of glioma are poorly understood, which is problematic for developing prevention strategies. As shown in table 1, environmental factors such as various occupations, diet (N-nitro compounds) and environmental carcinogens have been reported to be involved with small increased risk for developing glioma, but therapeutic X- ray radiation seems to be associated with a high risk of developing glioma (McKinney, 2004; Ohgaki and Kleihues, 2005).

**Table 1.1 List of environmental risk factors for brain tumours investigated in epidemiological studies (McKinney, 2004; Ohgaki and Kleihues, 2005).**

<b>Factors</b>	<b>Specific aspects</b>	<b>Evaluation of risk</b>
<b>Occupations</b>	Vinyl chloride, use of rubber and plastic products, petroleum refining.	Small risks but no mechanism or specific chemical known.
<b>Diet</b>	N-Nitro compounds such as Nitrosamide/ Nitrite/ Nitrate consumption, Aspartame, high intake of cholesterol, sodium, etc.	Small risk of glioma.
<b>Ionising radiation</b>	Therapeutic X-irradiation (dose)	High risk of glioma.
<b>Electromagnetic fields</b>	Residential and occupational exposure.	Weak association and little consistency, but research is ongoing.
<b>Head injury</b>	Trauma	No consistent evidence
<b>Allergy and immunological conditions</b>	Atopy	Small risk of glioma, further work needed to identify mechanisms.

Although these environmental risk factors have also been associated with glioma brain tumour, no conclusive evidence has been produced to date. Several familial cancer syndromes such as Li-Fraumeni syndrome (TP53 germline mutations), Turcot

syndrome (APC germline mutation), Neurofibromatosis 1 (NF1) and 2 (NF2) have also been reported to be associated with brain tumours (Ohgaki and Kleihues, 2005).

#### **1.4 Diagnostic imaging of glioma**

Brain magnetic resonance imaging (MRI) with or without contrast agents is the most sensitive and commonly preferred diagnosis modality of choice when a brain tumour is suspected, however, patients are often initially screened with a computed tomography (CT) x-ray scan (Grossman, 2003; Osborn *et al.*, 2004). CT x-ray imaging of malignant glioma typically show an irregular isodense (abnormality with same density as reference structure) or hypodense (less dense than the reference structure) mass with central hypodensity (representing the necrotic core), vascular infiltration of the tumour and vasogenic oedema. Vasogenic oedema is considered an indicator of the presence of tumour cells invading the parenchymal vasculature and releasing vascular permeability factors (Grossman, 2003). With contrast agents, the lesions appear with a heterogeneous (non-uniform) rim of enhancement in 95 % of such cases indicating the highly infiltrative nature of glioma.

Malignant glioma observed using MRI display image contrasts that are weighted to demonstrate different anatomical structures and presence of tumour (Figure 1.1). Each tissue returns to its equilibrium state after excitation by independent processes of T1 and T2 relaxation. Malignant glioma observed using MRI often appear as irregular lesions with cysts like appearance and irregular thick margins that are isointense or hypointense on T1-weighted images (Differences in T1 relaxation time, spin-lattice relaxation). Enhancement with gadolinium contrast agent shows lesions with a highly proliferative tumour region surrounding the central necrotic core and white matter indicating oedema (Provenzale *et al.*, 2006).

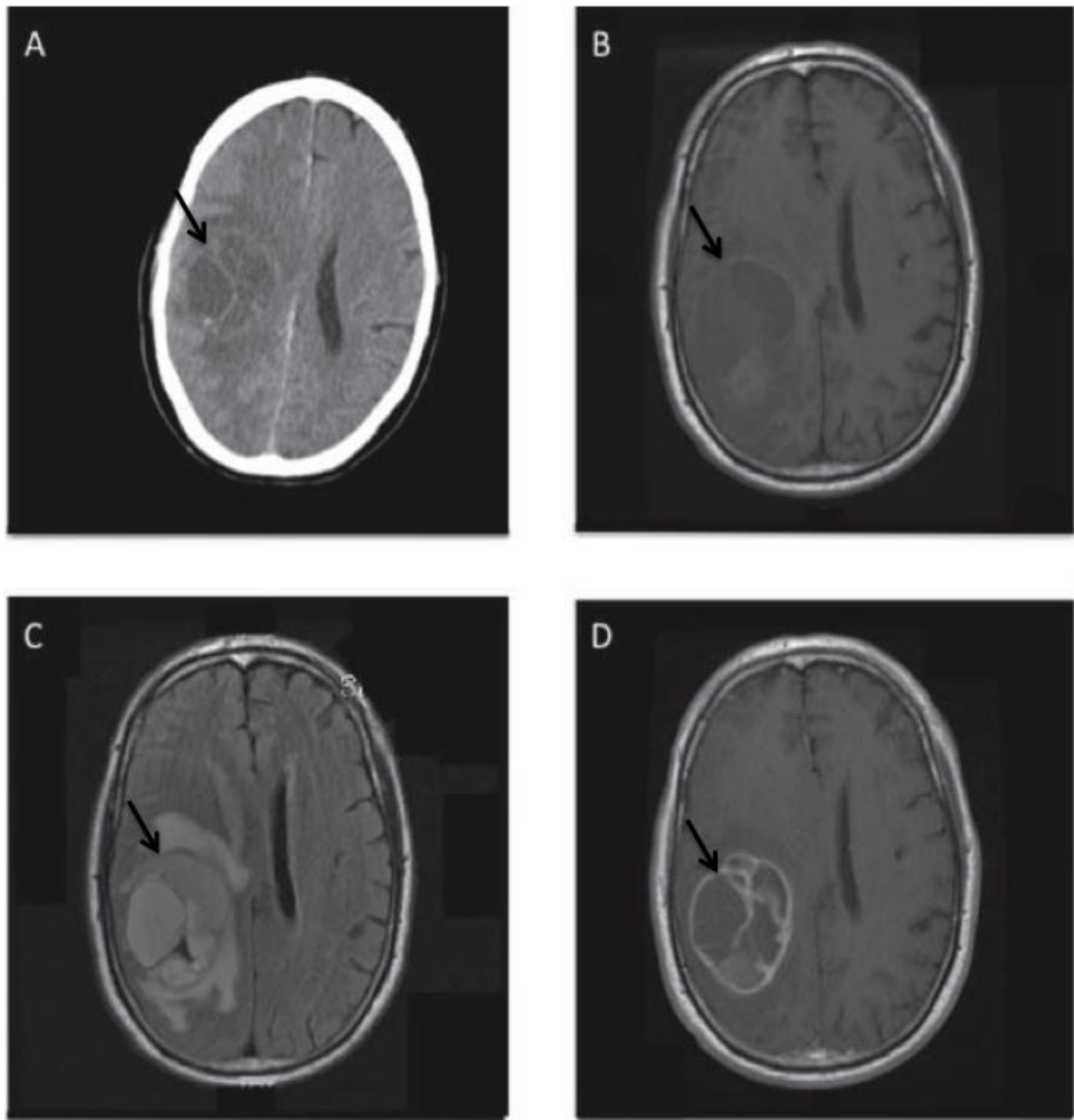


**Figure 1.1 Brain imaging of GBM.** Brain imaging from a 56 year old man who presented with headache, nausea, left hemiparesis, and left hand paresthesia that developed over the course of 3 weeks. Histological diagnosis was consistent with GBM. Arrows indicate region showing imaging by CT scan without contrast (**A**), and MRI which included non-contrast T1W1 showing a poorly delineated mass lesion (**B**), FLAIR (fluid attenuation inversion recovery) showing areas of hypersignal extending beyond the areas of contrast enhancement (**C**), and T1 with gadolinium contrast heterogeneously enhancing cystic/necrotic lesion (**D**), (Taken from Sonabend *et al.*, 2010).

T2-weighted images (differences in T2 relaxation time, spin-spin relaxation) and fluid attenuation inversion recovery (FLAIR) sequences demonstrate heterogeneous hyperintense lesions with surrounding vasogenic oedema and are specially employed in the assessment of tumour recurrence (Ludemann *et al.*, 2001). Novel promising imaging modalities such as perfusion MRI (information on tumour blood volume and vascular permeability; Barajas *et al.*, 2009), proton MR spectroscopy (differentiate high grade glioma from metastases; Server *et al.*, 2010), and positron emission tomography (PET, detecting glioma recurrence; Deng *et al.*, 2013) have potential implications for diagnosis of glioma.

### **1.5 The WHO based classification of glioma**

The tumours of the CNS have been differentiated and classified according World Health Organisation (WHO) (Louis *et al.*, 2007) with emphasis on morphological and immunohistochemical features including molecular pathogenesis such as cellularity, mitotic activity, microvascular proliferation and necrosis (Table 1.2). According to the classification, gliomas are categorised according to their grade, cell type, and location of the tumour. These include astrocytic tumours, namely, WHO classification grades I and II (astrocytoma), III (anaplastic astrocytoma) and IV (glioblastoma multiforme or GBM); oligodendrogliomas; ependymomas and mixed gliomas (Louis *et al.*, 2007). Grade I gliomas generally behave in a benign fashion and also can be circumscribed, whereas grade II-IV gliomas can diffusely infiltrate throughout the brain. The most frequent primary intracranial tumours diagnosed are diffuse gliomas comprised of astrocytic, oligodendroglial and ependymal lesions. The process of tumour progression from lower grade to higher grade is accompanied by the accumulation of genetic alterations resulting in heterogeneity at the histologic, biologic, and molecular levels.

**Table 1.2 Histological classification of diffuse gliomas and their overall survival** (Louis *et al.*, 2007; Ricard *et al.*, 2014).

Phenotype		Grading					Median survival (years)
		Differentiation	Cell density	Mitotic activity	Necrosis	Microvascular proliferation	
<b>Astrocytoma</b>							
Grade II	Fibrillary neoplastic astrocytes	Well differentiated	Moderate	Generally absent	Absent	Absent	6-8
Grade III	Fibrillary neoplastic astrocytes	Regional or diffuse anaplasia	Regionally or diffusely increased	Present	Absent	Absent	3
Grade IV	Pleomorphic astrocytic tumour cells	Poor	High	Marked	Present	Prominent	1-2
<b>Oligodendroglioma</b>							
Grade II	Monomorphic cells, uniform round nuclei	Well differentiated	Moderate	Absent or occasional mitosis	Absent or not clearly visible	Not prominent	12
Grade III	Monomorphic cells, uniform round nuclei	Regional or diffuse anaplasia	Increased	Usually prominent	Possible	Often prominent	3->10
<b>Mixed oligoastrocytoma</b>							
Grade II	Neoplastic glial cells with astrocytic or oligodendroglial phenotypes	Well differentiated	Moderate	No or low	Absent	Absent	6
Grade III	Neoplastic glial cells with astrocytic or oligodendroglial phenotypes	Anaplasia	High	High	Absent (if present: GBMO)	Might be present	3
GBMO- glioblastoma with oligodendroglial component							

Glioblastoma multiforme (GBM; WHO grade IV tumour) is the most malignant form of cerebral gliomas and accounts for approximately 50 % of such tumours (Louis *et al.*, 2007; Jung *et al.*, 2007). GBM can occur as a high-grade lesion arising *de novo* from the glial cells (also known as primary GBM) representing more than 90 % cases of GBM cases (Zulch, 1986; Ohgaki and Kleihues, 2007). GBM can develop from a lower-grade precursor lesion, such as WHO grade II astrocytoma and WHO grade III anaplastic

astrocytoma (also known as secondary or progressive GBM) (Kleihues and Ohgaki 1999; Jung *et al.*, 2007). GBM can occur in all age groups, however, it is commonly observed in adults above 50 years in age. With optimal treatment, the overall five years survival of patients diagnosed with glioma in UK is approximately 1.2 % and the median survival is 12-14.5 months (Stupp *et al.*, 2009; Sonabend *et al.*, 2010; Sehmer *et al.*, 2014). These incidence rates have remained constant over time during the last decade and also throughout all regions in UK. Factors affecting the survival changes include age, where younger groups fare better; gender, where males are more prone to develop glioma; and location and extent of tumour resection (Wen *et al.*, 2008; Van Meir *et al.*, 2010). A defining feature of GBM is poorly defined tumour border, which often results in incomplete resection of tumour and hence poor survival due to tumour recurrence (Van Meir *et al.*, 2010).

### **1.5.1 Limitations with current histological diagnosis**

Implementation of the WHO classification criteria plays a key role in the diagnosis glioma, however, classification is mostly based on subjective criteria and is variable among pathologists. This variability has also resulted to ambiguous diagnosis for some patients (van den Bent, 2010). In addition, the inability to anticipate individual patient outcome based solely on WHO classification has led to considerable research trying to understand the pathogenesis of glioma and to determine relevant prognostic biomarkers in terms of molecular alterations to accurately distinguish different grades of glioma (van den Bent, 2010; Ricard *et al.*, 2014). Past studies have discussed the further characterisation of tumours by molecular and genetic markers, which can act as useful prognostic indicators for tumour therapy (Davis and McCarthy, 2001; Wrensch *et al.*, 2002; McKinney, 2004).

### 1.6 Advances in diagnosis of glioma

The mechanisms underlying gliomagenesis have been ambiguous, but in recent years, considerable progress has been made in understanding the molecular genesis of gliomas. At the forefront of such development, the identification of 1p/19q codeletion and mutations involving the isocitrate dehydrogenase genes (IDH1 and/or IDH2) in specific tumour types has played a key role in classifying gliomas.

For example, tumours that contain unbalanced reciprocal chromosomal translocation of 19p to 1q have been associated with an oligodendroglial phenotype. Similarly, tumours that contain whole deletion of 1p in [t(1; 19)(q10; p10)] along with TP53 mutations have been associated with astrocytic phenotype (Idbaih *et al.*, 2005; de Groot, 2013; Ricard *et al.*, 2014). IDH1 and/or IDH2 mutations have been frequently identified in more than two-thirds of low-grade gliomas and anaplastic gliomas and also in secondary GBM, however, these mutations have been rarely identified (<10 %) in primary GBMs (Figure 1.2). In such cases, mutant IDH enzyme is unable to perform its normal activity in tricarboxylic acid (TCA) cycle to convert isocitrate into  $\alpha$ -ketoglutarate ( $\alpha$ KG), which is responsible for DNA and histone demethylation. Instead, the mutant IDH enzyme acquires the ability to reduce  $\alpha$ KG to oncometabolite 2-hydroxyglutarate and not NADPH, which results in depletion of intermediates in TCA cycle. This leads to epigenetic alterations and induces hypoxia that affects gene expression thereby resulting in inhibition of cellular differentiation and promotion of angiogenesis and neoplastic growth (Cohen *et al.*, 2013; Schaap *et al.*, 2013; Ricard *et al.*, 2014).

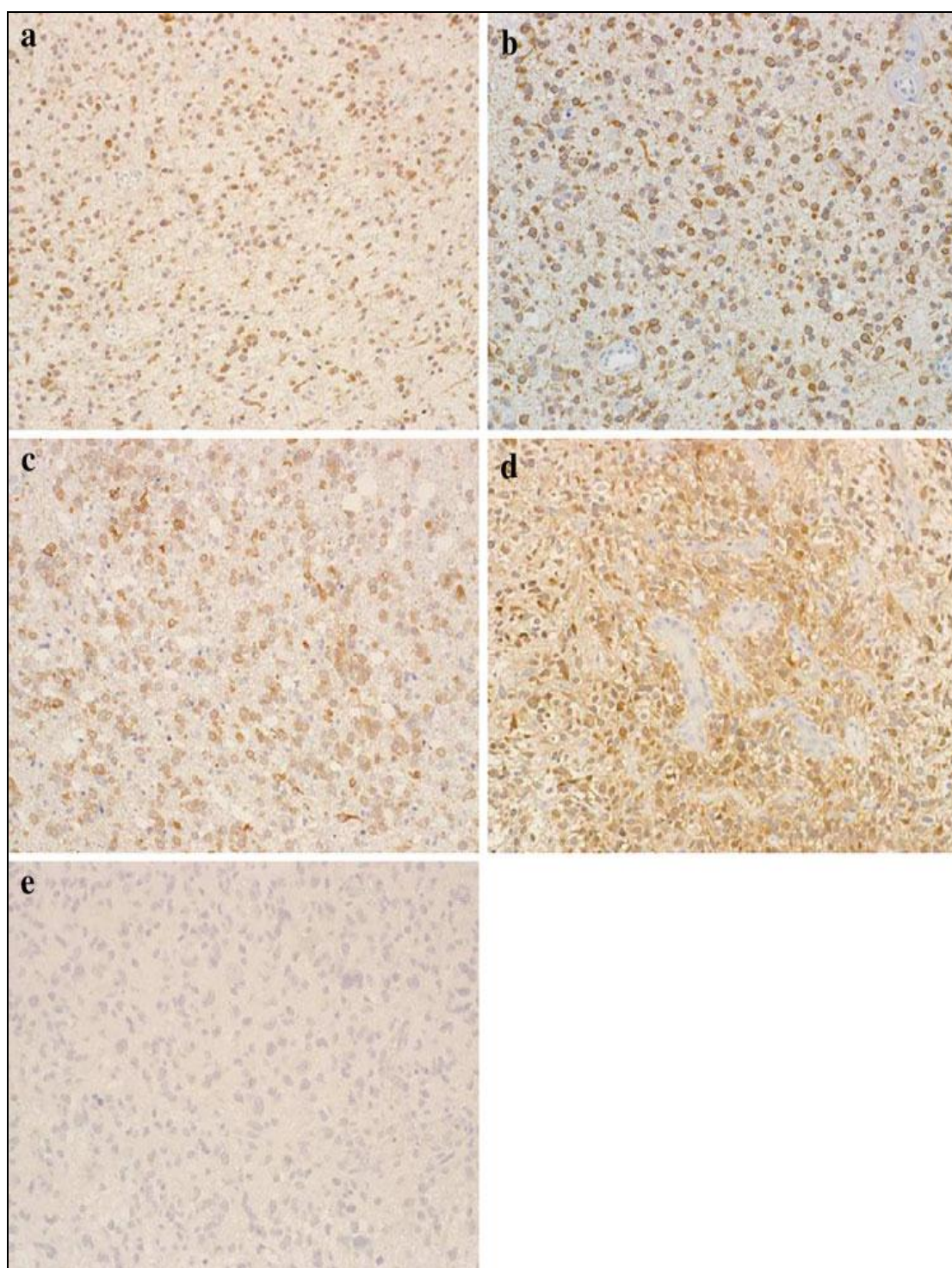


**Figure 1.2 IDH1 immunohistochemistry using IMAb-1 antibody (x 100).** a Diffuse astrocytoma, b anaplastic astrocytoma, c anaplastic oligoastrocytoma, d secondary glioblastoma, e primary glioblastoma. Note that IDH1 expression was not seen in grade IV primary glioblastomas (Taken from Takano *et al.*, 2011).

Primary GBM cases (> 90 % cases of all GBM) mainly affect elderly patients, and are genetically characterized by phosphatase and tensin homolog (PTEN) mutations, EGFR amplification and p16<sup>INK4A</sup> deletion (Figure 1.3). Secondary GBM (5 % cases) manifest mainly in younger patients and are often characterized by TP53 mutations with frequent G:C to A:T transitions at CpG (cytosine and guanine nucleotide in the linear sequence) sites. During progression to GBM, additional mutations occur; including, loss of heterozygosity (LOH) on chromosome 10q (10q25-qter) in both primary and secondary GBM (Ohgaki and Kleihues, 2007; Kakkar *et al.*, 2011 Raudino *et al.*, 2013).

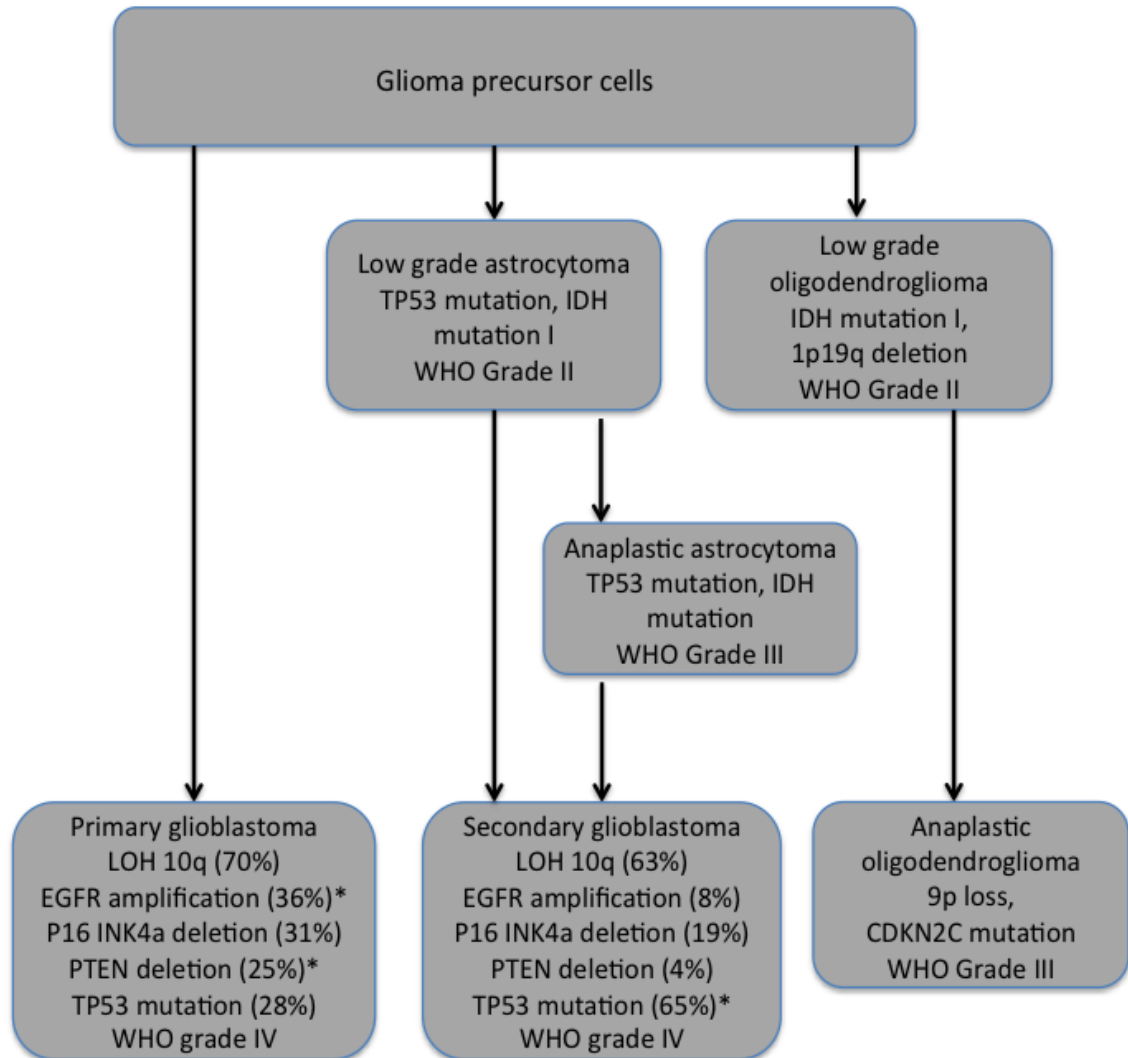


**Figure 1.3 Molecular and genetic characterization and pathways to primary and secondary GBMs at population level.** \*Frequency in genetic alterations differed significantly between primary and secondary GBMs (Ohkagi and Khleheius, 2007; Raudino *et al.*, 2013).

## 1.7 Establishment of tumour cell models

Use of *in vitro* cell lines as a model for glioma has been an essential mainstay for studying glioma biology and response to therapy (Wang *et al.*, 2005; Higgins *et al.*, 2010; Mullins *et al.*, 2013). Advances in cell-based assay techniques have facilitated the progress and understanding of the cellular and molecular processes involved in tumour initiation and progression (Laerum *et al.*, 2009). Cell culture has also been one of the fundamental tools for identification of novel therapeutic targets and high throughput screening of new chemical entities for desired pharmacological properties in drug design and development (Wang *et al.*, 2005; Breslin and O'Driscoll, 2013).

Cell culture models can be derived from primary human cells or immortalised human cell lines. Primary cultures are cells that have been isolated from human tissue resections, which may be further sub-cultured to form short-term cell lines with a finite replicative potential (Wang *et al.*, 2005). Immortalised cell lines have an infinite replicative potential, induced following exposure of cells to viruses such as monkey simian virus 40 (SV40) T antigen. An advantage of human immortalised cell lines is the ease of growth and maintenance and the consistency and reproducibility of the results obtained from a single cell type (Schindler, 1969; Wang *et al.*, 2005; Mullins *et al.*, 2013). A number of human malignant glioma cell lines were first developed by Poten and Westermark in the mid-1960s and 1970s and since then, a large number of well characterised cell lines for the major categories of brain tumours have been developed (Westermark, 1973; Poten, 1978; Masters and Palsson, 1999).

### 1.7.1 Applications of glioma cell lines to model human gliomas

Applications of GBM cell lines to model human gliomas have provided new

fundamental insight into potential and novel targets for therapeutics in cancer research. GBM cell lines have been used as a simple model system for glioma and have helped in finding new diagnostic and therapeutic modalities for these tumours. Various glioma derived cell lines such as 1321N1, U87MG, U251MG, GOS-3, TB10, LN-18, LN-229, T98G, and A172 have different malignant phenotypes and distinct genetic backgrounds. For example, U87MG (wild-type p53) and T98G (mutant p53) cell lines are both highly malignant and share similar altered cellular pathways, however, differ in the potential to form tumours in nude mice, with U87MG being highly tumorigenic *in vivo* (Cerchia *et al.*, 2009; Ramao *et al.*, 2012). U87MG also harbour higher levels of ErbB2 and phosphorylated extracellular signal- regulated protein kinase (ERK) than T98G (Cerchia *et al.*, 2009). The glioma cell culture models are more valuable to pharmaceutical scientists for evaluating new chemical entities as potential targets (Wang *et al.*, 2005; Mullins *et al.*, 2013).

### **1.7.2 Applications of pathological tissues to model human glioma**

One of the common procedures for cancer detection relies on the examination of tissue from biopsies, which are fixed under chemical conditions to preserve the integrity and antigenicity of tumour samples for later use. An important assay in examining cancer tissues is immunostaining, which can provide valuable diagnostic information for determination of malignancy. From fixed tissue, cancers have been categorised, subtyped and features enumerated to help elucidate the differences that exist between them. Several glioma related studies have used human tissue specimens as the primary source of investigational material for studying various prognostic markers involved in glioma (Dong *et al.*, 2005; Kalinina *et al.*, 2010; Sipayya *et al.*, 2012). They offer advantages over cell lines because they are more representative of the diagnosed

condition, not having undergone numerous passages and are reflective of the *in vivo* condition.

## **1.8 Current treatment strategies for malignant glioma**

The treatment of glioma, especially GBM remains difficult because no contemporary treatments have been curative (Preusser *et al.*, 2011). Multiple challenges for treating glioma persist because of the tumour heterogeneity, tumour location in the region where it is beyond the reach of local control, and rapid tumour relapse. While overall mortality rates remain high, recent work in the management of glioma combined with clinical trials are leading to more promising and tailored therapeutic approaches. Currently management of glioma is carried out in three modalities including surgery, radiotherapy, and chemotherapy.

### **1.8.1 Surgery**

The aim of brain tumour surgery is to maximise the removal of neoplastic tissue and minimise collateral damage to surrounding normal brain as well as vascular structures. Studies on glioma resection based on functional neuroimaging (MR imaging and magnetoencephalography), functional brain mapping and monitoring (fibre-tracking technique) (Mikuni and Miyamoto, 2010); and other functional neurosurgery methods such as neuro-navigation (Panciani *et al.*, 2012) and awake surgery (Yordanova *et al.*, 2011) are being reviewed to gain better treatment outcome. Combining these methods will allow safe and effective resection and may result in successful treatment. Conventional fluorophores and chromophore dyes have been used to identify tumour margins and have improved the extent of resection. Several studies also demonstrated that fluorescence imaging could be used to facilitate radical resection of glioblastoma during surgery (Laws *et al.*, 2003; Stummer *et al.*, 2006; Zhou *et al.*, 2009). The

discovery of photodynamic therapy (PDT) during 1980's involved the excitation of porphyrin derivatives to allow selective destruction of a tumour by means of apoptosis induced by cytochrome C. Photosensitisers such as 5-aminofluoresceinalbumin and mono-L-aspartyl chlorine have been used extensively in research. Stummer *et al.*, (2006) assessed the effect of fluorescence-guided resection with photosensitiser 5-aminolevulinic acid (5-ALA) on surgical radicality and demonstrated that intraoperative fluorescence imaging facilitated gross total resection and improved the prognosis of patients. Surgical treatment has therefore remained an important tool for the management of patients with GBM, however, complete surgical resection still continues to be the goal to reduce severe neurological, regional and systemic complications (Reardon and Wen, 2006; Lassen *et al.*, 2012; Wong *et al.*, 2012).

### **1.8.2 Radiotherapy**

Radiotherapy, an ionising radiation mainly affects rapidly dividing cells and is administered in short doses (fractions) to allow normal tissue to recover while rapidly dividing cells suffer an irreparable damage to DNA, cellular organelles and membranes thereby inducing cell death. Currently, the standard care for patients with newly diagnosed GBM includes maximal safe resection of the tumour followed by adjuvant radiotherapy (typical therapeutic dose of 60 Gy in 30 fractions) combined with chemotherapy (Stupp *et al.*, 2005; Mikuni and Miyamoto, 2010). The use of intensity-modulated and focal radiotherapy techniques has been increasingly preferred, however, because of the infiltrative diffusive nature of malignant glioma, there is currently a limited defined role for stereotactic radiosurgery or brachytherapy as first-line of treatment (Tsao *et al.*, 2005).

### 1.8.3 Chemotherapy

Several chemotherapeutic drugs including, tamoxifen (Brandes *et al.*, 1999), temozolomide (MacDonald, 2001; Strik *et al.*, 2008; Taal *et al.*, 2012), platinoids (Jeremic *et al.*, 1992; Francesconi *et al.*, 2010), topoisomerase inhibitors such as etoposide and irinotecan (Santisteban *et al.*, 2009), and procarbazine and vincristine (Schmidt *et al.*, 2006) are currently employed for the treatment option for glioma, with temozolomide paying special attention.

Temozolomide (TMZ), an alkylating agent is currently the most primarily used chemotherapeutic drug, given its ability to penetrate the blood brain-barrier and its acceptable toxicity profile. Analysis of patients with a tumour displaying promoter methylation of the DNA repair enzyme O<sup>6</sup>-methylguanine-DNA methyltransferase (MGMT) were most likely to have better prognosis with the addition of temozolomide to radiotherapy due to silencing of the DNA repair gene (Hegi *et al.*, 2005). GBM tumours carrying a non-methylated promoter (40-55 % of cases) responded poorly to TMZ dose (Hegi *et al.*, 2005; Sadones *et al.*, 2009), due to the functional MGMT enzyme repairing TMZ induced damage.

Carmustine or bis-chloroethylnitrosourea (BCNU) implants are biodegradable wafers implanted into the resected tumour area at surgery with the aim of improved chemotherapeutic targeting and passing the blood brain barrier (BBB). The biodegradable discs, Gliadel, infused with carmustine were approved by FDA in 2002. Though approved for treatment, the National Institute of Clinical health Excellence (NICE) appraisal noted no overall improvement in treatment response between patients treated with carmustine implants and patients treated with placebo at tumour resection

(Macbeth, 2007). The mean survival gain was however, observed for patients who had greater than 90 % tumour resection. NICE has therefore approved the use of carmustine implants in the conditional basis of greater than 90 % tumour resection, which is often unachievable in higher grade glioma due to the infiltrative nature (Macbeth, 2007). Moreover, carmustine wafers have also shown adverse effects in patients such as increased rates cerebrospinal fluid (CSF) leak and increased intracranial pressure secondary to oedema and mass effect (Gutenberg *et al.*, 2013).

### **1.9 Novel chemotherapeutics and issues identified while targeting and treating glioma**

The progress in genomics has provided the means for identification of novel targets and has enhanced progress in drug development and therapeutic regimes. Molecular targeting has been one of the novel approaches in the diagnosis of glioma as mentioned above. This approach is based on identifying a population of glioma cancer cells, which may express a unique receptor or antigen to be used as a targeting molecule for therapeutic purposes (Licha and Olbrich, 2005).

A large number of inhibitory agents targeting receptor tyrosine kinases such as epidermal growth factor receptor (EGFR), vascular endothelial growth factor receptor (VEGFR) and platelet derived growth factor receptor (PDGFR) along with transduction pathways inhibitors directed towards mTOR, PI3K, and histone deacetylase (HDAC) have also been evaluated in patients; however, the response rates have been variable and unpredictable (Table 1.3). Previous studies have identified a new mutant receptor of epidermal growth factor receptor (EGFR) known as EGFRvIII, which contains a unique polypeptide sequence with deletion of 269 amino acids and was expressed on several

malignant cells including GBM, but absent in non-cancerous healthy cells (Wickstrand *et al.*, 1995; Nash *et al.*, 2001; Sampson *et al.*, 2009). Although this initially appeared to be a unique marker of GBM, it was subsequently found that only 30 % of GBMs overexpressed EGFRvIII (Johnson *et al.*, 2012).

**Table 1.3 Selected agents tested in recurrent GBM.**

Agents	Target	Experimental design	Benefit	Reference
Self sufficiency in growth signals and insensitivity to growth suppressors				
Erlotinib, Gefitinib	EGFR	Phase II/III Ctr	Minimal as single agent. Some efficacy with TMZ	Van den Bendt <i>et al.</i> , 2009; Franceschi <i>et al.</i> , 2007
Enzasturin	PKC	Phase II Ctr	Minimal benefit	Wick <i>et al.</i> , 2010
Tipifarnib	Farnesyltransferase	Phase II Ctr	No benefit	Cloughesy <i>et al.</i> , 2006
Temsirolimus	mTOR	Phase II Ctr	Disease stabilisation and increased survival	Galanis <i>et al.</i> , 2005
Vorinostat	HDAC	Phase II Ctr	Modest activity	Galanis <i>et al.</i> , 2009
Imatinib	PDGFR	Phase II Ctr	Variable response	Wen <i>et al.</i> , 2006; Razis <i>et al.</i> , 2009
Induction of angiogenesis				
Bevacizumab	VEGF	Phase II/III Ctr	Active with and w/o TMZ and FDA approved for recurrent disease	Zhang <i>et al.</i> , 2012
Thalidomide	Fibroblast growth factors	Phase II Ctr	Minimal benefit as a single agent, some efficacy with carmustine	Fadul <i>et al.</i> , 2008
Invasion and metastasis				
Cilengitide	Integrins	Phase I/II Ctr	Some activity with TMZ	Stupp <i>et al.</i> , 2010
Abbreviations: Ctr, clinical trial; VEGF, vascular endothelial growth factor; EGFR, epidermal growth factor receptor; PDGFR, platelet derived growth factor receptor; PKC, protein kinase C; HDAC, histone deacetylase.				

Over expression of the receptors for Interleukin (IL)- 4R and IL-13R on various human brain tumour cells have also been identified (Debinski *et al.*, 1999). Studies on glioma found IL 13R2 was also highly expressed by GBM tumours. Interestingly, this receptor was found to be absent in normal brain tissues and therefore represented as a tumour-specific antigen for GBM, which may prove useful for diagnosis and imaging for patients with glioma (Debinski *et al.*, 1999; Mintz *et al.*, 2000; Nash *et al.*, 2001). These markers may potentially act as tumour associated targets (Kawakami *et al.*, 2002; Joshi *et al.*, 2003). This finding offered a novel approach to target malignant glial cells while sparing normal cells; however, the over-expression of the IL was not consistent due to the inherent heterogeneity of GBM (Liu *et al.*, 2003).

Vascular endothelial growth factor (VEGF) is a highly specific mitogen for vascular endothelial cells and induces endothelial cell proliferation, promotes cell migration, and inhibits apoptosis. The binding of VEGF to its receptor on blood vessels, promotes the proliferation, migration and survival and permeability of endothelial cells which forms building blocks of new vascular network for a malignant tumour (Ferrara *et al.*, 2003). Several studies have demonstrated the prevalence of VEGF expression and its isoforms and therefore have served as an important mediator of intense angiogenesis, which is a characteristic of glioblastoma (Oka *et al.*, 2007; Takano *et al.*, 2010; Xu *et al.*, 2013). A recent study demonstrated that VEGF is mainly expressed on the cell surface and also internalised in the early endosome compartment of the cytoplasm of the CD133<sup>+</sup> human glioma stem-like cells (GSCs) (Hamerlik *et al.*, 2012).

Bevacizumab (Avastin), an anti-VEGF inhibitor (FDA approved, 2009), has been studied in combination with radiotherapy and chemotherapy for potential use in

treatment of recurrent malignant glioma (Figure 1.4). It was also reported that combining bevacizumab with radiotherapy/temozolomide demonstrated improved quality of life, diminished steroid requirement, and statistically significant improvement in progression free survival (PFS) but not overall survival (Cloughsey *et al.*, 2006; Gilbert *et al.*, 2014). The results were encouraging, however, there is not enough available clinical trial data that provide convincing evidence that such combination therapy is superior to a single agent approach (Zhang *et al.*, 2012; Gilbert *et al.*, 2014). Moreover, prolonged treatment with bevacizumab has potential for serious adverse effects, with moderate survival benefit (Friedman *et al.*, 2009; Reardon *et al.*, 2012; Gilbert *et al.*, 2014).

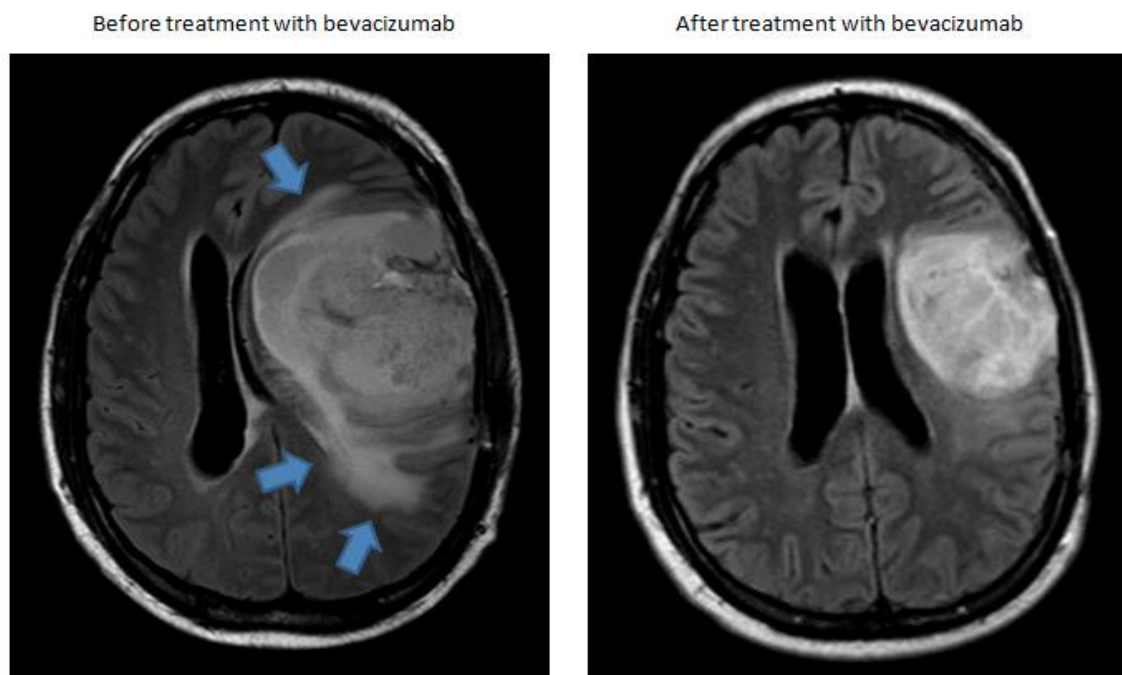


**Figure 1.4 Brain MRI image (FLAIR, axial plane) of a 44 years old man with recurrent GBM.** Note significant amount of tumour associated vasogenic oedema (arrows) and the midline shift (shift of the brain past its centre line). After treatment with bevacizumab, midline shift was resolved and amount of oedema significantly decreased leading to clinical improvement (Taken from Mrugala, 2013).

### 1.10 Future approaches towards targeting and treating glioma

Several studies have demonstrated that current therapies are limited by ineffective early diagnosis, insufficient drug concentrations reaching the tumour, drug toxicity, and poor therapeutic monitoring. There have been several cases, especially in diffusely invasive brain tumours, where a significant amount of residual tumour persists even after total resection (Albayrak *et al.*, 2004; Doherty, 2010). In addition, several aspects such as size of the therapeutic molecule, lipophilicity, presence of active efflux pumps and most importantly, integrity of the blood-brain barrier that is typically damaged by the invasive GBM have a great impact on drug access to CNS tumours (Neuwelt *et al.*, 2011). Major improvements in molecular imaging in a non-invasive manner are required to help with the early detection of disease and to help achieve gross total resection, and hence improve the outcome for the patient.

The rapid development of novel technologies for molecular diagnostics and tumour-targeted therapy has enabled the development of highly specific ligands for targeting cell surface or internalised molecules that are expressed differently in tumour cells and tissue (Cerchia and Franciscis, 2010; Yu *et al.*, 2011, Yu *et al.*, 2012). Recent advances in studying intercellular and intracellular biochemical process has significant impact on cell imaging and drug delivery (Cibiel *et al.*, 2011; Esposito *et al.*, 2014). Novel technologies including single molecular imaging, fluorescence resonant energy transfer (FRET) and gene regulation have greatly contributed to our understanding towards cellular functions and drug delivery (Xing *et al.*, 2012). The intrinsic heterogeneity in human tumours has meant there is a need for targeting ligands that can help in the identification of tumour specific signatures. The goal of targeted therapy is to improve diagnostics, predicted therapeutic response and as a result, a decline in unnecessary

treatment of unresponsive oncological patients.

Targeted drug delivery for cancer demands a ligand which can specifically carry the drug to cancer cells. A number of biological delivery systems have been used to selectively transport imaging probes to tumour cells with monoclonal antibodies receiving significant attention in the literature for more than three decades (Scott *et al.*, 2012). The antibody-drug conjugate (ADC) field has been developed for targeted delivery of potent anti-cancer drugs with the aim to deliver the cytotoxic drug to the target tumour cells and therefore passing the morbidity common to conventional chemotherapy. ADC consists of an antibody (or antibody fragment) linked to a biologically active cytotoxic payload or drug. Three such ADCs received FDA approval including Gemtuzumab ozogamicin (Mylotarg<sup>®</sup>) (2001), Brentuximab vedotin (Adcetris<sup>®</sup>, 2011) marketed by Seattle Genetics, and trastuzumab emtansine (Kadcyla, 2013) marketed by Genentech and Roche for the treatment of acute myelogenous leukemia, Hodgkin's Lymphoma and Her2<sup>+</sup> metastatic breast cancer, respectively.

Despite advances in this area, ADC still carry a number of limitations such as cancer cell specificity, tumour penetration, product heterogeneity, conjugation chemistry and manufacturing issues. For example, Gemtuzumab ozogamicin (Mylotag), FDA approved in 2001 for the treatment of patients with acute myelogenous leukemia was withdrawn from the market in June 2010 due to its significant side effects and negligible improvement in clinical benefit. Such limitations restrict the use of antibodies as drug carriers. By defining the advantages and disadvantages of ADC, it should be possible to develop a more rational approach to the application of targeted drug delivery strategies and develop therapies that are more effective for cancer patients.

The adoption of a new class of oligonucleotide- based molecular recognition elements have recently emerged as a rival of antibody based methods, serving an ever-increasing demand for versatility in the biomedical field.

### **1.11 Historical review of aptamers**

Aptamers are short single stranded DNA or RNA oligonucleotides, and could be ideal targeting agents for cancer. The DNA or RNA oligonucleotides were termed as “aptamers” with etymology stemming from the Greek word “aptus” meaning “to fit” (Shangguan *et al.*, 2008; Cibiel *et al.*, 2011; Meyer *et al.*, 2011). The highly defined three-dimensional structure of aptamers helps them to bind to their targeted molecules with nanomolar affinities and high specificity (Cerchia *et al.*, 2009; Bayrac *et al.*, 2011; Kong and Byun, 2013). Aptamers were discovered in the early 1990’s (Ellington and Szostak, 1990), and were found to bind to a range of targets from small organic compounds (Mannironi *et al.*, 1997), peptides (Nieuwlandt *et al.*, 1995), amino acids (Geiger *et al.*, 1996), proteins (Lupold *et al.*, 2002) and cells (Cerchia *et al.*, 2009). The speciality of aptamers is the small size, low immunogenicity, and low molecular weight (5-25 kDa), which correspond to binding affinity to targets in the low nanomolar to picomolar range. The specificity of aptamer – target binding was such that aptamers were shown to discriminate between closely related isoforms or different conformational states of the same targeted molecule (Cibiel *et al.*, 2011; Liu *et al.*, 2013).

Since their discovery, numerous aptamers have been engineered against various molecular targets and have been shown to exhibit inhibitory and modulatory activity towards their targets (Refer to section 1.16) (Keefe *et al.*, 2010; Cibiel *et al.*, 2011; Liu

*et al.*, 2013). Some of the key features of aptamers include, functional immobilisation on various substrates, long-term chemical stability by chemical modification of bases, uniform labelling, for instance with biotin or fluorescence reporters, and the ability to recover native active conformation after denaturation.

### **1.12 Secondary and tertiary structure of aptamers**

Aptamers are known to bind to target molecules on single stranded regions known as a 'bulge' or 'loop' which contribute to the spatial structure of binding (Hermann and Patel, 2000; Nery *et al.*, 2009; Cibiel *et al.*, 2011). Moreover, the overall structure is dominated by base pairings that are similar to those observed in the DNA double helix formation. The nucleotide sequence in an oligonucleotide chain allows Watson and Crick base pairing (guanine to cytosine, adenine to thymine/ uracil) as the single strand is folded back on itself. The folding pattern of such base pairing is known as the secondary structure of the aptamer (Figure 1.5, Klusmann, 2006; Bayrac *et al.*, 2011).

Ideally, an approximate knowledge of the aptamer secondary structure is required to understand and optimise the aptamer binding interactions with the target. The molecular recognition of aptamers results from intermolecular interactions such as stacking of aromatic rings, electrostatic and van der Waals interactions, or hydrogen bonding with a target compound (Hermann and Patel, 2000).

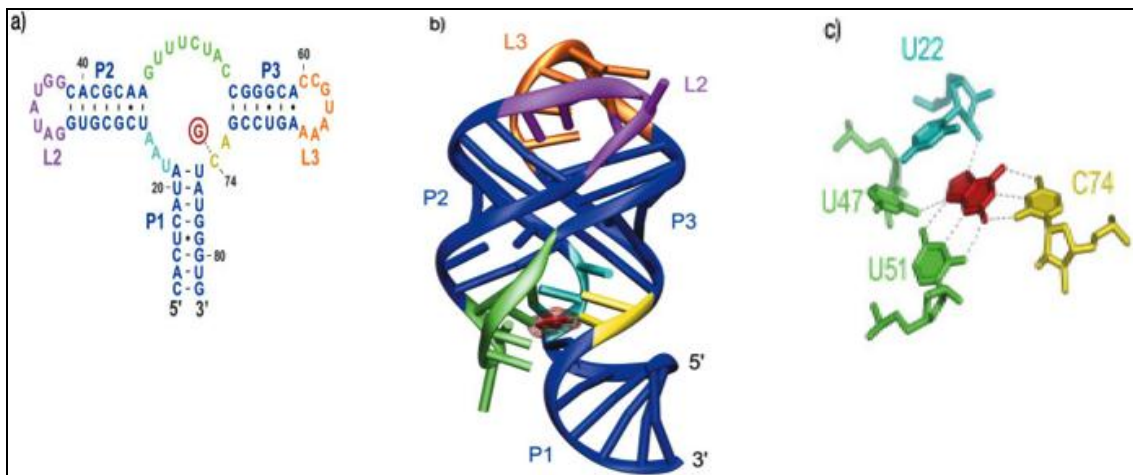


**Figure 1.5 Secondary and tertiary structure depictions of aptamers.**

a) Secondary structure of a RNA aptamer showing coloured loops due to unpaired nucleotides and kinks due to mismatched bases (base pairs are indicated by ‘-‘). The Watson-Crick interactions between aptamer and its ligand (circled) are depicted with dashed lines. b) Tertiary structure of the same RNA aptamer showing the binding site (red) where unbound bases in the loops binds to the target molecule. c) Exploded view of the binding site showing hydrogen bonding with the target molecule (red). (Taken from Klussmann, 2006).

The formation of unique three – dimensional structure by aptamers is mainly due to changing intramolecular base pairing, having a combination of stems, loops, quadraplexes, pseudoknots, bulges, and hairpins. Such unique properties of the aptamers justify them to be valuable for diagnostics, purification process, target validation, drug discovery, and therapeutic interventions (Cerchia and Franciscis, 2010; Esposito *et al.*, 2011; Cibiel *et al.*, 2011, Mencin *et al.*, 2013).

### **1.13 Generation of aptamers**

Over the past few years, considerable efforts have been made to improve the isolation and selection process for aptamers. The development of the Systemic Evolution of Ligands by Exponential enrichment (SELEX) process (first implemented at NascaCell IP Munic, Germany) in 1990 by Ellington and Szostak, significantly accelerated the generation of aptamers with a capacity of recognizing virtually any class of target molecules with high affinity and specificity. Since then several SELEX methods have been designed as the targets to generate aptamers conveniently and easily (Ellington and Szostak, 1990; Jayasena, 1999; Cerchia *et al.*, 2009; Ababneh *et al.*, 2013). During SELEX, general selection and amplification processes of nucleic acids are performed until the target interacting sequences dominate the population (Figure 1.6). A library of nucleic acid (DNA or RNA) molecules is incubated with the target and the non-binding sequences are partitioned away. The sequences with high affinity for the target are eluted and re-amplified by RT-PCR and transcription process to yield an enriched pool of molecules that bind to the protein of interest. Several rounds of selection (15-25) with increasingly stringent condition and amplification are performed to obtain high affinity target specific aptamers followed by cloning, sequencing, and characterization.

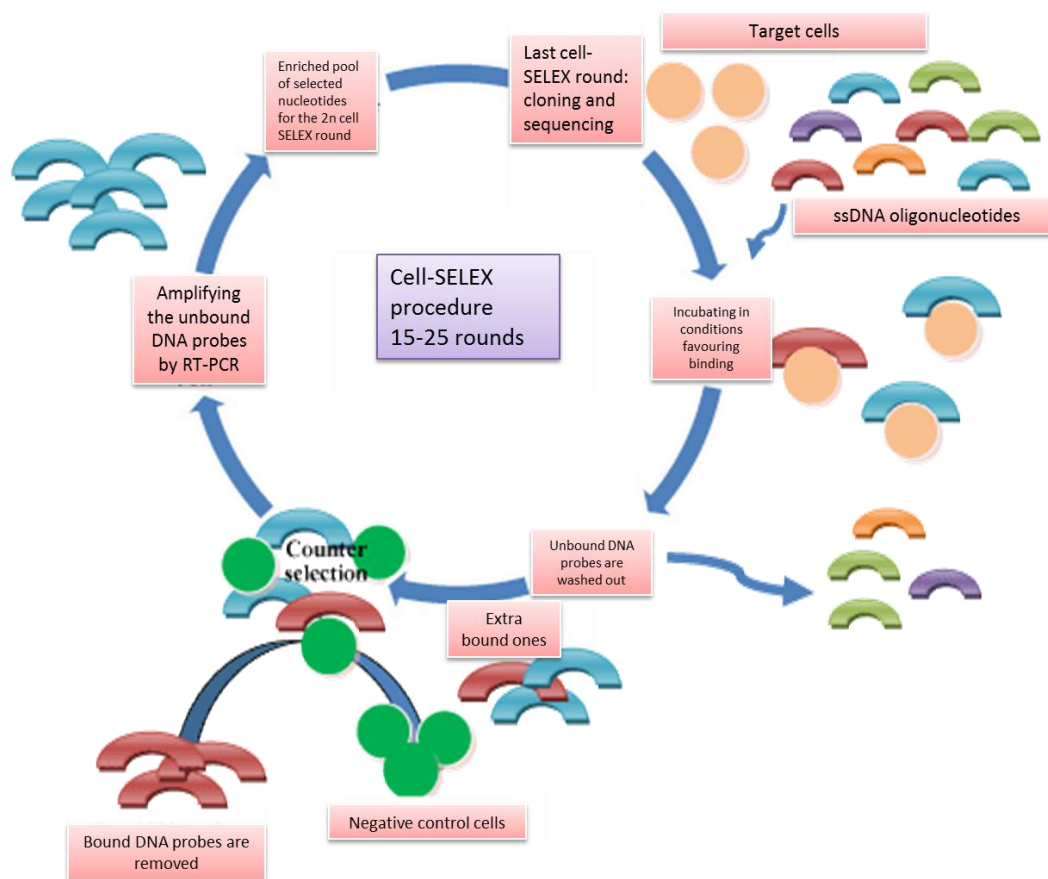


**Figure 1.6 General scheme of cell-SELEX procedure.**

Aptamers can be obtained through an iterative selection process known as SELEX (systematic evolution of ligands by exponential enrichment) by using single-stranded DNA or RNA. An initial pool of  $10^{14}$ - $10^{15}$  random oligonucleotide strands is subjected to binding with the target tumour cells. Unbound oligonucleotides are discarded and RT-PCR is performed to amplify the target-bound oligonucleotides. The target bound oligonucleotides are then subjected to counter-selection using control (non-cancerous) cells. This time the unbound sequences are collected and amplified. This selection process is repeated 15-25 times using amplified oligonucleotides as a new pool. This way, aptamers having high specificity and affinity are screened. Diverse molecules can be the target of the SELEX, including metal ion, protein, and organic compound (Taken from Marolt *et al.*, 2000).

During the selection process, the sequence diversity of oligonucleotide library is remarkably reduced and the overall affinity of the selected sequences increases in each successive SELEX. Once knowledge of particular aptamer sequence is elucidated, production can be easy and rapid via enzymatic *in vitro* transcription or chemical synthesis. Also, recent advances in selection processes and more detailed analysis of delivering nucleic acids to target cells and tissues should speed the process of drug development (Lee *et al.*, 2006; Cerchia *et al.*, 2009). Researchers have also developed *in vivo* SELEX, where instead of using *in vitro* cell-culture system, the whole experimental animal is used for aptamer generation (Mi *et al.*, 2010; Cheng *et al.*, 2013).

#### **1.14 Aptamers versus antibodies**

Aptamers can provide an excellent alternative to antibodies as aptamers have high affinity and sensitivity, very low detection limits and no problems with batch-to-batch variation (Baldrich *et al.*, 2004). Many experiments have compared aptamers and antibody based assays and has proven that aptamers show more accurate and specific results compared to antibodies (Blank *et al.*, 2001; Zeng *et al.*, 2010). Aptamers have also been used in ELISA- like assays and flow cytometry (Blank *et al.*, 2001). The time required for the generation of aptamers is comparatively shorter than that to obtain monoclonal or polyclonal antibodies. To date, antibody-based assays have also been developed for *in vivo* applications but, in most cases, antibodies have failed to reach expected adequate sensitivity because of the toxicity profile *in vivo* (Descotes, 2009).

The use of aptamers is currently limited to parenteral administration but has proven to be useful in animal models as mentioned in the previous sections. Aptamers have been

proven to address such requirements because of their small size and polyanionic nature, which help them to accumulate at the tumour site and show rapid blood clearance minimising their residence in liver and kidney. As a result of the small size (figure 1.7) and similarity to endogenous molecules, aptamers are thought to be poor antigens. In addition, aptamers include faster excretion than antibodies due to the small size and susceptibility to serum degradation when unmodified aptamers are used, however, this can be overcome by modifying the structure and adding stabilising groups (Refer to section 1.15). Clinical studies have confirmed that aptamers are thermally stable, have an unlimited shelf life, non-toxic and non-immunogenic molecules and so their applications have far exceeded the limitations (Table 1.4).

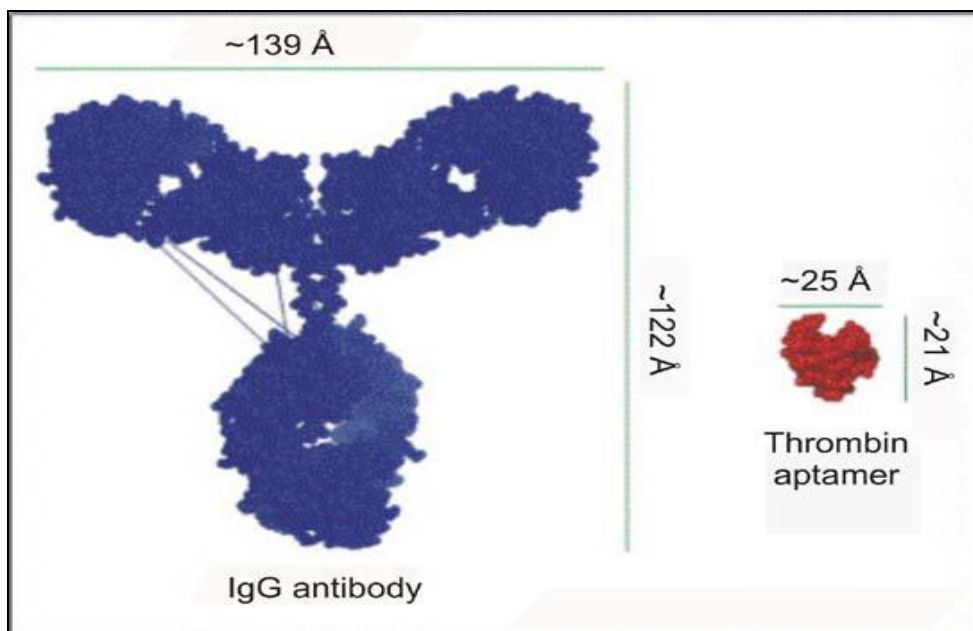


**Figure 1.7 Size comparison of an antibody and an aptamer** (Taken from Lee *et al.*, 2006).

Table 1.4 Properties of aptamers versus antibodies (Blank *et al.*, 2001; Proske *et al.*, 2005; Lee *et al.*, 2006).

	Aptamers	Antibodies
Size (figure 1.7)	Small, MW: 8-12 kDa	Large, MW: 150 kDa
Selection procedure	The whole selection is a chemical process carried out <i>in vitro</i> and can therefore target any protein.	The selection requires a biological system and therefore is difficult to raise antibodies to toxins or non-immunogenic targets which is not tolerated by animal.
Working conditions	Can select for ligands under a variety of conditions for <i>in vitro</i> diagnostics.	Limited to physiologic conditions for optimizing antibodies for diagnostics.
Activity	Consistent activity regardless of batch synthesis.	Activity of antibodies varies from batch to batch.
Modifications	Wide variety of chemical modifications to molecule for diverse functions	Limited modifications of molecule
Shelf-life	Unlimited shelf- life	Limited shelf-life
Immunogenicity	No evidence of immunogenicity	Significant immunogenicity

### 1.15 Modification of oligonucleotide aptamers to improve their function

One of the ultimate goals during aptamer selection is the biostability in clinical application; however, unmodified oligonucleotides *per se* are unstable in biological fluids due to enzymatic degradation or a short half-life (Gold, 1995; Dupont *et al.*, 2010). RNA aptamers are capable of forming a greater variety of spatial structures as compared with DNA aptamers, as a result of the presence of 2'-OH groups. RNA aptamers are however, more sensitive to the action of cell nucleases and therefore, various strategies have been established to increase the serum stability by the introduction and modification of additional protective group (Wang *et al.*, 2011;

Shigdar *et al.*, 2013). One common chemical modifications involved are substitutions of the 2'- hydroxyl group of the pyrimidine nucleotides with 2'- fluoro or 2'- amino although, 2'- fluoro RNAs appear superior to 2'- amino RNAs in terms of target affinity. Such modifications can improve the half – life considerably (Figure 1.8) (Esposito *et al.*, 2011). Phosphate and base modification are also used for this purpose. LNA has been designed to structurally protect 2' site offering stability. In addition, amino, thiol and carboxyl are introduced to strengthen the oligonucleotide backbone.

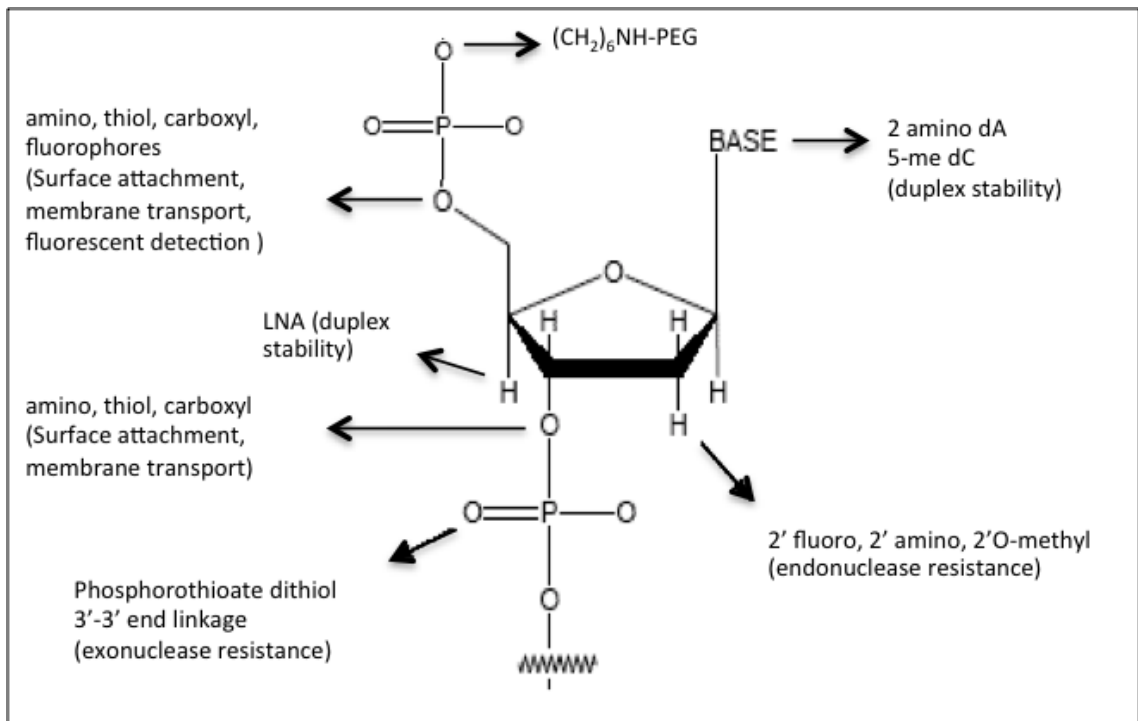


**Figure 1.8 Modifications employed to improve the function and pharmacokinetic profile of aptamers.** Such modifications can assist in stabilising the nucleic acids against enzymatic hydrolysis and renal filtration.

Recently, Pieve and his group performed a study on aptamers to improve the stability and provide resistance to nuclease degradation. They used  $^{99m}\text{Tc}$  labelled anti-MUC 1 (cell-surface mucin glycoprotein) aptamers (AptA and AptB) and conjugated with MAG2 and also modified their 3' end with an inverted thymidine. Such modification showed accumulation of the aptamer in the target tumour site along with reduced blood clearance (Pieve *et al.*, 2009).

Several authors have also conjugated polyethylene glycol (PEG) with aptamers to enhance the bioavailability and pharmacokinetic properties and increase the half-life of aptamers *in vivo* (Boomer *et al.*, 2005; Guo *et al.*, 2011). Aptamer anti-PDGF was conjugated with 40 kDa PEG to slow down the renal clearance thereby allowing the aptamer more time to perform its function (Floege, 1999). Similarly, Healy *et al.* (2004) conjugated an aptamer with 20 and 40 kDa PEG to increase its half-life in circulation.

Due to the small size and presence of high covalent bond between the aptamers and targets, aptamers have a high detection range and thus reduce the number of false-positive signals. Aptamers are chemically synthesised, and therefore, modification can be performed at either 5' or 3' - with any fluorescent dye or a chemical group or biotin using simple phosphoramidite chemistry without interfering with the aptamer binding to its target (Blank *et al.*, 2001; Sefah *et al.*, 2009; Jimenez *et al.*, 2012).

### **1.16 Applications of aptamers**

Aptamers are very effective tools owing to their easily modified chemical structure, specificity, non-immunogenicity, non-toxicity and wide range of targets and therefore, can be the ideal candidates for clinical application such as molecular imaging, target

diagnosis, cell detection, drug delivery, and therapeutic intervention.

### **1.16.1 Aptamer based molecular imaging**

Along with *in vitro* imaging, aptamers have been successfully employed for *in vivo* imaging, thus providing many potential applications in biomedicine. These imaging systems can be categorised according to their energy source (photons, positrons, X-rays, or sound waves), their spatial resolution (macroscopic or microscopic), or to the type of information that can be obtained (anatomical, cellular or molecular). Imaging technologies such as optical imaging, stereotactic navigation and intraoperative MRI, CT (computed tomography), PET (positron emission tomography), and SPECT (single photon emission computed tomography) have shown promising approaches to improve the extent of resection (Doherty, 2010).

#### **1.16.1.1 Optical imaging**

Optical methods such as confocal imaging, multiphoton imaging, microscopic imaging and near-infrared imaging have been adapted for current cancer research (Laws *et al.*, 2003; Sefah *et al.*, 2010; Lin *et al.*, 2014) These optical methods represent tissue-specific imaging and monitoring the progression of disease by utilizing new non-invasive imaging modalities, radioligands and contrast agents. Aptamer based optical imaging is a cost effective imaging technique that typically uses fluorescent or bioluminescent probes and can be categorised as a direct targeting probes that is able to be activated (Hong *et al.*, 2011). Several studies have been performed where simply conjugating a fluorescent molecule to the aptamer has proved to be a convenient way to image cellular target by fluorescence (Shi *et al.*, 2010; Cui *et al.*, 2011; Zhang *et al.*, 2012; Song *et al.*, 2013).

The use of aptamers as *in vivo* imaging probe was studied by Hicke *et al.*, (2006). In this publication, an aptamer generated against tenascin C (TTA1) was labelled with rhodamine red and <sup>99m</sup>Tc (radioisotope) to study uptake and biodistribution in glioblastoma (U251) and breast cancer (MDA-MB-436) cells by confocal microscopy and *in vivo* imaging, respectively. After intravenous injection, the aptamer showed accumulation in the tumour site within 10 min and by diffusion throughout tumour in 3 h followed by rapid renal and hepatic clearance from the circulatory system (Hicke *et al.*, 2006). The results were promising, and therefore encouraged the researchers to perform several more *in vivo* studies.

### 1.16.1.3 MRI

An approach by Dua *et al.*, (2011) was carried out to test the potential of RNA aptamer A10 against prostate cancer in tumour imaging. The study was performed by conjugating the A10 aptamer with a thermally cross-linked super paramagnetic iron oxide nanoparticle (TCL-SPION). This nanoparticle is often used as a contrast agent in MRI imaging and has low systemic toxicity. In this study, the A10 aptamer allowed TCL-SPION to bind specifically to prostate cancer cells expressing prostate specific membrane antigen (PSMA) thus enhancing the potential for tumour imaging capabilities of TCL-SPION to be localised to the prostate tumour (Dua *et al.*, 2011). A multimodality-imaging probe based on the AS1411 aptamer was evaluated by Hwang *et al.*, (2010). The biodistribution was studied by intravenously administering rhodamine labelled magnetic fluorescent nanoparticle conjugated to gallium-67 (<sup>67</sup>Ga) and nucleolin aptamer AS1411 into tumour bearing nude mice. The conjugates accumulated at the tumour site and also showed rapid blood clearance as observed by planar scintigraphic images and MRI (Hwang *et al.*, 2010).

#### 1.16.1.4 PET

PET, a widely used molecular imaging modality measures the signal originated from the radioactive decay of neutron-deficient radioisotopes such as  $^{11}\text{C}$ ,  $^{15}\text{O}$ ,  $^{64}\text{Cu}$  and  $^{18}\text{F}$  that are intravenously injected into the body. PET imaging application was studied using  $^{64}\text{Cu}$ -labelled A10-3.2 PSMA specific RNA aptamer to enable radiolabeling for *in vivo* imaging of tumours (Rockey *et al.*, 2011). In this study, the choice of chelators and radiolabeling parameters such as pH, temperature and aqueous conditions were investigated and found to be favourable for the development of  $^{64}\text{Cu}$ -labelled RNA-based targeted agents for potential PET imaging.

#### 1.16.1.5 SPECT

SPECT is a relatively new imaging technique similar to PET, however, the radionuclides used are Xenon-133, Technetium- 99 ( $^{99\text{m}}\text{Tc}$ ), and Iodine-123 which have longer decay times than those used in PET. A study performed by Pieve *et al.*, (2009) reported conjugation of radioactive substances to aptamers and antibodies showed quick distribution and rapid tumour uptake of the residual radioactive aptamers followed by clearance from the blood stream. This radionucleotide conjugation not only allowed for superior tumour imaging, but also decreased toxicity to healthy tissues that was often seen with radioactively labelled antibodies due to the slow clearance from the body. An example of the use of aptamers for *in vivo* imaging using SPECT was published by Charlton *et al.*, (1997) where, aptamers that were generated against activated neutrophil elastase, NX21909, a marker for inflammation in rats, were conjugated with  $^{99\text{m}}\text{Tc}$ , a metastable radioactive tracer. The results were compared with a negative control and the antibody counterpart, showing rapid clearance of the aptamer-radioactive tracer conjugate from circulation and higher signal-to-background

ratio.

### 1.16.2 Aptamers for target identification

The high binding affinity of aptamers to a target enables detection of cancer cells, resulting in early and sensitive diagnosis. Highly specific aptamers have been selected against a wide range of intracellular and extracellular targets such as tenascin-C (Hicke *et al.*, 2001), IFN- $\gamma$ -inducible CXCL10 chemokine (Marro *et al.*, 2005), nucleolin (Hwang *et al.*, 2010) or human epidermal growth factor receptor -3 (HER3) (Tan *et al.*, 2013). Table 1.5 lists some promising aptamers widely studied with the targets and clinical applications.

**Table 1.5 Promising aptamers involved in diagnostic imaging and treatment of various diseases.**

Name	Nucleotide	Target	Clinical applications	Reference
TTA1	RNA	Tenascin C	Imaging (SPECT)	Hicke <i>et al.</i> , 2006
AptA, AptB	DNA	Mucin	Imaging (SPECT/ Optical)	Pieve <i>et al.</i> , 2009; Savla <i>et al.</i> , 2011
AS1411	DNA	Nucleolin	Imaging (MRI/SPECT/Optical)	Hwang <i>et al.</i> , 2010 Kuo <i>et al.</i> , 2014
A10, A10-3, A10-3.2	RNA	PSMA	Prostate cancer therapy	Farokhzad <i>et al.</i> , 2006; Dhar <i>et al.</i> , 2008
gp120 aptamer	RNA	gp120	HIV therapy	Neff <i>et al.</i> , 2011
CD30	RNA	CD30	Imaging lymphoma	Zeng <i>et al.</i> , 2010

A new strategy for exploiting aptamers in the analysis of proteins and small molecules was developed by Yamamoto and Kumar in 2000, and was called aptamer beacons. Aptamers beacons produce fluorescent signals upon target binding and structural rearrangement (Yamamoto and Kumar, 2000). Vicens *et al.*, (2005) described these

molecular beacon aptamer as a high affinity synthetic DNA probe, which could detect the target in as little as 10 nanogram of platelet-derived growth factor (PDGF) per microgram of serum proteins from cell culture media.

Multiplexed aptamer-based proteomics has emerged as a potentially powerful analytical and quantification tool, which could complement mass-spectrometry (MS) based approaches for the purpose of drug and biomarker discovery. Using such technology, several thousands of proteins can be simultaneously measured and profiled with high accuracy from a tiny amount of serum or plasma, thus becoming an attractive technique for biomarker and clinical purposes. Shuangguan *et al.*, (2008) utilised T-cell acute lymphoblastic leukaemia (T-ALL) and identified a biomarker, PTK7 (protein tyrosine kinase 7), through cell SELEX and MS.

### **1.16.3 Aptamer as therapeutics - clinical trials of aptamers in medicine**

Angiogenesis is a crucial process in growth, development, and wound healing of tissue; however, it can also contribute to diseases such as tumour growth, cancer progression, and macular degeneration. In such cases, anti-angiogenic aptamers have shown to prevent or delay such unwanted neovascularisation (Eugene *et al.*, 2006). Since 2005, aptamer technology has achieved a breakthrough in the therapeutic application field when an aptamer drug Macugen (Pegaptanib) was developed for treatment of neovascular age related macular degeneration, a disease of the eye (FDA, 2004). The target for this anti-angiogenic aptamer was VEGF-165, (figure 1.9), which is a homodimeric protein and the most abundant VEGF isoform that regulates vascular permeability (Eugene *et al.*, 2006; Ferrara *et al.*, 2006). Table 1.6 lists few of the current aptamers, which are being tested in clinical trials.

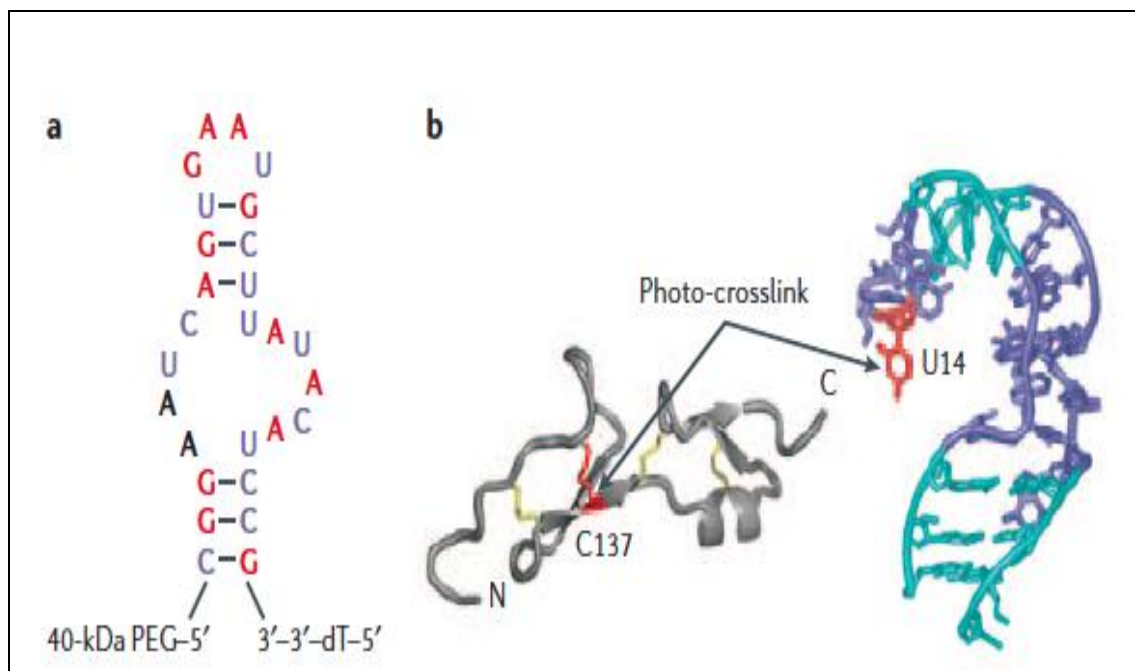


**Figure 1.9 Pegaptanib structure and target binding.** **a** Sequence and predicted secondary structure of pegaptanib with chemical modifications. 2'-O-methylated purines are shown in red, 2'-fluorine-modified pyrimidines are shown in blue and unmodified ribonucleotides are shown in black. The site of attachment of a 40-kDa polyethylene glycol moiety is shown. **b** Model showing interaction between the 55-amino-acid heparin-binding domain of vascular endothelial growth factor (VEGF)165 and pegaptanib. The interaction between cysteine-137 of VEGF-165 (cysteine-27 of the heparin-binding domain) and uridine-14 of the aptamer is indicated in red. (Taken from Eugene *et al.*, 2006).

**Table 1.6 Current therapeutic aptamers in various stages of clinical development.**

Name	Nucleotide	Target	Condition	Phase
<b>Pegaptanib</b>	RNA	VEGF	Macular Degeneration	FDA approved
<b>AS1411</b>	DNA	Nucleolin	Acute Myeloid Leukemia	Phase II
<b>NU172</b>	DNA	Thrombin	Heart disease	Phase II
<b>NOX-E36</b>	RNA	CCL2	Type 2 Diabetes Mellitus	Phase I
<b>E10030</b>	DNA	PDGF	Age-related macular degeneration	Phase II

The most advanced aptamer on the potential treatment of cancer is AS1411, a guanine rich aptamer previously known as AGRO100, developed by Antisoma (London, UK). AS1411 binds nucleolin on the cell surface and is able to internalise into the cancer cells. The therapeutic benefit of AS1411 is presumably attributed to interfere with intracellular pathways by disruption of nuclear factor kappa B (NF $\kappa$ B) signalling thereby inducing apoptosis (Bates *et al.*, 2009). AS1411 had also shown positive responses in patients with advanced solid tumours (including three renal and two pancreatic cancer cases) without adverse side effects (Laber *et al.*, 2005). In addition, in randomised phase II clinical trials, a 10 mg/kg/day or 40 mg/kg/day dose of AS1411 combined with high dose cytarabine (chemotherapeutic drug for acute myeloid leukaemia and Hodgkin lymphoma) was well tolerated and showed better efficacy and outcome with primary refractory or relapsed acute myeloid leukaemia (Stuart *et al.*, 2009). Other aptamers under clinical evaluation include NU172 targeting thrombin (Waters *et al.*, 2009), NOX-A12 and NOX-E36 targeting chemokine ligand 12 (CCL12) (Darisipudi *et al.*, 2011), and E10030 targeting PDGF (Keefe *et al.*, 2010).

#### 1.16.4 Aptamer conjugates for targeted drug delivery

To date, a large number of anti-cancer drugs have been approved by the Food and Drug Administration (FDA), however, most of them are not molecularly targeted which has caused significant toxicity and side effects. Successful delivery of anti-cancer drugs demands optimisation of many aspects including encapsulation, targeting, delivery, and controlled release. In addition, combining specific targeting and controlled drug release should be able to deliver sufficient doses of cytotoxic drugs to tumour cells over an extended period of time without significantly affecting the surrounding non-cancerous healthy tissues. Aptamers can potentially alterate and satisfy the aforementioned problems and challenges by use as recognition moieties and guide a variety of therapeutics to target diseased sites. Several aptamers have been selected against various cancer cell lines and have also demonstrated their targeted anti-tumour activity alone (Eugene *et al.*, 2006), or coupled with toxins (Chu *et al.*, 2006), siRNA (Liu and Gao, 2013), microRNA (Esposito *et al.*, 2014) chemotherapeutic drugs (Chen *et al.*, 2011), and metal oxides (Yigit *et al.*, 2008) with several characteristics attractive for their use in imaging and drug delivery probes.

As an example, Chen *et al.*, (2011) developed a smart functional nanostructure (SMN) composed of aptamer (scg8) and pegylated porous hollow magnetic nanoparticles (PHMNP) encapsulating doxorubicin (DOX), a commonly used anthracycline drug. This SMN worked as an imaging agent for MRI and was also shown to internalise by endocytosis into the target CEM (human T-cell lymphoblast) tumour cells (high expression of PTK7) resulting in inhibition of target cell proliferation. Hu *et al.*, (2012) developed an 86 base DNA aptamer (MA3) targeting MUC1 protein (overexpressed in adenocarcinoma and breast cancer cells) as a ligand for carrying DOX to cancer cells.

The aptamer-DOX conjugate was capable of carrying DOX to MUC1-positive tumour cells, while significant reduction in drug uptake and toxicity was observed in MUC1-negative cells.

Aptamers for intracellular targets have also been shown to regulate cellular functions causing cell death or proliferation, however, such aptamers have limited use due to low bioavailability and this becomes even more challenging when aptamers need to be delivered into cells *in vivo*. To characterise the biological effect of aptamers, Zamay *et al.*, (2013) attempted to inject the mixture of a natural polysaccharide product arabinogalactan (AG) as a carrier and aptamer NAS-24 intraperitoneally for 5 days into mice with adenocarcinoma. Coupled with AG, aptamer NAS-24 was delivered into the cytoplasm and caused apoptosis in Ehrlich ascites adenocarcinoma cells *in vitro* and *in vivo* leading to greater suppression of tumour growth compared to administration of free AG or the aptamer alone. Vimentin, which is over-expressed in tumour cells, was found to be the most probable protein target (Zamay *et al.*, 2013).

Micro-RNAs (mi-RNAs) play an important role in regulating multiple pathways integral to disease development and progression. There are however insufficient means for specific delivery of miRNAs to target tissues, therefore, researchers attempted to utilise aptamers as carriers for cell-targeted delivery by conjugating let-7g miRNA involved in tumour suppressor function with the established GL21.T aptamer that binds to and antagonises the oncogenic receptor tyrosine kinase Axl. Experiments performed in a xenograft model of lung adenocarcinoma showed reduced tumour growth using this multifunctional conjugate (Esposito *et al.*, 2014).

### 1.17 Aptamers and glioma

The use of aptamers in studying glioma is currently evolving. Research scientists have developed a series of aptamers via whole-cell SELEX that can bind to U87MG human glioma cell line. The GMT8 aptamer was shown to have highest binding affinity for U87MG cells compared to cell lines of other origin including MCF-7, CEM, RAMOS, HT29 and HBE-135 (Bayrac *et al.*, 2011). This GMT8 aptamer may be effective in improving drug accumulation in GBM cells enhancing tumour penetration for GBM targeting therapy (Gao *et al.*, 2012<sup>b</sup>).

Cerchia *et al.*, (2009) reported a differential cell-SELEX using target U87MG cells, yielding aptamers that selectively bind to the tumorigenic glioma cell lines (Cerchia *et al.*, 2009). The nuclease-resistant RNA aptamers were developed through the cell-SELEX process and the aptamers were capable of binding at high affinity to the target U87MG cells compared to the non-tumorigenic T98G cells. Likewise, aptamers such as GBM128 and GBM131 (Kang *et al.*, 2012) and apt 32 (Tan *et al.*, 2013) have been developed to target glioma cells. Chen *et al.*, (2008) demonstrated a new biosensing technique where a GBI-10 aptamer was conjugated to the quantum dot (QD) surface to construct a new kind of fluorescent QD labelled aptamer (QD-apt) nanoprobe. This nanoprobe was found to recognise the tenascin-C (overexpressed in glioma) on the surface of human glioma cells (Chen *et al.*, 2008).

Many chemotherapy regimes fail because of the limited blood-brain barrier (BBB) penetration and poor glioma targeting of the chemotherapeutics leading to unfavourable toxicity profiles (Serwer and James, 2012; Liu *et al.*, 2012). Effective treatment for brain glioma needs to conquer two barriers: the BBB and the brain-glioma barrier. Dual

targeting delivery systems were developed to conquer these two barriers and presented promising results (Gao *et al.*, 2012<sup>a</sup>; Yan *et al.*, 2012). These systems utilised AS1411 aptamer (glioma targeting ligand) and TGN peptide modified nanoparticles (AsTNPs, BBB targeting ligand) for precisely targeting glioma. It was demonstrated that the conjugation of both AS1411 and AsTNPs could effectively target brain glioma and improve survival of glioma bearing mice (Gao *et al.*, 2012<sup>a</sup>).

### **1.18 Scope for the present study**

Malignant glioma remains a challenging disease to treat. Despite recent advances in understanding the molecular heterogeneity of the disease and development in drug based multimodality therapy, customised therapy for GBM remains challenging (Wen and Kesari, 2008; Stupp *et al.*, 2010). Aptamers contribute a very promising and unique technology for the *in vitro* and *in vivo* imaging of live cells and tissues, with a potentially bright future in clinical diagnostics and therapeutics for malignant glioma. Considerable effort in developing novel aptamers against various cancers to improve specificity of drug delivery and targeting and to reduce adverse drug reactions due to cytotoxicity of healthy cells is on going. The use of aptamers for the treatment of glioma could be ideal, as not only could aptamers improve delivery of drugs across the BBB, but also healthy brain cells could be spared and maximal resection and targeted treatment of this diffuse cancer would hopefully minimise recurrence and increase life expectancy.

One of the major challenges for targeting drug delivery is to be able to direct the binding of the targeting aptamers to tumour cells instead of normal healthy cells. Aptamers (GL44 RNA, GL43 RNA and GL56 RNA) were adapted from Cerhcia *et al.*,

(2009) and modified by truncating the primer sequences from both ends. The aptamer sequences were studied for evaluation of their cellular localisation, uptake process, binding selectivity, and toxicity behaviour on glioma cells. From the literature, it was also identified there was a gap in the potential use of the aptamers for glioma diagnosis. To date, there have only been a few reports on the use of aptamers for the recognition of fixed clinical tissues (Li *et al.*, 2009; Zeng *et al.*, 2010; Han *et al.*, 2014; Lu *et al.*, 2014), with only one report for selectively recognising glioma tissues (Kang *et al.*, 2012). To explore the potential use of the aptamers for disease diagnosis, histochemistry was performed to screen the aptamers on various glioma, meningiomas and non-cancerous brain tissue sections

## **1.19 Aims and Objectives**

### **1.19.1 Main Aim**

The main aim of the study was to determine the potential of the aptamers to selectively target glioma cells and tissues.

### **1.19.2 Objectives**

- To evaluate the binding affinity of shortened aptamers (SA44 RNA, SA43 RNA and SA56 RNA) towards the target U87MG cells.
- To study the cellular localisation and binding selectivity of shortened aptamer sequences (SA44 RNA, SA43 RNA and SA56 RNA) for selective glioma targeting.
- To determine the difference in the binding affinity and selectivity of the selected DNA homolog sequences of the RNA aptamers towards the target glioma cells.
- To evaluate the internalisation and uptake process and toxicity behaviour of the

selected DNA aptamers on glioma cells and to compare with non-cancerous and non-glioma cells.

- To explore the potential use of the selected DNA aptamers for disease diagnosis by screening the aptamers on various pathological glioma, meningiomas and non-cancerous brain tissue sections.

## CHAPTER 2 MATERIALS AND METHODS

### 2.1 Cell lines

Cell culture experiments were carried out using different grades of human glioma cell lines including 1321N1 (malignant astrocytoma, sub-clone of grade IV U118MG, tumorigenic *in vivo*), U87MG (grade IV glioblastoma, tumorigenic *in vivo*), T98G (glioblastoma, non-tumorigenic *in vivo*) and non-cancerous foetal astrocytes SVGP12. The cell lines were obtained from the European Collection of Cell Cultures (ECACC, England, UK) and American Type Culture Collection (ATCC, Middlesex, UK). Two other non-glioma cell lines were also utilised for the study including MCF-7 (breast cancer) and T24 (bladder cancer), kindly donated by Royal Preston Hospital, UK and University of Leeds, UK respectively (Appendix 1).

#### 2.1.1 Materials

All media and supplements including DMEM, EMEM, FBS, L-glutamine, Sodium pyruvate solution, non-essential amino acid (NEAA) and penicillin/streptomycin (pen/strep) were obtained from scientific laboratory supplies (SLS), Lonza, Nottingham, UK (Appendix 2). Cell culture reagents including trypsin and DMSO were purchased from SLS, Lonza, Nottingham, UK. PBS and ethanol were purchased from Fisher scientific, Leicestershire, UK. All plasticware including tissue culture flasks, well plates with lids, centrifuge tubes, serological pipettes, unplugged pasteur pipettes, eppendorf tubes, syringes and membrane filters were purchased from Fisher scientific, Leicestershire, UK. Coverslips for confocal microscopy were purchased from Harvard apparatus, Kent, UK. All other chemicals were purchased from Sigma-Aldrich Ltd (Butterworth, UK) unless mentioned otherwise. Primary antibodies GFAP, VEGF and

beta actin were purchased from ABCAM, Cambridge, UK and secondary antibodies were purchased from Invitrogen, Paisley, UK.

### **2.1.2 Media and supplements**

The media and supplements that were used for each cell line were in accordance with the recommendations of ECACC and ATCC. The media preparations were carried out under aseptic conditions by the addition of required supplements as recommended by the suppliers (Appendix 1). Both DMEM and EMEM were supplied in 500 ml bottles, to which 50 ml of FBS and 5 ml of L-glutamine (200 mM) were aseptically added to achieve a final concentration of 10 % FBS and 2 mM L-glutamine, respectively. Sodium pyruvate (5 mM) and NEAA (5 mM) solution were added as supplements in EMEM media. The prepared media were stored at 4 °C for up to 4 weeks. All cell lines were routinely grown in 75 cm<sup>2</sup> or 25 cm<sup>2</sup> tissue culture flasks and maintained in a 37 °C humidified incubator supplied with 5 % CO<sub>2</sub>, 95 % O<sub>2</sub>. For all the experiments in the study, each of the cell lines were harvested when they reached 70-80 % confluence and were used between passages 5-25.

### **2.1.3 Routine cell culture and maintenance**

When the monolayer of cells reached 70-80 % confluency, cells were subcultured. The media was aspirated and the cells were washed with 0.1 M PBS, pH 7.4 to remove any traces of serum. The cells were detached by incubation with 0.25 % trypsin diluted in 0.1 M PBS, pH 7.4 for 2 minutes at 37 °C in a humidified incubator supplied with 5 % CO<sub>2</sub>, 95 % O<sub>2</sub>. After trypsin treatment, the flask was tapped gently and viewed under the inverted light microscope to ensure the detachment of cells. Media was then added to neutralise the trypsin reaction and mixed well to obtain homogenous and evenly distributed cell suspension. The cells were seeded at the ratio of 1:4 to each fresh flask.

## 2.2 Growth and biological characteristics of cells lines used in the study

### 2.2.1 Growth kinetics of cell lines

Growth curves were generated to evaluate the growth kinetics of the cultured cell lines such as their lag time, population doubling time (exponential phase) and saturation density. This assessment was done using the trypan blue exclusion method. Viable cells with intact membrane excluded trypan blue and cells stained blue were classified as dead cells. Cells at a density of  $6 \times 10^4$  cells/ml were then seeded into T25 flasks and incubated at 37 °C supplied with 5 % CO<sub>2</sub>, 95 % O<sub>2</sub>. At defined time points between 2 and 10 days, cells were trypsinised and resuspended in media prior to a 1:1 dilution of cell suspension and trypan blue. The number of viable cells were counted using a haemocytometer and light microscope (x10 magnification).

### 2.2.2 Data analysis

The average viable cell count per square (n=5 squares) was multiplied by the haemocytometer factor ( $10^4$ ) and the dilution factor (x 2) to give number of viable cells/mL. The experiment was performed in triplicate and cell count verses time was plotted to study growth kinetics. Accordingly, the lag, exponential and plateau phase of cell growth were determined. The growth curve also aided in determining the seeding density for each of the flat bottom 12, 24 and 96-well plate used on each day of the experiment using equation 1 stated below. The surface area and plating volume for each culture dish is given in table 2.1.

$$C_1 \times V_1 = C_2 \times V_2$$

Equation 1

Where:  $C_1$  = initial concentration of cells per flask;  $V_1$  = initial volume of medium with cells per flask;  $C_2$  = final concentration of cells needed per well; and  $V_2$  = final volume

of plating medium with cells per well.

**Table 2.1 Surface-area and plating volume in each culture dish used in the study**

Culture dish	Surface area per well (cm <sup>2</sup> )	Volume of plating medium (ml)
T25	25	5
T75	75	10
12-well plate	3.8	1
24-well plate	2	1
96-well plate	0.36	0.1

### 2.3 Characterisation of cell lines using Immunocytochemistry assay

The cell lines used in the study were characterised using specific markers to confirm the maintenance of the biological features of the cell lines. This was carried out using antibodies to Human leukocyte antigen (HLA; Santacruz biotechnology, Middlesex, UK) as a human cell marker, glial fibrillary acidic protein as a glial cell marker and vascular endothelial growth factor as a tumour cell marker. Primary antibodies were detected using Alexa fluor 488 secondary antibodies including goat anti-mouse and goat anti-rabbit. Isotype controls against each primary antibody such as mouse IgG and rabbit IgG were used to show that the labelling was specifically due to the primary antibody and to assess the level of background non-specific staining in the assay. Positive controls were included to confirm immunocytochemistry method by use of beta actin primary antibody and the goat anti-mouse secondary antibody. Detailed information regarding the primary and secondary antibodies with their working concentration diluted in 0.1 M PBS (pH 7.4) is mentioned in Table 2.2.

**Table 2.2 Antibodies used in the study and their working concentrations.**

<b>Protein</b>	<b>Antibody</b>	<b>Type</b>	<b>Final concentration</b>	<b>Isotype control</b>
<b>Beta Actin</b>	Primary	Mouse monoclonal to Beta actin	150 µg/ml	Mouse IgG
	Secondary	Goat anti- mouse IgG	20 µg/ml	
<b>GFAP</b>	Primary	Rabbit polyclonal to GFAP	4 µg/ml	Rabbit IgG
	Secondary	Goat anti- rabbit IgG	20 µg/ml	
<b>VEGF</b>	Primary	Mouse monoclonal to VEGF	10 µg/ml	Mouse IgG
	Secondary	Goat anti- mouse IgG	20 µg/ml	
<b>HLA</b>	Primary	Mouse monoclonal to HLA	4 µg/ml	Mouse IgG
	Secondary	Goat anti- mouse IgG	20 µg/ml	

### 2.3.1 Cell fixation

Glial cell lines (1321N1, U87MG, T98G and SVGP12), breast cancer cell line (MCF-7), and bladder cancer cell line (T24) were plated on 12 mm coverslips in a 24-well plate at a seeding density of  $3 \times 10^4$  cells/ well in media specified in section 2.1.2 and incubated in a 37 °C humidified incubator supplied with 5 % CO<sub>2</sub>, 95 % O<sub>2</sub> and were allowed to attach and grow for 36 hours. Post attachment, the cells were washed and fixed with 4 % paraformaldehyde (PFA; Sigma, UK) for 15 minutes at room temperature. The cells were rinsed three times with 0.1 M PBS (pH 7.4) for 10 minutes

followed by treatment with 0.01 % triton X-100 (Fisher Scientific, Leicestershire, UK) diluted in 0.1 M PBS (pH 7.4) for 5 minutes to permeabilise the cells. The cells were rinsed three times with 0.1 M PBS (pH 7.4) for 10 minutes and were ready for the staining experiments.

### **2.3.2 Cell staining and visualisation**

The fixed permeabilised cells were incubated with the 10 % blocking serum (goat serum) dissolved in 0.1 M PBS (pH 7.4) for 1 hour at room temperature. The cells were washed with 0.1 M PBS (pH 7.4) for 5 minutes and incubated with the primary antibodies for 1 hour at room temperature. The cells were then washed with 0.1 M PBS (pH 7.4) for 10 minutes and incubated with the respective secondary antibodies in the dark for 1 hour at room temperature. Post treatment with primary and secondary antibody, the cells were washed three times with 0.1 M PBS, pH 7.4 for 10 minutes and counterstained with VECTASHIELD<sup>®</sup> mounting medium with propidium iodide (PI) (1.5 µg/ml) (Vector laboratories, Peterborough, UK). The cells were visualised under 40 x using a Zeiss LSM510 confocal microscope (Zeiss LSM, Germany) equipped with appropriate filters sets for the detection of expression of various markers using FITC signal (excitation: 488 nm; emission: band pass filter 505-530 nm; detector gain: 897; amplifier offset: -0.06; amplifier gain: 1). The experiment was performed on three independent occasions and was analysed using in-built Zeiss LSM image browser.

### **2.4 Oligonucleotide synthesis and labelling**

Aptamers (oligonucleotides) were conjugated at the 5' end with Cy3 for confocal microscopy (section 2.6) and flow cytometry analysis (sections 2.5 and 2.7) and with biotin for histochemistry (sections 2.9 and 2.10) by Integrated DNA technologies (IDT, Glasgow, UK). Primary sequences of the single stranded RNA aptamers and their DNA

homologs are given in the table 2.3. Biotin labelled oligonucleotides were synthesised in desalted form, whereas the Cy3 labelled oligonucleotides were HPLC purified.

**Table 2.3 Primary sequences of aptamers used in the study.**

Test aptamer	Sequence 5' to 3'	Sugar	5' label	Reference
SA44 RNA	ACG UUA CUC UUG CAA CAC CCA AAC UUU AAU AGC CUC UUA UAG UUC	Ribose	Cy3	Cerchia <i>et al.</i> , 2009
SA43 RNA	ACG UUA CUC UUG CAA CAC AAA CUU UAA UAG CCU CUU AUA GUU C	Ribose	Cy3	Cerchia <i>et al.</i> , 2009
SA56 RNA	UGA UUU UGC AGC ACU UCU UGU UAU CUU AAC GAA CUG UUG AUG A	Ribose	Cy3	Cerchia <i>et al.</i> , 2009
SA44 DNA	ACG TTA CTC TTG CAA CAC CCA AAC TTT AAT AGC CTC TTA TAG TTC	Deoxyribose	Cy3/ Biotin	Cerchia <i>et al.</i> , 2009
SA43 DNA	ACG TTA CTC TTG CAA CAC AAA CTT TAA TAG CCT CTT ATA GTT C	Deoxyribose	Cy3/ Biotin	Cerchia <i>et al.</i> , 2009
SA56 DNA	TGA TTT TGC AGC ACT TCT TGT TAT CTT AAC GAA CTG TTG ATG A	Deoxyribose	Biotin	Cerchia <i>et al.</i> , 2009
SAN1 DNA	GGA AAA TTA TAC CCT CCA TTA AAT CCA CCA TTA CCA CAC CCU TTA	Deoxyribose	Cy3/ Biotin	In-house
SAN2 DNA	CCG TTA ATT AGG CCC TTA AAT GGC ATA AAA TTT GAA AGG GAA T	Deoxyribose	Cy3/ Biotin	In-house

## 2.5 Determining the binding affinity of the aptamers to the target U87MG cells by flow cytometry

Live U87MG cells were seeded in 12-well plate at a seeding density of  $4 \times 10^4$  cells/well in complete media specified in section 2.1.2 and were allowed to attach and grow for 36 hours at 37 °C in a 5 % CO<sub>2</sub> humidified incubator. The binding affinity of the test aptamers SA44, SA43 and SA56 was determined by incubating live adherent U87MG cells with varying concentrations (0.5 nM – 200 nM) of the Cy3 labelled aptamers in media for 90 mins at 37 °C in a 5 % CO<sub>2</sub> humidified incubator. This experiment also determined the effect of different concentrations of the selected aptamers on cells and

also aided in selecting a standard optimal concentration of each aptamer for determining their uptake on other cell lines. Untreated cells were incubated with complete growth medium alone. Post incubation, the cells were washed three times with 0.1 M PBS (pH 7.4) and detached using 0.25 % trypsin for 2 minutes. The suspended cells were transferred to an eppendorf tube and centrifuged at 224 x g for 5 minutes to remove the supernatant that contained unbound aptamer. The cells were then resuspended in PBS (0.26 ml, ideal volume for measuring at least 10000 events) for flow cytometry analysis. Fluorescence analysis was performed on BD FACSAria flow cytometer (BD Biosciences, San Jose, CA, USA) using phycoerythrin (PE) was detected at an excitation at 488 nm and emission at 578 nm where 10,000 events were collected for each sample. The mean fluorescent intensity (MFI) was determined using in-built FACS Diva version 4.1.2 software (BD biosciences). All the experiments for the binding assay were performed at least three times.

For calculation of the equilibrium dissociation constant ( $K_d$ ) of the aptamers and U87MG cell interaction, the average MFI value of cells was plotted against the fluorescently labelled aptamer concentration and a curve fitted using non-linear regression analysis (Graphpad Prism, Graphpad software, Inc, La Jolla, USA). Accordingly, the  $K_d$  value was obtained for each aptamer using the one site-specific binding equation (Equation 2) (Sefah *et al.*, 2010).

$$\text{Aptamer}_{\text{bound}} = (B_{\text{max}} \times C_{\text{aptamer}}) \div (K_d + C_{\text{aptamer}})$$

Equation 2

Where:  $B_{\text{max}}$  = maximum binding sites;  $C_{\text{aptamer}}$  = concentration of aptamer;  $K_d$  = dissociation constant (binding affinity).

## **2.6 Cellular uptake and localisation of aptamers by confocal microscopy**

All Cy3 labelled RNA and DNA aptamers were screened on various growing cell lines and confocal imaging was used to obtain three dimensional (3D) images and z-stacks to determine whether aptamer uptake or binding was selective and where the aptamer localised. The two steps involved were (a) determining the optimum standard concentration of each Cy3-labelled aptamer using the target U87MG cell line and (b) using the standard concentration of each aptamer on 1321N1, U87MG, SVGP12, T98G, T24 and MCF-7 cell lines to determine their binding selectivity.

Glioma cells (1321N1, U87MG, T98G), non-cancerous glial cells (SVGP12), breast cancer cells (MCF-7), and bladder cancer cells (T24) were plated on coverslips (12 mm) in 24 well plates at a seeding density of  $3 \times 10^4$  cells/ well in media specified in section 2.1.2 and allowed to grow for 36 hours. Post attachment, the following experiments (sections 2.6.1 – 2.6.2) were performed to study the uptake of aptamers by the cells.

### **2.6.1 Determining the optimum standard concentration for each Cy3-labelled aptamer using the target U87MG cells**

Live U87MG cells were incubated with varying concentrations (5 nM, 20 nM, 40 nM, 80 nM and 100 nM) of the Cy3 labelled aptamers SA44, SA43 and SA56 in media as previously specified in section 2.1.2 for 90 minutes at 37 °C in a 5 % CO<sub>2</sub> humidified incubator. Untreated cells were incubated with complete growth medium alone. Post incubation, the cells were washed three times with 0.1 M PBS (pH 7.4) to remove any unbound aptamer. Cells were fixed with 4 % PFA for 15 minutes at room temperature. After fixing, the cells were washed thrice with 0.1 M PBS, pH 7.4 and counter-stained using VECTASHIELD® mounting medium with DAPI (1.5 µg/ml) (Vector

laboratories, Peterborough, UK) in the dark to stain the nucleus. The cells were then visualised under 40 X magnification using a Zeiss LSM510 confocal microscope (Zeiss LSM, Germany) equipped with appropriate filter sets for the detection of Cy3 dye fluorescence (Excitation: 543; emission: long pass filter 560 or band pass filter 560-615; amplifier gain: 1; detector gain: 927; amplifier offset: - 0.06).

The images of aptamer uptake to the cells were acquired under 40 X oil immersion objective in z- stack mode with independent slice thickness determined by the software. 3D reconstruction with 64 projections of various z-stacks was then performed using Zeiss LSM image browser software. For all the staining experiments, cellular localisation was further confirmed by overlaying the fluorescence images (single plane image from the middle of Z-stack) with the nuclear DAPI stain. The experiments were performed at least three independent times and the fluorescence images reported in the study are representative of at least three captured images per experiment.

### **2.6.2 Assessing the uptake of the aptamers on live glial and non-glial cells**

Live 1321N1, U87MG, T98G, SVGP12, MCF-7, and T24 cells were incubated with suitable standard concentrations of the selected Cy3 labelled aptamers SA44, SA43, SA56 along with random sequenced aptamers in growth medium supplemented with FBS for 90 minutes at 37 °C in a 5 % CO<sub>2</sub> humidified incubator. Untreated cells were incubated with complete growth medium alone. Post incubation, the cells were washed three times with 0.1 M PBS (pH 7.4) to remove the unbound aptamer followed by the same treatment as mentioned in the section 2.6.1. The experiments were performed in triplicate and were analysed using same settings on Zeiss LSM image browser as mentioned in the section 2.6.1.

## **2.7 Cellular uptake and internalisation of aptamers by flow cytometry**

Aptamer uptake and internalisation on live cells was also assessed quantitatively by flow cytometry. Glioma cells (1321N1, U87MG, T98G), non-cancerous glial cells (SVGP12), breast cancer cells (MCF-7), and bladder cancer cells (T24) were seeded in 12-well plate at a seeding density of  $4 \times 10^4$  cells/ well in complete media specified in section 2.1.2 and were allowed to attach and grow for 36 hours at 37 °C in a 5 % CO<sub>2</sub> humidified incubator. Post attachment, the following experiments (sections 2.7.1- 2.7.3) were performed to analyse the aptamer uptake and internalisation by the live cells.

### **2.7.1 Assessing the aptamer uptake on live glial and non-glial cells**

Live 1321N1, U87MG, T98G, SVGP12, MCF-7, and T24 cells were used for the study. The binding selectivity of SA44, SA43, SA56 along with random sequence aptamers was determined by incubating the cells with suitable standard concentration of the aptamers at 37 °C (5 % CO<sub>2</sub>) for 90 minutes. Untreated cells were incubated with complete growth medium alone. The cells were washed with 0.1 M PBS (pH 7.4) followed by the same protocol for flow cytometry analysis as mentioned in the section 2.5. The mean fluorescent intensity (MFI) was determined using FACS Diva version 4.12 software. The binding assay experiments were analysed using windows multiple document interface (Win MDI) software (version 2.9) to determine the uptake of each aptamer on various cell types. The software creates single or dual-parameter histograms as frequency distribution based on the mean fluorescent intensity (MFI) for each sample. Evident peak shift compared to cells with no aptamers corresponded to an increase in the fluorescent signal which indicated increase in uptake and selectivity of the aptamers on the cells.

### **2.7.1.1 Data analysis**

To determine the binding selectivity and affinity for each aptamer on all cell lines, statistical analysis was performed on the MFI values using IBM SPSS statistics v20 software (IBM SPSS Statistics for Windows, Version 20.0, Armonk, NY). All MFI values of the untreated cells obtained from FACS Diva software were initially subtracted from the MFI values obtained from aptamer treated cells. Thereafter, the MFI of the random aptamer was subtracted from the MFI of the lead aptamers. A Shapiro-Wilk's test ( $p > 0.05$ ) (Shapiro & Wilk, 1965; Razali & Wah, 2011), an inspection of skewness and kurtosis measures and standard errors, and a visual inspection of their histograms, normal Q-Q plots and box plots was performed on the average MFI values from three individual experiments of each aptamer to test the normal distribution of the data. Statistical significance of differences in the means of average MFI values of each shortened aptamer between individual cell groups was then determined by using a one-way ANOVA (Ruxton and Beauchamp, 2008) followed by post hoc Bonferroni test (Ruxton and Beauchamp, 2008). The significant statistical difference was defined according to  $p$  value less than 0.05.

### **2.7.2 Effect of temperature on aptamer binding to the cells**

Live 1321N1, U87MG, and SVGP12 cells were used for the study. Cells were separated into two groups for the experiments and incubated with each aptamer (100 nM) at 4 °C and 37 °C simultaneously for 90 minutes. After incubation, cells were washed thrice with 0.1 M PBS, pH 7.4 following the same protocol for flow cytometry analysis in the section 2.7.1. The binding assay experiments were repeated at least three times and were analysed using WinMDI 2.9 software as mentioned in the section 2.7.1. Statistical significance of differences in the means of average MFI values of each shortened

aptamer between individual cell groups treated at 4 °C and 37 °C was then determined by using two-way ANOVA followed by Bonferroni post-hoc test (Ruxton and Beauchamp, 2008).

### **2.7.3 Effect of protease trypsin on aptamer binding to the cells**

To determine whether the entry of the lead aptamers was mediated through the cell surface receptors or through a different mechanism other than receptor-mediated pathway, cells were treated with trypsin protease before the aptamer treatment. The experiment also provided an idea about the nature of the aptamer target, whether it was mainly membrane bound or was intercellular. Live 1321N1, U87MG, and SVGP12 cells were used for the study and were separated into two groups for the experiments. One group was treated initially with aptamer and then trypsinised to remove any cell surface bound aptamers (similar experiment as mentioned in 2.7.1 and 2.7.2). Second group was initially incubated with 0.25 % trypsin at 37 °C (5 % CO<sub>2</sub>) for 10 minutes to remove the cell surface receptors. Media with FBS was then added to inhibit the protease activity. The cell suspension was then transferred to an eppendorf tube and centrifuged (MSE Microcentaur, DJB labcare) at 224 x g for 5 minutes. Each cell pellet was then resuspended with 500 µl complete growth media containing 100 nM aptamer and incubated for 90 minutes at 37 °C. Post treatment, the cells were washed and centrifuged at 224 x g three times to remove any unbound aptamer and taken for flow cytometry analysis. The binding assay experiments were repeated at least three times and were analysed using WinMDI 2.9 software (Section 2.7.1). Statistical significance of differences in the means of average MFI values between individual cell groups treated with aptamer before and after trypsin treatment was then determined by using two-way ANOVA followed by Bonferroni post-hoc test (Ruxton and Beauchamp,

2008).

## **2.8 Effect of aptamers on cell viability**

The effect of aptamers on cell viability was tested using the Presto blue assay. Presto blue reagent is a resazurin based solution that functions as cell viability indicator by using the reducing power of living cells to quantitatively measure the proliferation of cells (Boncler *et al.*, 2013). Briefly,  $2 \times 10^3$  cells/ well of 1321N1, U87MG, and SVGP12 cells were seeded in 96-well plates and incubated at 37 °C (5 % CO<sub>2</sub>) for 24 h. Cells were treated with four different concentrations (20 nM, 100 nM, 500 nM and 1000 nM) of biotinylated DNA aptamers SA44 and SA43 for 24, 48 and 72 hours. Cisplatin diluted in media (10 µM) was used as a positive control. To evaluate the cell viability following 24, 48 and 72 hours treatment, 10 µl of presto blue was added to each well and incubated for 1 hour at 37 °C. The assay was read using a TECAN genios pro multifunctional microplate reader (Tecan, Austria; software version 4.53) with excitation and emission wavelength of 535 nm and 612 nm respectively. Cell viability was expressed in percentage relative to control untreated cells grown in media.

## **2.9 Aptamer binding on fixed cells**

To determine the ability of the aptamers to bind to the targets of fixed cells, cells were treated with biotin labelled DNA aptamers post fixation.

### **2.9.1 Fixation and permeabilisation**

1321N1 (glioma cells) and SVGP12 (non-cancerous cells) were seeded on coverslips in 24 well plates at a seeding density of  $3 \times 10^4$  cells/ well in media previously detailed in section 2.1.2, and allowed to grow for 36 hours. Post attachment, the cells were washed three times and incubated with 4 % PFA for 15 minutes at room temperature. The cells

were then washed with 0.1 M PBS (pH 7.4) and permeabilised using 0.1 % Triton X-100 (diluted in PBS) for 5 minutes. Post permeabilisation, the cells were washed three times with 0.1 M PBS (pH 7.4) and incubated with 10 % biotin-blocking solution (Vector laboratories, UK) for 30 minutes at room temperature to mask the endogenous biotin binding.

### **2.9.2 Aptamer labelling and imaging**

The cells were then incubated with 100 nM concentration of each biotin labelled DNA aptamers for 60 minutes at room temperature. The cells were washed three times with 0.1 M PBS, pH 7.4 and incubated with VECTASTAIN<sup>®</sup> avidin biotin complex (ABC) reagent (Vector laboratories, Peterborough, UK) for 30 minutes at room temperature. Untreated cells were incubated with 0.1 M PBS (pH 7.4) alone followed by ABC reagent treatment. After three washes with 0.1 M PBS, pH 7.4, the cells were treated with 250  $\mu$ l of 3,3-diaminobenzidine (DAB) peroxidase substrate solution (Vector laboratories, Peterborough, UK) at room temperature for 5 minutes. Counterstaining of the cell nuclei was performed with 250  $\mu$ l Mayer's haematoxylin solution for 5 minutes. The cells were then rinsed with distilled water and dehydrated through an increasing series of ethanol washes (70 %, 90 % and 100 % twice for 2 minutes each). The coverslips were then placed into histoclear (Fisher scientific, UK) for 1 min and then mounted in DPX (distrene dibutyl- phatalate xylene) mounting medium. The treated cells were then examined using a Nikon light microscope under 40 X magnification equipped with digital eclipse camera system and screen, and analysed for their binding selectivity on fixed cells.

### **2.10 Aptamer binding selectivity to patient tissue samples**

The study also involved screening of the biotin labelled DNA aptamers SA44, SA43,

SA56, and random aptamer on patient serial tissue sections from the Brain Tumour North West (BTNW) bank. Different grades of glioma including grade I, grade II, grade III, grade IV glioblastoma, meningioma (grade II, grade III), and non-cancerous brain tissues were included in the study. The demographic details including the diagnosis and the tumour type for all the different patients used in the study are mentioned in appendix 4. Ethical approval and informed consent was obtained by the ethics committee for the use of above mentioned patients tissue sections.

### **2.10.1 Dewaxing of paraffin embedded sections**

Each excised tumour tissue sample and non-tumour portion were formalin-fixed and serially sectioned (4  $\mu\text{m}$ ) by pathologists Katherine Ashton and Dr Tim Dawson from the Royal Preston hospital. These paraffin-embedded tissue slides were deparaffinised with two changes of histoclear (Fisher scientific, UK), 15 minutes each and rehydrated through graded ethanol washes (100 %, 90 % and 70 %), 5 minutes each. Deparaffinised tissue slides were then rinsed in distilled water.

### **2.10.2 Antigen retrieval**

Antigen retrieval involved immersing the slides in 0.01 M citrate buffer at 97 °C for 20 minutes. The sections were allowed to stand at room temperature for 30 minutes to cool. The sections were rinsed in 0.1 M PBS, pH 7.4 twice for 2 minutes each.

### **2.10.3 Aptamer labelling and imaging**

To mask endogenous biotin binding, sections were treated with biotin-blocking solution (Vector laboratories, UK) for 30 minutes and then washed three times with 0.1 M PBS, pH 7.4. The tissue slides were incubated with 100 nM biotin labelled DNA aptamers for 60 minutes at room temperature. The slides were washed three times with 0.1 M PBS,

pH 7.4 for 5 minutes. The slides were then incubated with VECTASTAIN<sup>®</sup> ABC reagent for 30 minutes at room temperature. After three washes with 0.1 M PBS, pH 7.4, the tissues sections were treated with 200  $\mu$ l of DAB peroxidase substrate solution for 5 mins at room temperature for colour development. Counterstaining of the cell nuclei in tissue sections was performed with Mayer's haematoxylin solution for 5 minutes. The slides were then rinsed with distilled water and dehydrated through increasing series of ethanol washes (70 %, 90 % and 100 % two times for 2 minutes each). The sections were then placed into xylene for 5 minutes and then mounted in DPX mounting medium (Sigma, UK). The sections were then imaged and captured using bright field microscopy using Nikon microscope equipped with digital eclipse camera system (Nikon, UK) and analysed for the binding selectivity using a protocol mentioned below (Sections 2.10.4 and 2.10.5).

#### **2.10.4 Schematic explanation of the protocol for immuno-scoring**

A defined protocol was applied to analyse and count the cells stained with each DNA aptamer in the tissue sections. This protocol is based on that applied by Leake *et al.*, (2000) and is NEQAS approved for the scoring of BRCA1 positive cells in breast tumour tissue sections. The aptamers showed distinctive and remarkable staining in the tissue sections, which assisted in scoring them according to their staining intensity (Figure 2.1).

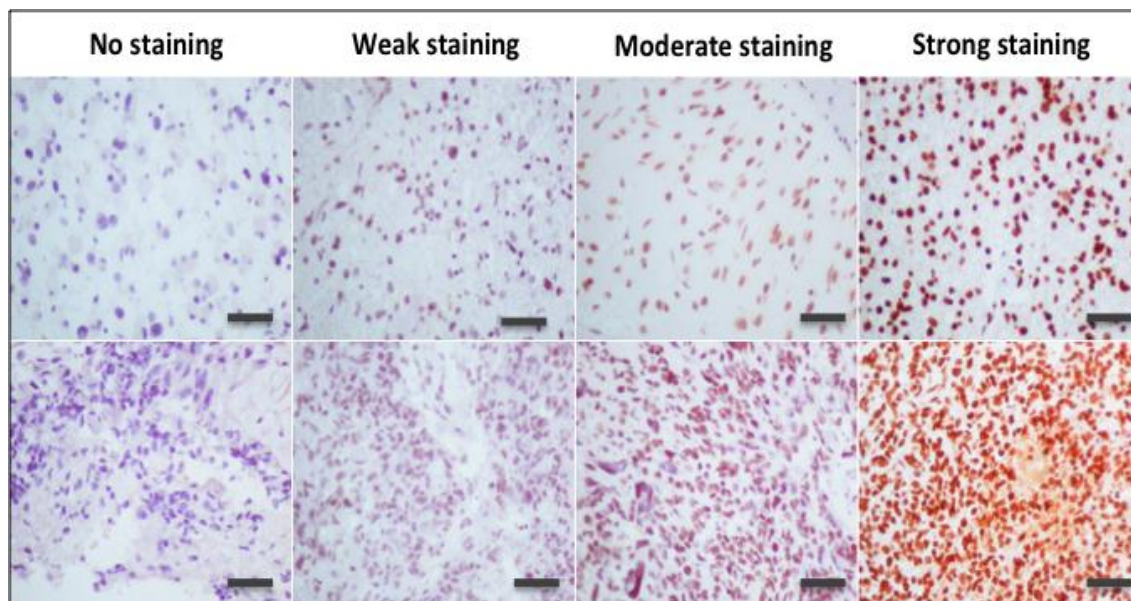


**Figure 2.1** Representative images from tumour tissues showing differential staining intensities with the studied DNA aptamers. All scale bars, 200  $\mu\text{m}$ .

A blind study without knowing the grades of tissues was then performed to be unbiased and therefore more accurate in analysing the binding results. The binding of the aptamers on tissue sections was identified by carefully examining each tissue section under 10 X and 40 X magnification. For accuracy, 10 different fields were selected per tissue section and counted. Initially, an intensity score was assigned, which represented the average staining intensity score of positive stained cells (Table 2.4). Thereafter, proportion score intensity was assigned, which represented the estimated proportion of positive stained tumour cells. The intensity and the proportion scores were then added together to obtain a total score, which ranged from 0 to 8. A total score of 3 or below was considered as negligible binding.

**Table 2.4 Suggested scoring system** (Leake *et al.*, 2000).

Score for staining intensity	Score for proportion intensity
<b>0= no staining</b>	0= no staining
<b>1= weak staining</b>	1= <1% cell staining
<b>2= intermediate/ moderate staining</b>	2= 1-10% cell staining
<b>3= intense/ strong staining</b>	3= 11-33% cell staining
	4= 34-66% cell staining
	5= 67-100% cell staining

### 2.10.5 Data analysis

To identify a clinically meaningful cut point for defining positive binding of aptamers to the cells on tissue sections, the results were examined on a scatter plot. A statistical test using one-way ANOVA followed by Bonfferoni post hoc test was applied to compare the overall mean binding scores for each aptamer on all glioma and meningioma tissues versus the non-cancerous tissues. Comparison of binding selectivity between the control (non-cancerous) group and tumour groups (grade I, grade II, grade III, grade IV, and meningioma) were further analysed by Fishers' exact test (Graph Pad Prism software, La Jolla, USA) using a 2 x 2 contingency table. A value of  $p < 0.05$  was considered to indicate a statistically significant differences of each aptamer between the non-cancerous and cancerous group. Morphological characteristics and cell type selectivity for each aptamer within each tissue sections was also analysed carefully using 40 X objective lens.

## **CHAPTER 3 GROWTH AND BIOLOGICAL CHARACTERISTICS OF CELL CULTURE MODELS**

### **3.1 Introduction**

Characterisation of the glioma cell lines is critical for the evidence of astrocytic differentiation and has been one of the most common parameters used for preliminary assessment in cell culture. Extensive cell culture may lead to problems such as cross-contamination in which a contaminant is another cell line or a micro-organism without handler's knowledge (Capes-Davis *et al.*, 2010). It was therefore essential to verify that the represented cell lines selected have a well-defined origin and growth. Immunological approaches have been one of the best methods for the evidence of the biological characteristics of the cell lines (Higgins *et al.*, 2010; Kamphuis *et al.*, 2012). This chapter aimed to determine the growth rate for each cell line to understand the growth pattern and ascertain appropriate seeding density for the downstream experiments. In addition, the chapter aimed to confirm the biological characteristics (glial and human origin, and cancerous) of each cell line using immunocytochemistry.

### **3.2 Results**

#### **3.2.1 Growth curves**

Growth curves were generated to evaluate the growth kinetics of the cultured glial (1321N1, U87MG, SVGP12 and T98G) and non-glial (T24 and MCF-7) cell lines used in the study. This assessment was done using trypan blue exclusion microscopy (Section 2.2). From the results shown in figure 3.1, it was evident that the 1321N1, T98G, T24 and MCF-7 cells proliferate more rapidly than SVGP12 and U87MG cells. All the cell lines exhibited a lag phase between days 1 and 2, an exponential growth

phase between the 3<sup>rd</sup> and the 7<sup>th</sup> day and reached the plateau or decline phase thereafter. The population doubling time was 36 - 48 hours for all the cell lines.

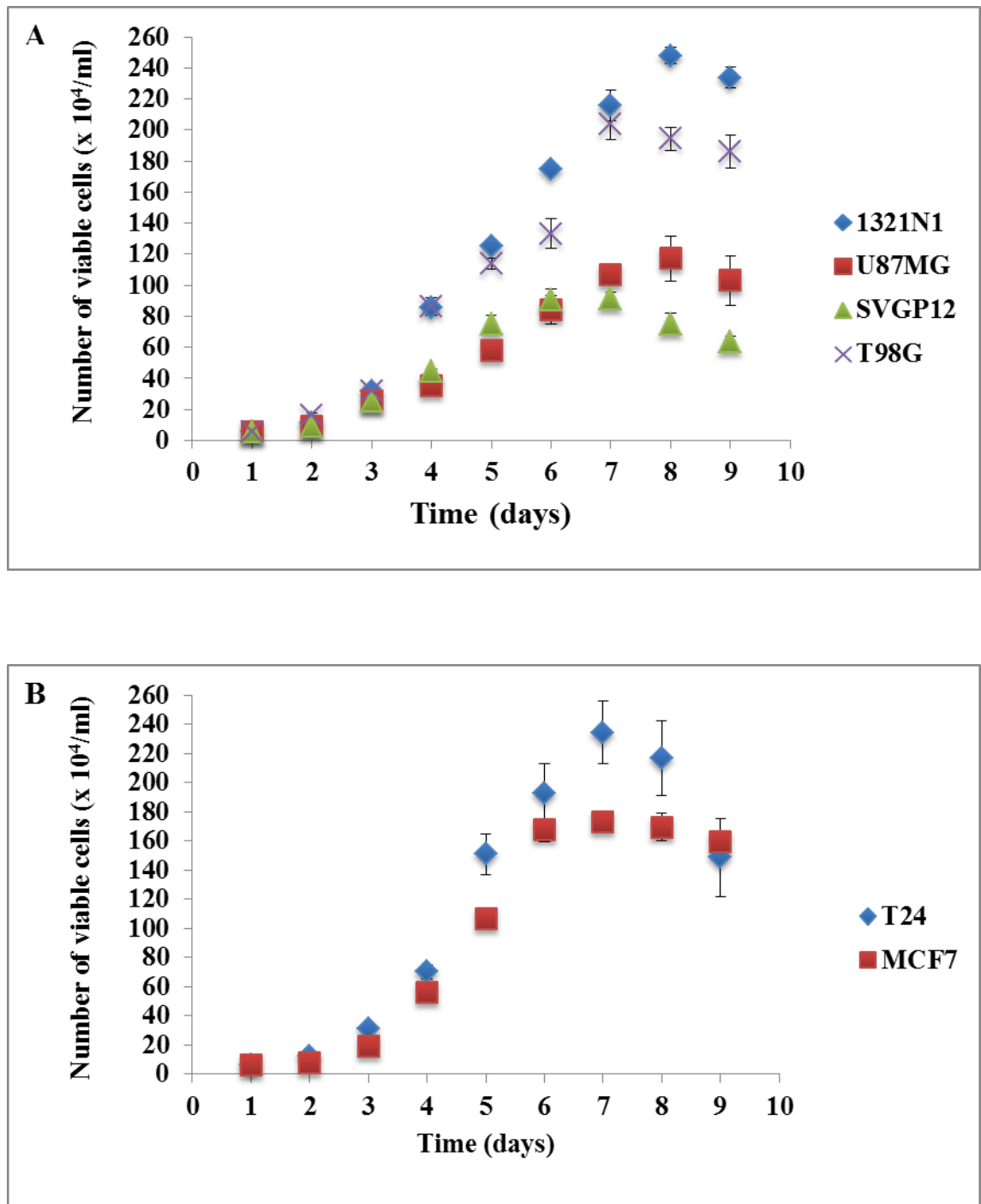


**Figure 3.1** The growth kinetics of cultured glial and non-glial cell lines used for the study. **A** Growth curve for glial cells 1321N1, U87MG, SVGP12, and T98G. **B** Growth curve for non-glial cells T24 and MCF-7. Each time point represents the average value of triplicates from three independent experiments and error bars represent standard error mean (S.E.M).

### **3.2.2 Immuno-cytochemical characterisation of various cell lines using specific markers**

1321N1, U87MG, T98G (glioma), SVGP12 (non-cancerous), T24 (bladder cancer), and MCF-7 (breast cancer) cells were characterised using a panel of antibodies raised against HLA-I, GFAP and VEGF to confirm the maintenance of biological features (Section 2.3). The antigens chosen to define the origin of the cell lines used in the study here were HLA-I to ensure the cells were human origin, GFAP to confirm glial origin for glial cells, and VEGF to confirm the cancerous nature of the tumour cells. C2C12 (mouse myoblast cell line, ATCC, UK) was used as a negative control to ensure the cells used for the study were human origin and was characterised using HLA-I antibody.

Immunocytochemical analysis of GFAP expression on the cell lines demonstrated that 1321N1, U87MG, SVGP12 and T98G cells were positive. Expression of GFAP was localised in the cytoplasm. In contrast, T24 and MCF-7 cells, and all isotype controls did not show staining above background levels (Figures 3.2 - 3.4). Similarly, all cell lines except C2C12 showed positive expression of human cell marker HLA-I. Moreover, all cancerous cells including glial and non-glial expressed positive staining for VEGF marker, except for weak to negligible staining on non-cancerous SVGP12 cells.

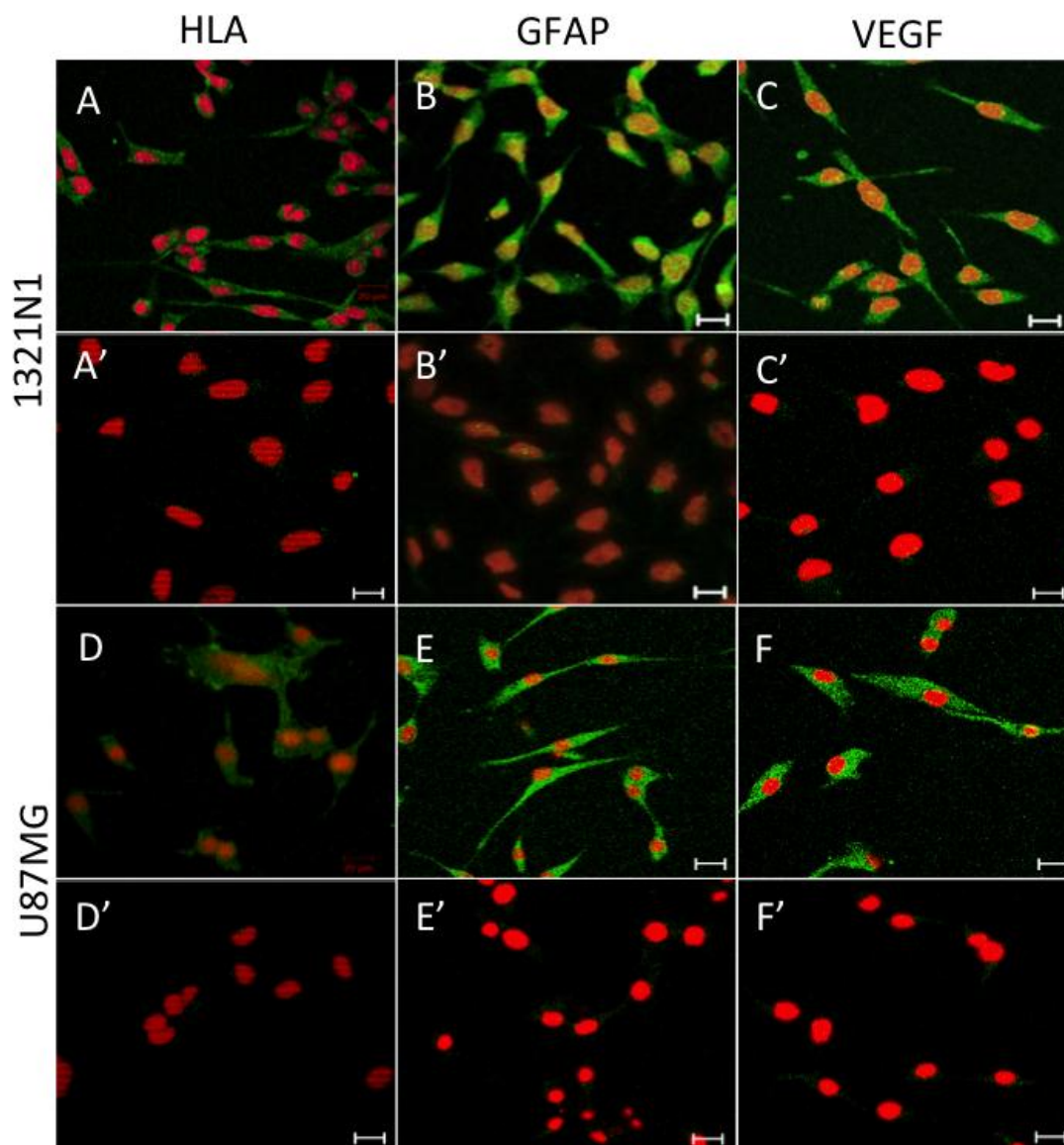


**Figure 3.2** Expression of HLA-I, GFAP and VEGF antigens (green) in cultured 1321N1 and U87MG cells. A, B, and C represent expression of HLA-I, GFAP and VEGF counterstained with PI (nuclear stain) respectively, in 1321N1 cells. A', B', and C' represent isotype controls against HLA-I, GFAP and VEGF counterstained with PI respectively, in 1321N1 cells. Similarly, D, E, and F represent expression of HLA-I, GFAP and VEGF counterstained with PI respectively, in U87MG cells. D', E', and F' represent isotype controls against HLA-I, GFAP and VEGF counterstained with PI respectively, in U87MG cells. Scale bar = 20  $\mu$ m.

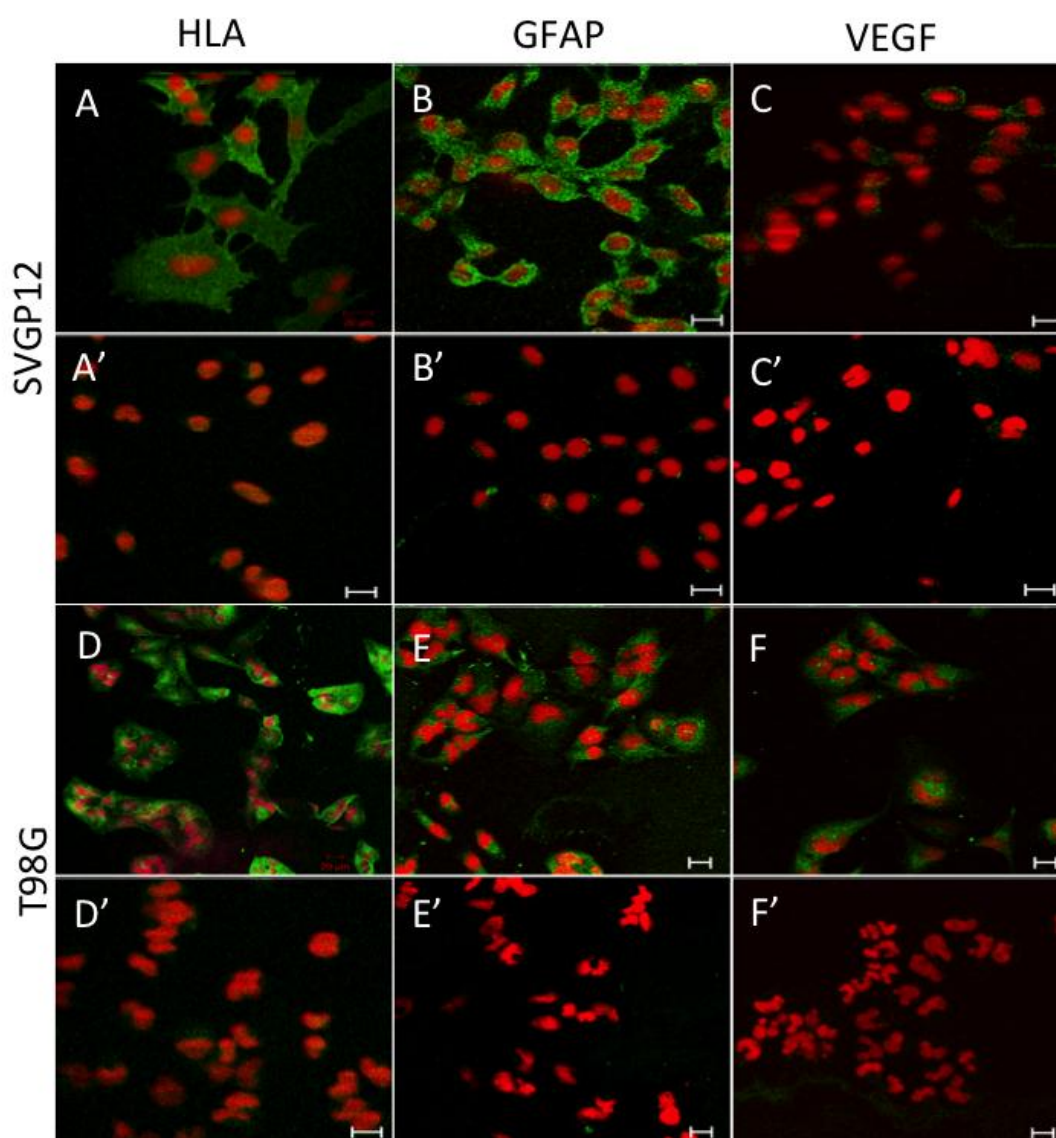


**Figure 3.3** Expression of HLA-I, GFAP and VEGF antigens (green) in cultured SVGP12 and T98G cells. A, B, and C represent positive expression of HLA-I, GFAP and negligible expression of VEGF counterstained with PI (nuclear stain) respectively, in SVGP12 cells. A', B', and C' represent isotype controls against HLA-I, GFAP and VEGF counterstained with PI respectively, in SVGP12 cells. Similarly, D, E, and F represent expression of HLA-I, GFAP and VEGF counterstained with PI respectively, in T98G cells. D', E', and F' represent isotype controls against HLA-I, GFAP and VEGF counterstained with PI respectively, in T98G cells. Scale bar = 20  $\mu$ m.

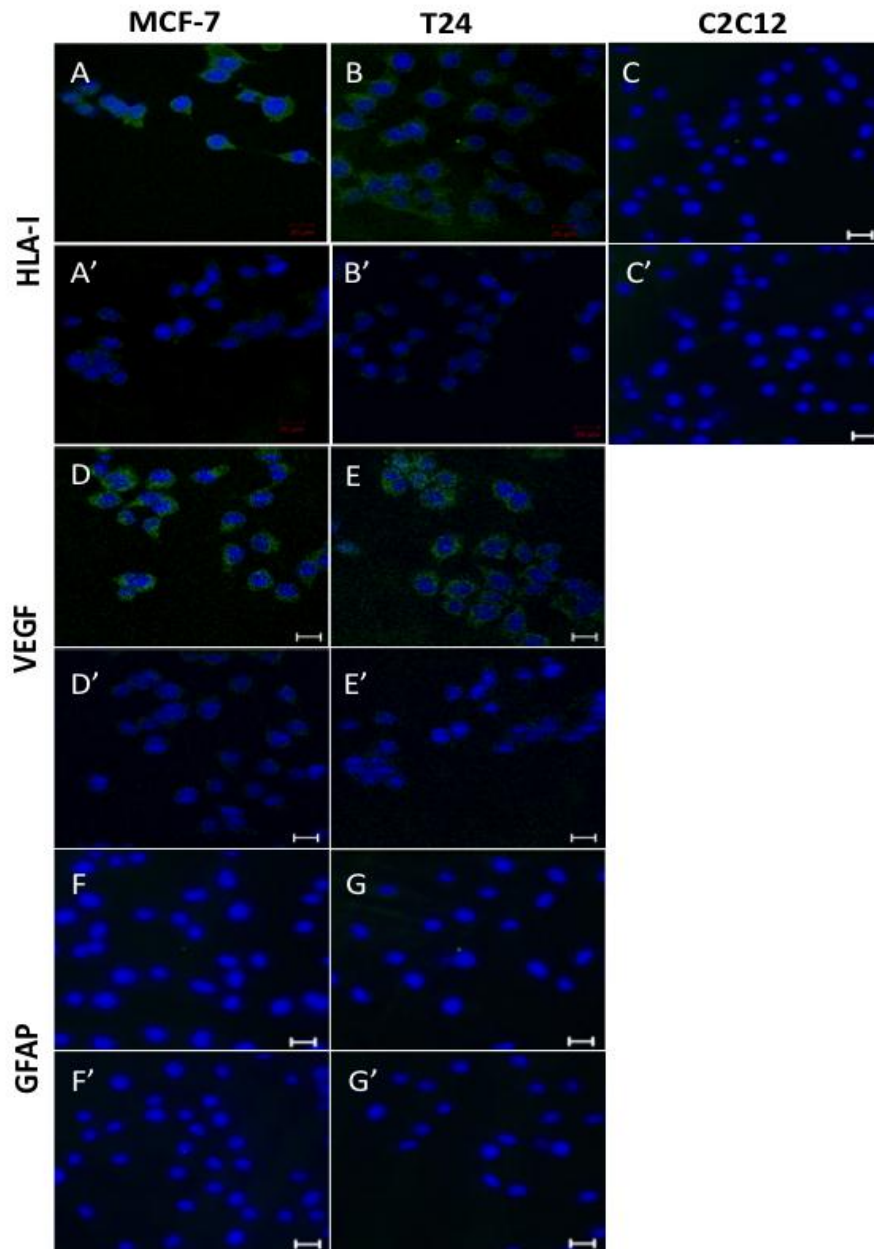


**Figure 3.4** Expression of HLA, VEGF, and GFAP antigens (green) in cultured MCF-7, T24, and C2C12 cells. **A** and **B** represent positive expression of HLA-I in MCF-7 and T24, respectively. **C** represents negligible expression of HLA counterstained with DAPI (nuclear stain) in C2C12 cells. **A'**, **B'** and **C'** represent isotype controls against HLA-I counterstained with PI respectively, in MCF-7, T24 and C2C12 cells, respectively. **D** and **E** represent positive expression of VEGF counterstained with PI respectively, in MCF-7 and T24 cells, respectively. **D'** and **E'** represent isotype controls against VEGF counterstained with PI respectively, in MCF-7 and T24 cells, respectively. **F** and **G** represent negligible expression of GFAP counterstained with PI respectively, in MCF-7 and T24 cells, respectively. **F'** and **G'** represent isotype controls against GFAP counterstained with PI respectively, in MCF-7 and T24 cells, respectively. Scale bar = 20  $\mu$ m.

### 3.3 Discussion

High heterogeneity in phenotypic and growth characteristics has been well identified between different glioma cell lines developing the need to study and confirm both the growth rate and biological characteristics of the individual cell line before screening and testing of various novel molecules (Mullins *et al.*, 2013). The characterisation of the glial and non-glial cell lines consisted of evaluating the proliferative capacity of cells using growth curve analysis and identification of biological features of the cell lines using glial, human and tumour specific markers.

Growth kinetic studies using trypan blue exclusion microscopy were useful in determining the cell density along with growth characteristics such as lag time, population doubling time (exponential phase) and saturation density of a cell line (Mather and Roberts, 1998; Li *et al.*, 2010; Assanga *et al.*, 2013). This assay also distinguished between viable and nonviable cells, based on the ability of cells with an intact plasma membrane (live cells) to exclude trypan blue while those cells that stained blue had impaired membrane integrity and were classified as non-viable cells, possibly undergoing necrosis or possible advanced apoptosis (Li *et al.*, 2010<sup>a</sup>; Assanga *et al.*, 2013). All the cell lines exhibited a lag phase between day 1 and day 2 which indicated the cells were adapting to culture conditions and ready to divide. An exponential growth phase was observed between the 3<sup>rd</sup> and the 7<sup>th</sup> day, which indicated maximum cell proliferative activity, hence maximum cellular function. The cells reached the plateau or decline phase thereafter, indicating that cell proliferation slowed due to cell population becoming over-confluent ultimately leading to cell death at this stage which was due to the natural path of the cellular cycle (Raaphorst *et al.*, 2004; Bai *et al.*, 2012;

Darzynkiewicz, 2012).

The next aim was to confirm the maintenance of the biological features of the original tumour and also to ensure that the cell lines had a well-defined human and glial origin. The cell lines were characterised for their expression of HLA-I, GFAP and VEGF to confirm that the cell lines were of human and glial origin and cancerous. These were compared to the respective isotype controls to measure the level of non-specific background signal caused by primary antibodies, based on the cell type.

HLA-I expression was observed on all human derived cells except C2C12 cells (animal derived), which suggested that the cells used in the study were of human origin. The results were in accordance with other related study where HLA marker was used to confirm human origin of human derived cells (Belkin *et al.*, 2013). GFAP expression was also observed on all glial cell lines confirming the glial origin. This was comparable to other studies, which reported that all astroglial cells, neural stem cells along with astroglial tumours such as astrocytoma and GBM characteristically express GFAP as their major filament protein (Abaza *et al.*, 1998; Doetsch, 2003; Brahmachari *et al.*, 2006; Kamphuis *et al.*, 2012). Non-cancerous astrocytes characteristically express glial fibrillary acidic protein (GFAP) as their major filament protein, but cells derived from malignant astrocytoma show less evidence of astrocytic differentiation and usually do not express this antigen after prolonged culture *in vitro* (Sultana *et al.*, 1998; Zhou and Skalli, 2000; Darling 2005). The GFAP expression was similar in all the glial cells, which suggested and verified that both non-cancerous and glioma cell cultures used in the study highly express GFAP as their filament protein and show high evidence of astrocytic differentiation. The prevalence of VEGF expression and isoforms has served as an important mediator of intense angiogenesis which is a characteristic of

glioblastoma. VEGF is normally expressed in healthy cells but over-expressed in the tumour cells predicting glioma aggressiveness (Leon *et al.*, 1996; Oka *et al.*, 2007; Takano *et al.*, 2010; Hamerlik *et al.*, 2012). In this study, VEGF was expressed in all tumour cells but weak to negligible expression was identified in non-cancerous SVGP12 cells. The results were comparable to other studies which demonstrated increased expression of VEGF in malignant glioma tissues compared to non-cancerous tissues with both ELISA and immunohistochemistry (Ferrara *et al.*, 2003; Takano *et al.*, 2010; Hamerlik *et al.*, 2012; Xu *et al.*, 2013).

Overall, characterisation of the cell lines confirmed that they had well defined origin and also depicted a defined proliferative growth rate. This data thereby confirmed suitability of the cell lines for the downstream experiments in determining the binding selectivity of aptamers using various techniques for targeting glioma.

## CHAPTER 4 BINDING ANALYSIS OF SHORTENED RNA AND DNA APTAMERS

### 4.1 Introduction

A key step in the identification and selection of aptamers is the evaluation of the aptamer binding affinity for the target molecules. Aptamers can be quite large (typical length between 80-200 nucleotides) including the primer regions but only specific nucleotides in the loop and bulge region are likely to be responsible for binding, thus it is possible to remove non-essential portions or primer regions whilst retaining specificity. Three out of eight aptamers from Cerchia *et al.*, (2009) publication (GL44, GL43, and GL56) were selected for the study as they had the lowest  $K_d$  (dissociation constant) and thus higher binding affinity towards U87MG cells (Cerchia *et al.*, 2009). These aptamers were identified through the standard SELEX process and comprised of 91 nucleotides (nt) for GL44, and 89 nt for GL43 and GL56 including the fixed primer sites of 23 nt on each side. The fixed primer sequences thus comprised of approximately 50 % of the full sequences and therefore, may have an impact on binding and penetration into the cells.

Generally, not all the nucleotides are necessary for target binding. Aptamer sequences can be optimised primarily towards the binding to targets by truncating few nucleotides within the aptamer sequence based on the secondary structure (Dey *et al.*, 2005; Simons *et al.*, 2012) or by simply deleting the primer sites from both ends (Jimenez *et al.*, 2012). Computational methods have suggested that aptamers with fixed primer sequences do not significantly influence the secondary structure and binding to the target (Cowperthwaite and Ellington, 2008). Other studies however, have reported

problems such as large numbers of false-positive binding sequences during selection process and also non-specific binding of the aptamers with primer sequences (Stoltenburg *et al.*, 2007; Pan and Clawson, 2009). Jimenez *et al.*, (2012) screened DNA aptamers sequences without primers and reported higher binding affinity and selectivity for lung adenocarcinoma cells. The study therefore hypothesised that removal of primer sites may improve the binding affinity towards the target and may result in high penetration into the target cells because of the smaller size. For the study here, the three aptamers were truncated at the primer ends and were subsequently renamed as shortened aptamers (SA44, SA43, and SA56).

The knowledge of functional secondary structures can have a significant impact on aptamer engineering for optimising desired properties and thereby modifying aptamer function (Refer to section 1.12 for more details) (Rockey *et al.*, 2011<sup>a</sup>; Fisher *et al.*, 2008). Studies based on aptamers and targets have also revealed complex folding structure where negative “Gibbs free energy” ( $\Delta G$ ) values plays a critical role for a successful aptamer sequence to function (Fischer *et al.*, 2008). This is typically predicted using *in silico* modelling techniques such as M-fold. The shortened aptamers were primarily characterised by evaluating the predicted secondary structures using M-Fold and binding affinity to the glioma cell line was compared with the aptamers published by Cerchia *et al.*, (2009) M-Fold predicted potential lowest free energy structures that can be generated from the primary sequence taking hairpin loops and other structural formations into account (Zuker, 2003). The binding selectivity and localisation of the shortened RNA aptamers for glioma cells and their DNA homologues were then analysed using confocal microscopy and confirmed by flow cytometry. For binding experiments, random nucleotide sequences (SAN1 DNA and SAN2 DNA) were

used as negative controls. The nucleotide composition length of the test and control aptamers were the same, however, due to the random primary sequence of the control aptamers, it was hypothesised that they would not fold into the exact secondary structure as the test DNA aptamers reported, and therefore will not show binding and selectivity to the target cells.

## 4.2 Results

### 4.2.1 Characterisation of published and shortened RNA aptamers

One (GL43 and GL56) or two (GL44) secondary structures were predicted per aptamer by the M-Fold program. All three aptamers (GL44, GL43 and GL56) also showed complex two - dimensional (2D) secondary structures, including four defined conserved stem-loop structures. The primer regions from the predicted secondary GL44 and GL43 aptamer differed by the presence of two cytosines (cyt42 and cyt43) at the 42<sup>nd</sup> and 43<sup>rd</sup> position in GL44 but not GL43, this however, did not alter affinity for the target cells (Figure 4.1). Truncating the primer ends from both the sides resulted in shorter base sequences and new predicted secondary structure with low free energies. A similar structure of a stem-bulge-stem-loop was predicted for the shortened aptamers SA44 and SA43 with similar Gibb's free energy (Figure 4.2). These stem-loop structures of aptamers are likely to play fundamental role in binding to a target molecule.

Aptamer-target complexes often reveal low dissociation constants that range from nanomolar to picomolar levels (Tombelli *et al.*, 2005; Cerchia *et al.*, 2009). As mentioned in section 4.1, Cerchia *et al.*, demonstrated that GL44 RNA, GL43 RNA and GL56 RNA showed higher binding affinity and specificity for the target U87MG cells (Cerchia *et al.*, 2009). The next approach was therefore to identify if the shortened

aptamers had similar binding capability to target U87MG cells (Refer to section 2.5). Binding curves were plotted using the average mean fluorescence intensity (MFI) of Cy3 labelled aptamers against various aptamer concentrations from three independent experiments (Figure 4.3). The binding assay showed that the shortened aptamers could strongly bind to target cells in the nanomolar range. Comparison of the  $K_d$  for the shortened aptamers showed that SA44 RNA and SA43 RNA bound with higher affinity ( $15.7 \pm 3.43$  nM and  $13.89 \pm 5.7$  nM) than SA56 RNA ( $41.48 \pm 16.96$  nM) to U87MG cells with their  $K_d$  values in nanomolar range. Comparison of maximum binding sites ( $B_{max}$ ) for the shortened aptamers showed that SA56 RNA had higher maximum binding capacity as indicated by the higher MFI ( $1571 \pm 201.3$ ) compared to SA44 RNA ( $460.2 \pm 64.21$ ) and SA43 RNA ( $303.8 \pm 20.47$ ) for U87MG cells. The shortened aptamers SA44 RNA and SA43 RNA also showed almost three times decrease in their  $K_d$  values indicating their higher binding affinity to U87MG compared to the GL44 ( $38 \pm 3$  nM) and GL43 RNA ( $44 \pm 4$  nM) (Cerchia *et al.*, 2009).

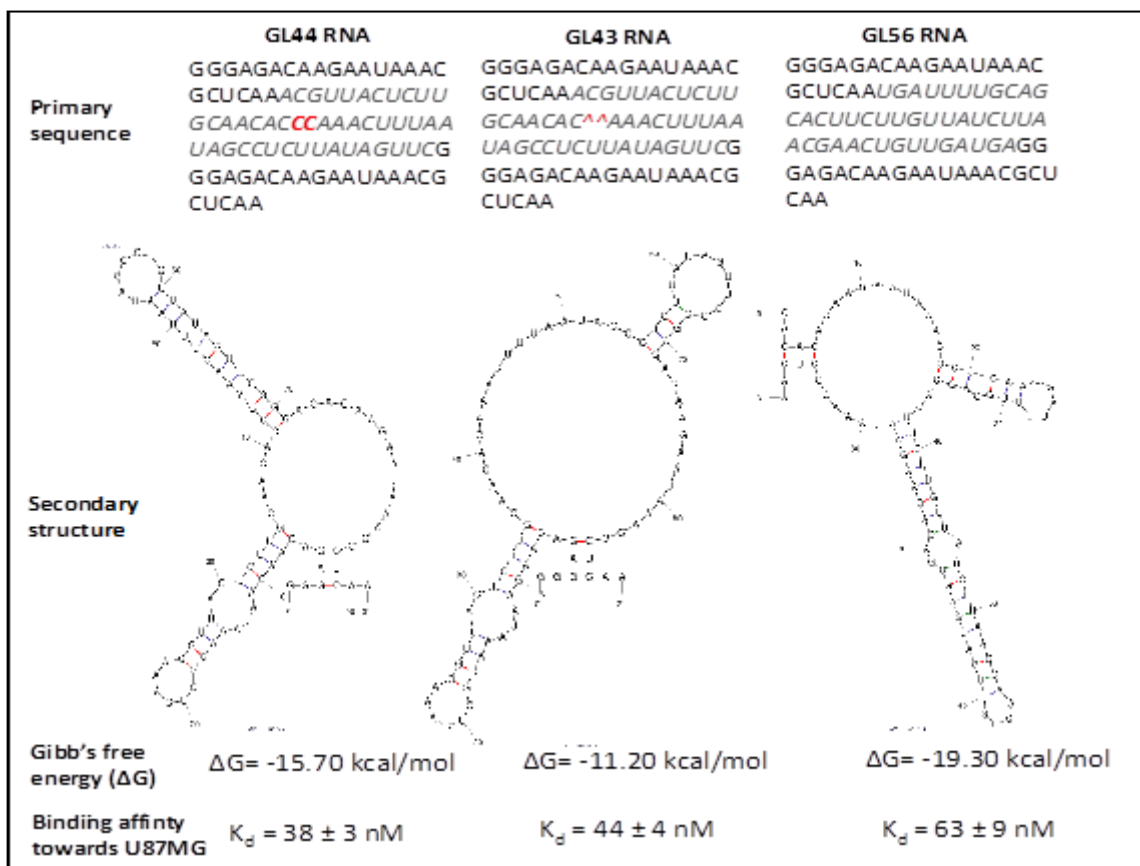


**Figure 4.1 Primary sequence and secondary structure of the selected published aptamers with high binding affinity for U87MG cells and lowest free energies.** From left to right, primary sequences showing 91 base length and 89 base length for selected single stranded RNA aptamers GL44 RNA, and GL43 RNA and GL56 RNA aptamers, respectively (Cerchia *et al.*, 2009). Note the difference in the sequences GL44 RNA and GL43 RNA with the presence of two cytosines (cyt42 and cyt43) in GL44 RNA which is absent in GL43 RNA (red). Sequences in bold were truncated to form new shortened aptamers. Predicted folding with lowest free energies of published aptamers using M-fold software (Zuker, 2003). Binding affinity ( $K_d$ ) values for target U87MG cells is also shown (Cerchia *et al.*, 2009). Dashes between nucleotides indicate Watson-Crick base pairs. All three aptamers showed complex 2D secondary structures, including four defined conserved stem-loop structures.

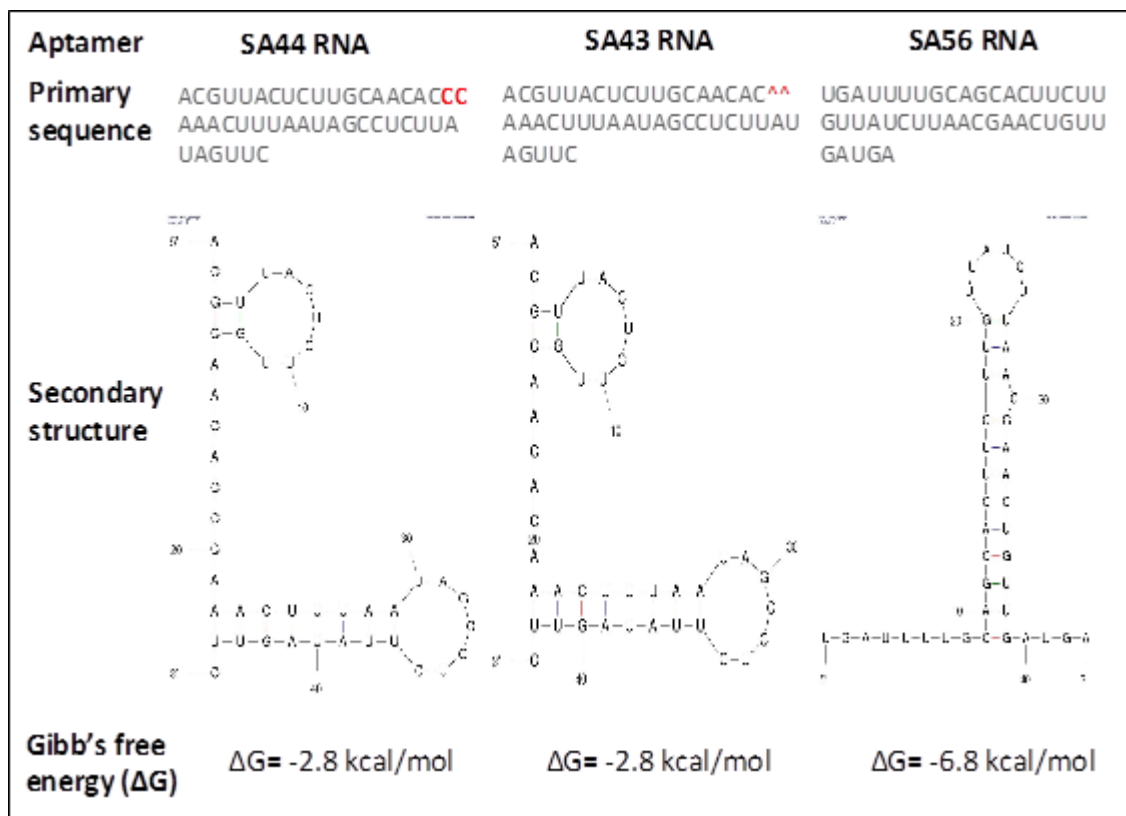


**Figure 4.2 Primary sequences and predicted secondary structures of shortened aptamers SA44 RNA, SA43 RNA, and SA56 with lowest free energies.** From left to right, primary sequences showing 45 base length and 43 base length for shortened single stranded RNA aptamers SA44 RNA, and SA43 RNA and SA56 RNA aptamers, respectively from Cerchia *et al.*, (2009) publication. Note the difference in the sequences SA44 RNA and SA43 RNA with the presence of two cytosines (cyt19 and cyt20) in SA44 RNA which is absent in SA43 RNA (red). Predicted folding with lowest free energies of shortened single stranded RNA aptamers using M-fold software (Zuker, 2003). Dashes between nucleotides indicate Watson-Crick base pairing.

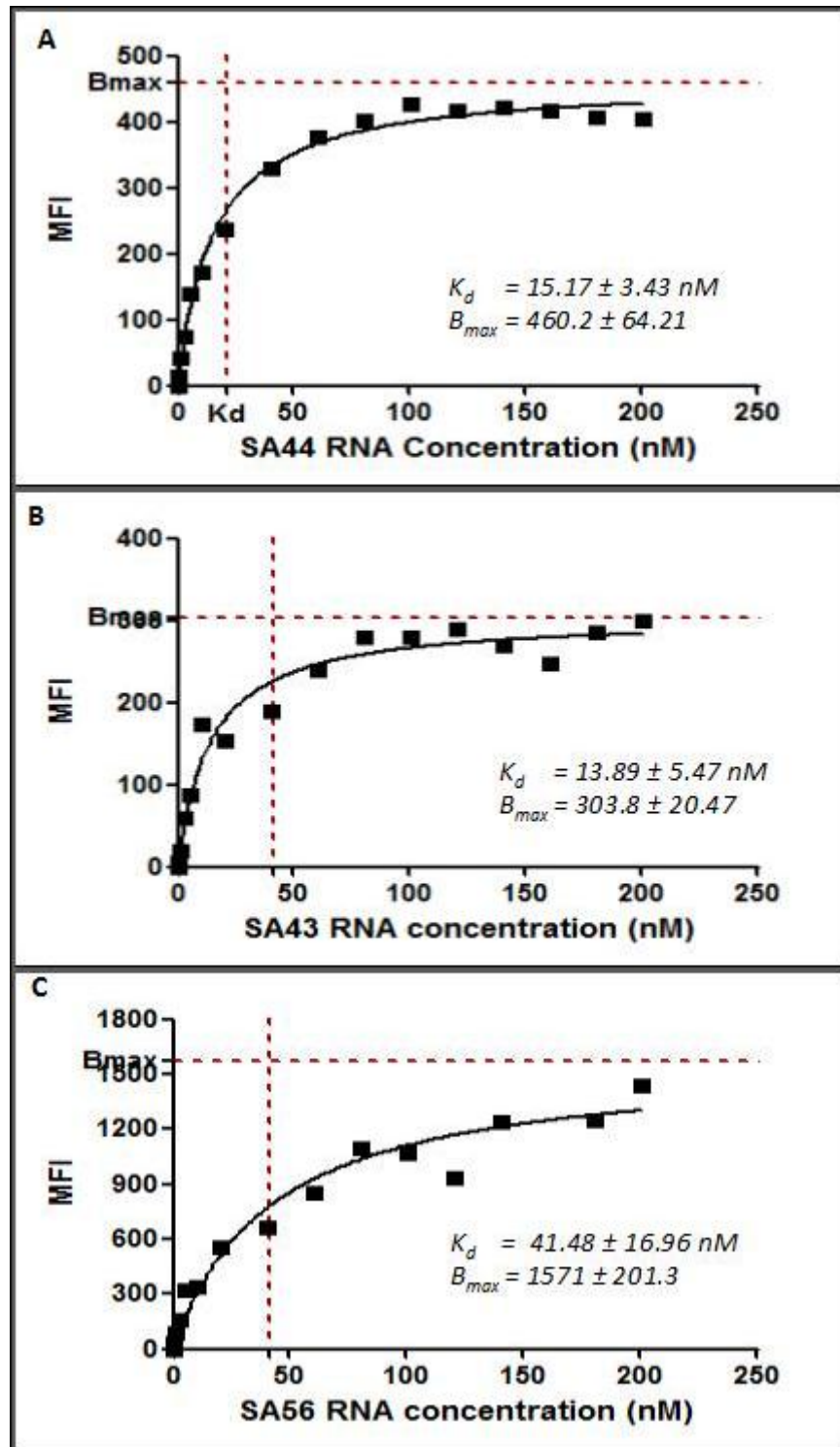


**Figure 4.3** Determination of binding affinity ( $K_d$ ) of the shortened aptamers SA44 RNA, SA43 RNA, and SA56 RNA to the target U87MG cells. Aptamers were incubated with live U87MG cells and analysed by flow cytometry. The average mean fluorescence intensity (MFI) of the cells was plotted against varying concentrations of the Cy3 labeled aptamers (0.5 – 200 nM) and analysed using non-linear regression analysis. (A) Binding curve of aptamer SA44 RNA, (B) binding curve of aptamer SA43 RNA, and (C) binding curve of aptamer SA56 RNA on U87MG cells (n = 3).

### 4.2.2 Concentration dependent binding study of shortened aptamers in live U87MG cells

The binding assay results in section 4.2.1 also helped to determine the optimum concentration of each shortened Cy3-labelled aptamer for binding live U87MG cells. This was accomplished using flow cytometry to measure the aptamer concentration at which  $K_d$  values started reaching saturation point. The mean fluorescence intensity (MFI) values of the Cy3 labelled aptamers bound to the live U87MG cells increased with an increasing aptamer concentration until reaching the plateau phase at 100 nM after 90 min incubation (Figure 4.3), hence this concentration was chosen for further analysis.

Confocal microscopy was used to confirm the concentration dependent uptake and to determine the localisation of the aptamers in U87MG cells. Live U87MG cells were incubated with Cy3- labelled aptamers with increasing concentrations ranging from 5 nM to 100 nM for 90 min at 37 °C and then analysed using confocal microscopy (Section 2.6.1). Untreated cells were incubated with complete growth medium alone. Figures 4.4, 4.5, and 4.6 represent middle section single plane images of the Z- axis for the Cy3 labelled SA44 RNA, SA43 RNA, and SA56 RNA aptamers with live U87MG cells, respectively. The results from Z stacks imaging indicated that the uptake was concentration dependent with lower uptake on lower concentrations and higher uptake at higher concentrations. Negligible uptake was observed at lowest concentration 5 nM. The binding started at 20 nM showing minimal Cy3 signal concentration non-uniformly distributed in the cytoplasm, however, aptamer started accumulating in the cytoplasm with the increase in the aptamer concentration after 20 nM. Maximum Cy3 fluorescence

signal was observed starting from 80 nM and from 40 nM in the cytoplasm for aptamers SA44 and SA43 RNA (figures 4.4 and 4.5), and SA56 RNA (figure 4.6), respectively. The 100 nM aptamer concentration showed the best contrast between unstained nucleus and stained cell cytoplasm, suggesting that the aptamers were mainly localised in cell cytoplasm. The data from sections 4.2.1 and 4.2.2 led to further study of the shortened aptamers for their binding selectivity on other cell types.

**Figure 4.4 Concentration dependent uptake and cellular localisation of SA44 RNA aptamer.** Cy3 labelled SA44 RNA was incubated separately at varying concentrations ranging from 5 nM to 100 nM on live U87MG cells (red) and fixed using 4 % PFA. The nuclei were counterstained with DAPI (blue) and mounted. U87MG cells with no aptamer were used as control. Z-stacks were acquired under 40x magnifications at an excitation of 543 nm and emission of 560 nm under 1047-camera resolution (amplifier gain: 1; detector gain: 927; amplifier offset: - 0.06). Data are representative of three independent experiments with single plane images of a middle section of Z- axis. In each section, 1<sup>st</sup> column represents image of nucleus stained with DAPI; 2<sup>nd</sup> column represents Cy3 aptamer and 3<sup>rd</sup> column represents the merge of DAPI and Cy3 image. Uptake was observed in a concentration dependent manner and mainly localised in cytoplasm. **A** Untreated cells (control); **B** 5 nM, SA44 RNA; **C** 20 nM, SA44 RNA; **D** 40 nM, SA44 RNA; **E** 80 nM, SA44 RNA; **F** 100 nM, SA44 RNA. Bar = 20  $\mu$ m.

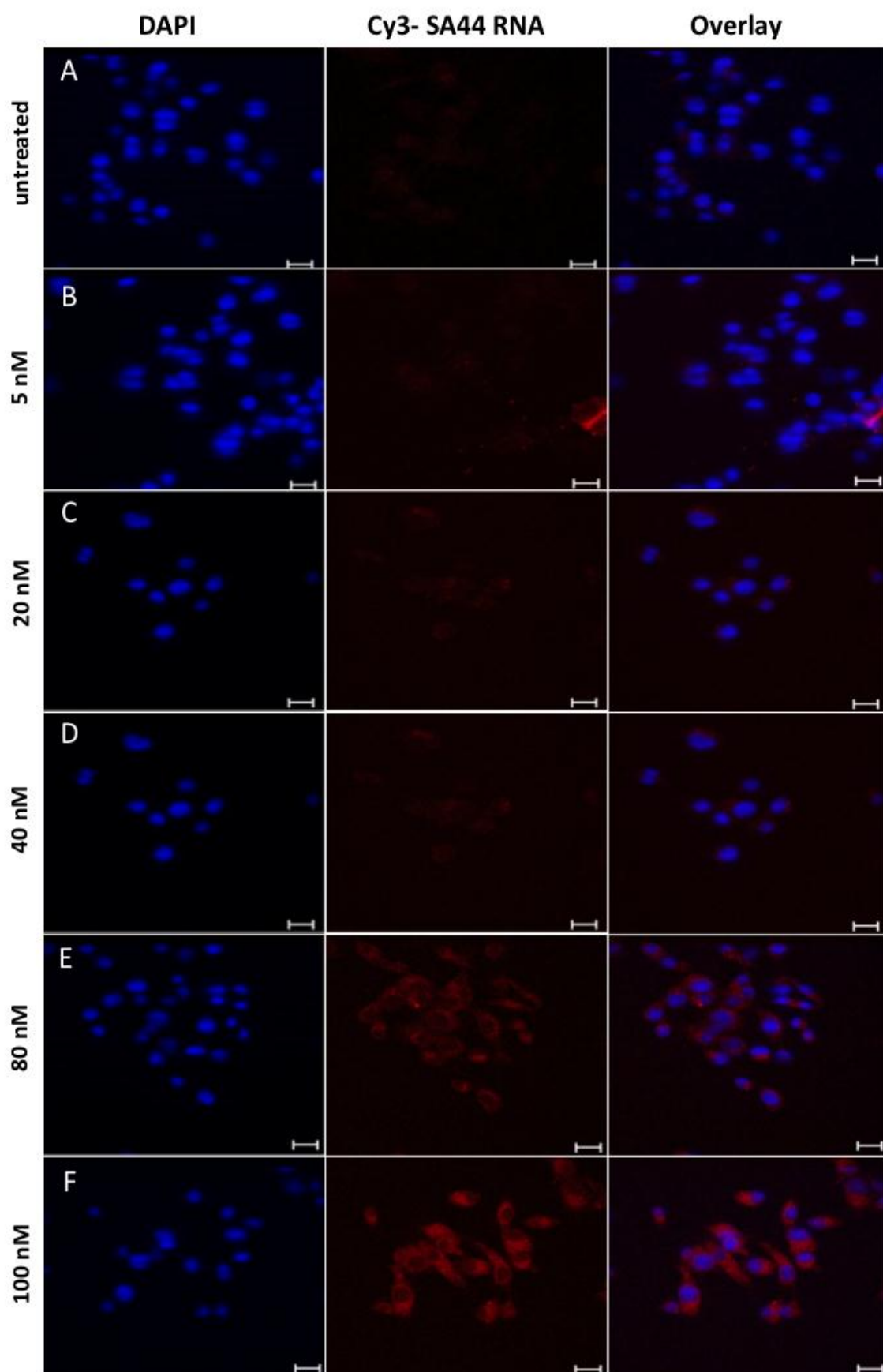


**Figure 4.5 Concentration dependent uptake and cellular localisation of SA43 RNA aptamer.** Cy3 labelled SA43 RNA was incubated separately at varying concentrations ranging from 5 nM to 100 nM on live U87MG cells (red) and fixed using 4 % PFA. The nuclei were counterstained with DAPI (blue) and mounted. U87MG cells with no aptamer were used as control. Z-stacks were acquired under 40x magnifications at an excitation of 543 nm and emission of 560 nm under 1047-camera resolution (amplifier gain: 1; detector gain: 927; amplifier offset: - 0.06). Data are representative of three independent experiments with single plane images of a middle section of Z- axis. In each section, 1<sup>st</sup> column represents image of nucleus stained with DAPI; 2<sup>nd</sup> column represents Cy3 aptamer and 3<sup>rd</sup> column represents the merge of DAPI and Cy3 image. Uptake was observed in a concentration dependent manner and mainly localised in cytoplasm. **A** Untreated cells (control); **B** 5 nM, SA43 RNA; **C** 20 nM, SA43 RNA; **D** 40 nM, SA43 RNA; **E** 80 nM, SA43 RNA; **F** 100 nM, SA43 RNA. Bar = 20  $\mu$ m.

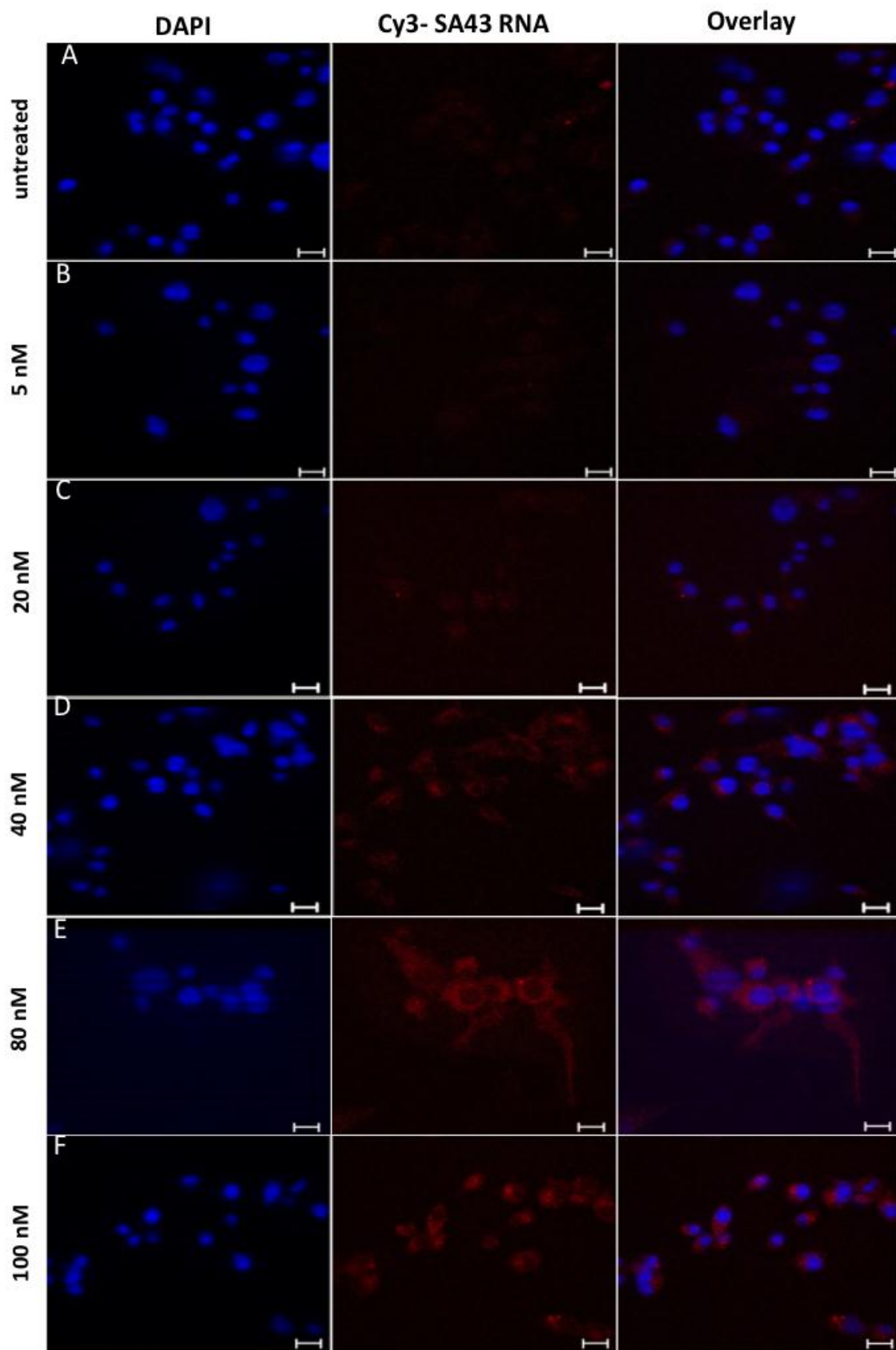
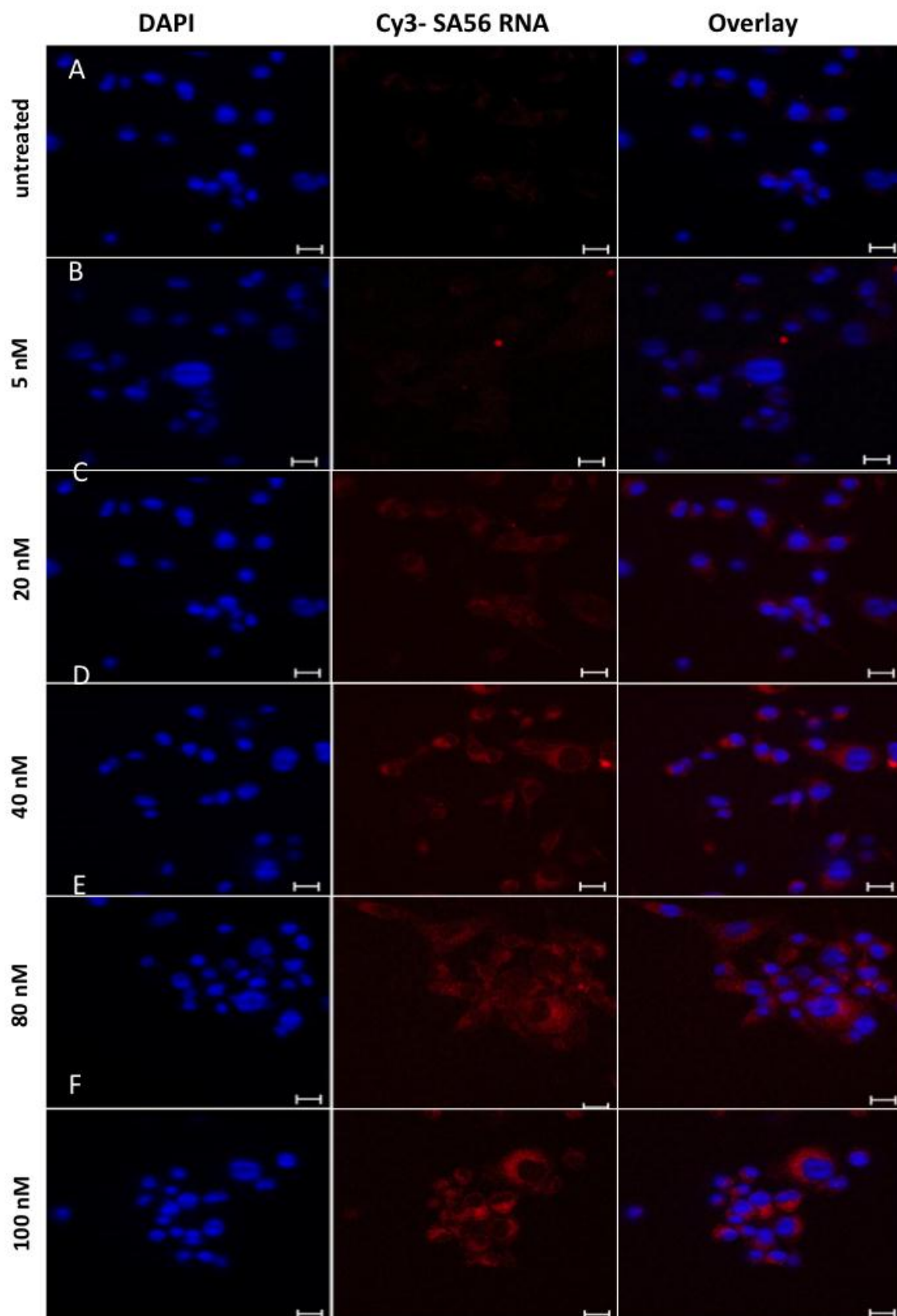


**Figure 4.6 Concentration dependent uptake and cellular localisation of SA56 RNA aptamer.** Cy3 labelled SA56 RNA was incubated separately at varying concentrations ranging from 5 nM to 100 nM on live U87MG cells (red) and fixed using 4 % PFA. The nuclei were counterstained with DAPI (blue) and mounted. U87MG cells with no aptamer were used as control. Z-stacks were acquired under 40x magnifications at an excitation of 543 nm and emission of 560 nm under 1047-camera resolution (amplifier gain: 1; detector gain: 927; amplifier offset: - 0.06). Data are representative of three independent experiments with single plane images of a middle section of Z- axis. In each section, 1<sup>st</sup> column represents image of nucleus stained with DAPI; 2<sup>nd</sup> column represents Cy3 aptamer and 3<sup>rd</sup> column represents the merge of DAPI and Cy3 image. Uptake was observed in a concentration dependent manner and mainly localised in cytoplasm. **A** Untreated cells (control); **B** 5 nM, SA56 RNA; **C** 20 nM, SA56 RNA; **D** 40 nM, SA56 RNA; **E** 80 nM, SA56 RNA; **F** 100 nM, SA56 RNA. Bar = 20  $\mu$ m.



### 4.2.3 Selective uptake of shortened RNA aptamers in live cell lines

The identification of a small set of aptamers SA44 RNA, SA43 RNA and SA56 RNA which showed high affinity for U87MG glioma cells raised an obvious question of whether these aptamers may bind as well to other cell types and whether they were able to discriminate cancerous from non-cancerous cells. To this aim, the cell type selectivity was determined by measuring the uptake of each aptamer at the same concentration, 100 nM, on a panel of unrelated cell lines. Glioma cells 1321N1 and U87MG (grade IV, tumorigenic *in vivo*), T98G (grade IV, non-tumorigenic *in vivo*) and non-cancerous foetal astrocytes SVGP12, including non-glioma cells MCF-7 (breast cancer) and T24 (bladder cancer) were utilised for the study. Aptamer uptake was assessed using confocal microscopy and further confirmed by flow cytometry.

#### 4.2.3.1 Selective uptake of aptamers SA44 RNA, SA43 RNA and SA56 RNA by confocal microscopy

The cells were treated with 100 nM of SA44 RNA, SA43 RNA and SA56 RNA aptamer for 90 minutes at 37 °C and then analysed using confocal microscopy. Z-stacks and 3D projections were obtained to determine the level of fluorescence obtained for each aptamer on each cell lines (Section 2.6). The presence of a more intense Cy3-fluorescence signal compared to the untreated control (no aptamer) indicated aptamer uptake and therefore the binding selectivity of the aptamers on various cell lines. Figures 4.7 and 4.8 indicated that tumorigenic cell lines U87MG and 1321N1 exhibited detectable Cy3-fluorescence (binding) in their cytoplasm for SA44 and SA43 RNA aptamers, when compared to the respective untreated controls. No detectable fluorescence was observed in SVGP12, T98G, T24, and MCF-7 cells compared to the untreated control. Similarly, SA56 RNA aptamer exhibited detectable Cy3-fluorescence

for U87MG and 1321N1 in the cytoplasm; however, it also showed moderate detectable Cy3 fluorescence in SVGP12, T98G, and T24 cells (Figure 4.9). The data suggested that SA44 RNA and SA43 RNA had increased uptake towards U87MG and 1321N1 compared to other cell lines. SA56 RNA, on the other hand showed no selective uptake on glioma cells, as the staining was prominent for other cells types too.

**Figure 4.7 Selective uptake of SA44 RNA on live cell lines assessed by confocal microscopy.** Cy3 labelled SA44 RNA (red) was incubated separately at a concentration of 100 nM on live 1321N1, U87MG, T98G, SVGP12, MCF-7, and T24 cells for 90 minutes at 37 °C and fixed using 4 % PFA. The nuclei were counterstained with DAPI (blue). Cells with no aptamer and media alone were used as control. Z-stacks were acquired under 40x magnifications at an excitation of 543 nm and emission of 560 nm under 1047-camera resolution (amplifier gain: 1; detector gain: 927; amplifier offset: -0.06). Data are representative of at least three independent experiments with single plane images of middle section of Z-axis. The Cy3 fluorescence signal of the aptamer for each cell line was compared to their respective untreated controls. **A** and **C** High uptake of SA44 RNA in U87MG and 1321N1 cells respectively. **A'** and **C'** Merged DAPI image of SA44 RNA localised in the cytoplasm of U87MG cells and 1321N1 cells respectively. **E**, **G**, **I**, and **K** Negligible uptake of SA44 RNA in SVGP12, T98G, T24, and MCF-7 cells, respectively. **E'**, **G'**, **I'**, and **K'** Merged DAPI image of SA44 RNA in SVGP12, T98G, T24, and MCF-7 cells, respectively. **B**, **D**, **F**, **H**, **J**, and **L** No detectable Cy3 fluorescence signal in untreated U87MG, 1321N1, SVGP12, T98G, T24, and MCF-7, respectively. **B'**, **D'**, **F'**, **H'**, **J'**, and **L'** Merged DAPI image of untreated U87MG, 1321N1, SVGP12, T98G, T24, and MCF-7 cells, respectively. Bar = 20µm.

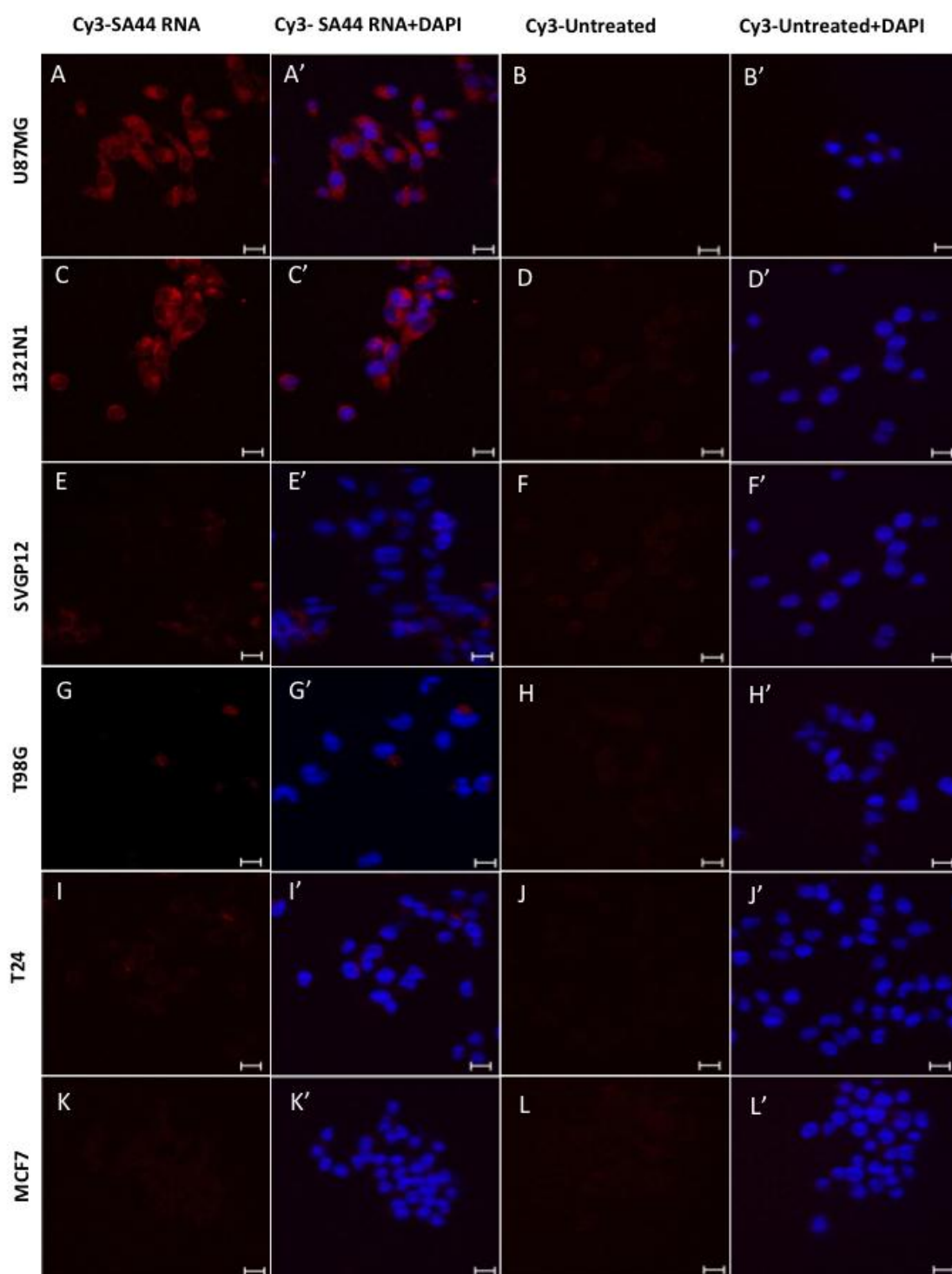


**Figure 4.8 Selective uptake of SA43 RNA on live cell lines assessed by confocal microscopy.** Cy3 labelled SA43 RNA (red) was incubated separately at a concentration of 100 nM on live 1321N1, U87MG, T98G, SVGP12, MCF-7, and T24 cells for 90 minutes at 37 °C and fixed using 4 % PFA. The nuclei were counterstained with DAPI (blue). Cells with no aptamer and media alone were used as control. Z-stacks were acquired under 40x magnifications at an excitation of 543 nm and emission of 560 nm under 1047-camera resolution (amplifier gain: 1; detector gain: 927; amplifier offset: -0.06). Data are representative of at least three independent experiments with single plane images of middle section of Z- axis. The Cy3 fluorescence signal of the aptamer on each cell lines were compared to their respective untreated controls. **A** and **C** High uptake of SA43 RNA in U87MG and 1321N1 cells respectively. **A'** and **C'** Merged DAPI image of SA43 RNA localised in the cytoplasm of U87MG cells and 1321N1 cells respectively. **E**, **G**, **I**, and **K** Negligible uptake of SA43 RNA in SVGP12, T98G, T24, and MCF-7 cells, respectively. **E'**, **G'**, **I'**, and **K'** Merged DAPI image of SA43 RNA in SVGP12, T98G, T24, and MCF-7 cells, respectively. **B**, **D**, **F**, **H**, **J**, and **L** No detectable Cy3 fluorescence signal in untreated U87MG, 1321N1, SVGP12, T98G, T24, and MCF-7, respectively. **B'**, **D'**, **F'**, **H'**, **J'**, and **L'** Merged DAPI image of untreated U87MG, 1321N1, SVGP12, T98G, T24, and MCF-7 cells, respectively. Bar = 20  $\mu$ m.

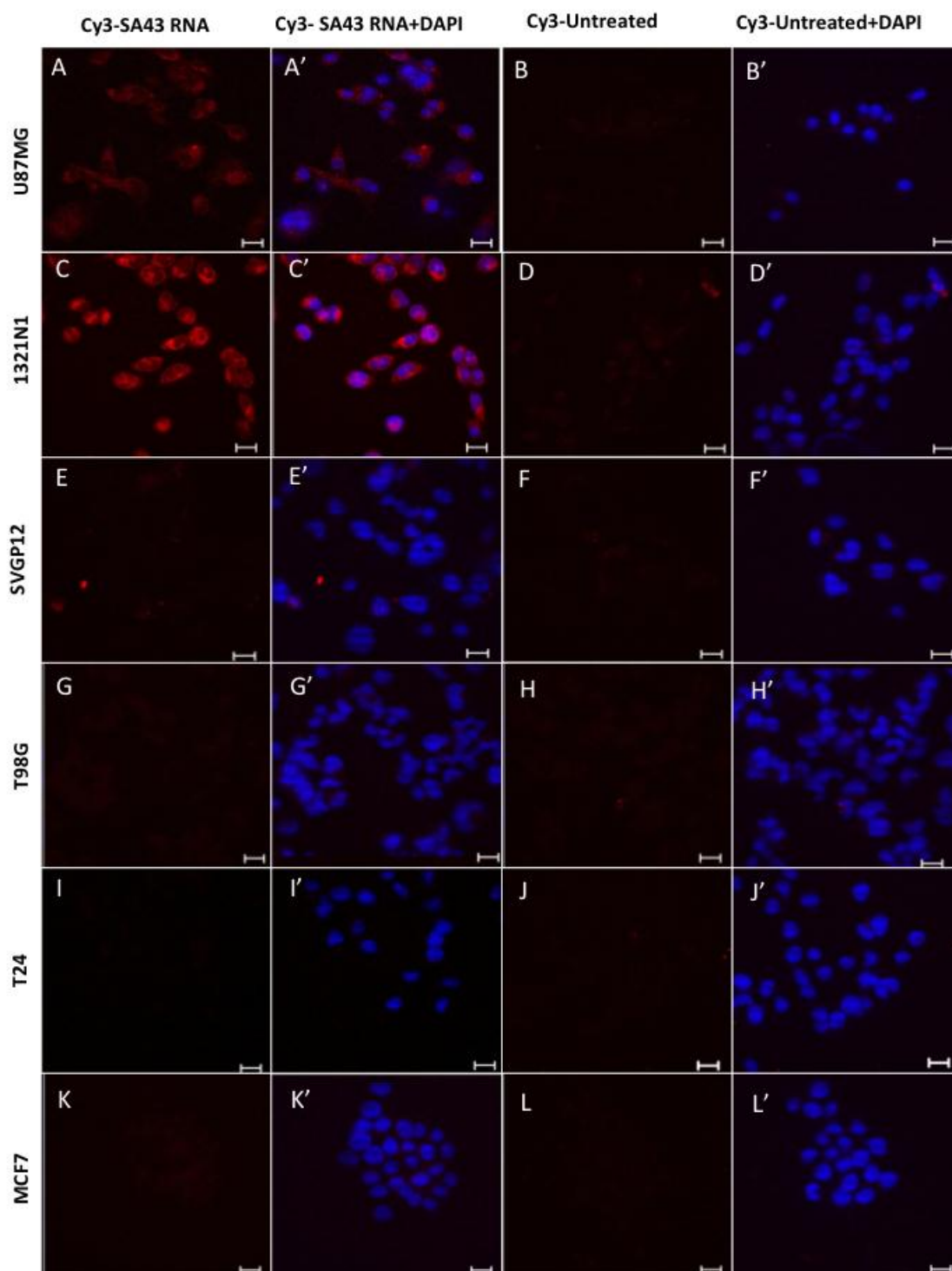
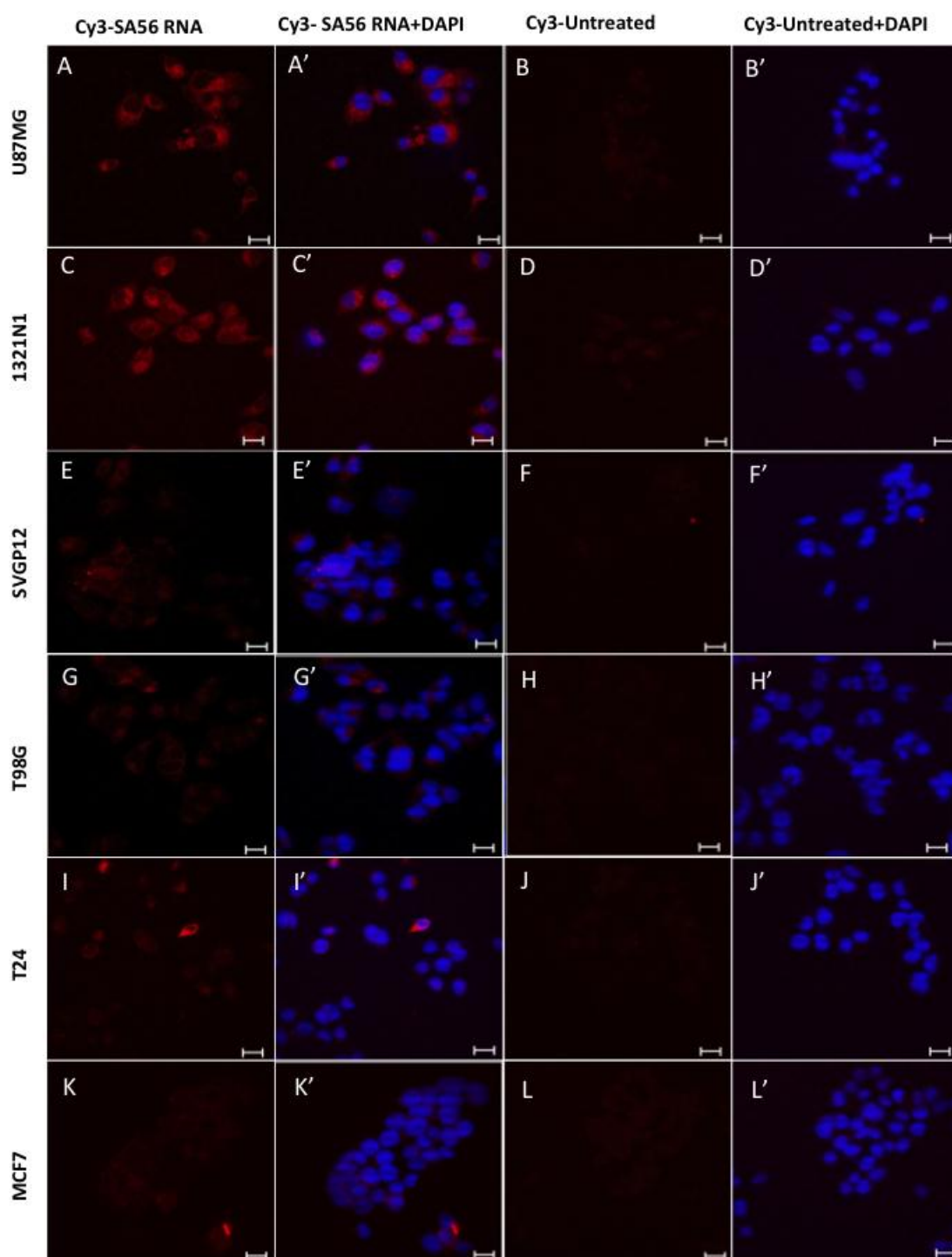


**Figure 4.9 Selective uptake of SA56 RNA on live cell lines assessed by confocal microscopy.** Cy3 labelled SA56 RNA (red) was incubated separately at a concentration of 100 nM on live 1321N1, U87MG, T98G, SVGP12, MCF-7, and T24 cells for 90 minutes at 37 °C and fixed using 4 % PFA. The nuclei were counterstained with DAPI (blue) and mounted. Cells with no aptamer and media alone were used as control. Z-stacks were acquired under 40x magnifications at an excitation of 543 nm and emission of 560 nm under 1047-camera resolution (amplifier gain: 1; detector gain: 927; amplifier offset: - 0.06). Data are representative of at least three independent experiments with single plane images of middle section of Z- axis. The Cy3 fluorescence signal of the aptamer on each cell lines were compared to their respective untreated controls. **A** and **C** High uptake of SA56 RNA in U87MG and 1321N1 cells respectively. **A'** and **C'** Merged DAPI image of SA56 RNA localised in the cytoplasm of U87MG and 1321N1 cells respectively. **E**, **G**, and **I** Moderate uptake of SA56 RNA in SVGP12, T98G, and T24 cells, respectively. **E'**, **G'**, and **I'** Merged DAPI image of SA56 RNA showing moderate Cy3 fluorescence signal localised in the cytoplasm in SVGP12, T98G, and T24, respectively. **K** Negligible uptake of SA56 RNA in MCF-7 cells. **K'** Merged DAPI image of SA56 RNA in MCF-7 cells. **B**, **D**, **F**, **H**, **J**, and **L** No detectable Cy3 fluorescence signal in untreated U87MG, 1321N1, SVGP12, T98G, T24, and MCF-7, respectively. **B'**, **D'**, **F'**, **H'**, **J'**, and **L'** Merged DAPI image of untreated U87MG, 1321N1, SVGP12, T98G, T24 and MCF-7 cells, respectively. Bar = 20 µm.



#### 4.2.3.2 Confirmation of selective uptake of the aptamers SA44 RNA, SA43 RNA and SA56 RNA by flow cytometry.

Glioma and glial cells (1321N1, U87MG, T98G and SVGP12), breast cancer cells (MCF-7) and bladder cancer cells (T24) were used for the study. The binding selectivity and uptake of SA44, SA43, SA56 was determined by incubating live cells with 100 nM concentration of the aptamers at 37 °C (5 % CO<sub>2</sub>) for 90 minutes (Section 2.7.1). Aptamers SA44 RNA and SA43 RNA demonstrated an increase in uptake towards U87MG and 1321N1 cells compared to other cell types (Figures 4.10 and 4.11). SA56 RNA showed increased uptake in 1321N1 and U87MG cells, however, non-specific uptake was also observed in SVGP12, T98G, T24, and MCF-7 cells (Figure 4.12).

A Shapiro-Wilk's test ( $p > 0.05$ ) showed that the sample data were normally distributed among the respected cell groups. One-way ANOVA test revealed that there was a significant difference in the means of average MFI values of each shortened RNA aptamer between cell groups ( $p < 0.05$ ). A post hoc Bonferroni test was therefore performed, which revealed that SA44 RNA and SA43 RNA showed significant differences in MFI values generated from 1321N1 and U87MG cells compared to SVGP12, T98G, T24 and MCF-7 cells ( $p < 0.01$ ) (Figure 4.13). There was no significant difference observed in MFI values between 1321N1 and U87MG cells, and between SVGP12, T98G, T24, and MCF-7 cells treated with the aptamers SA44 and SA43 RNA ( $p > 0.05$ ). On the contrary, SA56 RNA showed no significant difference between the MFI values of U87MG, 1321N1, SVGP12 ( $p > 0.05$ ) cells (Figure 4.14). There was however, a significant difference observed in MFI values of U87MG, 1321N1 and SVGP12 compared to T98G, T24, and MCF-7 cells ( $p < 0.01$ ), which suggested that aptamer SA56 RNA showed no significant selectivity for glioma cells

compared to the non-cancerous glial cells, yet the ability to distinguish tumorigenic glioma cells (U87MG and 1321N1) from non-tumorigenic (T98G) or non-glioma cells (MCF-7 and T24).

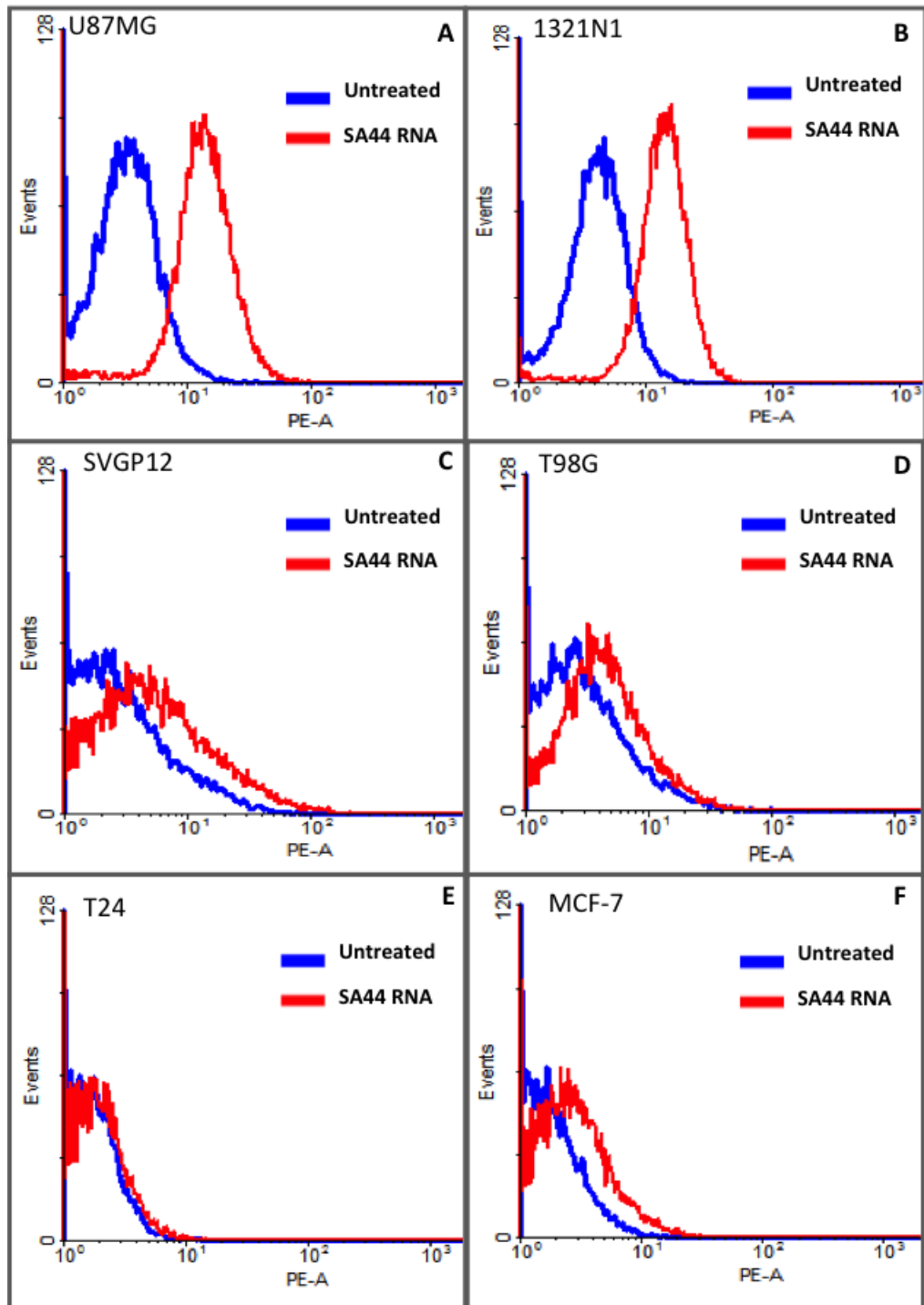


**Figure 4.10 Representative flow cytometry profiles and quantitative analysis of the uptake of SA44 RNA on various cell lines.** Cy3 labelled SA44 RNA aptamer (100 nM) was incubated with live U87MG, 1321N1, SVGP12, T98G, T24 and MCF-7 cells at 37 °C (5 % CO<sub>2</sub>) for 90 minutes. Untreated cells were incubated with complete growth medium alone. The blue curve represented the background mean fluorescence intensity (MFI) of the untreated cells (control) and the red curve represented the MFI (uptake) of the cells treated with SA44 RNA on U87MG (A), 1321N1 (B) SVGP12 (C), T98G (D), T24 (E), and MCF-7 cells (F).

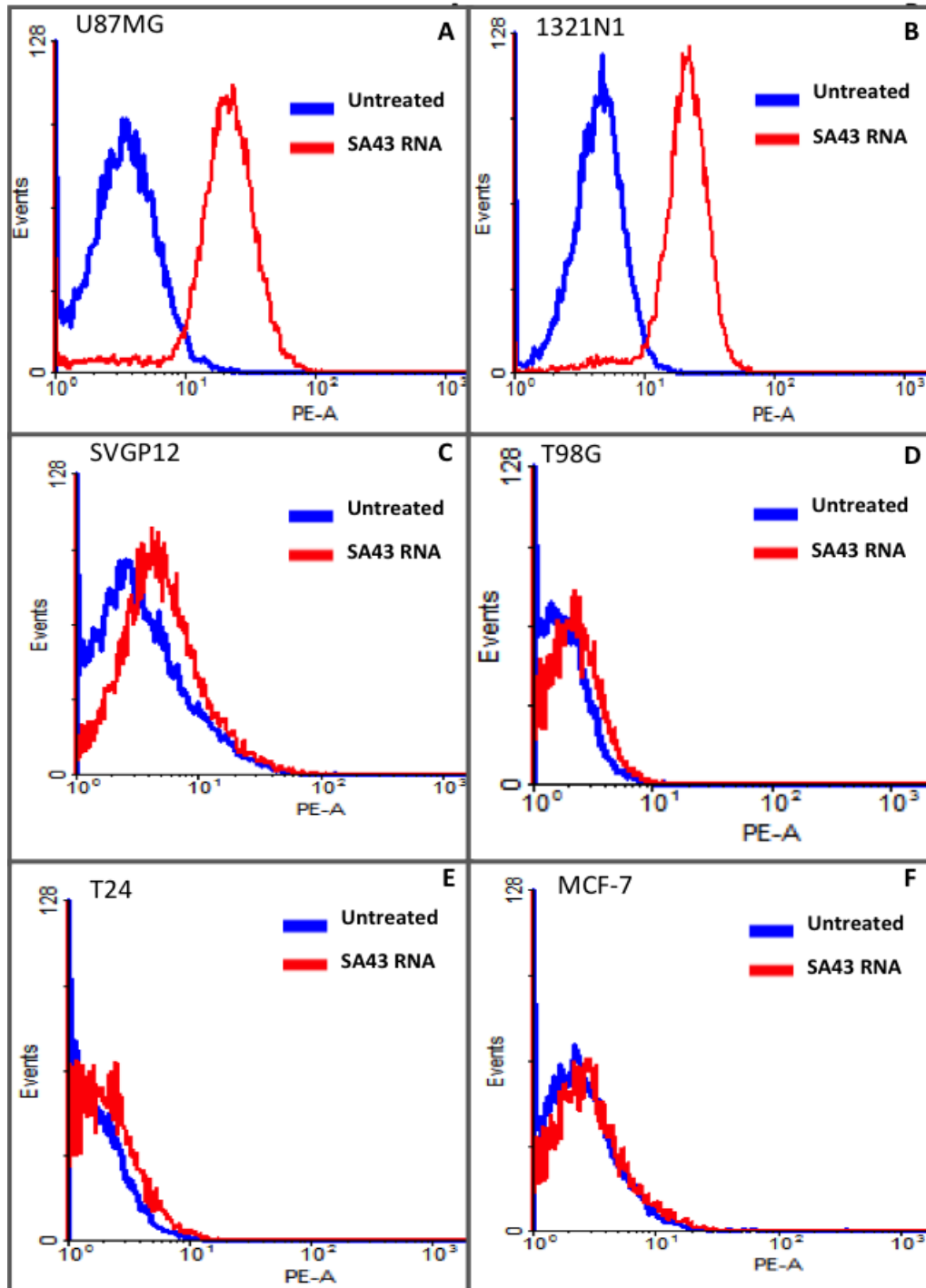


**Figure 4.11 Representative flow cytometry profiles and quantitative analysis of the uptake of SA43 RNA on various cell lines.** Cy3 labelled SA43 RNA aptamer (100 nM) was incubated with live U87MG, 1321N1, SVGP12, T98G, T24 and MCF-7 cells at 37 °C (5 % CO<sub>2</sub>) for 90 minutes. Untreated cells were incubated with complete growth medium alone. The blue curve represented the background mean fluorescence intensity (MFI) of the untreated cells (control) and the red curve represented the MFI (uptake) of the cells treated with SA43 RNA aptamer on U87MG (A), 1321N1 (B) SVGP12 (C), T98G (D), T24 (E), and MCF-7 cells (F).

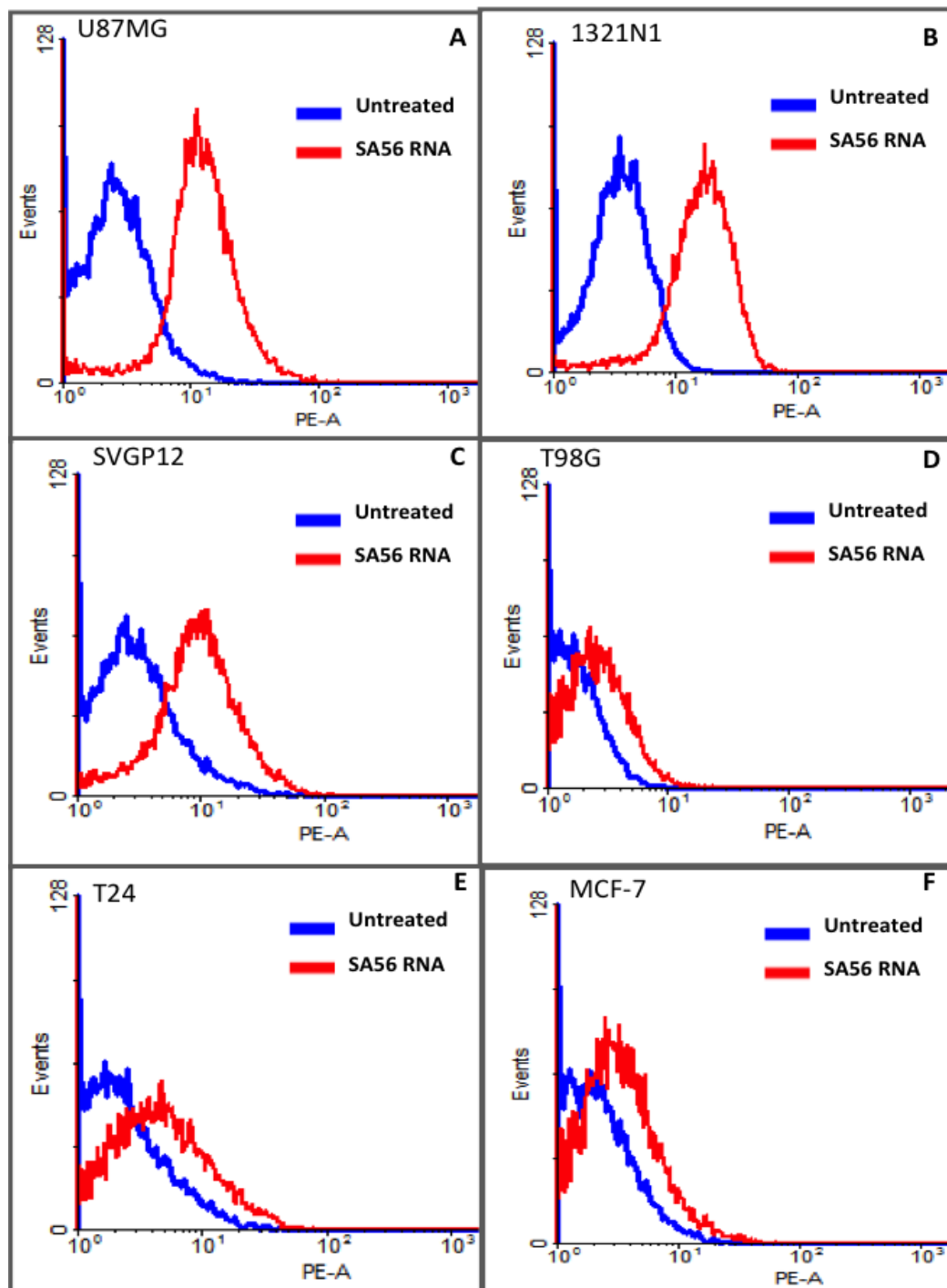


**Figure 4.12** Representative flow cytometry profiles and quantitative analysis of the uptake of SA56 RNA on various cell lines. Cy3 labelled SA56 RNA aptamer (100 nM) was incubated with U87MG, 1321N1, SVGP12, T98G, T24 and MCF-7 cells at 37 °C (5 % CO<sub>2</sub>) for 90 minutes. Untreated cells were incubated with complete growth medium alone. The blue curve represented the background mean fluorescence intensity (MFI) of the untreated cells (control) and the red curve represented the MFI (uptake) of the cells treated with SA56 RNA aptamer on U87MG (A), 1321N1 (B) SVGP12 (C), T98G (D), T24 (E), and MCF-7 cells (F).

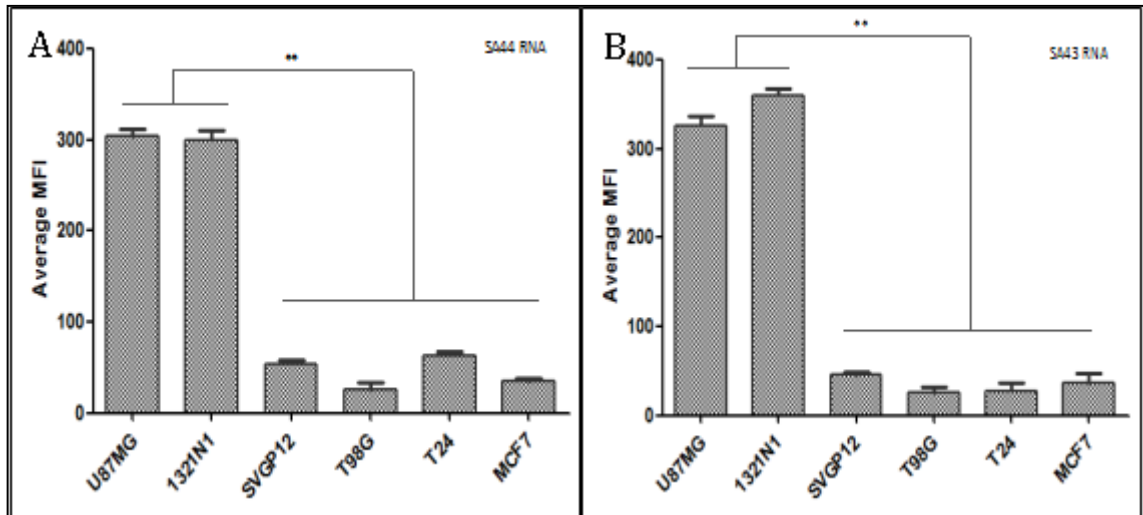


**Figure 4.13 Comparative binding selectivity of aptamers SA44 RNA and SA43 RNA across various cell lines.** Binding selectivity was measured using 100 nM concentration of SA44 RNA (A) and SA43 RNA (B) aptamers. The background MFI values for the untreated corresponding cells were subtracted. Statistical significance of the differences in MFI values of SA44 RNA referred to its high binding selectivity for U87MG and 1321N1 cells compared to SVGP12, T98G, T24, and MCF-7 cells (\*\* =  $p < 0.01$ ;  $n=3$ ).

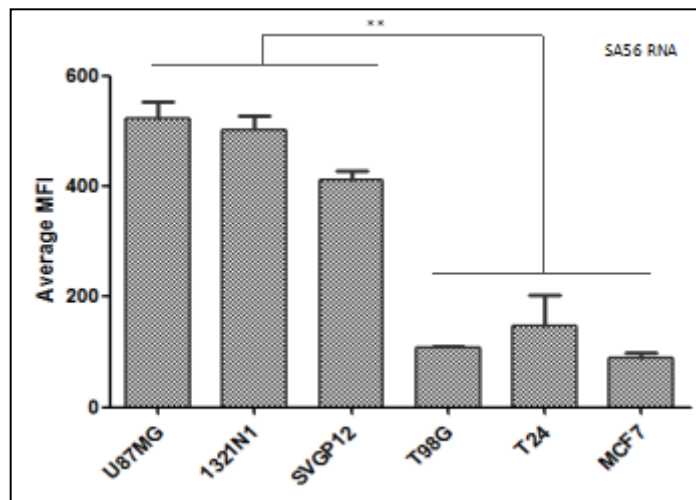


**Figure 4.14 Comparative binding selectivity of aptamer SA56 RNA across various cell lines.** Binding selectivity was measured using 100 nM concentration of SA56 RNA aptamer. The background MFI values for the untreated corresponding cells were subtracted. There was no significant difference in the uptake of SA56 RNA aptamer in U87MG, 1321N1 and SVGP12 cells, and between T98G, T24 and MCF-7 cells ( $p > 0.05$ ). Statistical significance of the differences in MFI values of SA56 RNA referred to higher uptake in U87MG, 1321N1 and SVGP12 cells compared to T98G, T24 and MCF-7 cells (\*\* =  $p < 0.01$ ;  $n = 3$ ).

#### **4.2.4 Comparison of binding affinity of the shortened RNA aptamers with the DNA homologs.**

An experiment was performed to compare the binding affinities of DNA and RNA homologues of the aptamers used in the study. As previously shown, SA44 RNA and SA43 RNA showed more uptake and binding selectivity towards glioma than SA56 RNA (Section 4.2.3), therefore, only the DNA homologues of these two aptamers (SA44 DNA and SA43 DNA) were further studied. The binding assay for the detection of Cy3 labelled aptamers bound to cells was measured by flow cytometry. The detected MFI showed that these DNA aptamers can also bind strongly bind to U87MG cells in nanomolar range. Moreover, like the RNA versions (section 4.2.1), similar binding affinity was observed for SA44 DNA ( $K_d$ ,  $21.11 \pm 3.30$  nM) and SA43 DNA ( $K_d$ ,  $21.56 \pm 4.60$  nM) for U87MG cells (Figure 4.15).

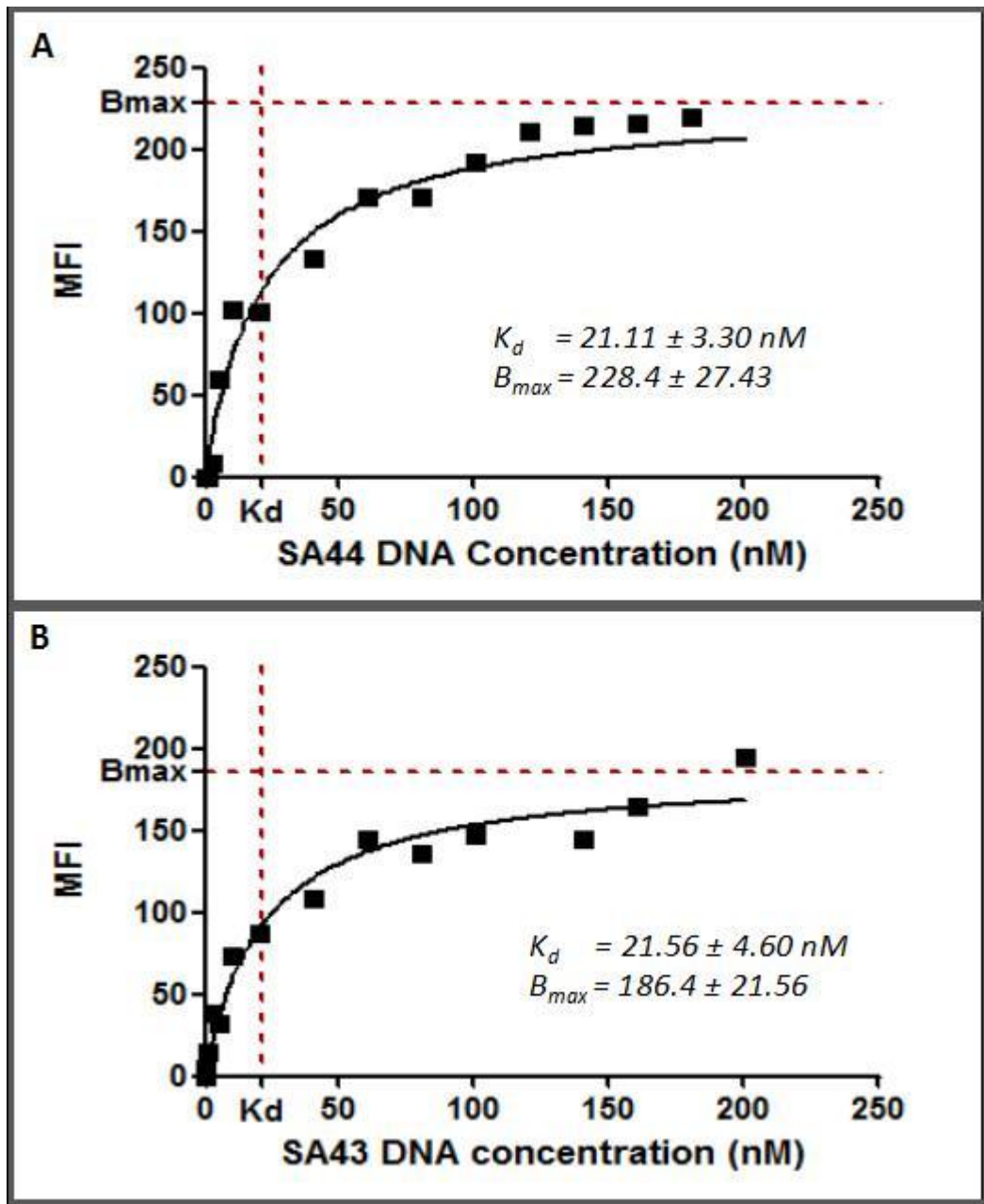


**Figure 4.15** Determination of binding affinity ( $K_d$ ) of aptamers SA44 DNA and SA43 DNA towards the target U87MG cells. Aptamers were incubated with live U87MG cells and analysed by flow cytometry. The average mean fluorescence intensity (MFI) of the cells was plotted against varying concentrations of the Cy3 labeled aptamers (0.5 – 200 nM) and analysed using non-linear regression analysis (A) Binding curve of aptamer SA44 DNA on U87MG cells. (B) Binding curve of aptamer SA43 DNA on U87MG cells.

#### **4.2.5 Selective uptake of the lead DNA aptamers on various cell types**

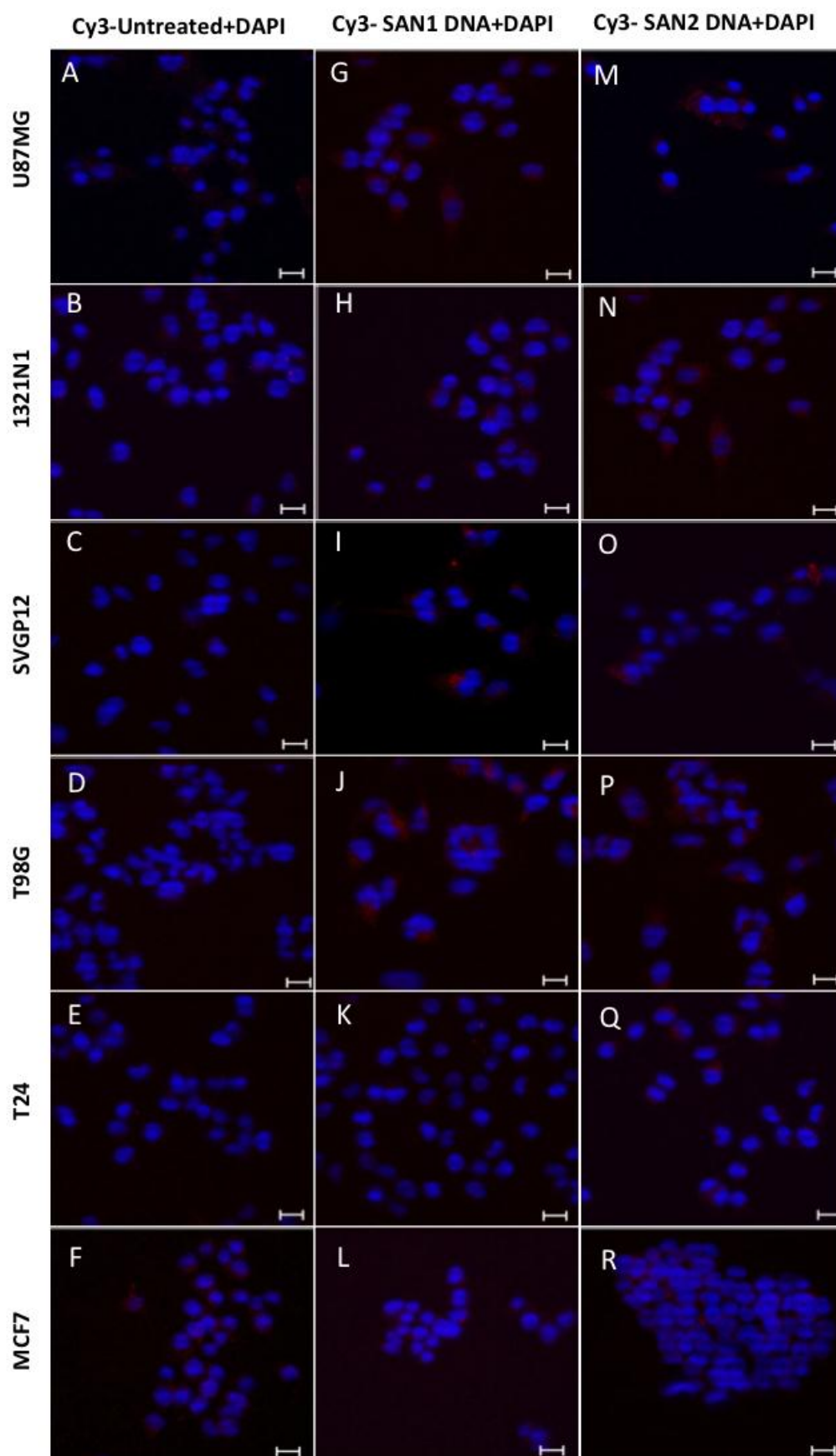
The uptake and binding selectivity of the DNA aptamers measured by confocal microscopy (Section 2.6.2) was further confirmed by flow cytometry (Section 2.7.1) under similar conditions to that of RNA aptamers. Before, performing the binding studies of the lead DNA aptamers (SA44 and SA43 DNA), a pilot study was performed to determine the uptake and binding selectivity of the random DNA aptamers (SAN1 and SAN2 DNA) by confocal microscopy (Section 2.6.2). No detectable Cy3 fluorescence was observed on all cells with SAN1 DNA and SAN2 DNA aptamer (Figure 4.16), which indicated that the aptamers were non-selective for any cell types. This suggested that both random sequence aptamers could act as a negative control for the study and either will be referred to as ‘random aptamer’ from here on in.

Figures 4.17 and 4.18 indicated that tumorigenic cell lines U87MG and 1321N1 exhibited detectable Cy3-fluorescence (binding) in the cytoplasm for SA44 and SA43 DNA aptamers, when compared to the respective untreated controls and the random aptamer as measured by confocal microscopy. No detectable fluorescence was observed on SVGP12, T98G, T24, and MCF-7 cells. The data suggested that SA44 DNA and SA43 DNA reflected the binding characteristics of RNA counterparts with increased cytoplasmic uptake and selectivity towards tumorigenic glioma compared to non-tumorigenic glioma, non-cancerous, and non-glioma cell types (Section 4.2.3).

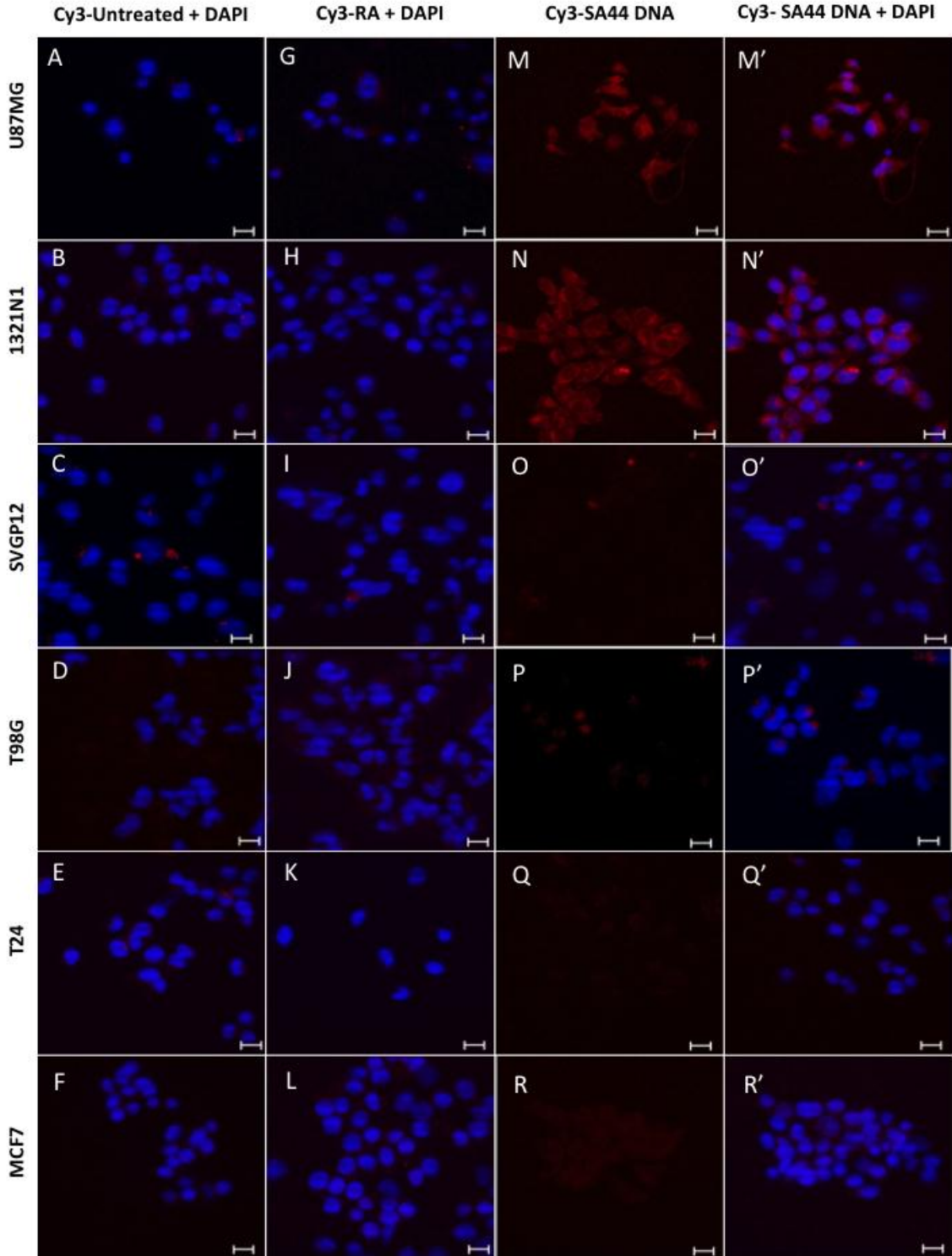
Aptamers SA44 DNA and SA43 DNA further demonstrated an increase in uptake towards U87MG and 1321N1 cells as compared to other cell types as measured by flow cytometry (Figures 4.19 and 4.20). A one-way ANOVA revealed that there was a significant difference in the MFI values of each shortened aptamer between individual

cell groups (Figure 4.21). Post hoc Bonferroni test revealed that SA44 DNA and SA43 DNA showed significant differences in their MFI values generated from 1321N1 and U87MG compared to SVGP12, T98G, T24, and MCF-7 cells ( $p < 0.05$ ). There was no significant difference observed in MFI values between SVGP12, T98G, T24, and MCF-7 cells ( $p > 0.05$ ). This confirmed that DNA aptamers SA44 and SA43 demonstrated significant binding selectivity for U87MG and 1321N1 cells compared to other cell lines. Overall, this data suggested that both shortened DNA and RNA aptamers were highly selective for tumorigenic glioma cells.

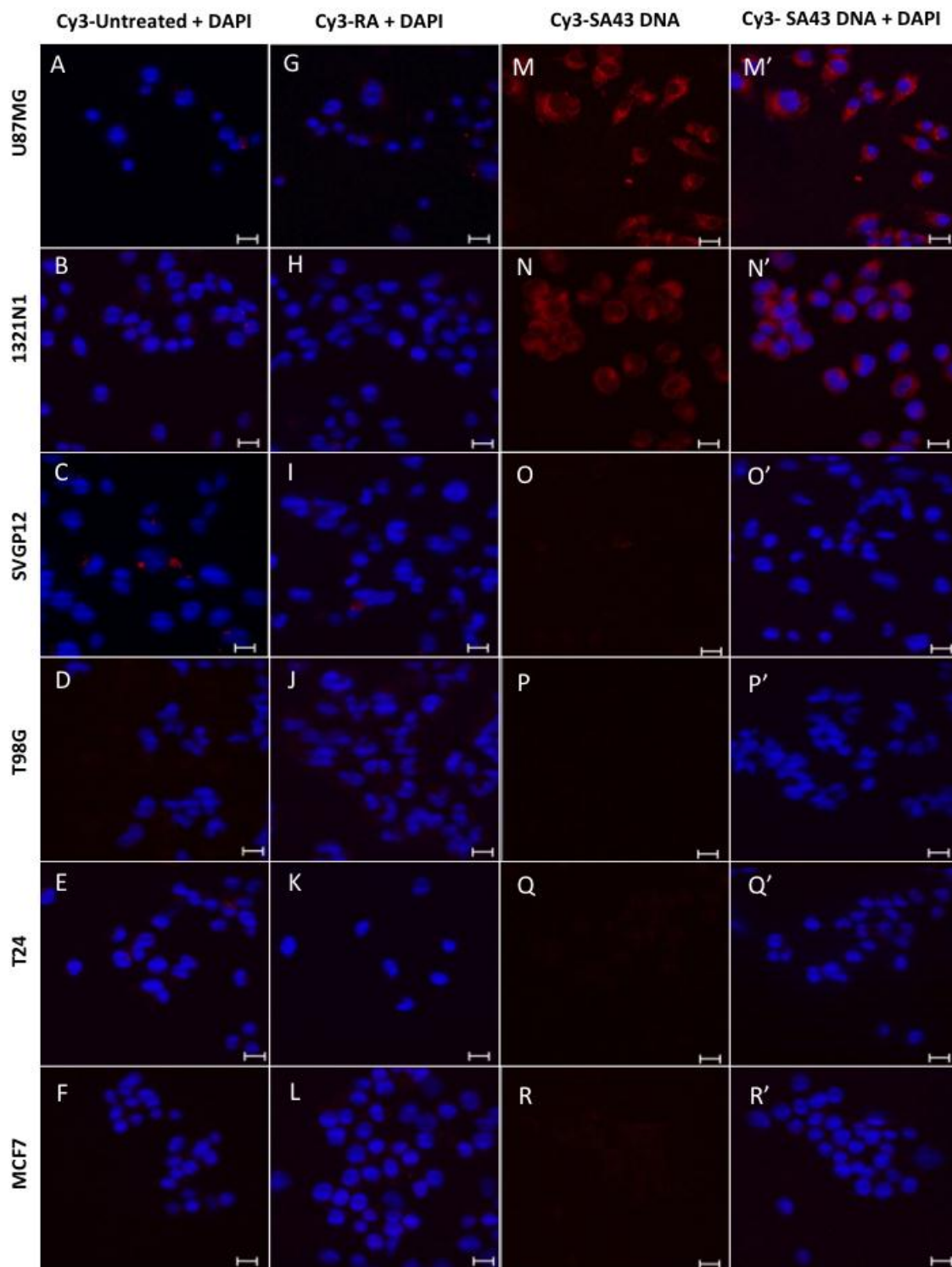
**Figure 4.16 Uptake of random aptamers SAN1 and SAN2 DNA on various cell lines by confocal microscopy.** Cy3 labelled SAN1 and SAN2 DNA (red) were incubated separately at a concentration of 100 nM on live 1321N1, U87MG, T98G, SVGP12, MCF-7, and T24 cells for 90 minutes at 37 °C and fixed using 4 % PFA. The nuclei were counterstained with DAPI (blue) and mounted. Cells with no aptamer and media alone were used as control. Z-stacks images were acquired under 40x magnifications at an excitation of 543 nm and emission of 560 nm under 1047-camera resolution (amplifier gain: 1; detector gain: 927; amplifier offset: - 0.06). Data are representative of three independent experiments with single plane images of middle section of Z- axis. The Cy3 fluorescence signal of the aptamer on each cells were compared to their respective untreated controls. **A, B, C, D, E,** and **F** represent merged Cy3 and DAPI image with no detectable Cy3 fluorescence on untreated U87MG, 1321N1, SVGP12, T98G, T24 and MCF-7, respectively. **G, H, I, J, K,** and **L** represent merged Cy3 and DAPI image with no detectable Cy3 fluorescence with SAN1 DNA treated U87MG, 1321N1, SVGP12, T98G, T24 and MCF-7 cells, respectively compared to the respective untreated cells. Similarly, **M, N, O, P, Q,** and **R** represent merged Cy3 and DAPI image with no detectable Cy3 fluorescence with SAN2 DNA treated U87MG, 1321N1, SVGP12, T98G, T24 and MCF-7 cells, respectively compared to the respective untreated cells. Scale bar = 20µm.



**Figure 4.17 Selective uptake of SA44 DNA on various cell lines using confocal microscopy.** Cy3 labelled SA44 DNA (red) and random aptamer (RA) were incubated separately at a concentration of 100 nM on live 1321N1, U87MG, T98G, SVGP12, MCF-7, and T24 cells for 90 minutes at 37 °C and fixed using 4 % PFA. The nuclei were counterstained with DAPI (blue). Cells with random aptamer and media alone were used as control. Z-stacks were acquired under 40x magnifications at an excitation of 543 nm and emission of 560 nm under 1047-camera resolution (amplifier gain: 1; detector gain: 927; amplifier offset: - 0.06). Data are representative of three independent experiments with single plane images of middle section of Z- axis. The Cy3 fluorescence signal of the SA44 DNA aptamer on each cells were compared to the random aptamer and respective untreated controls. **A, B, C, D, E,** and **F** represent merged Cy3 and DAPI image of untreated U87MG, 1321N1, SVGP12, T98G, T24, and MCF-7 cells, respectively. **G, H, I, J, K,** and **L** represent merged Cy3 and DAPI image of random aptamer (RA) showing negligible uptake and binding on U87MG, 1321N1, SVGP12, T98G, T24, and MCF-7 cells, respectively. **M (M')** and **N (N')** represents Cy3 and merged DAPI image showing high uptake and cytoplasmic binding of SA44 DNA in U87MG cells and 1321N1 cells respectively. **O (O'), P (P'), Q (Q'),** and **R (R')** represent Cy3 and merged DAPI image of SA44 DNA showing negligible uptake in SVGP12, T98G, T24, and MCF-7 cells, respectively. Bar = 20  $\mu$ m.



**Figure 4.18 Selective uptake of SA43 DNA on various cell types using confocal microscopy.** Cy3 labelled SA43 DNA (red) and random aptamer (RA) were incubated separately at a concentration of 100 nM on live 1321N1, U87MG, T98G, SVGP12, MCF-7, and T24 cells for 90 minutes at 37 °C and fixed using 4 % PFA. The nuclei were counterstained with DAPI (blue). Cells with random aptamer and media alone were used as control. Z-stacks were acquired under 40x magnifications at an excitation of 543 nm and emission of 560 nm under 1047-camera resolution (amplifier gain: 1; detector gain: 927; amplifier offset: - 0.06). Data are representative of three independent experiments with single plane images of middle section of Z- axis. The Cy3 fluorescence signal of the SA43 DNA aptamer on each cells were compared to the random aptamer and respective untreated controls. **A, B, C, D, E,** and **F** represent merged Cy3 and DAPI image of untreated U87MG, 1321N1, SVGP12, T98G, T24, and MCF-7 cells, respectively. **G, H, I, J, K,** and **L** represent merged Cy3 and DAPI image of random aptamer (RA) showing negligible uptake and binding on U87MG, 1321N1, SVGP12, T98G, T24, and MCF-7 cells, respectively. **M (M')** and **N (N')** represents Cy3 and merged DAPI image showing high uptake and cytoplasmic binding of SA43 DNA in U87MG cells and 1321N1 cells respectively. **O (O'), P (P'), Q (Q'),** and **R (R')** represent Cy3 and merged DAPI image of SA43 DNA showing negligible uptake in SVGP12, T98G, T24, and MCF-7 cells, respectively. Bar = 20 µm.



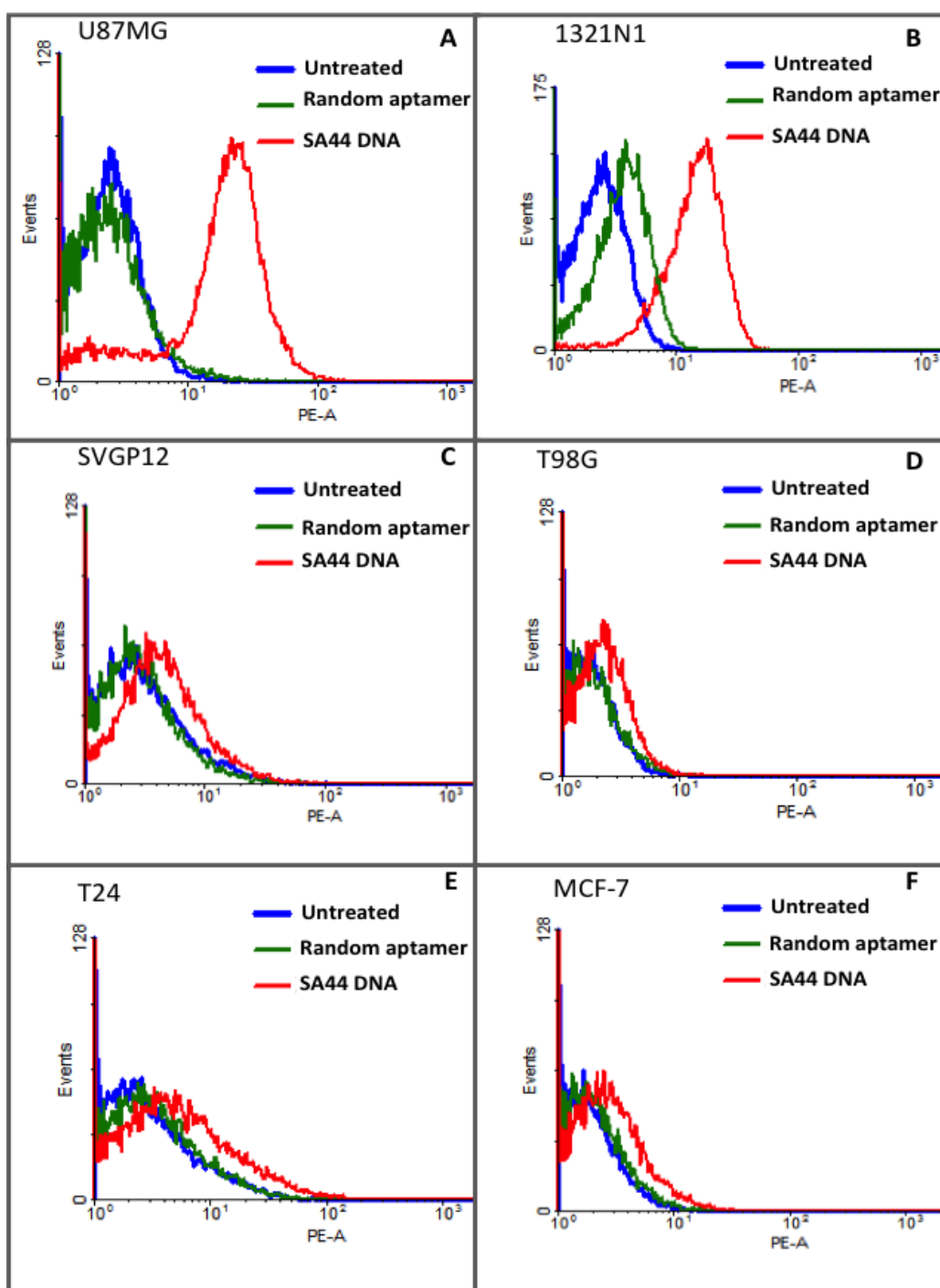


**Figure 4.19 Representative flow cytometry profiles of the uptake of SA44 DNA on various cell lines.** Cy3 labelled SA44 DNA aptamer and random aptamer (100 nM) were incubated separately with live U87MG, 1321N1, SVGP12, T98G, T24 and MCF-7 cells at 37 °C (5 % CO<sub>2</sub>) for 90 minutes. Untreated cells were incubated with complete growth medium alone. The blue curve represents the background mean fluorescence intensity (MFI) of the untreated cells (control). The green and red curve represents the MFI (uptake) of the cells treated with random aptamer and SA44 DNA aptamer respectively, on U87MG (A), 1321N1 (B) SVGP12 (C), T98G (D), T24 (E), and MCF-7 cells (F).

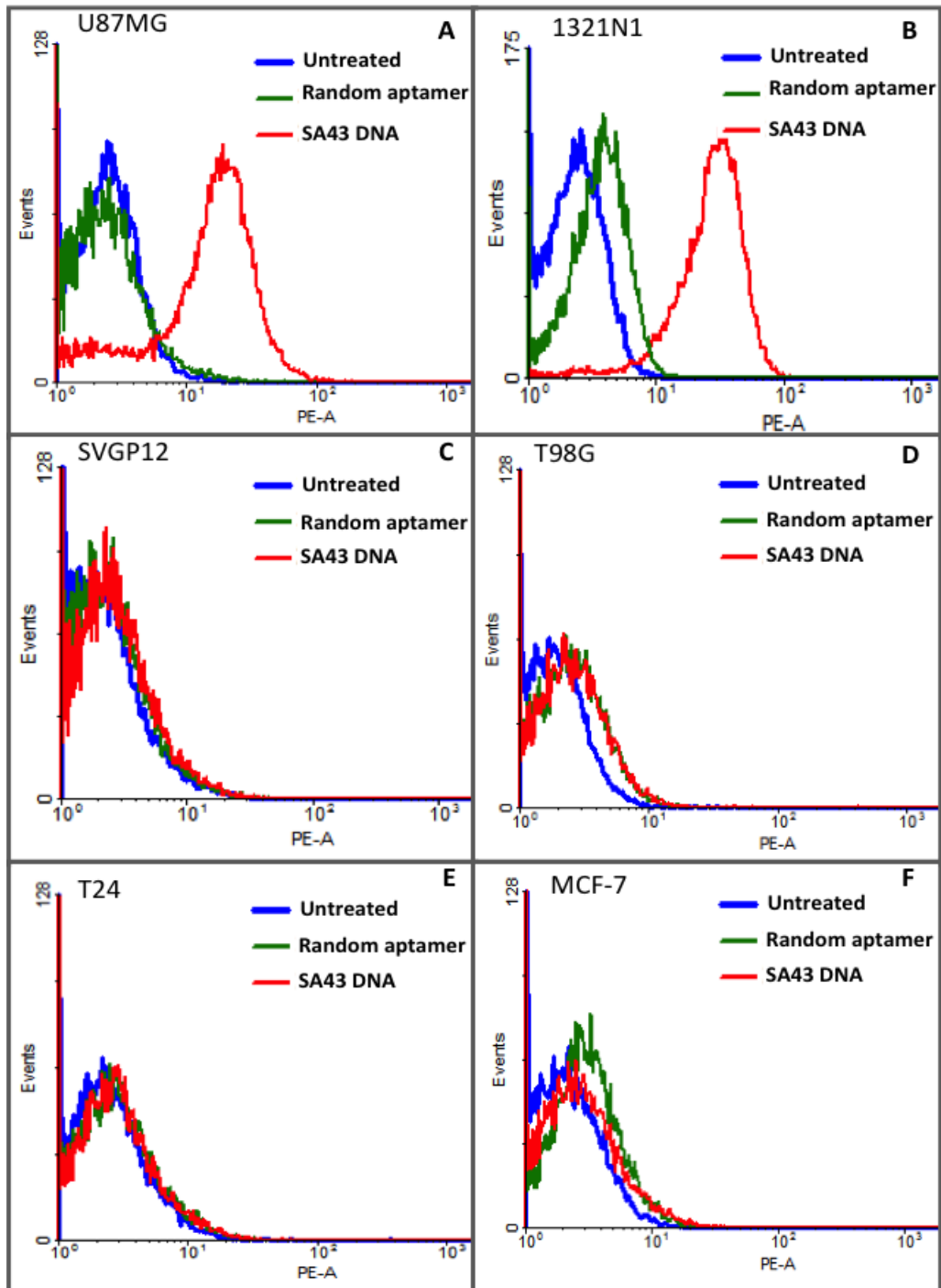


**Figure 4.20 Representative flow cytometry profiles of the uptake of SA43 DNA on various cell lines.** Cy3 labelled SA43 DNA aptamer and random aptamer (100 nM) were incubated separately with live U87MG, 1321N1, SVGP12, T98G, T24 and MCF-7 cells at 37 °C (5 % CO<sub>2</sub>) for 90 minutes. Untreated cells were incubated with complete growth medium alone. The blue curve represents the background mean fluorescence intensity (MFI) of the untreated cells (control). The green and red curve represents the MFI (uptake) of the cells treated with random aptamer and SA43 DNA aptamer respectively, on U87MG (A), 1321N1 (B) SVGP12 (C), T98G (D), T24 (E), and MCF-7 cells (F).

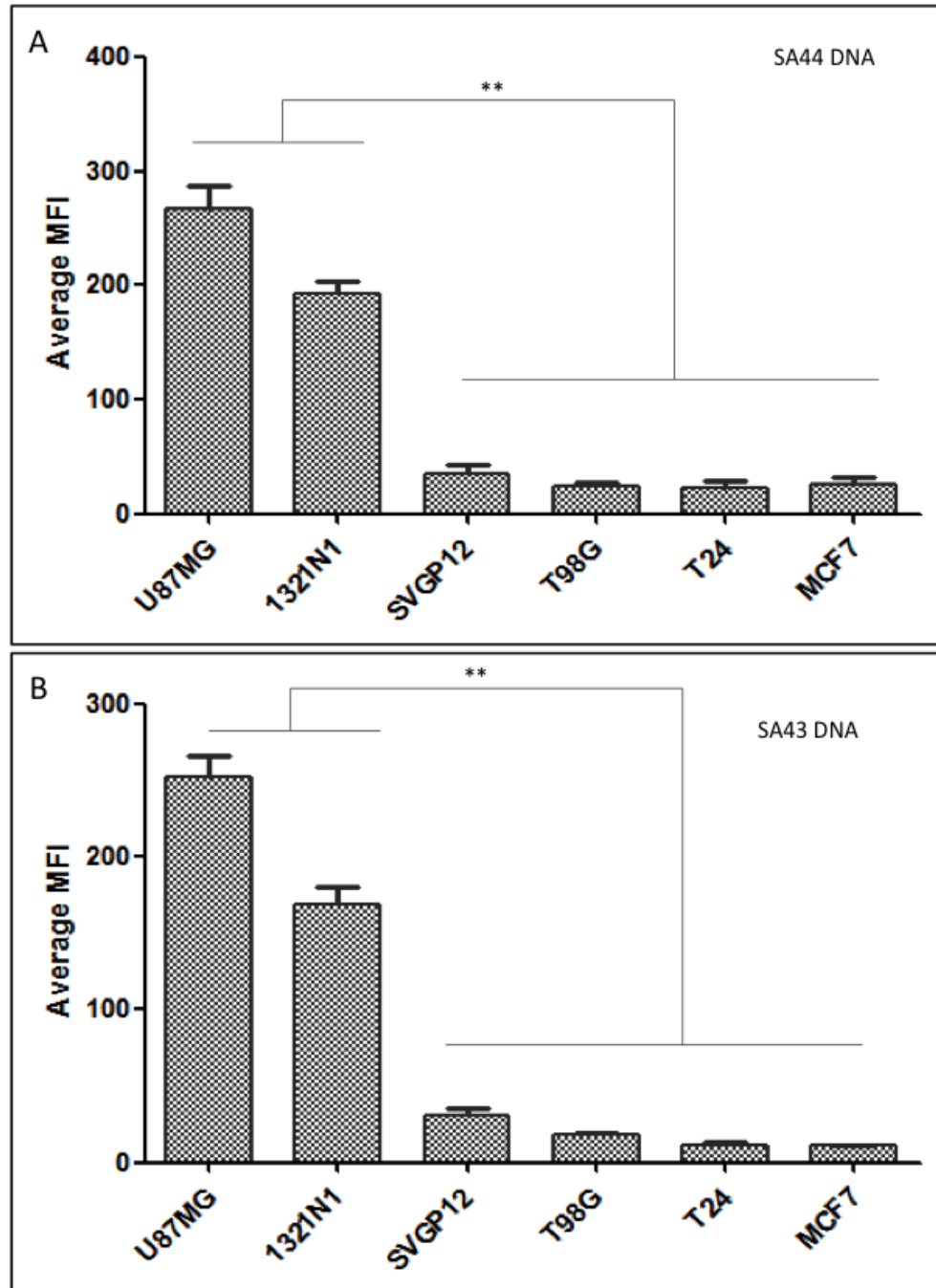


**Figure 4.21 Comparative binding selectivity of aptamer SA44 DNA and SA43 DNA across various cell types.** Binding selectivity was measured using 100 nM concentration of SA43 DNA (A) and SA43 DNA (B) aptamer. The background MFI values for the random aptamer treated cells were subtracted. Statistical significance of the differences in MFI values of SA44 DNA and SA43 DNA between U87MG and 1321N1 versus SVGP12, T98G, T24, and MCF-7 referred to its high binding selectivity for U87MG and 1321N1 cells (\*\* =  $p < 0.01$ ). No statistical difference was observed between U87MG and 1321N1 cells for both the aptamers ( $p > 0.05$ ;  $n = 3$ ).

#### 4.2.6 Summary of results for the binding selectivity of DNA and RNA aptamers

Following analysis of the images obtained from the confocal microscopy and quantitative data obtained from flow cytometry, a comparative summary of all aptamers on all cell lines was performed. The overall results were expressed by addition of data from confocal (strong binding) and flow cytometry (significant selectivity with high uptake) analysis (Table 4.1).

**Table 4.1 Summary of uptake and binding selectivity of aptamers on various cell types.**

	U87MG	1321N1	SVGP12	T98G	T24	MCF-7
SA44 RNA	++	++	-	-	-	-
SA43 RNA	++	++	-	-	-	-
SA56 RNA	++	++	+	-	-	-
SA44 DNA	++	++	-	-	-	-
SA43 DNA	++	++	-	-	-	-
++ higher binding (+ confocal and + flow cytometry), + moderate binding (+ confocal and - flow cytometry or - confocal and + flow cytometry) - negligible binding (- confocal and - flow cytometry).						

The overall data suggested that the shortened aptamers SA44 RNA and SA43 RNA and the DNA homologs showed similar and high binding selectivity to U87MG and 1321N1 cells compared to the other cell types. This indicated they were highly specific for tumorigenic glioma cells. SA56 RNA showed strong binding selectivity to tumorigenic glioma cells, however, binding was also observed in non-cancerous SVGP12 cells. This indicated that SA56 RNA was non-specific to glioma.

### 4.3 Discussion

It has previously been hypothesised that aptamers can be utilised for cancer detection (Shangguan *et al.*, 2008; Cerchia *et al.*, 2009; Bayrac *et al.*, 2012; Kang *et al.*, 2012; Jimenez *et al.*, 2012; Li *et al.*, 2014). The main aim of this chapter was to analyse the binding affinity and selectivity of the shortened aptamers to glioma cells. All three full length aptamers (GL44, GL43 and GL56) adopted from Cerchia *et al.*, (2009) showed complex 2D secondary structures, including four defined conserved stem-loop structures and negative  $\Delta G$  as predicted by the M-Fold program, which indicated that these stem-loop structures may be crucial for binding with higher stability and affinity (in nano-molar concentrations) to their target tumorigenic glioma cells. Shortened aptamers SA44 RNA, SA43 RNA and SA56 RNA were shown to have two stem-loop structures and negative  $\Delta G$  as predicted by M-Fold program, which indicated that the aptamers were capable of folding into complex tertiary structure with higher stability that is necessary for binding to the target molecule. It has been established that the lower the  $K_d$ , the higher the binding affinity of the aptamers to the targets (Cerchia *et al.*, 2009; Kang *et al.*, 2012). This was demonstrated by higher binding affinity of SA44 RNA and SA43 RNA towards U87MG cells with almost three times decrease in their  $K_d$  values as compared to the original full-length aptamers GL44 RNA and GL43 RNA. The increase in the binding affinity could be due to differences in secondary structures with nucleotides present in the stem-loops regions of shortened aptamers capable of binding to target sites with high affinity compared to those of original full-length aptamers. For example, the two stem-loop nucleotide regions in the shortened aptamers (SA) may be involved in binding to the targets on U87MG cells with more affinity than the nucleotides in four stem loop regions within the full length aptamers (GL) as predicted from the secondary structures. SA56 RNA ( $K_d$ ,  $41.48 \pm 16.95$  nM), however,

retained the same binding affinity as the full-length aptamer GL56 RNA ( $63 \pm 3$  nM), which indicated that the deletion of primer sequence of this aptamer did not alter the binding affinity to the target U87MG cells. Moreover, nucleotides “UAU” shared common regions within the stem-loops of secondary structures of GL56 and SA56 RNA aptamers, which indicated that these nucleotides might be involved in targeting U87MG cells. The results suggested that the shortened aptamers would be widely applicable, as they tightly bind to the target U87MG cells. In addition, because of the relatively small size, shortened aptamers may exhibit superior cell penetration (Hicke *et al.*, 2001).

One of the major challenges for *in vitro* targeting is the ability to direct the binding of the targeting aptamers to tumour cells instead of non-cancerous healthy cells (Bayrac *et al.*, 2011, Gao *et al.*, 2012). The aptamer specific for glioma cells compared to the other cell types can allow the specific identification of glioma without prior knowledge of any biomarkers or proteins present in the cells (Cerhcia *et al.*, 2009; Keefe *et al.*, 2010). U87MG and 1321N1 (wild-type p53, tumorigenic *in vivo*), T98G (mutant p53, non-tumorigenic *in vivo*), SVGP12 (non-cancerous foetal astrocytes), T24 (bladder cancer), and MCF-7 (breast cancer) cells were chosen to be the best model to analyse the binding selectivity of the shortened aptamers because of the well-defined origin and defined proliferative growth rate of the cells (chapter 3).

The tumour cell recognition was demonstrated by both confocal imaging and flow cytometry using Cy3 labelled aptamers at 100 nM concentration ( $K_d$  values reached saturation point). U87MG and 1321N1 cells exhibited intense Cy3-fluorescence staining in the cytoplasm after incubation with SA44 RNA and SA43 RNA aptamers, while the SVGP12 cells displayed no detectable fluorescence. Interestingly, T98G also

showed negligible uptake indicating the aptamers were specific to highly tumorigenic glioma cells and this was consistent with the GL44 and GL43 counterparts in Cerchia *et al.*, (2009). This indicated, although there is a difference in the binding affinity between the full length (GL44 and GL43) and shortened aptamers (SA44 and SA43), the similar cell type selectivity for U87MG and not for T98G demonstrates that the targets could be the same for both the aptamers (Cerchia *et al.*, 2009). Moreover, SA44 and SA43 RNA showed negligible uptake on bladder cancer and breast cancer cells, again, indicating selectivity towards tumorigenic glioma cells. Together, these results showed that the shortened aptamers SA44 RNA and SA43 RNA showed preferential binding to tumorigenic glioma cells. Similarly, SA56 RNA showed higher uptake on U87MG and 1321N1; however, it also showed moderate uptake in the cytoplasm of SVGP12, T98G and T24 cells and negligible uptake in MCF-7 cells. The overall confocal data suggested that either the binding of these aptamers could depend on the target present in cancer cells, or that malignant tumours from different origins have different malignant-related molecular determinants which are not recognised by the aptamers used in the study.

Further exploration of specific cell recognition by the selected aptamers was demonstrated by flow cytometry, which offered significant advantage in terms of quantification and statistical power compared to confocal microscopy. Similar to the findings observed in confocal microscopy, the flow cytometry results overall demonstrated that aptamers SA44 RNA and SA43 RNA showed higher uptake and significant binding selectivity ( $p < 0.05$ ) to tumorigenic glioma cells compared to the non-cancerous and non-glial cells. SA56 RNA aptamer however, showed no such selectivity for glioma cells U87MG and 1321N1 compared to the non-cancerous cells

SVGP12 ( $p > 0.05$ ). This quantitative data established that aptamers SA44 and SA43 only recognised targets presented on the 1321N1 and U87MG cells and therefore, showed potential as specific molecular probes for glioma tumour analysis. The results were comparable with other related studies, where aptamers have been selected using live cells as their target with selectivity for certain cell types. These aptamers were able to interact with particular molecules over-expressed on the cell surface of tumour cells (Pestourie *et al.*, 2005; Chu *et al.*, 2006; Shangguan *et al.*, 2008; Jimenez *et al.*, 2012; Kang *et al.*, 2012).

Similar binding affinity was observed for SA44 DNA ( $K_d$ ,  $21.11 \pm 3.30$  nM) and SA43 DNA ( $K_d$ ,  $21.56 \pm 4.60$  nM) for U87MG cells compared to the RNA versions. Moreover, SA44 DNA and SA43 DNA were highly selective for tumorigenic glioma cells. The study also proved that there was no difference between the RNA aptamers and the DNA homologs in terms of their selectivity for glioma. Previous analyses have reported that there is very little difference between RNA and DNA aptamers in terms of affinity and specificity (Gold, 1995). Some studies however, reported major differences in their affinity and specificity. For example, Lauhon and Szostak demonstrated that the DNA form of an RNA aptamer for riboflavin could still bind its target, albeit with lower affinity than RNA (Lauhon and Szostak, 1995). Similarly, in the study by Travascio *et al.*, (1999) a hemin-binding deoxyribozyme was converted to a ribozyme with a 30-fold loss of binding affinity to its targets. In another experiment, binding was abolished in the DNA homolog of the RNA aptamer for ATP (Dieckmann *et al.*, 1999). DNA and RNA vary based on their individual nucleotides: uracil being associated with RNA and thymine with DNA. Furthermore, the presence of the 2'-hydroxyl in RNA leading to  $\alpha$ -form structure in double helical regions, whereas, the absence of 2'-hydroxyl in DNA

leading to  $\beta$ -form structure can affect the major and minor groove widths, the rise per base pair, the average axial diameter, and the twist angle in the final structure (Walsh and DeRosa, 2009). This in turn could affect the overall binding of the RNA and DNA aptamers to the targets. This could be the reason why single stranded DNA aptamers exhibits a propensity for forming intricate tertiary structures that is not comparable to that of RNA when binding to its target even though they are similar in basic structure. In this study, both RNA and their DNA homologues showed similar affinity and selectivity for tumorigenic glioma cells indicating that the putative target could be similar and highly accessible for both the types. DNA aptamers have shown greater stability than RNA aptamers and therefore are less susceptible to degradation because of the absence of the hydroxyl (OH) group in DNA (Min *et al.*, 2008; Dupont *et al.*, 2010). Given the ease of synthesis, reduced cost, potentially increased stability of DNA aptamer compared to its RNA homologue, and similar binding selectivity towards glioma, DNA versions of the shortened RNA aptamers were selected for further experiments.

From the study, it can be concluded that the shortened aptamers SA44 RNA and SA43 RNA and the DNA homologs were highly selective for glioma cells, presumably due to selective affinity between the aptamers and their targets for glioma. The aptamers could have been taken up by the tumorigenic glioma cells via active transport because of the saturation of Cy3 fluorescence intensity (MFI) in U87MG cells at higher concentrations indicating an active process. If the uptake was through passive transport then MFI values would increase linearly. The saturable activity, selective binding and cytoplasmic localisation of the aptamers to tumorigenic glioma cells at physiological temperature together supported the hypothesis that the aptamers were actively transported and may

target the cell surface receptors that are overexpressed in glioma which allowed aptamers to internalise via an unknown endocytic pathway. In addition, the cells after incubation with aptamers, were challenged with protease trypsin to collect the cells for flow cytometry which could potentially degrade all aptamers bound to the cell surface receptors. Therefore, the signal (MFI) was from the cells that allowed the aptamers to internalise. In addition, internalisation of the aptamers also highlighted a question if the aptamers have had any effect on the cell viability. All of these inferences have been addressed in next chapter.

## CHAPTER 5 GLIOMA SPECIFIC INTERNALISATION STUDY OF THE DNA APTAMERS

### 5.1 Introduction

Aptamers which bind to cell-surface proteins such as cancer epitopes can be used for imaging applications and can differentiate between closely related cell types, such as non-cancerous and tumour cells (Hicke *et al.*, 2001; Hicke *et al.*, 2006; Cerchia *et al.*, 2009). Aptamers have been shown to inhibit cell growth on their own (Eugene *et al.*, 2006) or by conjugation with other moieties such as drug loaded nanoparticles (Li *et al.*, 2014). In addition, aptamers with cell-internalising properties can be developed for delivery of therapeutic agents such as small molecule drugs, radioisotopes, toxins, miRNAs and siRNAs into target cells (Dhar *et al.*, 2008; Cao *et al.*, 2009; Keefe *et al.*, 2010; Rocky *et al.*, 2011). The latter strategy is likely to increase efficacy as well as reduce the potential unwanted toxic effects of the therapy because the aptamers would deliver the drug selectively to the cancerous cells while sparing the non-cancerous healthy cells.

Several inherent factors such as the charge and size of the aptamer present potential barriers for cellular uptake. The presence of the negatively charged phosphate backbone in nucleic acid molecules could result in electrostatic repulsion from the negatively charged cell surface, which could be the primary cause of inadequate uptake into the cells. Moreover, aptamers longer than 25 bases have shown difficulty crossing the cell membrane because of the tendency to self hybridise thereby affecting the cellular uptake (Patil *et al.*, 2005). It would be highly desirable to develop aptamers that can be internalised directly into the cells in order to further explore the *in vivo* applications.

The previous chapter demonstrated that SA44 and SA43 DNA aptamers significantly bound to tumorigenic glioma cells with high affinity and selectivity compared to the control cells. Binding with high selectivity to U87MG and 1321N1 suggested a possible common cell surface target that is present in these two cell lines. Confocal data also demonstrated that these aptamers were localised in the cytoplasm of the target cells, suggesting that the aptamers had internalised into the cells. All of these experiments were performed with aptamers incubated on live cells under similar conditions such as physiological temperature (37 °C) for 90 minutes and before exposing the cells to protease (trypsin). To elucidate and confirm the uptake process, there was a need to investigate the uptake at 4 °C. If the rate of uptake was slower compared to the rate of uptake at 37 °C this would be highly indicative of an active transport process. This finding would also support the data obtained from concentration dependent saturation process and glioma cell selectivity of the aptamers, which indicated active transport from the previous chapter.

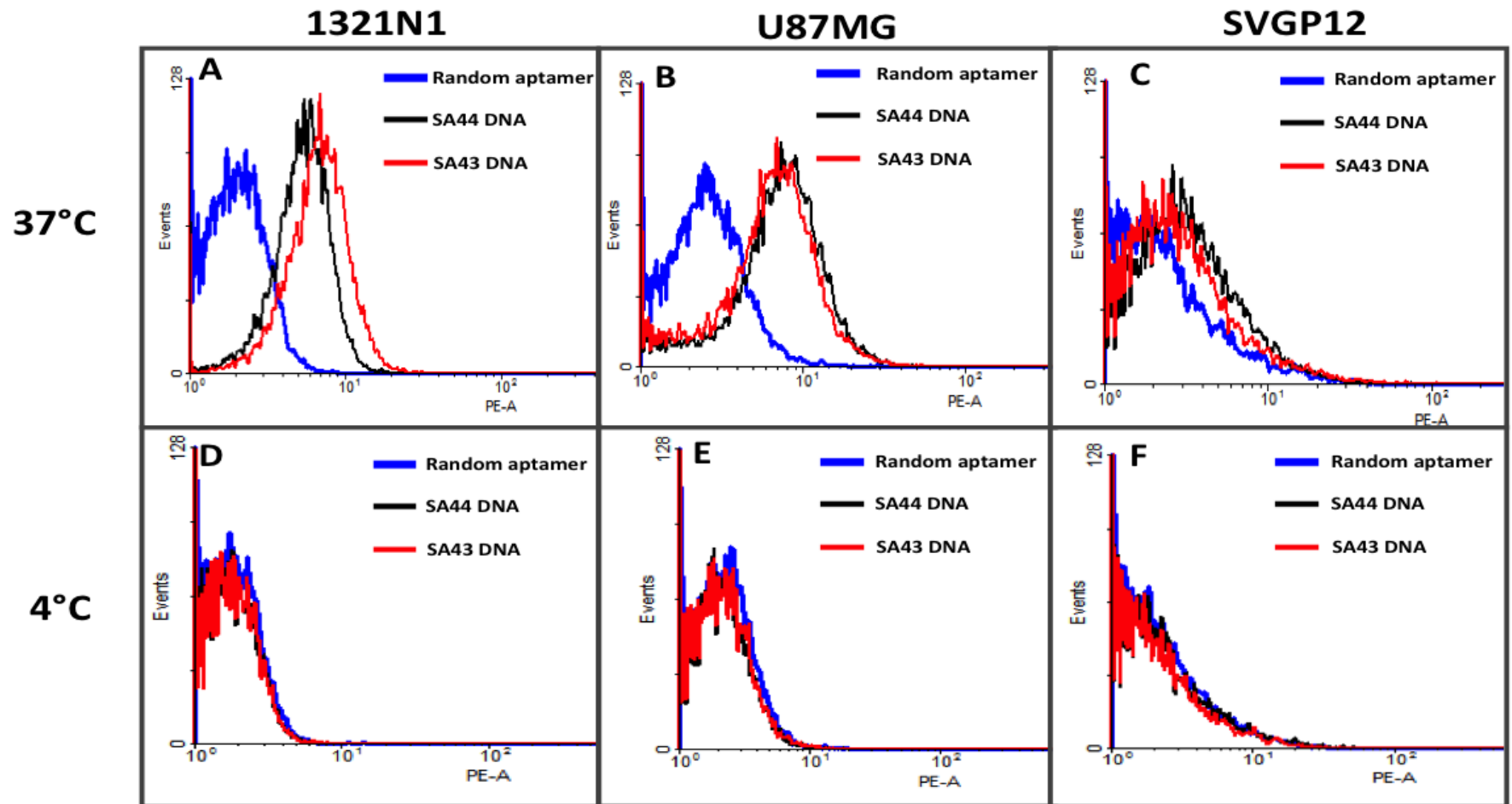
In addition, pre-trypsinisation treatment to cells was performed to distinguish whether the aptamer bound to a cell surface target ligand and follow internalisation by receptor-mediated pathway or an intracellular target ligand which could then follow distinct endocytic pathway other than receptor mediated. The aim of this chapter was therefore, to obtain more information underlying the uptake mechanism of the lead aptamers SA44 and SA43 DNA. In addition, the potential for the shortened aptamers to inhibit cell proliferation was assessed by performing a viability assay.

## 5.2 Results

### 5.2.1 Effect of temperature on aptamer binding to cells

A flow cytometry based assay was performed to monitor the uptake of aptamers that bound to the glioma cells (Section 2.7.2). Aptamers were added to live cells either at 37 °C (optimal for active transport) or at 4 °C (where active uptake is dormant) (Zueva *et al.*, 2010; Kang *et al.*, 2012) and were incubated for 90 minutes. A two-way ANOVA test revealed that both aptamers SA44 DNA and SA43 DNA showed significantly higher uptake in U87MG and 1321N1 cells compared to SVGP12 cells at 37 °C ( $p < 0.01$ ) (Figures 5.1 and 5.2). Cells treated at 4 °C showed no uptake in all the cell lines.

**Figure 5.1 Representative flow cytometry profiles showing temperature dependent uptake of SA44 DNA and SA43 DNA.** Cy3 labelled SA44 DNA and SA43 DNA aptamers (100 nM) were incubated separately with live U87MG, 1321N1 and SVGP12 cells at 37 °C (5 % CO<sub>2</sub>) or 4°C for 90 minutes. The blue curve represents the background mean fluorescence intensity (MFI) of the random aptamer. The black and red curve represents the MFI (uptake) of the cells treated with SA44 DNA and SA43 DNA aptamer, respectively. **A, B, and C** Uptake of SA44 DNA and SA43 DNA on U87MG, 1321N1, and SVGP12 cells, respectively at 37 °C. **D, E and F** Negligible uptake of SA44 DNA and SA43 DNA on U87MG, 1321N1 and SVGP12 cells, respectively at 4 °C.



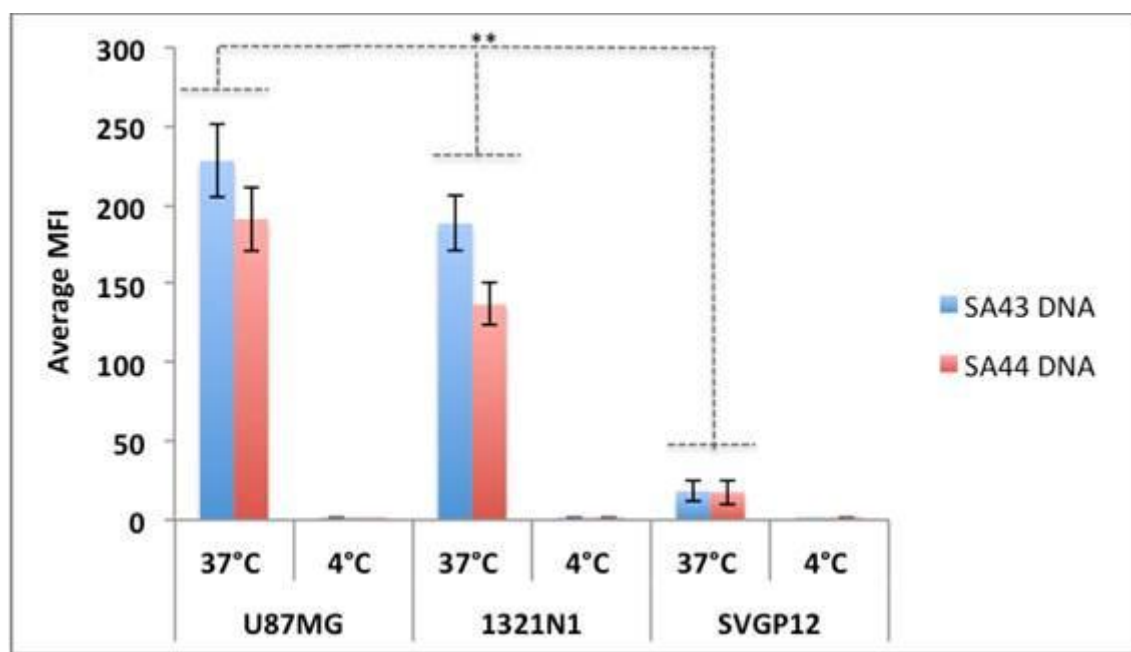


**Figure 5.2 Temperature dependent uptake of aptamer SA43 DNA and SA44 DNA.** Uptake was measured using 100 nM concentration of SA43 DNA and SA44 DNA aptamer. The background MFI values for the random aptamer (control) on corresponding cells were subtracted. Statistical significance of the differences in MFI values of SA43 DNA and SA44 DNA referred to its high uptake for U87MG and 1321N1 cells at 37 °C compared to 4 °C by a two way ANOVA test (\*\*=  $p < 0.01$ ). All experiments were repeated at least three times. Data are mean of three independent samples; bars, SEM.

### **5.2.2 Effect of trypsin protease digestion on aptamers binding to cells**

To test whether the targets of the aptamers were mainly cell surface receptors, which are membrane bound or whether the targets were intracellular, the cells were treated with protease (0.25 % trypsin) for 10 mins before adding the aptamer to the cells (Section 2.7.3). Only those aptamers that had been internalised without the receptor-mediated process remained after trypsin treatment and were detected by flow cytometry. As a control for internalisation, SVGP12 cells were used for negative binding. As shown in figures 5.3 and 5.4 the uptake of the aptamers SA44 and SA43 was not affected before or after trypsin treatment on U87MG, 1321N1, and SVGP12 cells. There was a statistical difference in the uptake of SA44 and SA43 DNA on U87MG, 1321N1 compared to SVGP12 both before and after trypsin treatment (\*\* $p < 0.01$ ).

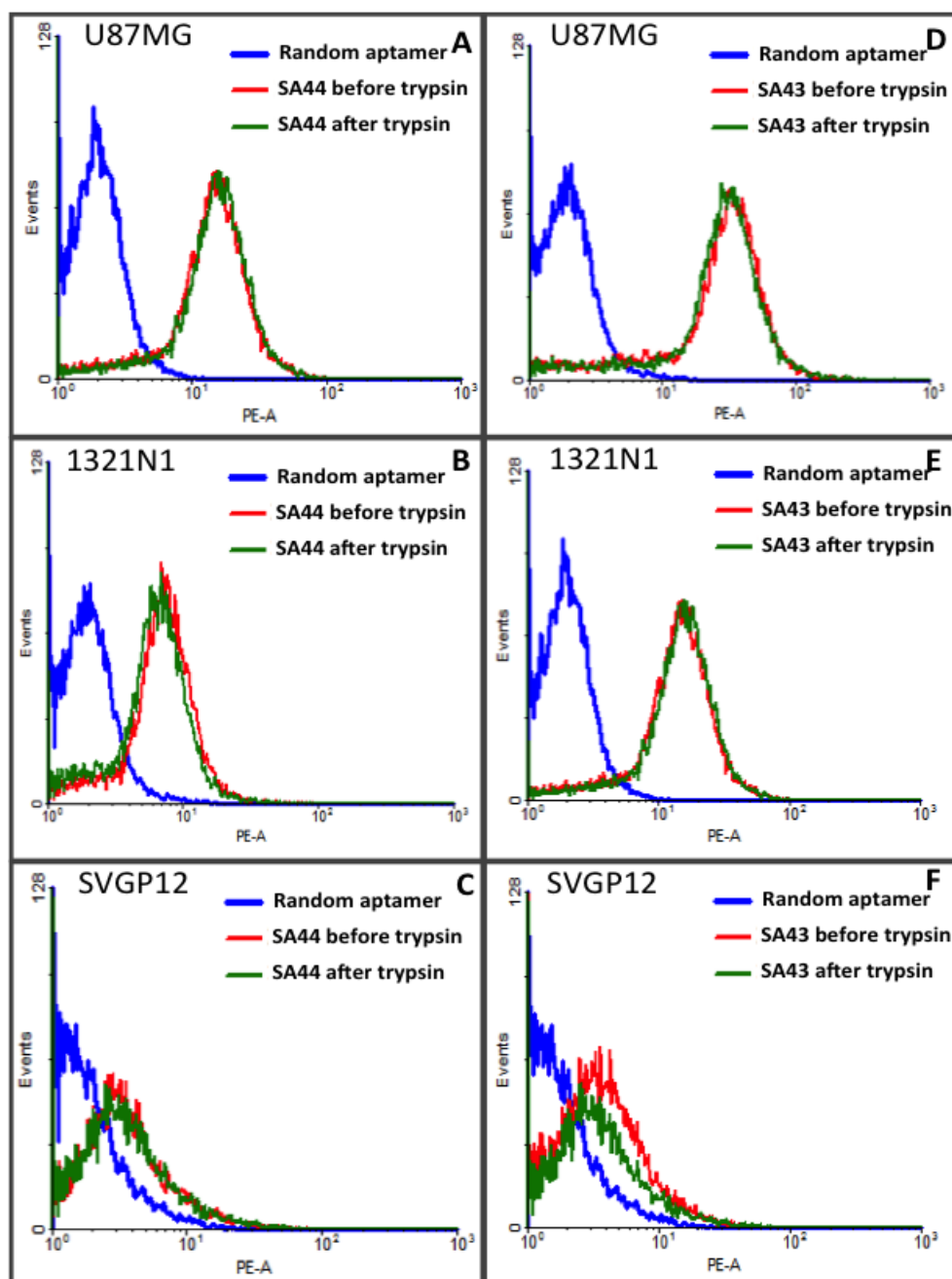


**Figure 5.3 Representative flow cytometry profiles showing the effect of trypsin protease digestion on aptamers binding to cells.** Cy3 labelled SA44 DNA and SA43 DNA (100 nM) were incubated with live U87MG, 1321N1 and SVGP12 cells at 37 °C (5 % CO<sub>2</sub>) for 90 minutes before or after treatment with 0.25 % trypsin (10 mins). The blue curve represented the background mean fluorescence intensity (MFI) of the random aptamer. The red and green curve represented the MFI (uptake) of the cells incubated with SA44 DNA aptamer before and after trypsin treatment, respectively. **A**, **B**, and **C** No difference in SA44 DNA uptake before and after trypsin treatment on U87MG, 1321N1, and SVGP12 cells respectively. **D**, **E**, and **F** No difference in SA43 DNA uptake before and after trypsin treatment on U87MG, 1321N1, and SVGP12 cells respectively.

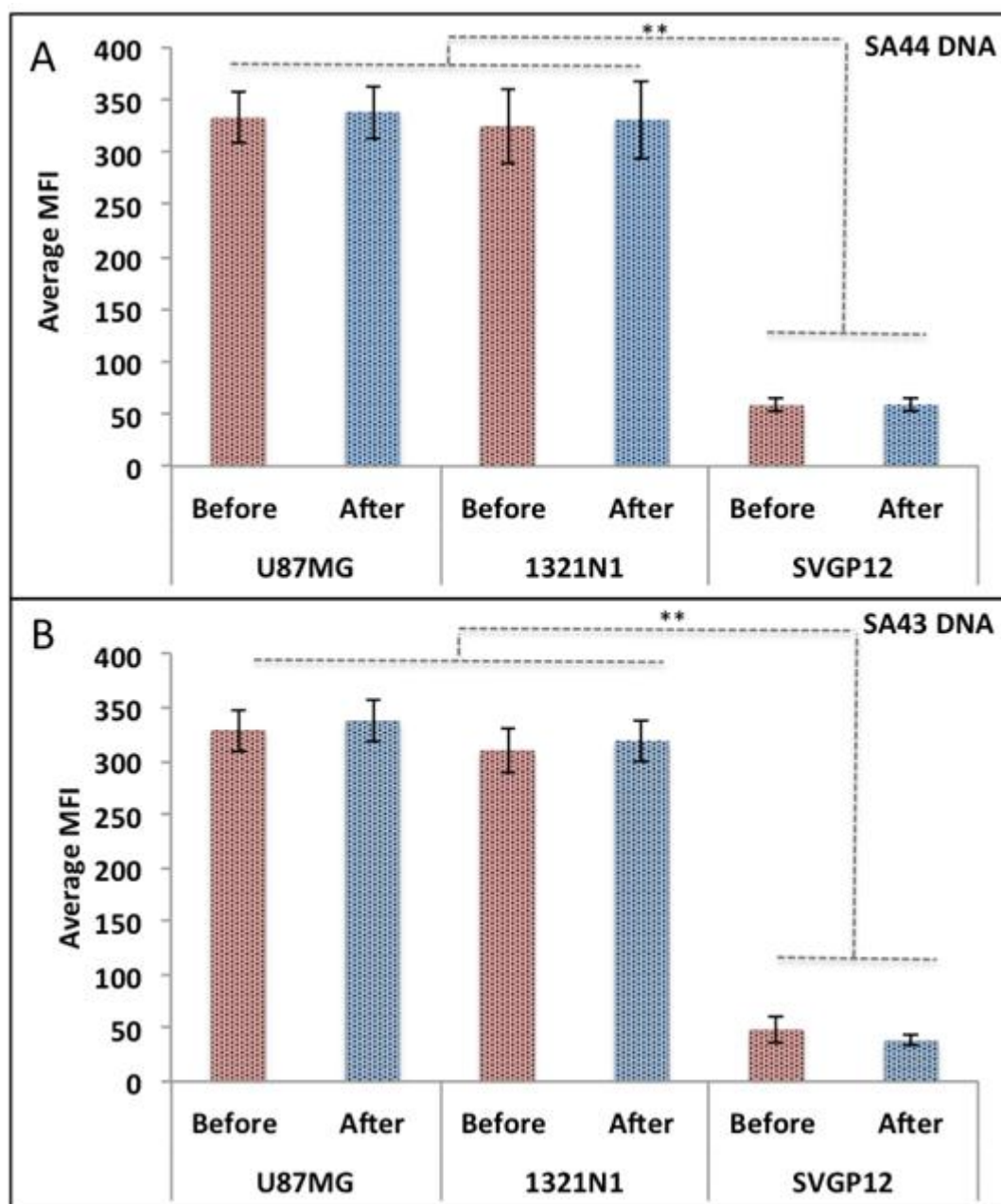


**Figure 5.4 Comparative effect of trypsin treatment on internalisation potential of SA44 DNA and SA43 DNA on U87MG, 1321N1, and SVGP12 cells.** Uptake was measured using 100 nM concentration of SA43 DNA and SA44 DNA aptamer. The background MFI values of random aptamer (control) on corresponding cells were subtracted. ANOVA test revealed no statistical significance of the differences in MFI values of SA43 DNA (A), and SA44 DNA (B) when incubated before and after trypsin treatment on U87MG, 1321N1 and SVGP12 cells ( $p > 0.05$ ). Statistical difference was observed in the internalisation of SA44 and SA43 DNA on before and after trypsin treated U87MG, 1321N1 compared to SVGP12 cells (\*\* $p < 0.01$ ). All experiments were repeated at least three times. Data are mean of three independent samples; bars, SEM.

### 5.2.3 Effect of aptamers on cell viability

After establishing the internalisation properties of aptamers, it was important to assess the function of SA44 DNA and SA43 DNA aptamers in terms of their effect on cell viability. Cells were incubated with 20 nM, 100 nM, 500 nM and 1000 nM of each aptamer and monitored for 24, 48 and 72 hours for cell viability using the presto blue assay (Section 2.8). To investigate the role of the DNA aptamers on cell viability, cells were treated with aptamers and viability was compared to the known cytotoxic cisplatin as a positive control. SA44 DNA and SA43 DNA showed the highest cell viability (approximately 100 %) and no significant change in viability was observed throughout the 3-day period (Figures 5.5 and 5.6). Microscopic observations also revealed that all cells appeared healthy after aptamer treatments without noticeable morphological changes (data not shown). Cells treated with cisplatin, 10  $\mu$ M (positive control) showed significant decrease in cell viability at 72 hours.

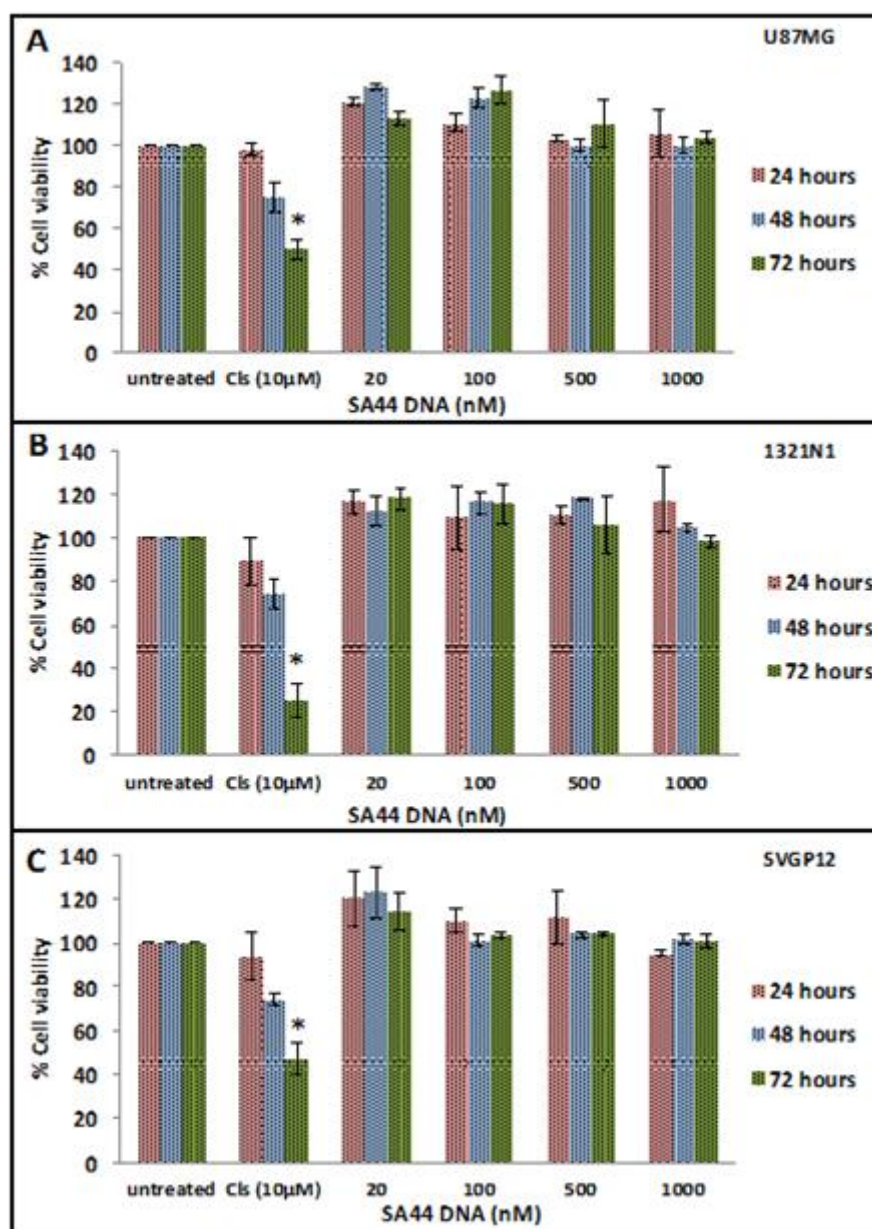


**Figure 5.5 Effect of SA44 DNA on cell viability using Presto blue assay.** Live cells U87MG, 1321N1 and SVGP12 were incubated with biotin tagged SA44 DNA aptamer at different concentrations such as 20 nM, 100 nM, 500 nM and 1000 nM at 37 °C (5 % CO<sub>2</sub>) and monitored for 24, 48 and 72 hours for cell viability using presto blue assay. Cisplatin at 10 μM concentration was used as positive control. A two-way ANOVA test was performed to analyse the difference in the percentage cell viability of the SA44 DNA against cisplatin and untreated controls. **A**, **B**, and **C** No statistical difference was observed between the percentage cell viability of SA44 DNA and untreated controls for U87MG, 1321N1 and SVGP12 cells, respectively ( $p > 0.05$ ). Cisplatin showed a significant decrease in the percentage cell viability at 72 hours when compared to SA44 DNA and untreated control (\*  $p < 0.05$ ). All experiments were repeated at least three times. Data are mean of three independent samples; bars, SD.

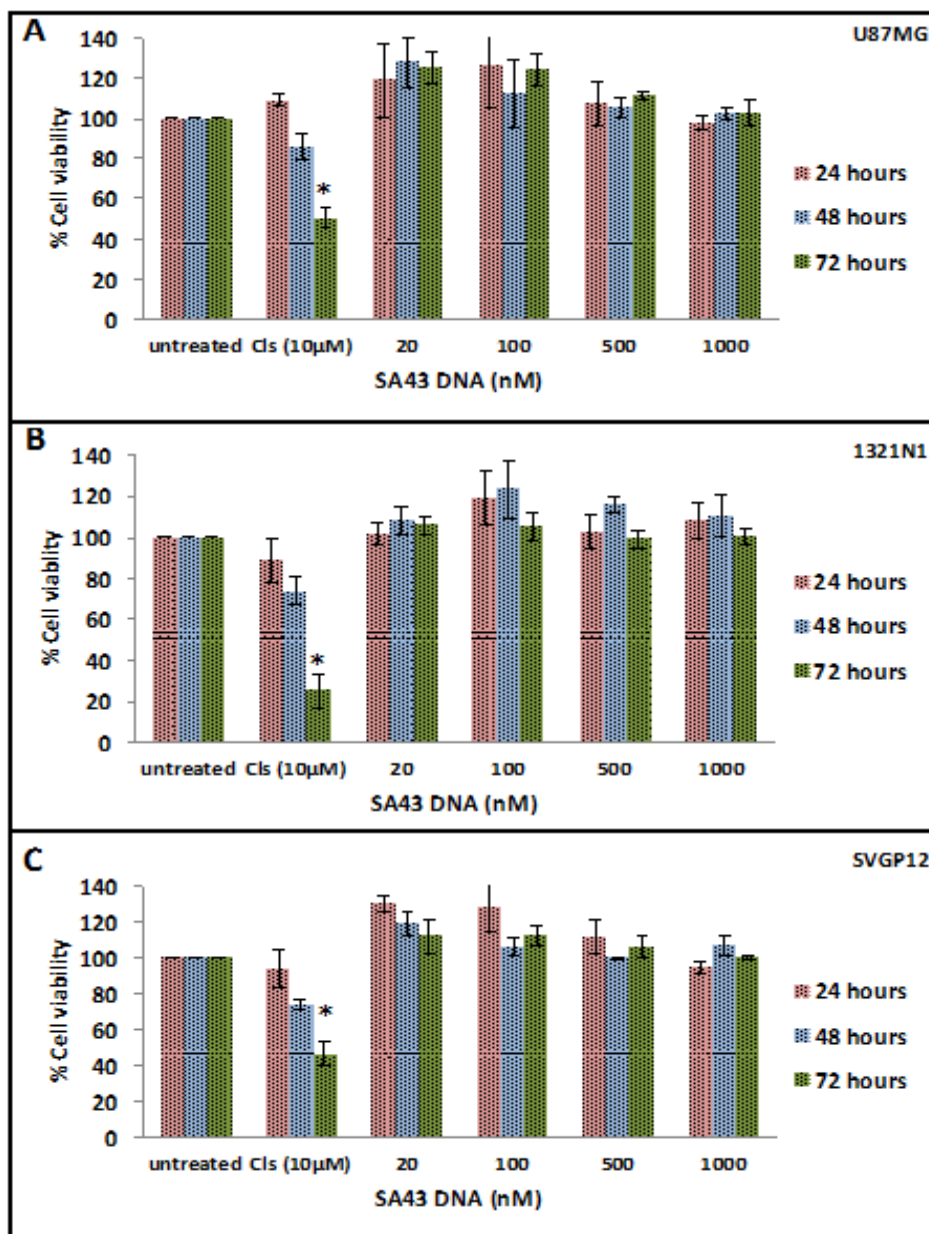


**Figure 5.6 Effect of SA43 DNA on cell viability using Presto blue assay.** Live cells U87MG, 1321N1 and SVGP12 were incubated with biotin tagged SA44 DNA aptamer at different concentrations such as 20 nM, 100 nM, 500 nM and 1000 nM at 37 °C (5 % CO<sub>2</sub>) and monitored for 24, 48 and 72 hours for cell viability using presto blue assay. Cisplatin at 10  $\mu$ M concentration was used as positive control. A two-way ANOVA test was performed to analyse the difference in the percentage cell viability of the SA43 DNA against cisplatin and untreated controls. A, B, and C No statistical difference was observed between the percentage cell viability of SA43 DNA and untreated controls for U87MG, 1321N1 and SVGP12 cells, respectively ( $p > 0.05$ ). Cisplatin showed a significant decrease in the percentage cell viability at 72 hours when compared to SA43 DNA and untreated control (\* =  $p < 0.05$ ). All experiments were repeated at least three times. Data are mean of three independent samples; bars, SD.

### 5.3 Discussion

By assessing the cellular distribution of aptamers by confocal microscopy in the previous chapter, there was a strong association with the cytoplasm, suggesting intracellular uptake. The objective of this chapter was to better understand the mechanism of cell uptake of the aptamers and to highlight the potential of oligonucleotides to serve as intracellular delivery agents to tumour cells. This was achieved by a flow cytometry quantitative method that allowed accurate measurement of aptamer internalisation. To explore this mechanism further, the influence of low temperature and protease activity on cellular uptake of the aptamers was determined.

Active and passive transport of any test molecule or drug by the cells have been assessed with commonly used method of parallel incubations at 37 °C and 4 °C, as active transport proteins are highly temperature dependent (Komai *et al.*, 1992; Thomas *et al.*, 2004). Although active transport is inhibited at low temperatures, passive processes might also be altered to some degree as membrane fluidity decreases (Neuhoff *et al.*, 2005). Preferably, temperature dependence studies should be combined with a concentration dependent study to assess whether transport is saturated at higher concentration of the test molecule or drug (Poirier *et al.*, 2008; Pang *et al.*, 2010). The study initially suggested that the uptake of aptamers could be via active transport by showing the saturation process and selectivity of aptamers to glioma cells at physiological temperature (37 °C) (Chapter 4, section 4.2.1). In order to confirm the active uptake, aptamers were incubated at 4 °C because active transport is inhibited at this temperature. As expected from an energy driven process, no internalisation was observed while the cells incubated at 4 °C; on the contrary, aptamers were rapidly internalised at 37 °C. Both SA44 and SA43 DNA aptamers retained specificity for

tumorigenic glioma cells at 37 °C. The results provided strong evidence that the uptake of aptamers depended on a cellular process related to active transport assisted by enzymes requiring energy.

Methods for assessing cell specific internalisation of aptamers have been crucial to the development of powerful reagents capable of delivering therapeutics such as siRNAs or small molecule drugs to the target cells. In previous studies to confirm internalisation, trypsin treatment has shown to be a convenient and straightforward method to achieve this goal (Huang *et al.*, 2009; Orava *et al.*, 2010; Van Simaey *et al.*, 2010; Kang *et al.*, 2012; Zhang *et al.*, 2012<sup>a</sup>; Wu *et al.*, 2014). Cell trypsinisation causes a loss of extracellular components of membrane proteins, which are then restored after several hours after the cells have been replated at lower density (Huang *et al.*, 2010). This was in agreement with other related studies where expression of cell membrane proteins such as HSP 60, HSP 90 beta, protein disulphide isomerase, and integrins reduced drastically after trypsinisation which were recovered within 24 hours after replating cells (Cruz *et al.*, 1997; Huang *et al.*, 2010; Sutradhar *et al.*, 2010).

Using trypsin treatment, numerous aptamers have shown to be selective for cell surface targets (Hicke *et al.*, 2001; Hicke *et al.*, 2006; Kang *et al.*, 2012; Xiao *et al.*, 2008; Zhou and Rossi, 2009; Zhang *et al.*, 2012). The confirmation of aptamer internalisation requires that aptamers bound to the cell surface be removed. Previous chapter have detailed experiments whereby aptamer was incubated with live cells and then trypsinised (for flow cytometry) to remove any cell surface bound aptamers. Only those aptamers that have been internalized remained and were detected by flow cytometry (Figure 5.7, A). The study initially hypothesised that the SA44 and SA43 DNA aptamer

may be binding to cell surface receptors, which may help the aptamer to internalize via a receptor-mediated endocytic pathway when considered with the saturation process data (Chapter 4, section 4.2.4). The question arose whether the cell surface receptors were involved in the internalisation of the aptamers or whether the aptamers entered the cells without the assistance of cell-surface receptors. Prior cleavage with trypsin would abrogate internalisation of the aptamers if the cell-surface receptors were involved. The internalisation potential of SA44 and SA43 DNA even after the cell-surface receptors were cleaved by trypsin (aptamer incubation after trypsin treatment) suggested that the aptamer may have internalised via some distinct pathway other than receptor mediated endocytic pathway and the target was mainly intracellular (Figure 5.7, B), however, further studies warrant to confirm the mechanism (discussed in chapter 8).

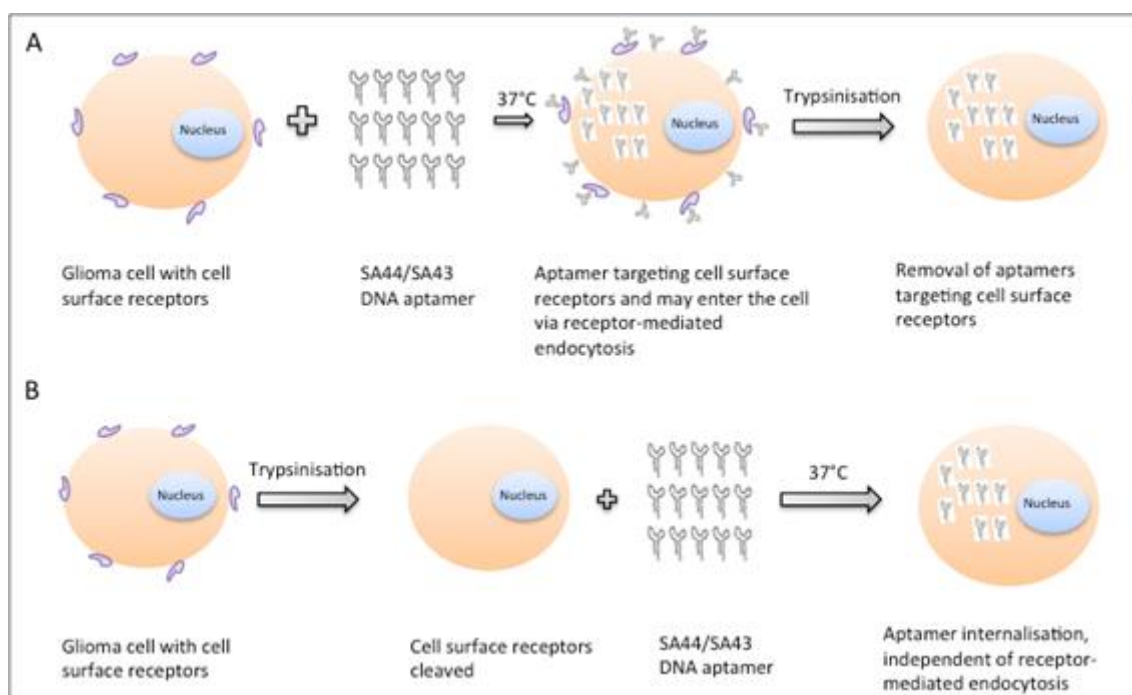


**Figure 5.7 Internalisation property of the aptamer SA43 DNA in glioma cells. A** Trypsin treatment after aptamer incubation suggesting aptamer may internalise the cells via receptor-mediated endocytosis. **B** Trypsin treatment before aptamer incubation confirmed that aptamer internalise the glioma cells via different pathway other than receptor-mediated endocytic process.

Currently, the lack of cellular selectivity of cancer chemotherapeutic drugs results in a poor toxicity profile (Lee and Nan, 2012). Studies based on aptamers have provided a proof of concept that aptamers with minimal cytotoxicity can mediate cell type-specific delivery through conjugation with toxins, chemotherapeutic drugs, imaging agents and siRNAs (Dassie *et al.*, 2009; Kim *et al.*, 2010; Li *et al.*, 2010; Kotula *et al.*, 2012). Following the internalisation of the DNA aptamers, the influence on cell viability was yet to be observed. Short-term toxicity of SA44 DNA and SA43 DNA aptamer was assessed using presto blue cell viability assay. The known cytotoxic cancer drug cisplatin has been previously shown to be taken up by cells via passive transport because of linear and non-saturable activity indicating reduced drug uptake (Eastman, 1990; Sedlestska *et al.*, 2005), however some past studies have postulated the involvement of several transporters such as Na<sup>+</sup>, K<sup>+</sup> - ATPase and members of solute carriers involved indicating some type of active facilitated transport (Arnesano *et al.*, 2013). Studies, however, have shown the cytotoxicity effect (IC<sup>50</sup>) of cisplatin to occur in a concentration dependent manner for glioma cells (Carminati *et al.*, 2010; Taghavi *et al.*, 2013). A short pilot study was therefore performed to determine the concentration dependent cytotoxicity of cisplatin on glioma cells over three days (data not shown). The results showed significant reduction in cell viability following 10 µM cisplatin treatment at 72 hours which was chosen to be ideal concentration to compare the effect of aptamer on cell viability. Cells treated with aptamers SA44 DNA and SA43 DNA showed the highest cell viability (approximately 100 %) even at high aptamer concentrations compared to the cisplatin and throughout the same incubation period. This suggested that the DNA aptamers showed no grow inhibitory effect on cells suggesting them to be non-cytotoxic at the concentrations tested and are therefore ideal

candidates for delivery of therapeutic payloads.

In summary, the selected aptamers not only showed high affinity to the target glioma cells with nanomolar dissociation constants as described in the previous chapter, but also were able to internalise into cells actively without influencing the cell viability. Although the cells had been treated with trypsin before and after aptamer application at 37 °C, an evident increase in cellular fluorescence intensity in tumour cells was shown compared to the experiments carried out at 4 °C, whereby active transport was inhibited and cellular uptake was completely eliminated. No internalisation was detected for SVGP12 cells. Together these data confirmed that the shortened aptamers are non-toxic and retained target specific cell internalisation properties and thus, can be developed into effective targeted delivery agents for glioma (Further discussed in chapter 8) (Rockey *et al.*, 2011). A definitive conclusion to confirm selective targeting of aptamers (SA44 and SA43 DNA) to glioma cells compared to non-cancerous cells by mere studying on selected cell lines is not enough because glioma as whole disease is heterogeneous, hence the study needed to be extended to glioma tissues. Clinical tissue sections are more representative of diseased state and therefore, there was a question highlighted whether these shortened aptamers could recognise and differentiate between different grades of glioma and non-cancerous brain tissues. Combining the selectivity of aptamers on live glioma cells and fixed glioma tissues will be the main highlight of the study and would prove the specificity of shortened aptamers for glioma, which will be addressed in next chapter.

## CHAPTER 6 HISTOCHEMICAL ANALYSIS OF DNA APTAMERS

### 6.1 Introduction

Data in the previous two chapters suggested that SA44 and SA43 DNA aptamers were more selective to tumorigenic glioma cells compared to the other cell types (Chapter 4 and 5). While aptamers show great promise in targeting glioma cells, there have been very limited reports of clinical applications as probes for histochemistry in studying glioma (Blank *et al.*, 2001; Kang *et al.*, 2012). This chapter explored the potential of aptamers to function clinically as a glioma-selective targeting molecule. Using histochemistry, the selected biotin conjugated aptamers were studied on various grades of glioma, meningioma, and non-cancerous patient tissue sections.

### 6.2 Results

#### 6.2.1 Binding analysis of aptamers on fixed cells.

Prior to assessing the potential of aptamers recognising targets in the fixed histological clinical tissues, binding was assessed in fixed cells. To this aim, a pilot study was initially performed to determine the binding capability of the selected biotin labelled aptamers under fixed conditions. Cells 1321N1, U87MG and SVGP12 were fixed with 4 % PFA prior to the incubation with biotin labelled aptamers (Section 2.9). As shown in figure 6.1, SA44 and SA43 DNA showed higher binding selectivity to fixed and permeabilised 1321N1 and U87MG cells compared to non-cancerous SVGP12. The binding was localised mainly in the nucleus with some cytoplasmic staining of the target glioma cells. SA56 showed no binding selectivity as nuclear staining was observed on both 1321N1 and SVGP12 cells. Random aptamer (RA) on the other hand showed negligible staining on both 1321N1 and SVGP12 cells. This indicated that the

aptamers SA44 and SA43 DNA could selectively bind to the targets on tumour cells even under fixed conditions. These results strongly suggested that the aptamers SA44 and SA43 DNA would have the potential to be used as glioma recognition molecules in clinical samples compared to SA56 DNA.

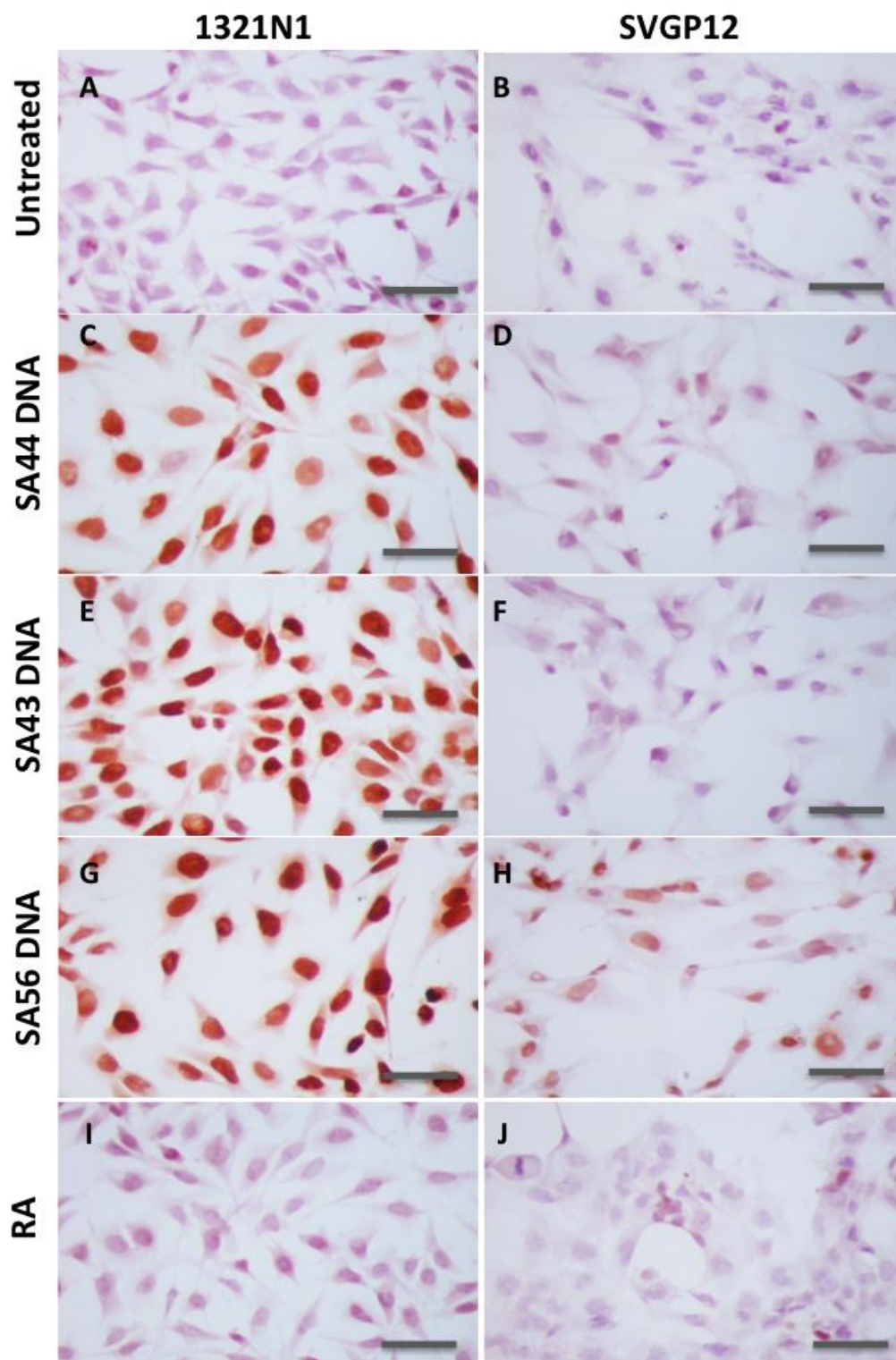


**Figure 6.1 Binding analysis of DNA aptamers on fixed cells.** The left panel shows 1321N1 tumour cells treated with no aptamer (A), SA44 DNA (C), SA43 DNA (E), SA56 DNA (G), and random aptamer (I). The right panel shows the non-cancerous SVGP12 cells treated with no aptamer (B), SA44 DNA (D), SA43 DNA (F), SA56 DNA (H), and RA (J). All scale bars, 200  $\mu$ m.

### 6.2.2 Binding analysis of aptamers on fixed clinical tissues

To determine if aptamers could be used as probes for histochemical analysis on specific grade of glioma, histochemistry (HC) was performed on fixed cancerous and non-cancerous tissue sections. The study involved screening of the biotin labelled DNA aptamers SA44, SA43, SA56, and random aptamer (RA) on serial tissue sections from the BTNW tissue bank including non-cancerous brain, grade I, grade II, grade III, grade IV glioma, and meningioma from a total of 61 patients (Section 2.10). Overall, the main aim was to identify and discriminate aptamers binding to tumour tissues and not to healthy non-cancerous tissue. Figures 6.2 – 6.4 shows representative images of tissue sections from non-cancerous and different pathological grades of glioma and meningioma tissues stained with the biotinylated DNA aptamers. A defined protocol was applied to analyse and count the cells stained with each DNA aptamer in the tissue sections (Section 2.10.4). The stained tissue sections were blindly scored without knowing the grade of the tissue using an established quantitative scoring system, which showed remarkable and distinctive staining intensities and proportion rate for all the aptamers (Appendices 4,5,6,7,8 and 9) (Harvey *et al.*, 1997; Leake *et al.*, 2000; Rhodes *et al.*, 2010). RA showed comparatively negligible binding to the non-cancerous and tumour tissues and therefore served as the best negative control for the experiment. SA44 DNA showed moderate to strong nuclear staining in glioma tissues with an average mean score ranging from 5.3 - 6.5, however, most of the non-cancerous tissues also showed strong nuclear staining with the SA44 DNA aptamer with an average score of 4.5. SA56 DNA showed strong nuclear staining on most tumour tissues including the non-cancerous sections with an average mean score ranging from 5.7 - 7.25. With regards to SA43 DNA aptamer, there was a differential staining on tumour tissues when compared to non-cancerous tissues. The aptamer showed moderate to strong nuclear

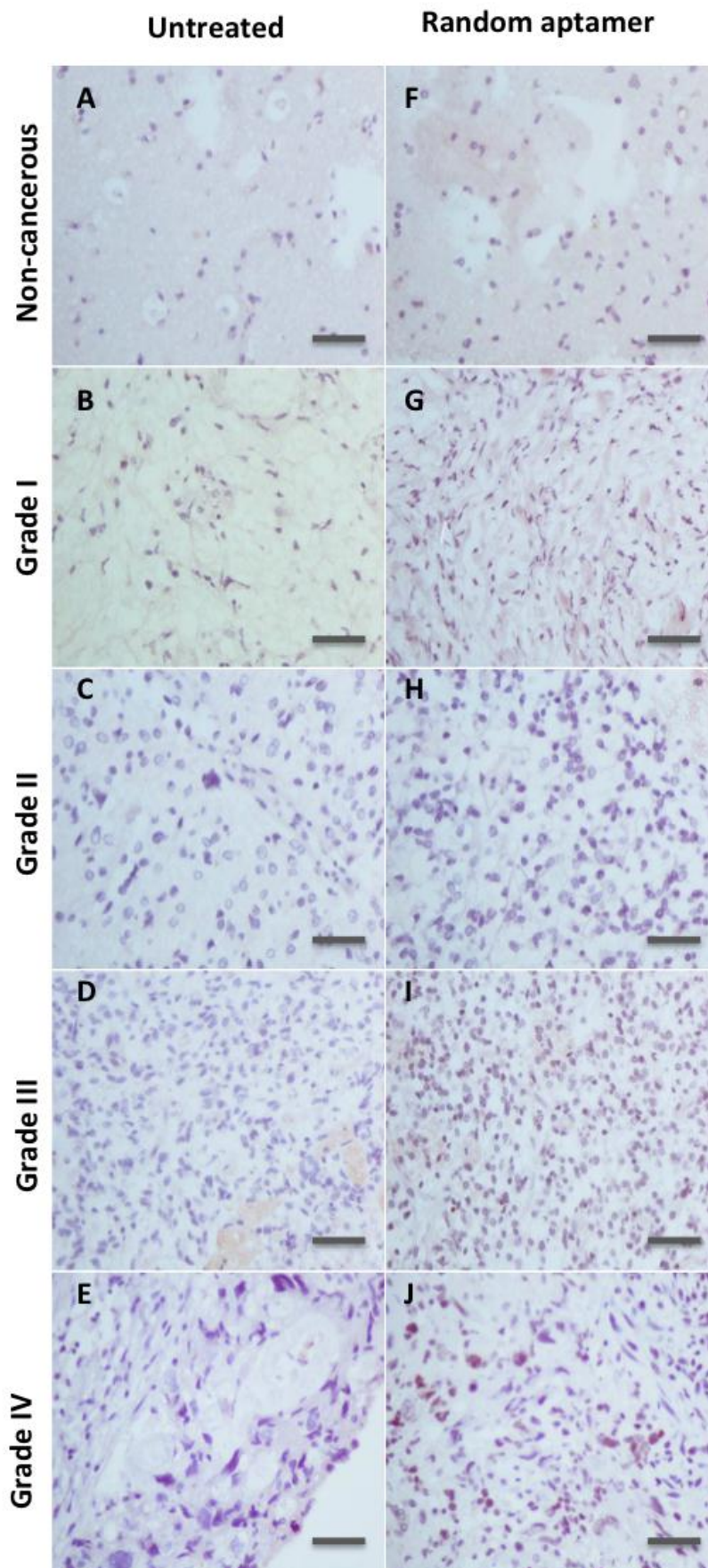
staining in tumour tissues with a mean score ranging from 4 – 6.6, whereas, in non-cancerous tissues, the average score was only 2.9. This indicated that, SA43 DNA could potentially discriminate tumour tissues from the non-cancerous tissues. To confirm these findings, further data analysis was performed as described below.

To identify a clinically meaningful cut off point for defining positive binding of aptamers to the cells on tissue sections, the results were examined on a scatter plot (Figure 6.5). A statistical test using one-way ANOVA followed by Bonfferoni post hoc test was applied to compare the overall mean binding scores for each aptamer on all glioma and meningioma tissues compared to the non-cancerous tissues. SA44 DNA and SA56 DNA showed no significant difference in mean binding score between all glioma grades, including meningioma and non-cancerous brain. SA43 DNA, on the contrary, showed significant difference in binding score between all grades of glioma and non-cancerous brain. The cut off value of 3 as analysed from the blind study was found to be more precise, as scores of 2 or 3 did match non-cancerous tissue samples which included patients with less than 1 % or 10 % cells weakly or moderately stained. Moreover, it could be inappropriate to include patients with less than 1 % to 10 % weakly stained cells to be included with the groups showing more than 10 % staining because it would provide false positive results. Each tissue section was therefore defined as positive aptamer binding if the total HC score was greater than 3 and negative aptamer binding if the total score was less than or equal to 3.

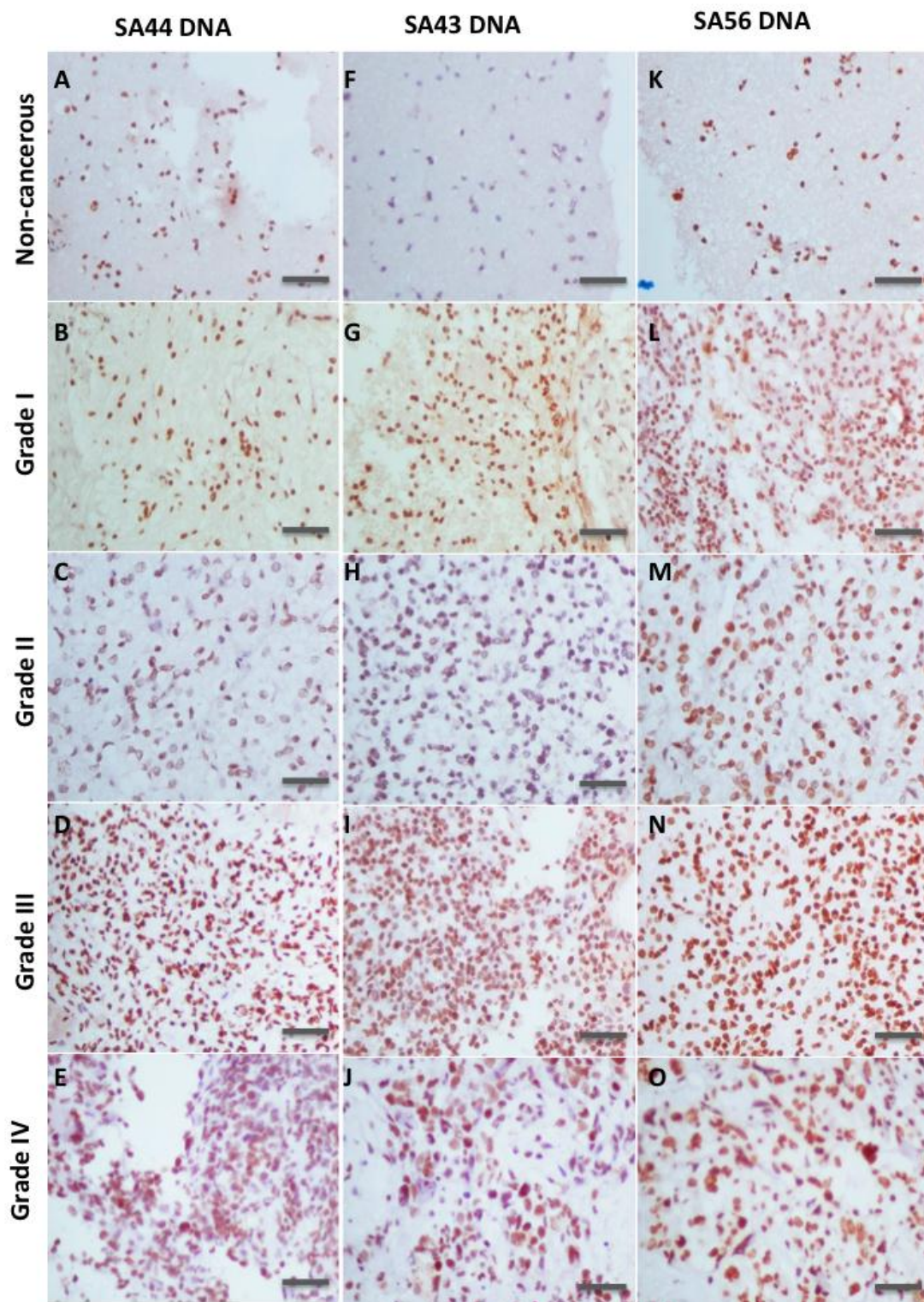
Comparison between the control (non-cancerous) group and tumour groups (grade I, grade II, grade III, grade IV, and meningioma) were then analysed using Fishers' exact test (Table 6.1). A significant difference in binding selectivity between non-cancerous

group and tumour groups with grade I, II, III, and IV was observed with SA43 DNA aptamer ( $p < 0.05$ ), however, no significant difference was observed for meningiomas ( $p > 0.05$ ). SA44, SA56 and random aptamer showed no significant difference in binding selectivity between non-cancerous and all grades of glioma, including meningioma. This indicated that SA43 DNA could potentially discriminate between all glioma grades and non-cancerous tissues.

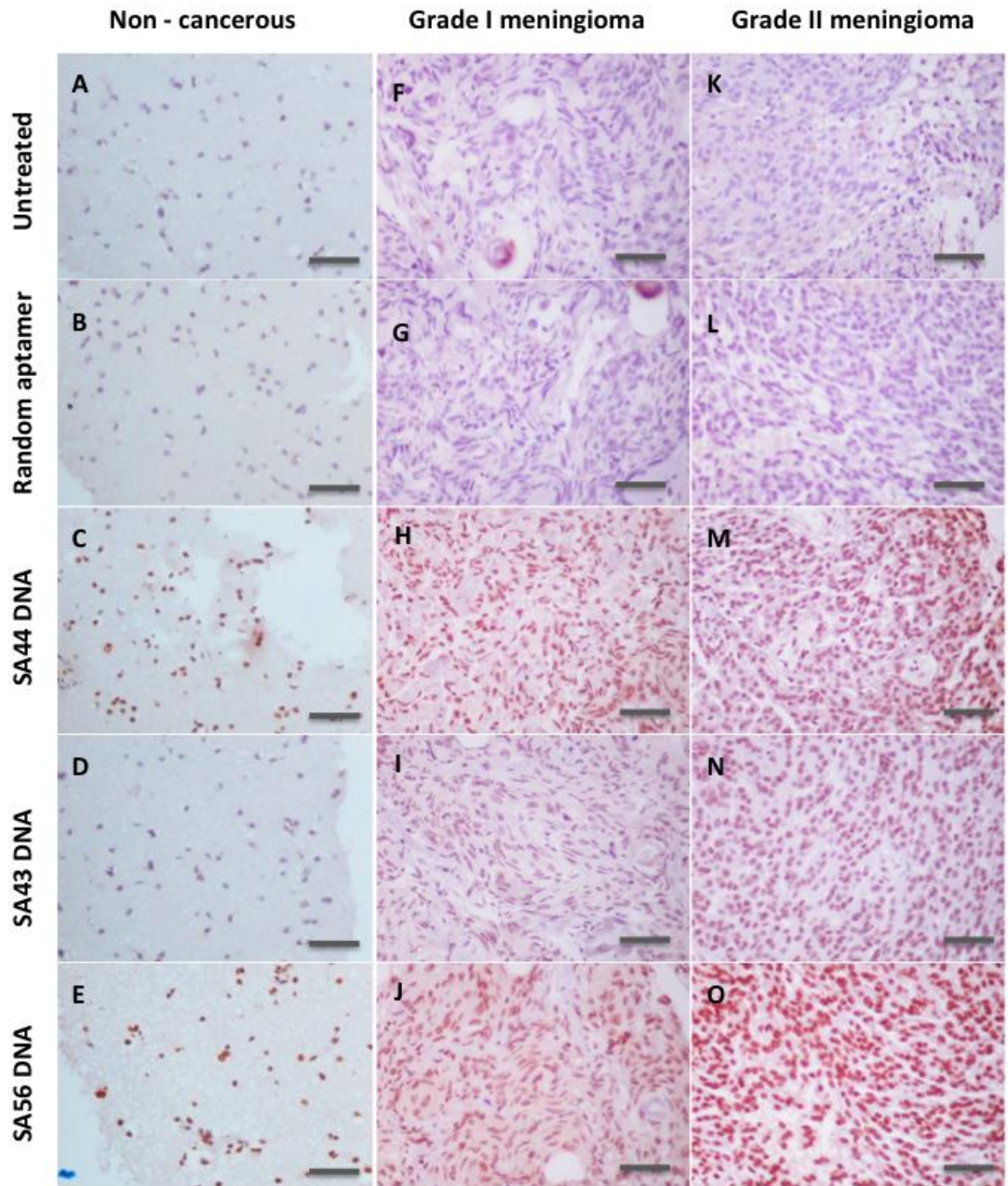
**Figure 6.2 Representative images of tissue sections from non-cancerous (BTNW no. 596) and different pathological grade glioma (BTNW no 814, grade I; 726, grade II; 738, grade III; and 1077, grade IV) patients stained with a biotinylated random sequence aptamer.** Biotin labeled aptamers were incubated with the tissue sections for 60 min followed by incubation with AB reagent for 30 min. DAB substrate was then added which resulted in brown colour product upon reacting with avidin biotin complex. The nuclei were counterstained with haematoxylin. **A-E** untreated tissues (no aptamer); **F-J** Random aptamer treated. With mean scores greater than 3, random aptamer showed negligible staining in all non-cancerous, grade I, and grade II tissues; however, showed moderate nuclear staining in 2/12 grade III, and 3/10 grade IV tissues. All scale bars, 200  $\mu\text{m}$ .



**Figure 6.3** Representative images of tissue sections from non-cancerous (BTNW no. 596) and different pathological grade glioma (BTNW no 814, grade I; 726, grade II; 738, grade III; and 1077, grade IV) patients stained with biotinylated SA44, SA43 and SA56 DNA aptamers. Biotin labeled aptamers were incubated with the tissue sections for 60 min followed by incubation with AB reagent for 30 min. DAB substrate reagent was then added which resulted in brown colour product upon reacting with avidin biotin complex. The nuclei were counterstained with haematoxylin. **A-E** SA44 DNA treated; **F-J** SA43 DNA treated; **K-O** SA56 DNA treated. With mean scores greater than 3, SA44 DNA showed moderate to strong nuclear staining in 9/13 non-cancerous, 7/7 grade I, 12/14 grade II, 10/12 grade III, and 8/10 grade IV tissues. SA43 DNA showed weak to moderate nuclear staining in 3/13 non-cancerous tissues. Strong nuclear staining was observed in 6/7 grade I, 11/14 grade II, 11/12 grade III, and 8/10 grade IV tissues with SA43 DNA aptamer. SA56 DNA showed strong nuclear staining in 12/13 non-cancerous tissues, 6/7 grade I, 11/14 grade II, 11/12 grade III, and 9/10 grade IV tissues. All scale bars, 200  $\mu$ m.



**Figure 6.4 Representative images of tissue sections from different pathological grade meningioma grade I (BTNW no. 759), and meningioma grade II (BTNW no. 760) patients stained with biotinylated random aptamer, SA44, SA43 and SA56 DNA aptamers.** Biotin labeled aptamers were incubated with the tissue sections for 60 min followed by incubation with AB reagent for 30 min. DAB substrate reagent was then added which resulted in brown colour product upon reacting with avidin biotin complex. The nuclei were counterstained with haematoxylin. **A, F, K** untreated tissues (no aptamer); **B, G, L** Random aptamer treated; **C, H, M** SA44 DNA DNA treated; **D, I, N** SA43 DNA treated; and **E, J, O** SA56 DNA treated. With mean scores greater than 3, random aptamer showed moderate staining on 1/3 grade I, and no staining on any of grade II/III (0/2) meningioma tissues. SA44 DNA and SA56 DNA showed strong nuclear staining on all 3/3 grade I, and 1/2 grade II meningioma. SA43 DNA showed moderate nuclear staining on 2/3 grade I, and 1/2 grade II meningioma tissues. All scale bars, 200  $\mu\text{m}$ .



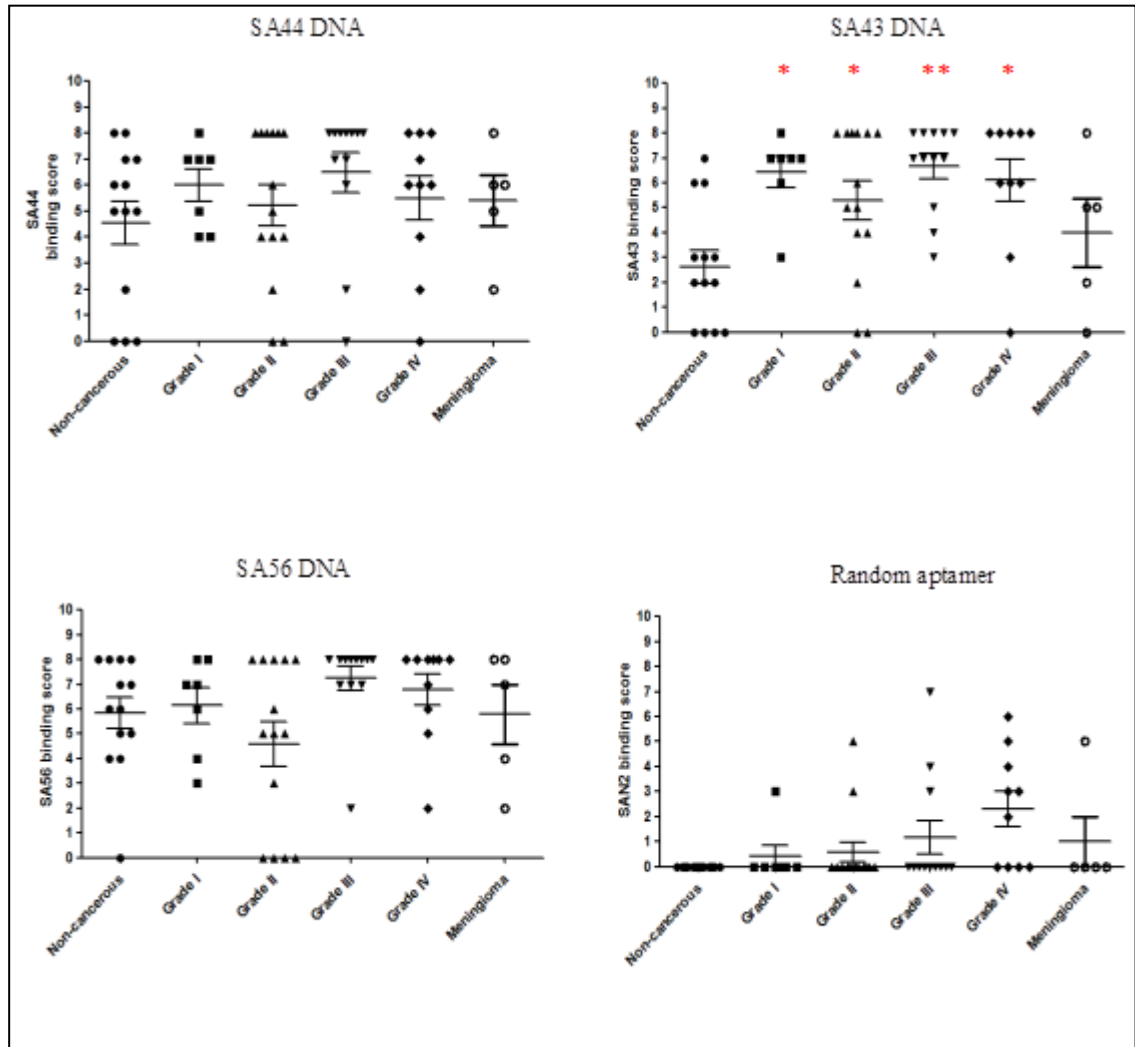


Figure 6.5 Scatter plot showing the mean and the distribution of average scores for each aptamer on patients tissue sections. Using ANOVA and post hoc Bonferroni test, SA44 DNA, SA56 DNA and random aptamer showed no statistical difference in the average binding scores between tumour and non-cancerous tissues. SA43 DNA showed statistical difference in the average binding scores between all pathological grades (I, II, III, IV) of glioma tissues compared to the non-cancerous tissues (\*,  $p < 0.05$ ; \*\*,  $p < 0.01$ ).

**Table 6.1 Comparison of each DNA aptamer binding on non-cancerous tissues against various glioma grade and meningioma tissues using Fishers exact test.**

Grade	Random aptamer	SA44	SA43	SA56
<b>Non-Cancerous</b>	0/13	9/13	3/13	12/13
<b>I</b>	0/7 ( <i>p</i> = 1.000)	7/7 ( <i>p</i> = 0.2487)	6/7 ( <i>p</i> = 0.0166)	6/7 ( <i>p</i> = 1.000)
<b>II</b>	1/14 ( <i>p</i> = 1.000)	11/14 ( <i>p</i> = 0.6776)	11/14 ( <i>p</i> = 0.0070)	11/14 ( <i>p</i> = 1.000)
<b>III</b>	2/12 ( <i>p</i> = 0.2200)	10/12 ( <i>p</i> = 0.6447)	11/12 ( <i>p</i> = 0.0010)	11/12 ( <i>p</i> = 1.000)
<b>IV</b>	3/10 ( <i>p</i> = 0.0678)	8/10 ( <i>p</i> = 0.6600)	8/10 ( <i>p</i> = 0.0123)	9/10 ( <i>p</i> = 1.000)
<b>Meningioma</b>	1/5 ( <i>p</i> = 0.2778)	4/5 ( <i>p</i> = 1.000)	3/5 ( <i>p</i> = 0.2682)	4/5 ( <i>p</i> = 0.4902)

**6.2.3 Detailed histological analysis of SA43 DNA aptamer (exceptional cases).**

SA43 DNA showed significant binding selectivity to glioma tumour tissues compared to the non-cancerous tissues (Table 6.1), therefore, detailed histological analysis was performed on the tissues stained with SA43 DNA aptamer, to determine cellular localisation and cell type selectivity with the help of an experienced pathologist from Royal Preston Hospital (RPH). SA43 DNA showed moderate staining on three of the non-cancerous tissues studied (Figure 6.6). Tissue section from patient no. 713, a non-cancerous brain sample adjacent to breast metastasis in cerebellum showed staining with all test aptamers including SA43 DNA. This initially suggested that metastasised breast tumour cells present in the cerebellar part could be recognised selectively by the aptamer, and that this biopsy was not a suitable non-cancerous control. The cerebellar tissue however, was stated to be hyper cellular (particularly granule cells) in nature and

non-cancerous by the pathologist upon closer inspection. This suggested that tumour in the cerebellar part could not be selectively recognised by the aptamer SA43 DNA. Upon closer inspection, there was selectivity between the cells on the tissue (no.713) with this particular aptamer (SA43). The aptamer showed binding to granular cells of the cerebellum, but not molecular cells (Figure 6.6) and Purkinje cells (Figure 6.7). Patient tissue no. 1085 and 1039 from the non-cancerous category was excised from around a grade I trigeminal schwannomas (tumours of Schwann cell origin) and from around a frontal carcinoma of unknown origin and showed staining with all test aptamers. This initially suggested that, there could be some cells infiltrated from the tumour part which might have shown binding to the aptamers, however, the tissues were stated to be non-cancerous by the pathologist (Further discussed in section 6.3).

SA43 DNA was more selective to glioma tissues, however, three high-grade tissue samples showed negligible staining with the aptamer (Figure 6.8). These tissues were in the category of necrotic glial tumour with pleomorphism, microvascular proliferation, and thrombosed vessels, however, other tissues showing staining also had similar peculiarities. Glioma tissues consist of heterogeneous cells; hence, the tissue sample may contain cell populations that do not express the aptamer target.

Another noteworthy observation was that the aptamer showed negligible binding to endothelial cells of all of the glioma tissues from all the pathological grades including meningioma a representative image showing absence of binding to the endothelial cells is shown in figure 6.9. The overall findings for the study showed that SA43 DNA is an aptamer, which can be utilised for HC to potentially discriminate between glioma tissues and non-cancerous brain tissues.

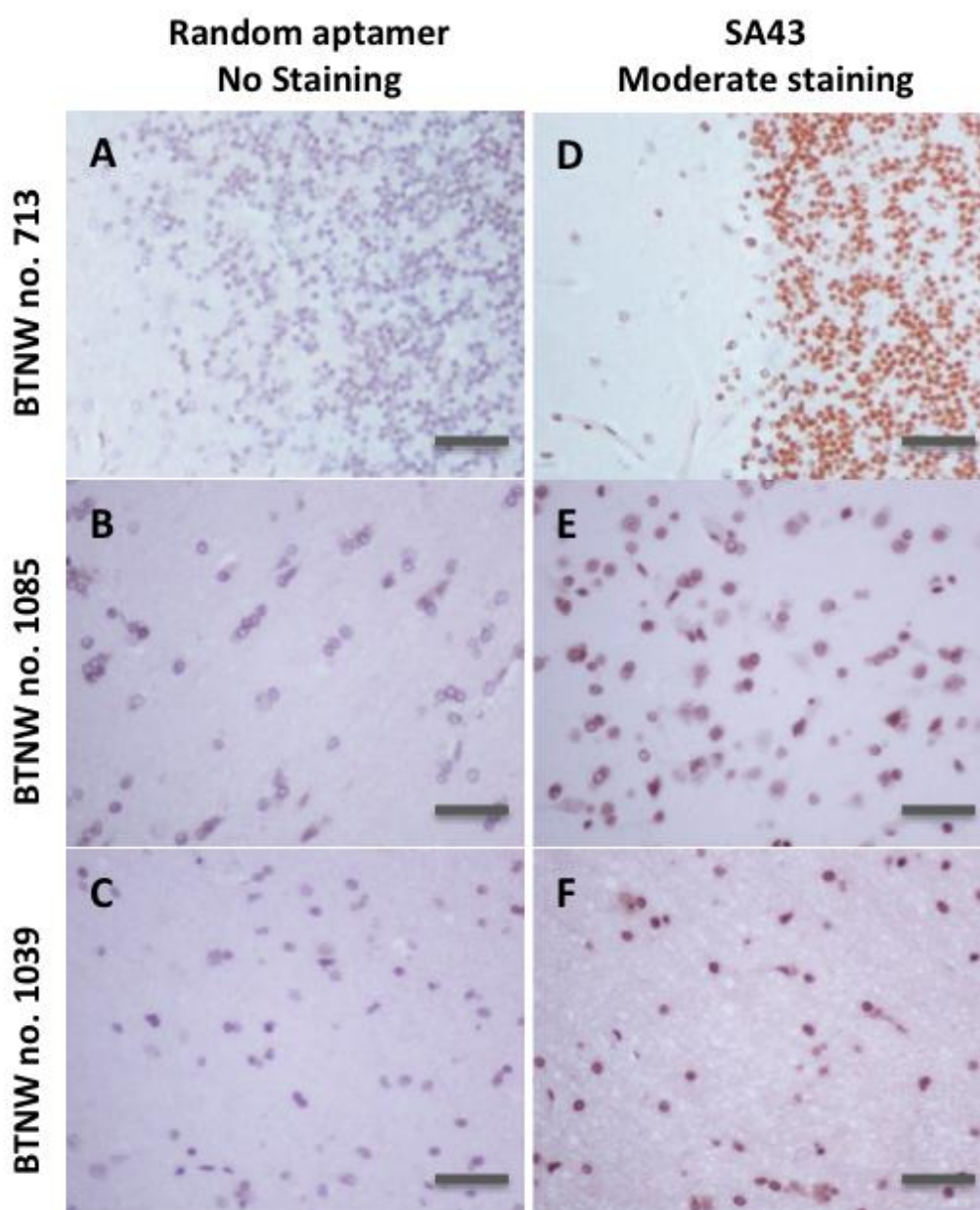


**Figure 6.6 SA43 DNA aptamer showing moderate staining in three non-cancerous tissues. A B and C** Non-cancerous tissues showing negligible staining with random aptamer. **D E and F** Non-cancerous tissues showing moderate nuclear staining with SA43 DNA aptamer. All scale bars, 200  $\mu$ m.

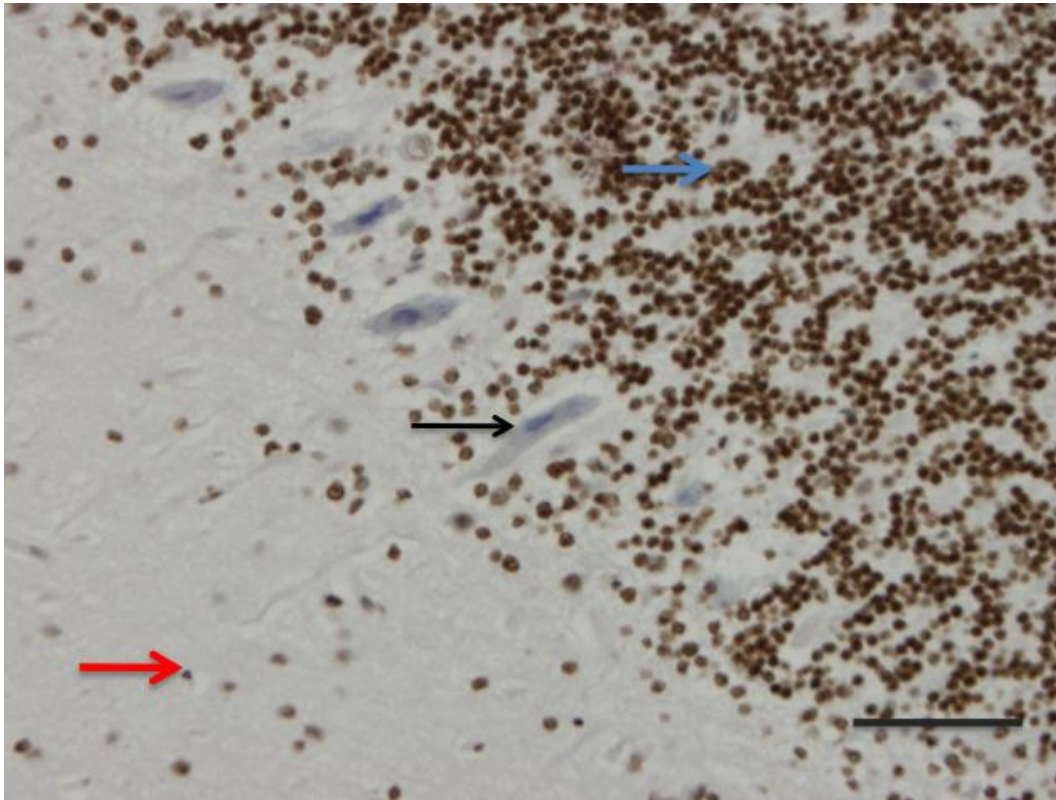


**Figure 6.7 SA43 DNA selectivity within the cells of the cerebellar tissue.** SA43 DNA aptamer showed binding on granular cells (region highlighted in blue arrow), molecular layer cells (red arrow), and negligible binding to Purkinje cells (black arrow). Scale bar, 200  $\mu\text{m}$ .

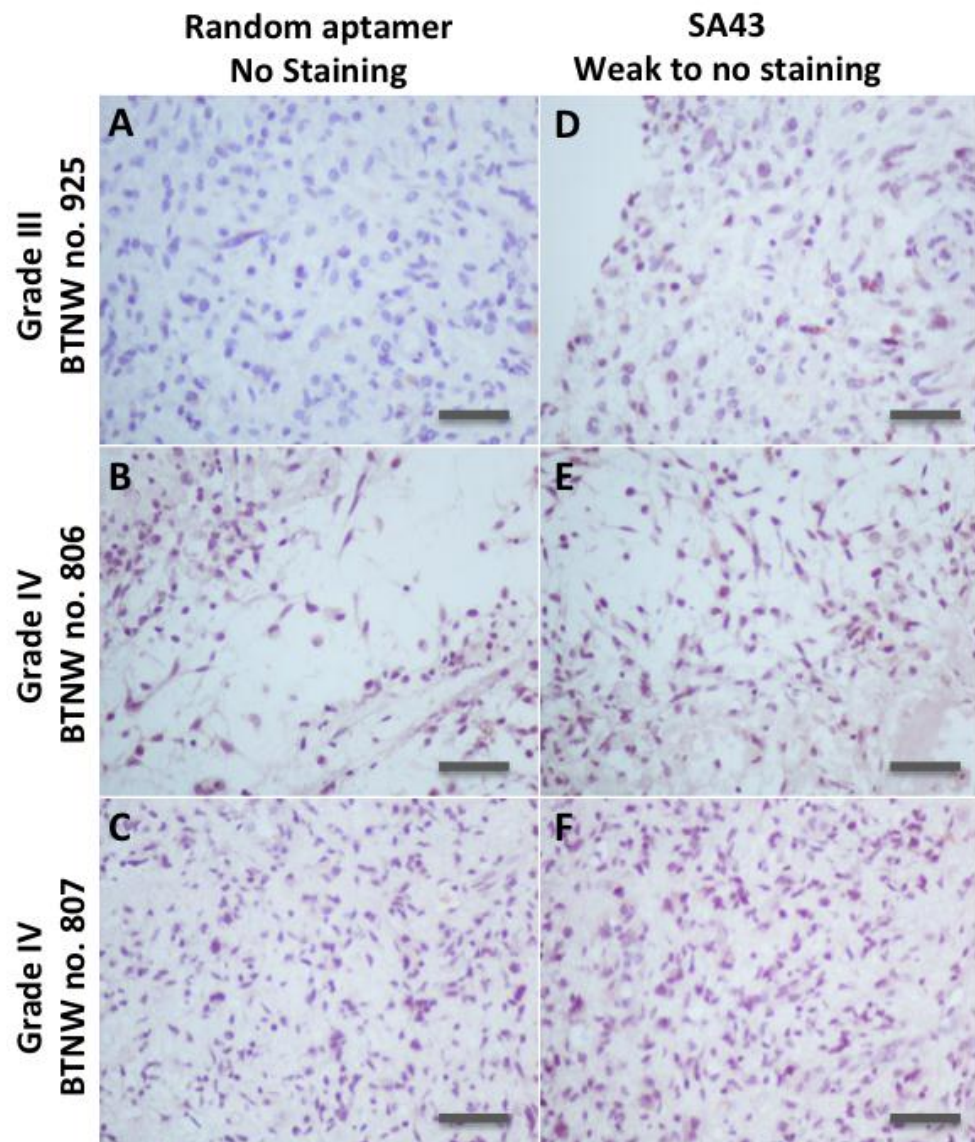


**Figure 6.8 SA43 DNA aptamer showing weak to no staining in three high-grade glioma tissues. A B and C High-grade glioma tissues showing negligible staining with random aptamer. D E and F High-grade glioma tissues showing weak to negligible staining with SA43 DNA aptamer. All scale bars, 200  $\mu$ m.**

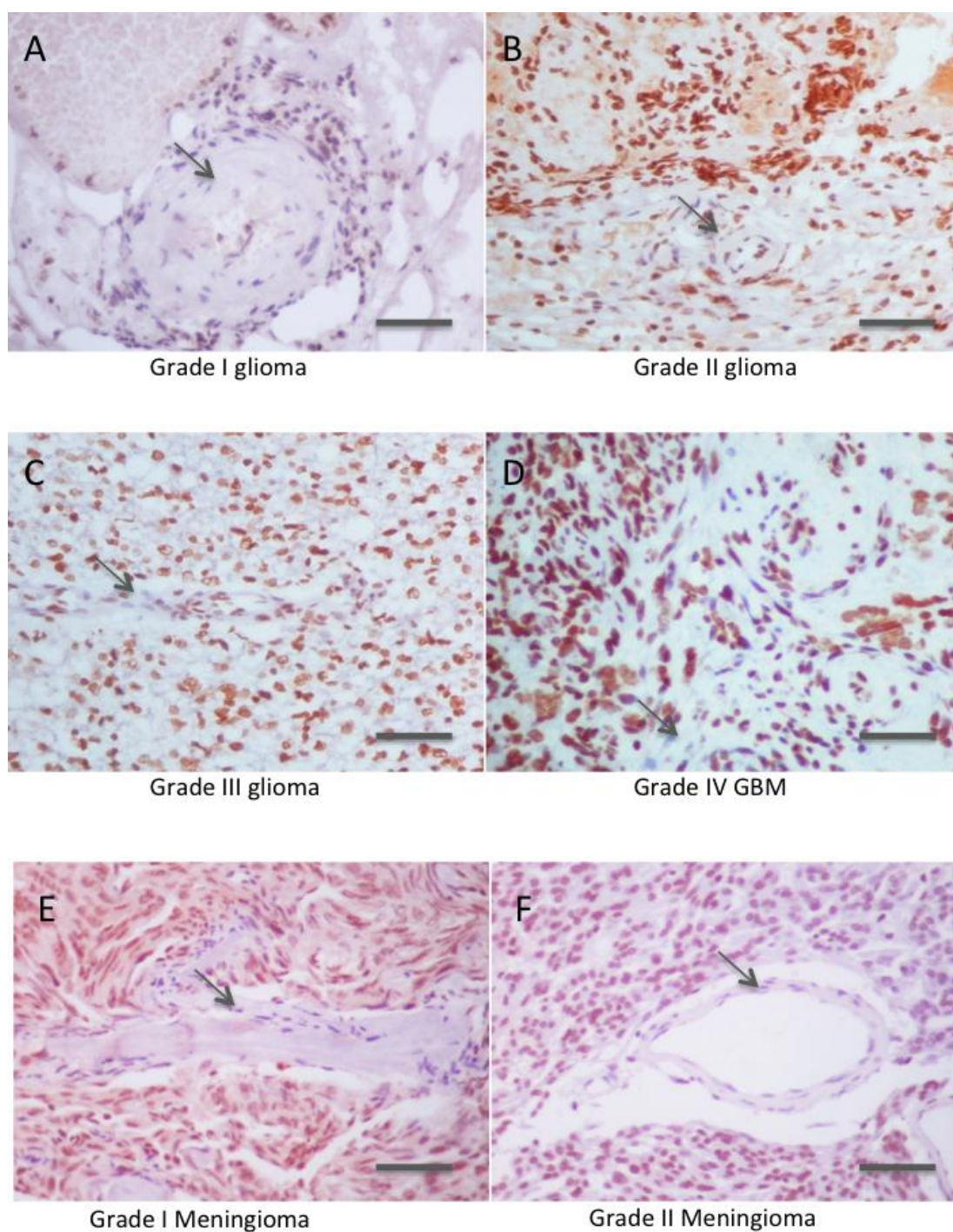


**Figure 6.9** Representative images from various glioma pathological grades including meningiomas showing negligible binding to endothelial cells with SA43 DNA aptamer. Arrows indicate absence of SA43 DNA binding to endothelial cells in grade I glioma (A), grade II glioma (B), grade III glioma (C), grade IV GBM (D), grade I meningioma (E), and grade II meningioma (F). All scale bars, 200  $\mu\text{m}$ .

### 6.3 Discussion

An important tool in cancer diagnosis is immunostaining, in which freshly dissected clinical tissues are fixed prior to the treatment with probes, such as antibodies and aptamers, specifically for tumour markers. In research, clinical tissue specimens are more representative of disease than cultured cell lines, in that the former are separated and preserved in the disease state while the latter may be influenced by *in vitro* factors as discussed in chapter 3 (Li *et al.*, 2009). The ultimate usefulness of aptamer binding assessment by histochemistry (HC) as a diagnostic tool resides in the ability of aptamers to distinguish cancerous from non-cancerous cells.

Initial binding studies were conducted on the fixed cells to determine if the DNA aptamers were capable to bind to their cell targets under chemical fixation using standard avidin-biotin complex staining technique (de Matos *et al.*, 2010). SA44 and SA43 DNA both retained binding capability to fixed and permeabilised 1321N1 glioma cells compared to the non-cancerous SVGP12 cells. The binding was mainly localised in the nucleus along with some cytoplasmic staining indicating that the target was localised in both cytoplasm and nucleus of the tumour cells. SA56 DNA showed no selectivity, which was also supported the live cells data (Chapter 4).

To elucidate the application of aptamers in HC, analysis was performed on glioma tissues of various pathological grades including non-cancerous brain tissues as a control. An established scoring system was used as previously it has been found to be highly reproducible, correlated with established biochemical assays and provided equally significant predictive and prognostic information regarding patient samples

(Harvey *et al.*, 1999; Leake *et al.*, 2000). The optimal cut off point in the study was a total HC score of greater than 3, which considered more than 10 % cells positively stained with the aptamers. This was in agreement with many clinical and commercial laboratories choosing 10 % or even 20 % positive tumour cells as the cut off value for defining estrogen receptor (ER), progesterone receptors (PR), and HER2 positivity (Harvey *et al.*, 1999; Leake *et al.*, 2000; Wolf *et al.*, 2007). Using this scoring system and through physical observation, the present study showed differential binding with SA43 aptamer on tumour tissues compared to the non-cancerous tissues. Moreover, the binding was localised in the nucleus and selective for a certain cell type. This proved that the results achieved were not an artefact or non-specific staining but were in accordance with the fact that the aptamers can be used for staining specific targets on cells within the tissue sections.

SA43 DNA showed significant binding to glioma tumour tissues compared to the non-cancerous tissues. SA44 DNA mimicked SA43 DNA in binding to glioma tissues; however, it also showed binding to most of the non-cancerous tissues. SA44 DNA differed in the presence of nucleotide bases 'CC' compared to SA43 DNA, however, the absence of nucleotides did not alter the secondary structure. Whether the binding to the non-cancerous tissues is because of the presence of nucleotides bases CC in SA44 DNA aptamer, still remains an unsolved question. Structural studies with aptamer-target interactions have however demonstrated diversity in tertiary structures of aptamers associated with folding upon binding to the target (Gold *et al.*, 1995). If this is the case for SA44 and SA43 aptamers, the deletion of the two cytosines from the SA44 sequence might then adopt a different 3-dimensional (3D) conformation more preferable for targeting tumour cells. This suggested that aptamer 3D conformation might play an

important role in its specific tumour targeting and also suggested for further studies on aptamer-target interactions to provide a conclusive remark. The binding characteristics of SA56 DNA to tissues mimicked the live cells data, as it also showed binding to both glioma and non-cancerous tissues. This could be explained by its binding to targets that may be equally expressed in glioma and non-cancerous cells. The project therefore focussed on SA43 DNA aptamer, as it undoubtedly showed similar binding characteristics on both live cells, fixed cells and fixed clinical tissues, therefore, further in-depth analysis was performed on the data obtained with this aptamer.

An in depth analysis of SA43 DNA aptamer binding to three non-cancerous tissues showed some distinct observations. One of the tissues was non-cancerous cerebellar tissue around metastatic breast tissue. The layers of cerebellum are indicated as internal granular layer, Purkinje cell layer, and molecular layer (outer layer of the cortex of the cerebellum) (Moncalero *et al.*, 2011). The aptamer showed distinctive binding to granular cells and molecular cells, but showed no binding to Purkinje cells. This observation initially suggested that tumours in the cerebellar region could not be able to be recognised selectively by the aptamer, if such indiscriminate binding to granular and molecular layer cells was present. Furneaux *et al.*, (1990), however, reported that Purkinje cells antigen namely, Purkinje neuronal protein termed cdr2 was highly expressed in tumours from tissues with paraneoplastic cerebellar degeneration (PCD) but was absent in normal tissues. PCD is one of the several immune-mediated paraneoplastic neurologic disorder that develop as a remote effect of systemic cancers (Darnell and Posner, 2006; O'Donovan *et al.*, 2010). This suggested that further studies warrant identifying if the aptamer can bind to purkinje cells in PCD, which could assist in identifying and discriminating the PCD from normal tissues. The other two non-

cancerous tissues were excised around a grade I trigeminal schwannoma and a frontal carcinoma of unknown origin. These tissues showed highest total binding score (7) with SA43 along with aptamers SA44 and SA56. Grade I trigeminal schwannoma are very rare arising from Schwann cells, which function as supporting cells in peripheral nervous system (PNS) similarly to how glial cells act as supporting cells in CNS. The question was raised whether the aptamer SA43 DNA would be able to show selectivity in tumour tissues within PNS as it also binds to the non-cancerous tissue. Analysis from one such tissue would not provide such conclusive remark and therefore, further studies are needed to confirm aptamer selectivity within the cells of PNS. The non-cancerous tissue of the brain biopsy around frontal carcinoma of unknown origin also showed binding to SA43 DNA including SA44, and SA56, however, as the origin of the tumour was unknown, it was difficult to comment on the binding with the aptamers, whether it was on the non-cancerous tissue excised or possibly to the infiltrative cells from the surrounding tumour tissue.

A number of aptamers have been reported to bind targets on endothelial cells of brain tumour with a view to distinguish them from the endothelial cells in non-cancerous brain (Blank *et al.*, 2001; Mann *et al.*, 2010). Nucleolin, a well establish target for the AS1411 aptamer is also highly expressed in the plasma membrane of both cancer cells and endothelial cells in the angiogenic blood vessels (Christian *et al.*, 2003). Another study by Blank *et al.* used endothelial cells as targets and selected DNA aptamers that could be used as histological markers of microvessles in brain tumours (Blank *et al.*, 2001). These papers demonstrated that aptamers binding to endothelial cells is an advantage in diagnostic and therapeutic purposes, in such a way that aptamers can internalise via endothelial cells and can easily pass through blood brain barrier (BBB).

The study here however showed negligible binding of SA43 DNA to the endothelial cells, which was therefore, initially thought to be a hindrance, considering its entry into BBB. The BBB, mediated by endothelial tight junctions, however, has been reported to be defective and leaky in malignant gliomas, resulting in cerebral oedema as visualised by immunohistochemistry of plasma proteins using biopsy specimens (Seitz and Wechsler, 1987) and contrast enhancement upon neuro-radiological examination (Roberts *et al.*, 2000). Moreover, Schneider *et al.* including few other researchers have reported that malignant gliomas have acquired the ability to actively degrade tight junctions by secreting soluble factors, eventually leading to BBB disruption within invaded brain tissue (Schneider *et al.*, 2004; Wolburg *et al.*, 2012; Agarwal *et al.*, 2013). Moreover, immunohistochemical studies have revealed that some abnormal function of the transmembrane tight junction components are mostly down regulated in malignant gliomas and has therefore been associated with loosening of the BBB (Liebner *et al.*, 2000; Papadopoulos *et al.*, 2001; Nitta *et al.*, 2003).

The enhanced permeability and retention (EPR) effect describes the intrinsic ability of macromolecules and particles of a certain size to accumulate in solid tumour tissues (Iyer *et al.*, 2006; Yang *et al.*, 2013). Features that have been identified as EPR mediators include vascular permeability enhancing and vasodilating factors such as vascular endothelial growth factor, bradykinin, prostaglandins, and nitric oxide that are upregulated or present in large quantities in tumour compared to normal tissue (Iyer *et al.*, 2006). Anatomical differences in tumour vasculature also contribute, such as the lack of a smooth muscle layer surrounding the vessels that leads to increased blood flow volume to tumours during hypertension and hence more leakage of macromolecules into the surrounding tissue (Iyer *et al.*, 2006). SA43 DNA aptamer showed negligible

binding to endothelial cells, the study therefore proposes this to be an advantage because the aptamer can potentially gain entry into malignant glioma tissue by the EPR effect (increased potential entry when conjugated with nano-particles, discussed in chapter 8) and through the leaky vasculature without any non-specific binding to the surrounding endothelial cells.

Overall, a substantial amount of data proves the potential of SA43 DNA aptamer being more selective for glioma when compared to the non-cancerous tissue. The study has opened many new horizons and avenues to further explore the applications of aptamers in targeting tumour cells and tissues. There was however, a point to be noted that the aptamer SA43 DNA showed strong binding in the nucleus of the fixed cells and tissues, whereas, the binding was shown to be localised in the cytoplasm on live tumorigenic glioma cells at 90 min incubation time. The question was raised whether the aptamer still resided in cytoplasm after 90 min or did it reach the nucleus over time. Performing longer time over 24 hours would provide an answer to the question, which will be addressed in next chapter.

## **CHAPTER 7 DETERMINING THE FATE OF SA43 DNA APTAMER IN TUMOUR CELLS**

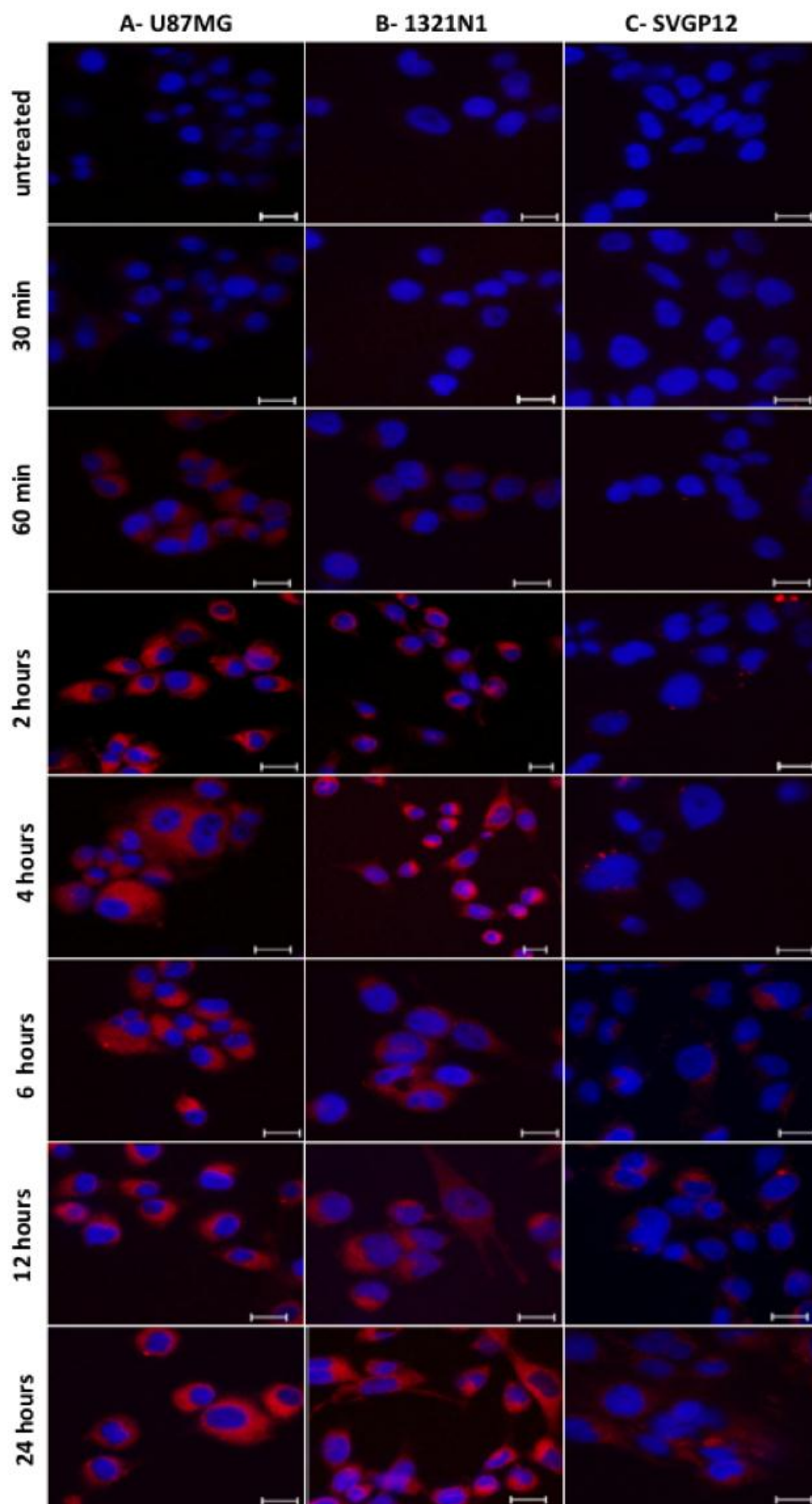
### **7.1 Introduction**

The previous chapters gathered a considerable amount of data stating SA43 DNA was able to recognise the targets on both live and fixed tumour cells and tissues compared to the non-cancerous cells and tissues. The localisation of aptamer SA43 DNA in the cytoplasm and around the periphery of the nucleus in the live tumour cells at 90 minutes was however, distinct to the localisation in nucleus of fixed tumour cells and tissues. Considering the current scenario of both live cytoplasmic and fixed nuclear localisation, a longer time course study was performed to understand if the aptamer entered the nucleus of live cells over 24 hours. Confocal microscopy was used to track the localisation and internalisation potential of the aptamer on live tumour and non-cancerous cells at specific time points.

### **7.2 Results**

SA43 DNA uptake was detectable as early as 60 minutes in 1321N1 and U87MG cells, whereas the uptake started from 6 hours in SVGP12 cells, which was minimal compared to the 1321N1 and U87MG cells (Figures 7.1, Appendix 3). Moreover, there was no obvious difference between the distributions of SA43 DNA aptamer at 2 hours and 24 hours in tumour cells 1321N1 and U87MG as the fluorescence remained localised in the cytoplasm even at 24 hours, which suggested that the aptamer was unable to reach the nucleus.

**Figure 7.1 Time dependent uptake and cellular localisation of SA43 DNA by U87MG, 1321N1 and SVGP12 cells.** Cy3 labelled SA44 DNA was incubated separately at a concentration of 100 nM on live U87MG, 1321N1 and SVGP12 cells (red) which were then fixed using 4 % PFA. The nuclei were counterstained with DAPI (blue) and mounted. Cells with no aptamer were used as control. Z-stacks images were acquired under 40x and 63x magnifications at an excitation of 543 nm and emission of 560 nm under 1047-camera resolution (amplifier gain: 1; detector gain: 927; amplifier offset: - 0.06). Data are representative of three independent experiments with single plane images of middle section of Z- axis. The Cy3 fluorescence signal of the aptamer on each cells were compared to their respective untreated controls. **A, B** and **C** represent time dependent uptake of SA43 in live U87MG, 1321N1 and SVGP12 cells. Scale bar = 20  $\mu\text{m}$ .



### 7.3 Discussion

A longer time course assay was performed in order to assess whether the different binding localisation events on live cells observed will lead to same localisation of binding as fixed cells. The aptamer resided in the cytoplasm of live tumour cells even at 24 hours incubation suggesting that the aptamer was unable to penetrate through the nuclear membrane even after 24 hours of incubation. With such observations, the study proposed that aptamers would internalise into the tumour cells rapidly by unknown endocytosis mechanism and culminate to lysosomes for degradation and hence, unable to reach the nucleus. The entrapment of internalised aptamer in endocytic compartments may have then prevented further intracellular transport towards the nucleus, because of degradation of aptamer. This was in agreement with a few studies where the aptamer was shown to internalise through an endocytosis mechanism, which led to endosomal and cytoplasmic localisation in live cells (McNamara *et al.*, 2006; Dassie *et al.*, 2009; Li *et al.*, 2010). Moreover, if SA43 DNA managed endosomal escape, the aptamer must have traversed the cytosol to access the nucleus, which could be then challenged by the complex environment of the cytosol, containing cytosolic nucleases, which can further degrade the aptamer. To date, only one aptamer AS1411, which targets nucleolin, has been identified which internalises through macropinocytosis (Reyes Reyes *et al.*, 2010) allowing nuclear localisation and the apparent ability to escape the endosomal or lysosomal pathway (Kotula *et al.*, 2012). The method employed in this study, however, utilised Cy3 dye as a probe, which would accumulate in the cytoplasm with or without degradation of the aptamer used, herein. Therefore, a mere observation of fluorescence in the cytoplasm does not necessarily represent intact DNA aptamer as the Cy3 dye will fluoresce independent of its attachment to the aptamer, full-length or otherwise.

Uptake was observed in non-cancerous SVGP12 cells from 6 hours indicating longer incubation time could enhance non-specific uptake of SA43 DNA *in vitro* and reduce the binding specificity. The staining was however minimal compared to tumour cells even at 24 hours, and therefore SA43 DNA would be able to still differentiate the aptamer binding between the tumour and non-cancerous cells. Such observations warrant further studies understanding the exact mechanism of the uptake and the localisation of the aptamer within the sub-cellular compartments over time (Discussed in chapter 8).

## CHAPTER 8 GENERAL DISCUSSIONS AND FUTURE WORK

### 8.1 Challenges for glioma targeted therapy and overall summary

The overall aim of this project was to examine the potential of RNA and DNA aptamers as a targeting agent for targeting tumour cells. Taking into account the available literature, it was hypothesised that aptamers can be applied for cancer diagnosis and treatment (Cerchia *et al.*, 2009; Bayrac *et al.*, 2012; Kang *et al.*, 2012; Nicol *et al.*, 2013; Li *et al.*, 2014). Glioma cells and tissues were chosen as a model for tumour targeting because they are the most common primary central nervous system tumours with a dismal prognosis, and are widely incurable. Surgery followed by radiotherapy and/or chemotherapy has been the standard treatment; however, due to the infiltrative growth of gliomas, it is hard to completely resect the tumour. Most of the chemotherapies have also failed because of the blood brain barrier (BBB) resistance and poor glioma targeting of the chemotherapeutics (Pardridge, 2007; Serwer and James, 2012). For example, temozolomide has poor efficacy in the treatment of glioma, however, the mean survival time of the glioma patient is only extended by approximately 6 months (Serwer and James, 2012). Overall, as human gliomas are highly heterogeneous tumours, the sensitivity to therapeutic approaches has been difficult to predict.

The ultimate aim for an aptamer to be successfully used for targeted drug delivery for glioma is the capability to distinguish tumour cells from non-cancerous cells in clinical samples for effective targeted delivery. Moreover, the aptamer should be able cross the BBB and internalise into the target tumour cells for successful drug delivery without influencing the cell viability of surrounding non-cancerous cells. An effective approach

was adopted to identify a molecular probe to recognise and target glioma cells and tissues. The project here reported a preliminary study focussed on selecting RNA and DNA aptamers for targeting glioma cells assessed by powerful approaches such as confocal laser imaging and flow cytometry. Shortened aptamers SA44 RNA and SA43 RNA were shown to target live glioma cells with high affinity and specificity compared to the non-cancerous glial cells, breast cancer, and bladder cancer cells. The DNA homologs of the RNA aptamers also showed similar binding tendency to glioma cells.

One of the major challenges for *in vitro* targeting is to be able to direct the binding of the targeting aptamers to tumour cells instead of healthy non-cancerous cells. Confocal imaging and flow cytometry on live cells at 90 minutes incubation with both the DNA aptamers (SA44 and SA43) showed that the aptamers internalised rapidly in the target glioma cells, however, from the data obtained from studying pathological glioma tissues, SA43 DNA showed significant binding selectivity for glioma tissues compared to non-cancerous tissues. This data obtained from the tissue sections is novel because few studies have investigated aptamer binding in glioma tissue (Blank *et al.*, 2001; Kang *et al.*, 2012). Considering both the live cells and pathological tissue data, SA43 DNA was selected as a promising aptamer for targeting glioma.

## **8.2 Internalisation property of SA43 DNA aptamer and its implication on targeted drug delivery**

Targeted aptamer-drug delivery has been shown to have great potential for cancer therapy, as aptamers provide enhanced delivery and hence increased efficacy and reduced side effects (Huang *et al.*, 2009; Keefe *et al.*, 2010; Rockey *et al.*, 2011). Although aptamers can specifically bind to various molecular targets, the contact and

internalising property may produce the best possible results if the aim is to deliver conjugated chemotherapeutics that act internally on the cells. Indeed, intracellular delivery of aptamer-drug conjugates results in higher drug concentration inside the cells, and thus its efficacy is more than non-internalised aptamer therapeutics or by using standard chemotherapeutic agents alone (Orava *et al.*, 2010; Esposito *et al.*, 2011). The study showed that SA43 DNA aptamer not only showed high affinity to the target glioma cells with nanomolar dissociation constants as described in chapter 4, but also was able to actively internalise rapidly into live tumour cells compared to the non-cancerous and non-glioma cells (Chapter 4 and 5).

The ability of the aptamer SA43 DNA to selectively bind and rapidly internalise into the glioma cells was comparable over the other published aptamers such as GM128 and GM131 (Kang *et al.*, 2012), which showed higher binding affinity and selectivity to U118-MG glioma cells, however, also lost binding efficiency after trypsin treatment (Kang *et al.*, 2012). Zhang *et al.*, (2012<sup>a</sup>) reported the development of cancer-cell-specific DNA aptamer probe, KMF2 – 1a, that successfully internalised to the endosomes of the targets on breast cancer cells, however, the internalisation failed after trypsin treatment. Moreover, other aptamers targeting glioma and other cancer cell types lost their binding efficiency after trypsin protease treatment, and unable to internalise thereby suggesting their most likely target could be proteins on cell surface (Shangguan *et al.*, 2008; Sefah *et al.*, 2010; Ara *et al.*, 2012; Jimenez *et al.*, 2012; Meyer *et al.*, 2012; Zhang *et al.*, 2012<sup>a</sup>; Hernandez *et al.*, 2013; Wu *et al.*, 2014). These aptamers have been shown to internalise via receptor-mediated endocytosis, due to the involvement of cell surface receptors in aptamer uptake. The ability of the aptamer SA43 DNA to bind and internalise in the tumourigenic glioma cells even after trypsin

treatment hypothesised that either the aptamer entered the cells via some other endocytic process other than receptor mediated pathway or the target could be resistant to trypsin cleavage if it was present on the cell surface (Further discussed in section 8.4). Such selective internalisation property of the aptamer (irrespective of trypsin treatment) would be of great relevance in designing strategies for targeted therapy of glioma. This is because internalisation of the aptamer may occur via an endocytic pathway, thereby improving drug accumulation in targeted glioma cells and tissues thus enhancing the targeted therapy.

### **8.3 Putative target for SA43 DNA aptamer (in relation to the parallel study)**

Considering the nanomolar affinity of SA43 DNA aptamer and selective targeting to glioma cells and tissues, it could be possible that the aptamer may bind to an essential protein, which is overexpressed in glioma cells. A parallel project for determining the target for SA43 DNA aptamer was carried out simultaneously based on immunoprecipitation (IP) analysis in our laboratory, but subsequently termed aptoprecipitation (AP). The results revealed that more than 30 % pull down was only to Ku heterodimer (Ku 70/80) proteins on 1321N1 and U87MG cells including primary glioblastoma cells (BTNW 914) by the aptamer SA43 DNA (unpublished data). The remaining 70 % pull down was distributed among cytoplasmic and nuclear proteins such as mitochondrial proteins and nucleolin, however, very few surface proteins were present.

Ku 70/80 is a DNA-repair protein involved in the repair of double stranded breaks required for non-homologous end joining (NHEJ) pathway and is ubiquitously

expressed in the nucleus of most untransformed cells, however, it has been reported to be expressed on the cell surface, cytoplasm or nucleus in various tumour cells (Muller *et al.*, 2005; Fransson and Borrebaeck, 2006; Persson *et al.*, 2010). With regards to glioma, this antigen has been reported to be highly expressed in U87MG cells (Canazza *et al.*, 2011) and glioma tissues (Persson *et al.*, 2010). Such observation was in agreement with the parallel study, where the SA43 aptamer target was found to be expressed in both the cytoplasm and nucleus of fixed 1321N1 and U87MG cells compared to non-cancerous SVGP12 cells and normal human astrocytes (NHA cells; unpublished data). The localisation of Ku heterodimer outside of the nucleus in tumours suggests that this protein is serving additional roles besides its main function in DNA repair such as, cell adhesion, migration, and invasion, however, they are yet poorly understood (Fransson and Borrebaeck, 2006). Considering the fact that Ku 70/80 is also expressed predominantly in the nucleus of non-cancerous cells, the absence of binding to non-cancerous cells and tissues with SA43 DNA aptamer demonstrated aptamer sensitivity to detect the target in glioma and hence could be utilised in histological glioma diagnosis.

Overall, the parallel aptoprecipitation analysis on the aptamers strongly supported that the SA43 DNA aptamer targeted Ku heterodimer proteins, which was overexpressed in the tumour cells, compared to the non-cancerous cells. Moreover, the selectivity of SA43 DNA on glioma tissue sections highly supported the parallel study demonstrating aptamer SA43 DNA sensitivity to the target in tumour cells by showing least binding to the non-cancerous tissues, as Ku 70/80 was also shown to be expressed in non-cancerous cells. In addition, strong cytoplasmic and nuclear binding of SA43 on live cells, and fixed tumour cells and tissues respectively (present study), and both

cytoplasmic and nuclear binding of Ku 70/80 on fixed cells (parallel study) again demonstrates the sensitivity of the aptamer to the target and warrants further study to understand the aptamer-target interaction.

#### **8.4 Predicting the mechanism of the uptake of SA43 DNA aptamer**

Confocal imaging with Z-stacks showed intracellular distribution of SA43 DNA in the cytoplasm and towards one edge of the periphery of the nucleus of some tumour cells, possibly suggesting that the aptamer entered the cells via endocytosis and was deposited in or near the endoplasmic reticulum. This was supported by a reduction in cellular uptake of the aptamer at 4 °C when energy dependent processes, including endocytosis, are reduced. Although it is recognised that passive diffusion is also reduced at 4 °C, it is unlikely the aptamer is uptaken by a passive process because of the saturable activity of the aptamer as discussed in chapter 5. Moreover, the parallel study (section 8.3) further supported the transport to be active and highly restrictive; as non-cancerous cells would have also showed binding to the aptamer considering Ku 70/80 is present in the non-cancer cells too. The experiments where aptamers were incubated for increased duration (24 hours) also suggested that the aptamer was able to follow the endosomal and lysosomal pathway, leading to deposition of aptamer throughout the cell cytoplasm and enabling their interaction with other cellular components including lysosomes which potentially would have degraded the aptamer and hence was unable to reach the nucleus (Holt *et al.*, 2010).

Most of the aptamers showing active uptake and sensitivity to trypsin treatment have been shown to internalise via receptor-mediated endocytosis as mentioned in section 8.2. Most of the recent work have also shown that internalisation of DNA can be

mediated through macropinocytosis, an actin-driven, ligand independent mechanism (Wittrup *et al.*, 2007; Fumoto *et al.*, 2009). The AS1411 aptamer which targets nucleolin with an active process, has been shown to be internalised into cancer cells (DU145, MCF7 and MDA-MB-321) by macropinocytosis (Reyes-Reyes *et al.*, 2010). It was therefore difficult to predict the exact mechanism of the aptamer SA43 DNA to tumour cells as it showed active uptake and also entered the cells independent of trypsin treatment. If the aptamer was taken up by receptor mediated transport, then there could be some cell surface protein or any other moiety involved (including Ku 70/80, if it was present on the cell surface too), which could be resistant to trypsin cleavage and may have help the aptamer to internalise into the target cells. With respect to Ku 70/80, the protein consists of total 560 amino acids and the number of cleavages with trypsin has shown to be 82 (14.6 %) with arginine and lysine as the targets for cleavage (ExPASy peptide cutter tool by Gasteiger *et al.*, 2005). The small percentage of amino acids involved in trypsin cleavage could therefore suggest a possibility of Ku 70/80 being resistant to a 10-minute trypsin treatment if Ku 70/80 was present on cell surface along with its localisation in cytoplasm and nucleus, as the aptamer showed internalisation even after trypsin treatment. The antibody INCA-X binding to Ku 70/80 has shown to internalise in the tumour cells (pancreatic carcinoma) undergoing receptor-mediated endocytosis involving clathrin - mediated endocytosis after binding to the antigen (Fransson and Borrebaeck, 2006). In addition, different antibodies directed against Ku 70/80 have shown different abilities to target the antigen, in relation to its presentation of the cell surface or intracellular localisation (Persson *et al.*, 2010). Such cellular internalisation may also proceed by a number of other different mechanisms including phagocytosis, macropinocytosis, or clathrin and caveolae-independent endocytosis (Liu and Shapiro, 2003; Xin *et al.*, 2011). Cargo entering via these different routes is

transported to a series of intracellular compartments from where it is either recycled or directed to degradative compartments such as late endosomes and lysosomes. Clathrin mediated endocytosis, used by all eukaryotic cells to internalise nutrients and degrade or recycle substances is well known for its role for selective uptake of molecules through specific receptors (Mahmoudi *et al.*, 2011). Usually, the particles ingested via clathrin – mediated pathway and macropinocytosis initially reside in endosomes and macropinosomes respectively, which are acidified and fused with lysosomes afterwards. Understanding the exact mechanism of the uptake of the aptamer SA43 DNA would provide an idea of aptamer-target interaction and the role of Ku 70/80 in harbouring the entry of aptamer in the cytoplasm. Moreover, silencing of Ku 70/80 will further confirm and verify whether this is indeed the target. The study did not examine the specific pathway of endocytosis relevant for the aptamer uptake, which could be further clarified using individual pathway inhibitors. Sucrose and chlorpromazine, blocking agents for clathrin- coated pit formation; filipin, a special inhibitor of calveolae associated endocytosis, nocodazole, an inhibitor of macropinocytosis and cytochalasin D, a microtubule-disrupting agent could be used to confirm the actual mechanism of aptamer uptake by the cells. Understanding the uptake and trafficking within the cells will undoubtedly facilitate design improvements in aptamer therapeutics. In the context of drug delivery, the endosomal compartment is usually acidic, and many internalised molecules change their structures at low pH to release their bound substance. As such, the internalised aptamer SA43 DNA could potentially respond to these conditions to release their drug payloads. For example, one such acid – labile linkage was used by Huang *et al.* for sgc8c (aptamer)- Dox (drug) conjugate, where it was found that the aptamer – drug conjugate was cleaved inside the acidic endosomal environment, resulting in Dox release (Huang *et al.*, 2009).

Advances in microscope have increased resolution to a point where sub-cellular compartments can be visualised. In addition, because of the wide range of different fluorescent labels, multiple fluorescent labels can be used in a single sample allowing co-localisation studies. Using these approaches, it will be interesting to observe and identify aptamer internalisation, tracking the sub-cellular localisation, and identify the transport pathway of aptamers into the cells.

### **8.5 Aptamer and its entry through BBB**

The large molecular weight of the SA43 DNA aptamer (14 kDa) may preclude its crossing blood brain barrier (BBB) through paracellular transport (unless specific transporters are present). As discussed in chapter 6, aptamer SA43 DNA may have a high chance for crossing the blood brain barrier through paracellular transport without any non-specific binding to endothelial cells in the case of glioma (Section 6.3). Parallel studies in the laboratory have also shown that the aptamer can cross artificial tumour BBB culture systems (unpublished data), however, further studies are required to be performed *in vivo* to confirm these findings.

A recent study by Cheng *et al.*, found that an aptamer A15 was capable of crossing the BBB *in vivo*, suggesting that, BBB *in situ* could be the optimal platform compared to the artificial BBB culture systems for selecting aptamers that could afford central nervous system delivery through BBB (Cheng *et al.*, 2013<sup>a</sup>). While the exact mechanism of the brain uptake of the BBB penetrating aptamer (A15) was unclear, given the large molecular weight of the aptamer (23 kDa), the study proposed the most likely mechanism could be through absorptive-mediated transcytosis or fluid-phase

pinocytosis. The small size of the aptamer SA43 DNA compared to the A15 aptamer including its non-toxicity for the cells and active binding selectivity for glioma tumour tissues can enable the aptamer to cross the blood brain barrier and hence can hold a powerful promise in animal model systems to dynamically visualise and target the tumour tissues *in vivo*. Moreover, strategies combining aptamer with nanoparticles (further discussed in section 8.6) has also shown to increase the efficacy of their entry to blood brain barrier (Yu *et al.*, 2012; Liu *et al.*, 2014).

### **8.6 The bigger picture: Future perspectives of combined strategies for cancer therapy using aptamer–nanoparticle–drug conjugate model for controlled drug release**

The major challenges of recent research include finding ways to maximise the tolerated dose of chemotherapeutic drug given whilst balancing this with an acceptable toxicity profile by increasing selectivity to cancerous cells (Markman, 2008; Yallapu *et al.*, 2010; Li *et al.*, 2014). The study here already succeeded in demonstrating SA43 DNA aptamer as an excellent targeting ligand for the sensitive and selective recognition of particular cancer cell populations in glioma cell lines and tissues. The identification of the potential aptamer SA43 DNA targeting glioma will allow the possibility of coupling therapeutic agents directly to the aptamer for targeting glioma cells. Overall, the rapid uptake and tumour cell internalisation of the aptamer SA43 DNA in the cytoplasm will be advantageous, for quick release and action of the drug to the tumour cells (Li *et al.*, 2010; Kotula *et al.*, 2012). This could lower the therapeutic doses of the drugs required and would therefore reduce any harmful side effects resulting from the use of high doses of chemotherapeutics (Kim *et al.*, 2010; Li *et al.*, 2010; Kotula *et al.*, 2012). These findings will further support the hypothesis that aptamer SA43 DNA can serve as promising agent for cell type specific intracellular delivery with both diagnostic and

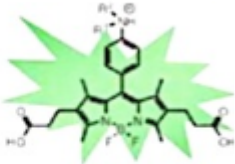
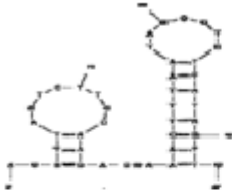
therapeutic implications.

The development of material science, however, must also satisfy the need for aptamers to have chemical properties that allow long circulation in the blood, maintain biocompatibility and exhibit control release. Aptamer distribution throughout the blood plasma compartment may be subjected to degradation by nucleases present in the blood (Chung *et al.*, 2013). In addition, some unmodified aptamers have half-lives in the blood that can be as short as 2 minutes because of their small size (Griffin *et al.*, 1993). The smaller molecular mass for most of the aptamers (5-15 kDa) including SA43 DNA (14 kDa) could be susceptible to renal filtration even if they are resistant to nuclease degradation. To overcome such difficulties, pyrimidine modifications at the 2'-fluorine position or chemical modifications with PEG have been used to enhance the bioavailability and pharmacokinetics properties (Bouchard *et al.*, 2010). The best-characterised aptamers for targeted delivery are 2'-fluoro-pyridine aptamers generated against the extracellular domain of prostate-specific membrane antigen (PSMA) (Lupold *et al.*, 2002). These aptamers have been used to deliver, self – assembled polymeric nanoparticles (Kolishetti *et al.*, 2010; Farokhzad *et al.*, 2006), and QDs (Bagalkot *et al.*, 2007) with increased efficacy for their targets.

Table 8.1 shows the strengths and weaknesses of small molecules (drugs), aptamers and nanoparticles. The aptamer SA43 DNA can also overcome the challenges of being degraded in blood and quick renal filtration by designing a model consisting of drug encapsulated high polymeric nanoparticle – aptamer bioconjugates as an effective targeting delivery systems (Figure 8.1).

Taking the advantage of the enhanced permeability and retention (EPR) effect strategy, nanoparticles can enter the interstitium and be entrapped in the tumour, and have higher retention times than normal tissues (Gao *et al.*, 2013; Zhou *et al.*, 2014). Cancer targeting entirely based on EPR (passive targeting mechanism) however, has undesirable systemic effects and suboptimal antitumour efficacy (White *et al.*, 2006; Woo *et al.*, 2008), which can be improved significantly by delivery vehicles with active tumour-targeting capability (Cao *et al.*, 2009). The excellent property of SA43 DNA showing rapid active tumour targeting will enhance the NPs loaded drug uptake into tumour cells.

**Table 8.1 Strengths and weaknesses of drugs, aptamers and nanoparticles during targeted tumour therapy.**

	<b>Drug</b>	<b>Aptamer</b>	<b>Nanoparticle</b>
<b>Molecular probe</b>			
<b>Strengths</b>	Intracellular imaging, quick therapeutic action	Small size, intracellular imaging, Low immunogenicity, High diversity, High affinity, high penetration	Narrow emission spectra, resistant to degradation, high chances of endosomal escape, improved circulation time and EPR effect
<b>Weaknesses</b>	High molecular weight, non-specific binding, high systemic toxicity	Degradable in blood or cells	Low light penetration in tissues

Drugs whether hydrophilic or hydrophobic, could be encapsulated into and protected by these delivery systems. The controlled release of chemotherapeutic drugs providing the optimum dosage for long periods will increase the efficacy of the drug, maximising patient compliance and enhance the ability to use highly toxic, poorly soluble, or relatively unstable drugs. A very recent study developed a curcumin (CUR)-encapsulated nano-particle (NP) tri-conjugate consisting of RNA aptamer (Apt-CUR-NPs) against epithelial cell adhesion molecule (EpCAM) and lipid polymer lecithin hybrid nanoparticles encapsulating curcumin for targeted delivery to colorectal adenocarcinoma cells. The tri-conjugates exhibited enhanced uptake and increased binding to HT29 colon cancer cells compared to CUR-NPs conjugated with a control aptamer, as measured by confocal microscopy and flow cytometry ( $p < 0.01$ ). In addition, a substantial improvement in cytotoxicity towards target HT29 cells was achieved along with increased bioavailability of delivered CUR was observed *in vivo* over a period of 24 hours compared to that of free CUR (Li *et al.*, 2014).

There have also been reports where uptake of ligand functionalised nano-particles conjugates can occur via an endocytic mechanism (mostly macropinocytosis related) other than receptor mediated pathway (Iversen *et al.*, 2012). In addition, the increased endosomal escape with nanoparticles has been demonstrated by few other studies, and therefore, combining the strategies of aptamer, nano-particle and drug delivery to target tumour cells will be potentially effective in glioma treatment (Pittella *et al.*, 2011; Gilleron *et al.*, 2013). Moreover, such combination of targeted drug delivery and controlled release technology may pave the road to more effective yet safe chemotherapeutic options for glioma therapy. Thus, further studies need to be carried out to elucidate the interaction between aptamer-nanoparticle drug conjugate for

optimising the drug delivery system, however, the interaction between aptamers and the target still needs to be understood, which will facilitate the action of these tri-conjugates. In addition, much work remains to be done before these conjugated materials can be used in clinical practice such as understanding the transport of aptamers to the cancer locale, the interactions between aptamers and cancer cells, the intracellular trafficking of aptamers within cancer cells and the subcellular density. The study utilised paraffin-embedded formalin fixed tissue samples for determining the potential of aptamers in histological diagnosis of glioma. Use of such fixed tissues however, may have a possibility of altering the composition or structure of epitopes during the tissue processing methods. Use of unfixed frozen tumour tissues over fixed waxed tissues can minimize tissue processing and preserve the natural presentation of epitopes. Treating aptamers on frozen tissues will further assist to acquire clearer conclusions and support the current findings on aptamer targeting to tumour tissues.

In conclusion, the results of the study have laid the foundation for future work that will demonstrate the therapeutic value of targeted drug delivery through the conjugation of aptamer – nanoparticle - drug. It is indicated that the aptamer target molecules may also provide useful information for explaining the mechanism of oncogenesis. Meanwhile, although the study has produced abundance of *in vitro* data stating that the reported aptamer SA43 DNA have more binding selectivity for glioma cells and tissues compared to the control cells and tissues, it is of paramount importance to fill the gaps of the current knowledge by understanding the exact mechanism, stability, and aptamer-target interaction.

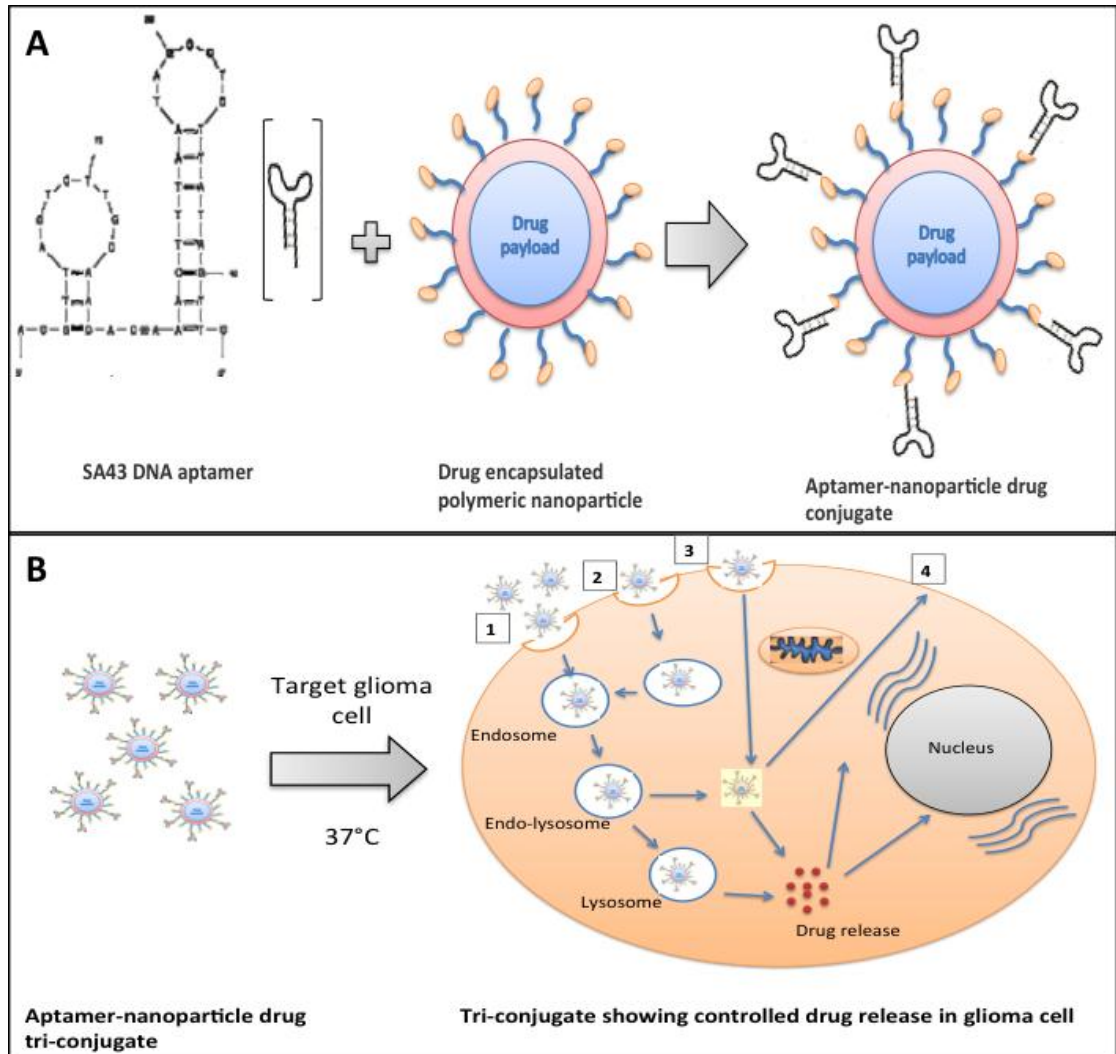


**Figure 8.1 Predicted mechanisms for targeted drug release through the use of aptamer-nanoparticle-drug conjugate. A** Model consisting of aptamer-nanoparticle drug conjugate, **B** Tri-conjugate showing cellular association (1), internalisation via endocytosis, endosomal escape of the tri-conjugate, lysosomal degradation of tri-conjugate, therapeutic drug freely diffuses into cytoplasm leading to controlled drug release, cytoplasmic transport of therapeutic drug to the target organelle; (2), Internalisation via macropinocytosis or phagocytosis; (3), cellular internalisation and releasing the drug without any association with endosomes or lysosomes, (4) recycling and exocytosis of nano-particles.

## 8.6 Summary

In summary, the results provided a proof-of-concept for the use of RNA and DNA aptamers in targeting glioma cells. The assays described in the study provided a powerful tool for assessing and confirming the internalisation potential and cellular localisation of the selected aptamers. The selective binding capability of aptamers studied, suggested that the interaction of the aptamer and target largely depends on the nature of the aptamer sequence. From the shortened aptamers studied, SA43 DNA exhibited selective *in vitro* targeting on tumour targets on both live and fixed glioma cells, and most importantly glioma tissues. The key consequence of the internalising property of the aptamer SA43 DNA is the ability to accumulate inside the tumour cells, thus routing their therapeutic cargoes to intracellular sites relevant to their action. The current approach will hold particular promise in aptamer – nanoparticle – drug delivery for studying targeted therapeutics. The selective binding capability of aptamer SA43 DNA and the sensitivity to glioma tissues will hold promise in histochemical diagnosis of glioma. Moreover, the small size of the aptamer, non-toxicity to cells, and negligible binding to endothelial cells will potentially allow the aptamer to cross BBB via EPR effect. This will further allow testing the potential of aptamer-nanoparticle-drug conjugate for their enhanced efficacy in targeting tumour cells *in vivo*. Importantly, these efforts promise to expedite the development of the aptamer- based approaches for delivering therapeutic drugs to the cytoplasm of the target cells and possibly facilitate a more rapid translation for therapeutics to humans.

## APPENDICES

### Appendix 1. Description and specifications of the cell lines and their media.

Cell lines	Description	Culture Medium (Lonza, UK)	Media constituents
1321N1	Astrocytoma WHO grade II	Dulbecco's Modified Eagle Medium (DMEM), 10 % FBS and L-glutamine (2 mM)	1 mM sodium bicarbonate 1.0 g/l glucose 25 mM Hepes 0.0011 g/l phenol red
T24	Highly malignant grade III human urinary bladder carcinoma		
U87MG	Glioblastoma WHO grade IV	Eagle's Minimum Essential Medium (EMEM), 10% FBS, L-glutamine (2 mM), Sodium pyruvate (5 mM) and NEAA (5 mM)	2.2 g/l sodium bicarbonate 4.5 g/l glucose 10 mM Hepes 0.0053 g/l phenol red
T98G	Grade IV glioblastoma		
SVGPI2	Non-cancerous foetal astrocytes		
MCF-7	Human mammary gland adenocarcinoma cell line		

### Appendix 2. Formulation and storage conditions of reagents used in cell culture.

Reagent	Storage	Constituents	Supplier
Fetal Bovine serum (FBS)	-20°C	Heat inactivated FBS	Lonza, UK
L-glutamine	-20°C	200 mM L-glutamine	Lonza, UK
Non essential amino acid	2-8°C	100x non essential amino acid	Lonza, UK
Phosphate buffer saline (PBS, 1x)	Room temperature	8 g/l NaCl, 0.2 g/l KCl, 1.44 g/l Na <sub>2</sub> PO <sub>4</sub> 0.24 g/l KH <sub>2</sub> PO <sub>4</sub> , pH 7.4.	Fisher scientific, UK
Trypsin EDTA	-20°C	0.5 g Porcine trypsin 0.2 g EDTA	Lonza, UK
Dimethyl-sulfoxide (DMSO)	Room temperature	99.5% dimethyl sulfoxide, 0.81% sodium chloride	Lonza, UK
Trypan blue	Room temperature	0.81% (w/v) sodium chloride 0.06% (w/v) potassium phosphate dibasic	Sigma, UK

**Appendix 3.** DVD inserted showing Z stacks and merged Cy3 and DAPI image of SA43 DNA on U87MG, 1321N1 and SVGP12 at various time points as measured by confocal microscopy.

**Appendix 4. Patient's demographics**

BTNW no.	Diagnosis	Bx site	Age	Gender
625	Normal brain	R frontal	51	F
713	Normal brain	R posterior fossa	39	F
596	Normal brain	L frontal	60	M
7	Normal brain	R temporal	66	M
106	Normal brain	R temporal	42	F
136	Normal brain	R temporal	51	F
678	Normal brain	R frontal	48	F
713	Normal brain	R posterior fossa	39	F
8	Normal brain	R frontal	38	F
83	Normal brain	L temporal	57	M
225	Normal brain	R temporal	26	F
321	Normal brain	L parietal	72	M
356	pilocytic astrocytoma I	Posterior fossa	25	M
720	pilocytic astrocytoma I	Posterior fossa	65	F
814	pilocytic astrocytoma I	L cerebellar pontine angle	23	F
1043	Ganglioglioma I	R frontal	16	M
422	Pilocytic astrocytoma I	L posterior fossa	25	M
632	Ganglioglioma I	L temporal	38	F
801	Subependymoma I	4th ventricle	52	M
680	astrocytoma II	R temporal	59	M
726	oligoastrocytoma II	R occipital	45	M
736	astrocytoma II	L temporal	63	F
740	astrocytoma II	L frontal	46	M
761	astrocytoma II	L temporal	24	M
934	Diffusely infiltrating LGG II	L frontal	30	M
1005	Mixed glioma / Glioneuronal II	R occipital	43	F
1028	Gemistocytic astrocytoma II	Not stated	40	M
1044	Infiltrating LGG II	R frontal	27	M
1047	Ependymoma II	L occipital	52	F
681	astrocytoma III	L occipital	75	M
629	astrocytoma III	R parietal	39	F
686	oligoastrocytoma III	R parietal	56	M

703	oligoastrocytoma III	R frontal	46	M
738	oligodendroglioma III	L frontal	66	M
883	Oligodendroglioma III	L frontal	59	F
925	Astrocytoma III	R parietal	78	M
962	Astrocytoma III	L parietal	66	F
1021	Astrocytoma III	L frontal	56	F
1051	Astrocytoma III	L occipital	34	M
1066	Oligodendroglioma III	R temporal	59	M
933	Cavernoma high grade	R frontal	41	M
693	GBM IV	L frontal	74	M
748	GBM IV	L frontal	49	M
749	GBM IV	L frontal	45	F
758	GBM IV	L frontal	49	M
769	GBM IV	L frontal	70	M
789	GBM IV	L frontal	41	M
794	GBM IV	R parietal	77	M
806	GBM IV	R parafalcine	66	F
807	GBM IV	L frontal	79	M
1054	GBM IV	R frontal	42	M
1077	GBM IV	R frontal	65	M
1078	GBM IV	R parieto-occipital	79	M
1086	GBM IV	R frontotemporal	41	M
1088	GBM IV	L frontal	74	M
1090	GBM IV	L parietal	73	F
1094	No tumour biopsy	R frontal	32	M
13	Oligoastrocytoma II	R temporal	52	F
20	Astrocytoma II	L frontal	26	M
62	Ependymoma II	4th ventricle	34	F
65	Diffuse astrocytoma II	L frontal	25	M
158	Diffuse astrocytoma II	L temporal	74	M
160	Astrocytoma II	L tempero-frontal	35	M

**Appendix 4.** Total binding scores for each aptamer treated on non-cancerous tissues.

BTNW No.	Diagnosis	Random Aptamer	SA44 DNA	SA43 DNA	SA56 DNA
7	Non-cancerous tissue	0	0	0	4
8	Non-cancerous tissue	0	7	3	7
83	Non-cancerous tissue	0	6	3	6
106	Non-cancerous tissue	0	2	0	6
136	Non-cancerous tissue	0	0	0	4
225	Non-cancerous tissue	0	6	3	8
321	Non-cancerous tissue	0	5	4	5
596	Non-cancerous tissue	0	5	2	7
678	Non-cancerous tissue	0	0	0	0
713	Non-cancerous tissue	0	8	6	8
1039	Non-cancerous tissue	0	7	7	8
1085	Non-cancerous tissue	0	8	7	8
1094	Non-cancerous tissue	0	5	3	5
Average		0.0	4.5	2.9	5.8

**Appendix 5.** Total binding scores for each aptamer treated on Grade I patients tissues

BTNW No.	Diagnosis	Random Aptamer	SA44 DNA	SA43 DNA	SA56 DNA
356	pilocytic astrocytoma I	0	5	6	4
422	pilocytic astrocytoma I	0	8	8	8
632	ganglioglioma I	3	4	7	6
720	pilocytic astrocytoma I	0	7	7	8
801	Subependymoma I	0	7	7	7
814	pilocytic astrocytoma I	0	7	7	7
1043	ganglioglioma I	0	4	3	3
Average		0.4	6.0	6.4	6.1

**Appendix 6.** Total binding scores for each aptamer treated on Grade II patients tissues

BTNW No.	Diagnosis	Random aptamer	SA44 DNA	SA43 DNA	SA56 DNA
13	Oligoastrocytoma II	0	8	8	8
62	Ependymoma II	3	8	8	8
65	Diffuse astrocytoma II	0	8	8	8
158	Diffuse astrocytoma II	0	8	8	8
160	Astrocytoma II	0	8	8	8
726	Oligoastrocytoma II	0	5	5	6
736	Astrocytoma II	0	4	5	5
740	Astrocytoma II	0	4	4	5
761	Astrocytoma II	0	4	4	5
934	Diffusely infiltrating LGG II	0	0	0	0
1005	Mixed glioma/glioneuronal II	0	6	6	8
1028	Gemistocytic astrocytoma II	5	8	8	8
1047	Ependymoma II	0	2	2	3
1044	Infiltrating LGG II	0	0	0	0
<b>Average</b>		<b>0.6</b>	<b>5.2</b>	<b>5.3</b>	<b>5.7</b>

**Appendix 7.** Total binding scores for each aptamer treated on Grade III patients tissues

BTNW No.	Diagnosis	Random aptamer	SA44 DNA	SA43 DNA	SA56 DNA
629	Astrocytoma III	0	7	7	7
686	Oligoastrocytoma III	3	8	7	7
703	Oligoastrocytoma III	0	8	8	8
738	Oligoastrocytoma III	0	8	8	7
772	Chondrosarcoma III	0	8	7	8
883	Oligoastrocytoma III	0	7	5	8
925	Astrocytoma III	0	2	3	8
933	Cavernoma	0	8	7	8
962	Astrocytoma III	0	0	4	2
1021	Astrocytoma III	0	8	8	8
1051	Astrocytoma III	7	8	8	8
1066	Oligoastrocytoma III	4	6	8	8
<b>Average</b>		<b>1.2</b>	<b>6.5</b>	<b>6.7</b>	<b>7.3</b>

**Appendix 8.** Total binding scores for each aptamer treated on Grade IV tissues

BTNW No.	Diagnosis	Random aptamer	SA44 DNA	SA43 DNA	SA56 DNA
769	GBM	5	8	6	8
794	GBM	2	6	6	6
806	GBM	0	2	3	5
807	GBM	0	0	0	2
1054	GBM	3	8	8	8
1077	GBM	6	7	8	8
1078	GBM	4	8	8	8
1086	GBM	3	6	8	8
1088	GBM	0	4	6	7
1090	GBM	0	6	8	8
<b>Average</b>		<b>2.3</b>	<b>5.5</b>	<b>6.1</b>	<b>6.8</b>

**Appendix 8.** Total binding scores for each aptamer treated on meningioma tissues

BTNW No.	Diagnosis	Random aptamer	SA44 DNA	SA43 DNA	SA56 DNA
625	Meningioma I	0	6	0	4
759	Meningioma I	5	6	5	7
779	Meningioma I	0	8	8	8
811	Meningioma II	0	2	2	2
760	Meningioma II	0	5	5	8
<b>Average</b>		<b>1</b>	<b>5.4</b>	<b>4</b>	<b>5.8</b>

**REFERENCES**

- Ababneh N, Alshaer W, Allozi O, Mahafzah A, El-Khateeb M, Hillaireau H, Noiray M, Fattal E, & Ismail S (2013). *In vitro* selection of modified RNA aptamers against CD44 cancer stem cell marker. *Nucleic Acid Ther* **23**, 401-407.
- Abaza MS, Shaban F, Narayan RK, & Atassi MZ (1998). Human glioma associated intermediate filament proteins: over-expression, co-localisation and cross-reactivity. *Anticancer Research* **18**, 1333-1340.
- Agarwal S, Manchanda P, Vogelbaum MA, Ohlfest JR, & Elmquist WF (2013). Function of the blood-brain barrier and restriction of drug delivery to invasive glioma cells: findings in an orthotopic rat xenograft model of glioma. *Drug Metab Dispos* **41**, 33-39.
- Albayrak B, Samdani AF, & Black PM (2004). Intra-operative magnetic resonance imaging in neurosurgery. *Acta Neurochir (Wien)* **146**, 543-556.
- Ara MN, Hyodo M, Ohga N, Hida K, & Harashima H (2012). Development of a novel DNA aptamer ligand targeting to primary cultured tumor endothelial cells by a cell-based SELEX method. *PLoS ONE* **7**, e50174.
- Arnesano F, Losacco M, & Natile G (2013). An update view of cisplatin transport. *European journal of inorganic chemistry* **15**, 2701-2711.
- Assanga I, Salido A, Lujan L, Durazo A, Acosta-Silva AL, Rivera Castaneda EG, & Rubio-Pino JL (2013). Cell growth curves for different cell lines and their relationship with biological activities. *Academic journals* **4**, 60-70.
- Bagalkot V, Zhang L, Levy-Nissenbaum E, Jon S, Kantoff PW, Langer R, & Farokhzad OC (2007). Quantum dot-aptamer conjugates for synchronous cancer imaging, therapy, and sensing of drug delivery based on bi-fluorescence resonance energy transfer. *Nano Lett* **7**, 3065-3070.
- Bai R, Shi Z, Zhang J, Li D, Zhu Y, & Zheng S (2012). ST13, a proliferation regulator that inhibits growth and migration of colorectal cancer cell lines. *J Zhejiang Univ-Sci B (Biomed & Biotech)* ISSN, 1862-1783.
- Baldrich E, Restrepo A, & O'Sullivan CK (2004). Aptasensor development: elucidation of critical parameters for optimal aptamer performance. *Anal Chem*, **76**, 7053-7063.

- Barajas RF, Chang JS, Sneed PK, Segal MR, McDermott MW, & Cha S (2009). Distinguishing recurrent intra-axial metastatic tumour from radiation necrosis following gamma knife radiosurgery using dynamic susceptibility-weighted contrast-enhanced perfusion MR imaging. *Am J Neuroradiol* **30**, 367-372.
- Bates PJ, Kahlon JB, Thomas SD, Trent JO, & Miller DM (1999). Antiproliferative activity of G-rich oligonucleotides correlates with protein binding. *J Biol Chem* **274**, 26369-26377.
- Bates PJ, Laber DA, Miller DM, Thomas SD, & Trent JO (2009). Discovery and development of the G-rich oligonucleotide AS1411 as a novel treatment for cancer. *Exp Mol Pathol* **86**, 151-164.
- Bayrac AT, Sefah K, Parekh P, Bayrac C, Gulbakan B, Oktem HA, & Tan W (2011). *In vitro* selection of DNA Aptamers to Glioblastoma Multiforme. *ACS Chem Neurosci* **2**, 175-181.
- Belkin DA, Chen J, Mo JL, Rosoff JS, Goldenberg S, Poppas DP, Krueger JG, Herschman M, Mitsui H, Felsen D, & Carucci JA (2013). An animal explant Model for the study of human cutaneous squamous cell carcinoma. *PLoS ONE* **8**, e76156.
- Blank M, Weinschenk T, Priemer M, & Schluesener H (2001). Systematic evolution of a DNA aptamer binding to rat brain tumor microvessels: selective targeting of endothelial regulatory protein pigpen. *Journal of Biological Chemistry* **276**, 16464-16468.
- Boncler M, Różalski M, Krajewska U, Podśędek A, & Watala C (2014). Comparison of PrestoBlue and MTT assays of cellular viability in the assessment of anti-proliferative effects of plant extracts on human endothelial cells. *Journal of Pharmacological and Toxicological Methods* **69**, 9-16.
- Boomer RM, Lewis SD, Healy JM, Kurz M, Wilson C, & McCauley TG (2005). Conjugation to polyethylene glycol polymer promotes aptamer biodistribution to healthy and inflamed tissues. *Oligonucleotides* **15**, 183-195.
- Bouchard PR, Hutabarat RM, & Thompson KM (2010). Discovery and development of therapeutic aptamers. *Annu Rev Pharmacol Toxicol* **50**, 237-257.
- Brahmachari S, Fung YK, & Pahan K (2006). Induction of glial fibrillary acidic protein expression in astrocytes by nitric oxide. *J Neurosci* **26**, 4930-4939.

- Brandes AA, Ermani M, Turazzi S, Scelzi E, Berti F, Amista P, Rotilio A, Licata C, & Fiorentino MV (1999). Procarbazine and high-dose tamoxifen as a second-line regimen in recurrent high-grade gliomas: a phase II study. *J Clin Oncol* **17**, 645-650.
- Breslin S & O'Driscoll L (2013). Three-dimensional cell culture: the missing link in drug discovery. *Drug discovery today*. **18**, 240-249.
- Canazza A, De Grazia U, Fumagalli L, Brait L, Ghielmetti F, Fariselli L, Croci D, Salmaggi A, & Ciusani E (2011). *In vitro* effects of Cyberknife-driven intermittent irradiation on glioblastoma cell lines. *Neurol Sci* **32**, 579-588.
- Cao Z, Tong R, Mishra A, Xu W, Wong GC, Cheng J, & Lu Y (2009). Reversible cell-specific drug delivery with aptamer-functionalized liposomes. *Angew. Chem. Int. Ed. Engl* **48**, 6494-6498.
- Capes-Davis A, Theodosopoulos G, Atkin I, Drexler HG, Kohara A, MacLeod RA, Masters JR, Masters JR, Nakamura Y, Reid YA, Reddel RR, & Freshney RI (2010). Check your cultures! A list of cross-contaminated or misidentified cell lines. *Int. J. Cancer* **127**, 1-8.
- Carminati PO, Mello SS, Fachin AL, Junta CM, Sandrin-Garcia P, Callotti CG, Donadi EA, Passos GA, & Sakamoto-Hojo ET (2010). Alterations in gene expression profiles correlated with cisplatin cytotoxicity in the glioma U343 cell line. *Genet Mol Biol* **33**, 159-168.
- Cerchia L & de Franciscis V (2010). Targeting cancer cells with nucleic acid aptamers. *Trends Biotechnol* **28**, 517-525.
- Cerchia L, Esposito CL, Jacobs AH, Tavitian B, & Franciscis V (2009). Differential SELEX in human glioma cell lines. *Plos one* **4**(11), e7971. Doi: 10.1371/0007971.
- Charlton J, Sennello J, & Smith D (1997). *In vivo* imaging of inflammation using an aptamer inhibitor of human neutrophil elastase. *Chem Biol* **4**, 809-816.
- Chen T, Shukoor MI, Wang R, Zhao Z, Yuan Q, Banrungsap S, Xiong X, & Tan W (2011). Smart multifunctional nanostructure for targeted cancer chemotherapy and magnetic resonance imaging. *ACS Nano* **5**, 7866-7873.

- Chen XC, Deng YL, Lin Y, Pang DW, Qing H, Qu F, & Xie HY (2008). Quantum dot-labeled aptamer nanoprobe specifically targeting glioma cells. *Nanotechnology* **19**, 235105.
- Cheng C, Chen YH, Lennox KA, Behlke MA, & Davidson BL (2013<sup>a</sup>). *In vivo* SELEX for Identification of brain-penetrating aptamers. *Mol Ther Nucleic Acids* **2**, e67.
- Cheng Y, Morshed RA, Auffinger B, Tobias AL, & Lesniak MS (2013). Multifunctional nanoparticles for brain tumor imaging and therapy. *Adv Drug Deliv Rev* **66**, 42-57.
- Christian S, Pilch J, Akerman ME, Porkka K, Laakkonen P, & Ruoslahti E (2003). Nucleolin expressed at the cell surface is a marker of endothelial cells in angiogenic blood vessels. *JCB* **163**, 871-878.
- Chu TC, Marks JW 3<sup>rd</sup>, Lavery LA, Faulknew S, Rosenblum MG, Ellington AD, & Levy M (2006). Aptamer:toxin conjugates that specifically target prostate tumor cells. *Cancer res* **66**, 5989-5992.
- Chung CH, Kim JH, Jung J, & Chung BH (2013). Nuclease-resistant DNA aptamer on gold nanoparticles for the simultaneous detection of Pb<sup>2+</sup> and Hg<sup>2+</sup> in human serum. *Biosensors and Bioelectronics* **41**, 827-832.
- Cibiel A, Dupont DM, & Duconge F (2011). Methods To Identify Aptamers against Cell Surface Biomarkers. *Pharmaceuticals (Basel)* **4**, 1216-1235.
- Cloughesy TF, Wen PY, Robins HI, Chang SM, Groves MD, Fink KL, Junck L, Schiff D, Abrey L, Gilbert MR, Lieberman F, Kuhn J, DeAngelis LM, Mehta M, Raizer JJ, Yung WK, Aldape K, Wright J, Lamborn KR, & Prados MD (2006). Phase II trial of tipifarnib in patients with recurrent malignant glioma either receiving or not receiving enzyme-inducing antiepileptic drugs: a North American Brain Tumor Consortium Study. *J Clin Oncol* **24**, 3651-3656.
- Cohen AL, Holmen SL, & Colman H (2013). IDH1 and IDH2 mutations in gliomas. *Curr Neurol Neurosci rep* **13**, 135.
- Coomer BL, Stewart PA, Hayakawa K, Farrell CL, & Del Maestro RF (1985). Quantitative morphology of human glioblastoma multiforme microvessels: structural basis of blood-brain barrier defect. *J Neurooncol* **5**, 299-307.
- Cowperthwaite MC & Ellington AD (2008). Bioinformatic analysis of the contribution of

- primer sequences to aptamer structures. *J. Mol. Evol* **67**, 95-102.
- Cruz HJ, Yanase Y, & Carrondo MJT (1997). Cell dislodging methods under serum-free conditions. *Appl Microbiol Biotechnol* **47**, 482-488.
- Cui ZQ, Ren Q, Wei HP, Chen Z, Deng JY, Zhang ZP, & Zhang XE (2011). Quantum dot-aptamer nanoprobe for recognizing and labeling influenza A virus particles. *Nanoscale* **3**, 2454-2457.
- Darisipudi MN, Kulkarni OP, Sayyed SG, Ryu M, Migliorini A, Sagrinati C, *et al.* (2011). Dual blockade of the homeostatic chemokine CXCL12 and the proinflammatory chemokine CCL2 has additive protective effects on diabetic kidney disease. *Am J Pathol* **179**, 116-124.
- Darling JL (2005). *In Vitro Culture of Malignant Brain Tumors*, in *Culture of Human Tumor Cells* (eds R. Pfragner and R. I. Freshney), *John Wiley & Sons, Inc.*, Hoboken, NJ, USA. doi: 10.1002/0471722782.ch14.
- Darnell RB & Posner JB (2006). Paraneoplastic syndromes affecting the nervous system. *Semin Oncol* **33**, 270-298.
- Darzynkiewicz Z (2012). Cycling into future: mass cytometry for the cell-cycle analysis. *International Society for Advancement of Cytometry* **81**(7), 546-548.
- Dassie JP, Liu XY, Thomas GS, Whitaker RM, Thiel KW, Stockdale KR, Meyerholz DK, McCaffrey AP, McNamara JO 2<sup>nd</sup>, & Giangrande PH (2009). Systemic administration of optimized aptamer-siRNA chimeras promotes regression of PSMA-expressing tumors. *Nat Biotechnol* **27**, 839-849.
- Davis FG & McCarthy BJ (2001). Current epidemiological trends and surveillance issues in brain tumours. *Expert Rev Anticancer Ther* **1**, 395-401.
- De Groot JF (2013). Prediction of response to chemotherapy in anaplastic glioma: how many markers does it take? *J Clin Oncol* **31**, 297-298.
- De Matos LL, Trufelli DC, de Matos MG, & da Silva Pinhal MA (2010). Immunohistochemistry as an important tool in biomarkers detection and clinical practice. *Biomark insights* **5**, 9-20.

- Debinski W, Gibo DM, Hulet SW, Connor JR, & Gillespie GY (1999). Receptor for interleukin 13 is a marker and therapeutic target for human high-grade gliomas. *Clin Cancer Res*, **5**: 85-990.
- Deng SM, Zhang B, Wu YW, Zhang W, & Chen YY (2013). Detection of glioma recurrence by <sup>11</sup>C-methionine positron emission tomography and dynamic susceptibility contrast-enhanced magnetic resonance imaging: a meta-analysis. *Nucl med commun* **34**, 758-766.
- Dey AK, Griffiths C, Lea SM, & James W (2005). Structural characterization of an anti-gp120 RNA aptamer that neutralizes R5 strains of HIV-1. *RNA* **11**, 873-884.
- Dhar, S., Gu, FX, Langer R, Farokhzad OC, & Lippard SJ (2008). Targeted delivery of cisplatin to prostate cancer cells by aptamer functionalized Pt (IV) prodrug-PLGA PEG nanoparticles. *Proc. Natl. Acad. Sci* **105**, 17356-17361.
- Dieckmann T, Butcher SE, Sassanfar M, Szostak JW, & Feigon J (1997). Mutant ATP binding RNA aptamers reveal the structural basis for ligand binding. *J. Mol. Biol.* **273**, 467-478.
- Doetsch F (2003). The glial identity of neural stem cells. *Nat Neuroscience* **6**, 1127-1134.
- Doherty G. (2010) Current diagnosis and treatment: surgery. *McGraw- Hill Companies*, **13**, 841.
- Dong S, Nutt CL, Betensky RA, Stemmer-Rachamimov AO, Denko NC, Ligon KL, Rowitch DH, & Louis DN (2005). Histology-based expression profiling yields novel prognostic markers in human glioblastoma. *J Neuropathol Exp Neurol* **64**, 948-955.
- Dua P, Kim S, & Lee DK (2011). Nucleic acid aptamers targeting cell-surface proteins. *Methods* **54**, 215–225.
- Dupont DM, Madsen JB, Hartmann RK, Tavitian B, Ducongé F, Kjems J, & Andreasen PA (2010). Serum-stable RNA aptamers to urokinase-type plasminogen activator blocking receptor binding. *RNA* **16**, 2360-2369.
- Eastman A (1990). Activation of programmed cell death by anticancer agents: cisplatin as a model system,” *Cancer Cells* **2**, 275–280.
- Ellington AD & Szostak JW (1990). *In vitro* selection of RNA molecules that bind specific ligands. *Nature* **346**, 818–822.

- Esposito CL, Cerchia L, Catuogno S, De Vita G, Dassie JP, Santamaria G, Swiderski P, Condorelli G, Giangrande PH, & de Franciscis V (2014). Multifunctional aptamer-miRNA conjugates for targeted cancer therapy. *Molecular therapy* **22**, 1151-1163.
- Esposito CL, Passaro D, Longobardo I, Condorelli G, Marotta P, Affuso A, de Franciscis V, & Cerchia L (2011). A Neutralizing RNA aptamer against EGFR Causes Selective Apoptotic Cell Death. *PLoS ONE* **6**, e24071.
- Eugene WM, Shima DT, Calias P, Cunningham ET, Guyer DR, & Adamis AP (2006). Pegaptanib, a targeted anti-VEGF aptamer for ocular vascular disease. *Nature reviews drug discovery* **5**, 123-132.
- Fadul CE, Kingman LS, Meyer LP, Cole BF, Eskey CJ, Rhodes CH, Roberts DW, Newton HB, & Pipas JM (2008). A phase II study of thalidomide and irinotecan for treatment of glioblastoma multiforme. *J Neurooncol* **90**, 229-235.
- Farokhzad OC, Cheng J, Teply BA, Sherifi I, Jon S, Kantoff PW, Richie JP, & Langer R (2006). Targeted nanoparticle-aptamer bioconjugates for cancer chemotherapy *in vivo*. *Proc Natl Acad Sci* **103**, 6315-6320.
- Ferrara N, Gerber HP, & LeCouter J (2003). The biology of VEGF and its receptors. *Nat. Med* **9**, 669-676.
- Ferrara N, Mass RD, Campa C, & Kim R (2006). Targeting VEGF-A to treat cancer and age-related macular degeneration. *Annual review of medicine* **58**, 491-504.
- Fischer NO, Tok JB-H, Tarasow TM (2008). Massively parallel interrogation of aptamer sequence, structure and function. *PLoS ONE* **3**, e2720.
- Floege J, Ostendorf T, Janssen U, Burg M, Radeke HH, Vargeese C, Gill SC, Green LS, & Janjić N (1999). Novel approach to specific growth factor inhibition *in vivo*: antagonism of platelet-derived growth factor in glomerulonephritis by aptamers. *Am. J. Pathol* **154**, 169-179.
- Franceschi E, Cavallo G, Lonardi S, Margini E, Tosoni A, Grosso D, Scopece L, Blatt V, Urbini B, Pession A, Tallini G, Crino L, & Brandes AA (2007). Gefitinib in patients with progressive high-grade gliomas: a multicentre phase II study by Gruppo Italiano Cooperativo di Neuro-Oncologia (GICNO). *Br J Cancer* **96**, 1047-1051.

- Francesconi AB, Dupre S, Matos M, Martin D, Hughes BG, Wyld DK, & Lickliter JD (2010). Carboplatin and etoposide combined with bevacizumab for the treatment of recurrent glioblastoma multiforme. *J Clin Neurosci* **17**, 970-974.
- Fransson J & Borrebaeck CA (2006). The nuclear DNA repair protein Ku70/80 is a tumor-associated antigen displaying rapid receptor mediated endocytosis. *Int J Cancer* **119** (10), 2492-2496.
- Frézard F & Garnier-Suillerot A (1998). Permeability of lipid bilayer to anthracycline derivatives: role of the bilayer composition and of the temperature. *Biochim Biophys Acta* **1389**, 13-22.
- Friedman HS, Prados MD, Wen PY, Mikkelsen T, Schiff D, Abrey LE, Yung WK, Paleologos N, Nicolas MK, Jensen R, Vredenburgh J, Huang J, Zheng M, & Cloughesy T (2009). Bevacizumab alone and in combination with irinotecan in recurrent glioblastoma. *J Clin Oncol* **27**, 4733-4740.
- Fumoto S, Nishi J, Ishii H, Wang X, Miyamoto H, Yoshikawa N, Nakashima M, Nakamura J, & Nishida K (2009). Rac-mediated macropinocytosis is a critical route for naked plasmid DNA transfer in mice. *Mol. Pharmaceutics* **6**, 1170-1179.
- Furneaux HM, Rosenblum MK, Dalmau J, Wong E, Woodruff P, Graus F, & Posner JB (1990). Selective expression of Purkinje-cell antigens in tumour tissue from patients with paraneoplastic cerebellar degeneration. *N Engl J Med* **322**, 1844-1851.
- Galanis E, Buckner JC, Maurer MJ, Kreisberg JI, Ballman K, Boni J, Peralba JM, Jenkins RB, Dakhil SR, Morton RF, Jaeckle KA, Scheithauer BW, Dancey J, Hidalgo M, & Walsh DJ (2005). Phase II trial of temsirolimus (CCI-779) in recurrent glioblastoma multiforme: a North Central Cancer Treatment Group Study. *J Clin Oncol* **23**, 5294-5304.
- Galanis E, Jaeckle KA, Maurer MJ, Reid JM, Ames MM, Hardwick JS, Reilly JF, Loboda A, Nebozhyn M, Fantin VR, Richon VM, Scheithauer B, Giannini C, Flynn PJ, Moore DF Jr, Zwiebel J, & Buckner JC (2009). Phase II trial of vorinostat in recurrent glioblastoma multiforme: a north central cancer treatment group study. *J Clin Oncol* **27**, 2052-2058.

- Gao H, Qian J, Cao S, Yang Z, Pang Z, Pan S, Fan L, Xi Z, Jiang X, & Zhang S (2012<sup>a</sup>). Precise glioma targeting of and penetration by aptamer and peptide dual-functioned nanoparticles. *Biomaterials* **33**, 5115-5123.
- Gao H, Qian J, Yang Z, Pang Z, Xi Z, Cao S, Wang Y, Pan S, Zhang S, Wang W, Jiang X, & Zhang Q (2012<sup>b</sup>). Whole-cell SELEX aptamer-functionalised poly (ethyleneglycol)-poly ( $\epsilon$ -caprolactone) nanoparticles for enhanced targeted glioblastoma therapy. *Biomaterials* **33**, 6264-6272.
- Gasteiger E, Hoogland C, Gattiker A, Duvaud S, Wilkins MR, Appel RD, & Bairoch A (2005). Protein identification and analysis tools on the ExPASy server. John M Walker (ed): The proteomics protocols handbook, Human Press.
- Geiger A, Burgstaller P, von der Eltz H, Roeder A, & Famulok M (1996). RNA aptamers that bind L-arginine with sub-micromolar dissociation constants and high enantioselectivity. *Nucleic Acids Res* **24**, 1029-1036.
- Gilbert MR, Dignam JJ, Armstrong TS, *et al.*, (2014). A randomised trial of Bevacizumab for newly diagnosed glioblastoma. *N Engl J Med* **370**, 699-708.
- Gilleron J, Querbes W, Zeigerer A, Borodovsky A, Marsico G, Schubert U, Manygoats K, Seifert S, Andree C, Stoter M, Epstein-Barash H, Zhang L, Kotliansky V, *et al.*, (2013). Image-based analysis of lipid nanoparticle-mediated siRNA delivery, intracellular trafficking and endosomal escape. *Nat Biotechnol* **31**, 638-646.
- Gold L, Polisky B, Uhlenbeck O, & Yarus M (1995). Diversity of oligonucleotide functions. *Annu Rev Biochem* **64**, 763-797.
- Griffin LC, Tidmarsh GF, Bock LC, Toole JJ, & Leung LL (1993). *In vivo* anticoagulant properties of a novel nucleotide-based thrombin inhibitor and demonstration of regional anticoagulation in extracorporeal circuits. *Blood* **81**, 3271-3276.
- Grossman SA (2003). Arguments against the routine use of currently available adjuvant chemotherapy in high-grade gliomas. *Semin Oncol* **30**, 19-22.
- Guo J, Gao X, Xia H, Gu G, Pang Z, Jiang X, Yao L, Chen J, & Chen H (2011). Aptamer-functionalized PEG-PLGA nanoparticles for enhanced anti-glioma drug delivery. *Biomaterials* **32**, 8010-8020.

- Gutenberg A, Bock HC, Bruck W, Doerner L, Mehdorn HM, Roggendorf W, Westphal M, Felsberg J, Reifenberger G, & Giese A (2013). MGMT promoter methylation status and prognosis of patients with primary or recurrent glioblastoma treated with carmustine wafers. *Br J Neurosurg* **27**, 772-778.
- Hambardzumyan D, Squatrito M, Carbajal E, & Holland EC (2008). Glioma formation, cancer stem cells, and Akt Signalling. *Biomedical and life sciences* **4**, 203-210.
- Hamerlik P, Lathia JD, Rasmussen R, Wu Q, Bartkova J, Lee M, Moudry P, Bartek J, Fischer W, Lukas J, Rich JN, & Bartek J (2012). Autocrine VEGF-VEGFR2-Neuropilin-1 signaling promotes glioma stem-like cell viability and tumor growth. *J Exp Med* **209**, 507-520.
- Han ME, Baek S, Kim HJ, Lee JH, Ryu SH, & Oh SO (2014). Development of an aptamer-conjugated fluorescent nanoprobe for MMP2. *Nanoscale research letter* **9**, 104.
- Han W, Xin Z, Zhao Z, Bao W, Lin X, Yin B, Zhao J, Yuan J, Qiang B, & Peng X (2013). RNA-binding protein PCBP2 modulate glioma growth by regulating FHL3. *J Clin Invest*. **123**, 2103-2118.
- Harmann T & Patel DJ (2008). Adaptive recognition by nucleic acid aptamers. *Science* **287**, 820-825.
- Harvey JM, Clark GM, Osborne CK, & Allred DG (1999). Estrogen receptor status by immunohistochemistry is superior to the ligand-binding assays for predicting response to adjuvant therapy in breast cancer. *J Clin Oncol* **17**, 1474-85.
- Hatiboglu MA, Wei J, Wu ASG, & Heimberger AB (2010). Immune therapeutic targeting of glioma cancer stem cells. *TargOncol* **5**, 217-227.
- Healy JM, Lewis SD, Kurz M, Boomer RM, Thompson KM, Wilson C, McCauley TG (2004). Pharmacokinetics and biodistribution of novel aptamer compositions. *Pharm. Res* **21**, 2234-2246.
- Hegi ME, Diserens AC, Gorlia T, Hamou MF, de Tribolet N, Weller M, Kros JM, Hainfellner JA, Mason W, Mariani L, Bromberg JE, Hau P, Mirimanoff RO, Cairncross JG, Janzer RC, & Stupp R (2005). MGMT gene silencing and benefit from temozolomide in glioblastoma. *N Engl J Med* **352**, 997-1003.

- Hermann T & Patel DJ (2000). Adaptive recognition by nucleic acid aptamers. *Science* **287**, 820-825.
- Hernandez LI, Flenker KS, Hernandez FJ, Klingelhutz AJ, McNamara JO II, & Giangrande PH (2013). Methods for evaluating cell-specific, cell-internalising RNA aptamers. *Pharmaceuticals* **6**, 295-319.
- Hicke B, Stephens A, Gould T, Chang Y, Lynott C, Heil J, Borkowski S, Hilger C, Cook G, Warren S, & Schmidt PG (2006). Tumor targeting by an aptamer. *J Nucl Med* **47**, 668-678.
- Hicke BJ, Marion C, Chang YF, Gould T, Lynott CK, Parma D, Schmidt PG, & Warren S (2001). Tenascin-C aptamers are generated using tumor cells and purified protein. *J Biol Chem* **276**, 48644-48654.
- Higgins SC, Steingrimsdottir H, & Pilkington GJ (2010). Human, mouse or rat? Species authentication of glioma-derived cell cultures. *J. Neurosci Methods* **194**, 139-143.
- Holt BD, Short PA, Rape AD, Wang YL, Islam MF, & Dahl KN (2010). Carbon nanotubes reorganize actin structures in cells and *ex vivo*. *ACS Nano* **4**, 4872-4878.
- Hong H, Goel S, Zhang Y, & Cai W (2011). Molecular imaging with nucleic acid aptamers. *Curr. Med. Chem* **18**, 4195-4205.
- Hu Y, Duan J, Zhan Q, Wang F, Lu X, & Yang XD (2012). Novel MUC1 Aptamer Selectively Delivers Cytotoxic Agent to Cancer Cells *In Vitro*. *PLoS ONE* **7**, e31970.
- Huang YF, Shangguan D, Liu H, Phillips JA, Zhang X, Chen Y, & Tan W (2009). Molecular assembly of an aptamer–drug conjugate for targeted drug delivery to tumor cells. *Chembiochem* **10**, 862-868.
- Huse JT & Holland EC (2010). Targeting brain cancer: advances in molecular pathology of malignant glioma and medulloblastoma. *Nature reviews cancer* **10**, 319-331.
- Hwang do W, Ko HY, Lee JH, Kang H, Ryu SH, Song IC, Lee DS, & Kim S (2010). A nucleolin-targeted multimodal nanoparticle imaging probe for tracking cancer cells using an aptamer. *J Nucl Med* **51**, 98-105.
- Idbaih A, Marie Y, Pierron G, Brennetot C, Hoang-Xuan K, Kujas M, Mokhtari K, Sanson M, Lejeune J, Aurias A, Delattre O and Delattre JY (2005). Two types of chromosome 1p losses with opposite significance in gliomas. *Ann Neurol* **58**, 483-487.

- Ignatova TN, Kukekov VG, Laywell ED, Suslov ON, Vrionis FD & Steindler DA (2002). Human cortical glial tumours contain neural stem-like cells expressing astroglial and neuronal markers *in vitro*. *Glia* **39**, 193-206.
- Iversen TG, Frerker N, & Sandvig K (2012). Uptake of ricinB-quantum dot nanoparticles by a macropinocytosis-like mechanism. *J Nanobiotechnology* **10**, 33.
- Iyer AK, Khaled G, Fang J, & Maeda H (2006). Exploiting the enhanced permeability and retention effect for tumor targeting. *Drug Discov Today* **11**, 812-818.
- Jayasena S.D. (1999) Aptamers: an emerging class of molecules that rival antibodies in diagnostics. *Clin Chem* **45**, 1628-1650.
- Jeremic B, Grujicic D, Jevremovic S, Stanisavljevic B, Milojevic L, Djuric L, & Mijatovic L (1992). Carboplatin and etoposide chemotherapy regimen for recurrent malignant glioma: a phase II study. *J Clin Oncol* **10**, 1074-1077.
- Jimenez E, Kwame Safah, Lopez-Colon D, Simaey DV, Chen HW, Tockman MS, & Tan W (2012). Generation of Lung adenocarcinoma DNA aptamers for cancer studies. *PLoS ONE* **7**(10), e46222.
- Jin W, Bi W, Huang ES, & Cote GJ (1999). Glioblastoma cell specific expression of fibroblast growth factor receptor – 1 beta requires an intronic repressor of RNA splicing. *Cancer Res* **59**, 316-319.
- Johnson H, Del Rosario AM, Bryson BD, Schroeder MA, Sarkaria JN, & White FM (2012). Molecular characterization of EGFR and EGFRvIII signaling networks in human glioblastoma tumor xenografts. *Mol Cell Proteomics* **11**, 1724-1740.
- Joshi BH, Leland P, & Puri RK (2003). Identification and characterisation of interleukin – 13 receptor in human medulloblastoma and targeting these receptors with interleukin-13- pseudomonas exotoxin fusion protein. *Croat Med J* **44**, 455-462.
- Jung CS, Unterberg AW, & Hartmann C (2011). Diagnostic markers for glioblastoma. *Histol Histopathol* **26**, 1327-1341.
- Kakkar A, Suri V, Jha P, Srivastava A, Sharma V, Pathak P, Sharma MC, Sharma MS, Kale SS, Chosdal K, Phalak M, & Sarkar C (2011). Loss of heterozygosity on chromosome 10q in glioblastomas, and its association with other genetic alterations and survival in Indian patients. *Neurol India* **59**, 254-261.

- Kalinina J, Peng J, Ritchie JC, & Van Meir EG (2010). Proteomics of gliomas: Initial biomarker discovery and evolution of technology. *Neuro-oncology* **13**, 926-942.
- Kamphuis W, Mamber C, Moeton M, Kooijman L, Sluijs JA, Jansen AH, Verveer M, de Groot LR, Smith VD, Rangarajan S, Rodriguez JJ, Orre M, & Hol EM (2012). GFAP Isoforms in Adult Mouse Brain with a Focus on Neurogenic Astrocytes and Reactive Astrogliosis in Mouse Models of Alzheimer Disease. *PLoS One* **7**, e42823.
- Kang D, Wang J, Zhang W, Song Y, Li X, Zou Y, Zhu Z, Chen F, & Yang CJ (2012). Selection of DNA aptamers against glioblastoma cells with high affinity and specificity. *PLoS ONE* **7**, e42731.
- Kawakami M, Kawakami K, & Puri RK (2002). Intratumor administration of interleukin 13 receptor-targeted cytotoxin induces apoptotic cell death in human malignant glioma tumor xenografts. *Mol Cancer Ther* **1**, 999-1007.
- Keefe AD, Pai S, & Ellington A (2010). Aptamers as therapeutics. *Nat Rev Drug Discov* **9**, 537-550.
- Kim E, Jung Y, Choi H, Yang J, Suh JS, Huh YM, Kim K, & Haam S (2010). Prostate cancer cell death produced by the co-delivery of Bcl-xL shRNA and doxorubicin using an aptamer-conjugated polyplex. *Biomaterials* **31**, 4592-4599.
- Kleihues P & Ohgaki H (1999). Primary and secondary glioblastomas: from concept to clinical diagnosis. *Neuro Oncol* **1**, 44-51.
- Klussman S (2006). The aptamer handbook: functional oligonucleotides and their applications. ISBN: 978-3-527-31059-3.
- Koley D & Bard AJ (2010). Triton X-100 concentration effects on membrane permeability of a single HeLa cell by scanning electrochemical microscopy (SECM). *Proc Natl Acad Sci USA* **107**, 16783-16787.
- Kolishetti N, Dhar S, Valencia PM, Lin LQ, Karnik R, Lippard SJ, Langer R, & Farokhzad OC (2010). Engineering of self-assembled nanoparticle platform for precisely controlled combination drug therapy. *Proc Natl Acad Sci* **107**, 17939-17944.
- Komai T, Shigehara E, Tokui T, Koga T, Ishigami M, Kuroiwa C, & Horiuchi S (1992). Carrier-mediated uptake of pravastatin by rat hepatocytes in primary culture. *Biochem Pharmacol* **43**, 667-670.

- Kong HY & Byun J (2013). Nucleic acid aptamers: New methods for selection, stabilisation, and application in biomedical science. *Biomol Ther (Seoul)* **21**, 423-434.
- Kotula JW, Pratico ED, Ming X, Nakagawa O, Juliano RL, & Sullenger BA (2012). Aptamer-Mediated Delivery of Splice-Switching Oligonucleotides to the Nuclei of Cancer Cells. *Nucleic Acid Ther* **22**, 187-195.
- Kuo T, Lai W, Li C, Wun Y, Chang H, Chen J, Yang P, & Chen C (2014). AS1411 aptamer-conjugated Gd<sub>2</sub>O<sub>3</sub>: Eu nanoparticles for target-specific computed tomography/magnetic resonance/fluorescence molecular imaging. *Nano research* **7**, 658-669.
- Kurpad SN, Zhao XG, Wikstrand CJ, Batra SK, McLendon RE, & Bigner DD (1995). Tumour-antigen in astrocytic glioma. *Glia* **15**, 244-256.
- Laber DA, Sharma VR, Bhupalam L, Taft B, Hendler FJ, & Barnhart KM (2005). Update on the first phase 1 study of AGR100 in advanced cancer. *J Clin Oncol* **23**, 3064.
- Laerum OD, Steinsvag S, & Bjerkvig R (2009). Cell and tissue culture of the central nervous system: Recent developments and current applications. *Acta neurologica Scandinavica*, **72**, 529-549.
- Langer R (2001). Drug delivery. Drugs on target. *Science* **293**, 58-59.
- Laske DW, Youle RJ, & Oldfield EH (1997). Tumor regression with regional distribution of the targeted toxin TFCRM107 in patients with malignant brain tumors. *Nat Med* **3**, 1362-1368.
- Lassen B, Helseth E, Egge A, Due-Tonnessen BJ, Ronning P, & Meling TR (2012). Surgical mortality and selected complications in 273 consecutive craniotomies for intracranial tumours in pediatric patients. *Neurosurgery* **70**, 936-943.
- Lauhon CT & Szostak JW (1995). RNA aptamers that bind flavin and nicotinamide redox cofactors. *J. Am. Chem. Soc.* **117**, 1246-1257.
- Laws ER, Parney IF, Huang W, Anderson F, & Morris AM (2003). Survival following surgery and prognostic factors for recently diagnosed malignant glioma: data from the Glioma Outcomes Project. *J Neurosurgery*, **99**: 467-473.
- Leake R, Barnes D, Pinder S, Ellis I, Anderson L, Anderson T, Adamson R, Rhodes T, Miller K, & Walker R (2000). Immunohistochemical detection of steroid receptors in breast cancer: a working protocol. *J Clin Pathol* **53**, 634-635.

- Lee J, Kotliarova S, Kotliarov Y, Li A, Su Q, Donin NM, Pastorino S, Purow BW, Christopher N, Zhang W, Park JK, & Fine HA (2006). Tumour stem cells derived from glioblastomas cultured in bFGF and EGF more closely mirror the phenotype and genotype of primary tumors than do serum-cultured cell lines. *Cancer Cell* **9**, 391-403.
- Leon SP, Folkerth RD, & Black PM (1996). Microvessel density is a prognostic indicator for patients with astroglial brain tumors. *Cancer* **77**, 362-72.
- Levy-Nissenbaum E, Radovic-Moreno AF, Wang AZ, Langer R, & Farokhzad OC (2008). Nanotechnology and aptamers: applications in drug delivery. *Trends Biotechnol* **26**, 442-449.
- Li F, Vijayasankaran N, Shen A, Kiss R and Amanullah A (2010<sup>a</sup>). Cell culture processes for monoclonal antibody production. *Landes bioscience* **2**, 466-477.
- Li L, Xiang D, Shigdar S, Yang W, Li Q, Lin J, Liu K, & Duan W (2014). Epithelial cell adhesion molecule aptamer functionalized PGLA-lecithin-PEG nanoparticles for targeted drug delivery to human colorectal adenocarcinoma cells. *International journal of nanomedicine* **9**, 1083-1096.
- Li N (2010). Detection of non-nucleic acid targets with an unmodified aptamer and a fluorogenic competitor. *JALA Charlottesv Va* **15**, 189-197.
- Li N, Larson T, Nguyen H, Sokolov K & Ellington A (2010). Directed evolution of gold nanoparticle delivery to cells. *Chem. Commun. (Camb.)* **46**, 392-394.
- Li S, Xu H, Ding H, Huang Y, Cao X, Yang G, Li J, Xie Z, Meng Y, Xiaobing Li, Zhao Q, Shen B, & Shao N (2009). Identification of an aptamer targeting hnRNP AI by tissue slide-based SELEX. *Journal of pathology* **218**, 327-336.
- Licha K & Olbrich C (2005). Optical imaging in drug discovery and diagnostic applications. *Advanced drug delivery reviews*. **57**, 1087-1108.
- Liebner S, Fischmann A, Rascher G, Duffner F, Grote EH, Kalbacher H, Wolburg H (2000). Claudin-1 and claudin-5 expression and tight junction morphology are altered in blood vessels of human glioblastoma multiforme. *Acta Neuropathol* **100**, 323-331.
- Lin Z, Qiang Ma, Xiaofang F, Zhang H, & Su X (2014). A novel aptamer functionalized CuInS<sub>2</sub> quantum dots probe for daunorubicin sensing and near infrared imaging of prostate cancer cells. *Analytica Chimica Acta* **818**, 54-60.

- Liu HY & Gao X (2013). A universal protein tag for delivery of SiRNA-aptamer chimeras. *Sci Rep* **3**, 3129.
- Liu J & Shapiro JI (2003). Endocytosis and signal transduction: basic science update. *Biol Res Nurs* **5**, 117-128.
- Liu K, Lin B, & Lan X (2013). Aptamers: A promising tool for cancer imaging, diagnosis, and therapy. *Journal of cellular biochemistry* **114**, 250-255.
- Liu Q, Jin C, Wang Y, Xiaohong F, Zhang X, Chen Z, & Tan W (2014). Aptamer-conjugated nanomaterials for specific cancer cell recognition and targeted cancer therapy. *NPG Asia Nanomaterials* **6**, e65.
- Liu TF, Tatter SB, Willingham MC, Yang M, Hu JJ, & Frankel AE (2003). Growth factor receptor expression varies among high-grade gliomas and normal brain: epidermal growth factor receptor has excellent properties for interstitial fusion protein therapy. *Mol Cancer Ther* **2**, 783.
- Liu Y & Lu W (2012). Recent advances in brain tumor-targeted nano-drug delivery systems. *Expert Opin Drug Deliv* **9**(6), 671-686.
- Louis DN, Ohgaki H, Wiestler OD, Cavenee WK, Burger PC, Jouvet A, Scheithauer BW, & Kleihues P (2007). The 2007 WHO classification of tumours of the central nervous system. *Acta Neuropathol* **114**, 97-109.
- Lu B, Wang J, Zhang J, Zhang X, Yang D, Wu L, Luo Z, Ma Y, Zhang Q, Pei X, Yu H, & Liu J (2014). Screening and verification of ssDNA aptamers targeting human hepatocellular carcinoma. *Acta Biochim Biophys Sin (Shanghai)* **46**, 128-135.
- Ludemann L, Grieger W, Wurm R, Budzisch M, Hamm B, & Zimmer C (2001). Comparison of dynamic contrast enhanced MRI with WHO tumour grading for gliomas. *Eur Radiol* **11**, 1231-1241.
- Lupold SE (2011). Prostate-targeted radio sensitization via aptamer-shRNA chimeras in human tumor xenografts. *J. Clin. Invest.*, **121** (6): 2383–2390.
- Lupold SE, Hicke BJ, Lin Y, & Coffey DS (2002). Identification and characterization of nuclease-stabilized RNA molecules that bind human prostate cancer cells via the prostate-specific membrane antigen. *Cancer Res* **62**, 4029-4033.

- Macbeth F (2007). Carmustine implants and temozolomide for the treatment of newly diagnosed high-grade glioma. *NICE technology appraisal guidance* **121**, London: NICE.
- MacDonald DR (2001). Temozolomide for recurrent high-grade glioma. *Semin Oncol* **28**, 3-12.
- MacDonald TJ, DeClerck YA, & Laug WE (1998). Urokinase induces receptor mediated brain tumor cell migration and invasion. *J Neurooncol* **40**, 215-226.
- Mahmoudi M, Azadmanesh K, Shokrgozar MA, Journeay WS, & Laurent S (2011). Effect of nanoparticles on the cell life cycle. *Chem Rev* **111**, 3407-3432.
- Mallikaratchy P, Tang Z, Sefah K, Meng L, Shangguan D, & Tan W (2007). Aptamer directly evolved from live cells recognizes membrane bound immunoglobulin heavy mu chain in Burkitt's lymphoma cells. *Mol Cell Proteomics* **6**, 2230-2238.
- Mann P, Somasunderam A, Nieves-Alicea R, Li X, Hu A, Sood AK, Ferrari M, Gorrenstein DG, & Tanaka T (2010). Identification of thioaptamer ligand against E-selectin: potential application for inflamed vasculature targeting. *PLoS ONE* **5**, e13050. .
- Mannironi C, Di Narbo A, Fruscoloni P, & Tocchini-Valentini GP (1997). *In vitro* selection of dopamine RNA ligands. *Biochemistry*, **36**, 9726-9734.
- Marimuthu C, Tang TH, Tominaga J, Tan SC, & Gopinath SCB (2012). Single-stranded DNA (ssDNA) production in DNA aptamer generation. *Analyst* **137**, 1307-1315.
- Markman M. Pharmaceutical management of ovarian cancer: current status (2008). *Drugs* **68**, 771-789.
- Marolt U, Cencic A, Gorenjak M, & Potrc S (2012). Generating aptamers for cancer diagnosis and therapy. *Clin Exp Pharmacol* **2**, 111.
- Marro ML, Daniels DA, Andrew DP, Chapman TD, & Gearing KL (2006). *In vitro* selection of RNA aptamers that block CCL1 chemokine function. *Biochem Biophys Res Commun* **349**, 270-276.
- Marro ML, Daniels DA, McNamee A, Andrew DP, Chapman TD, Jiang MS, Wu Z, Smith JL, Patel KK, & Gearing KK (2005). Identification of potent and selective RNA antagonists of the IFN-gamma-inducible CXCL10 chemokine. *Biochemistry* **44**, 8449-8460.

- Maslon MM & Hupp TR (2010). Drug discovery and mutant p53. *Trends Cell Biol* **20**, 542-555.
- Masters JRW & Palsson B (1999). Human Cell Culture. *Kluwer Academic Publishers* **2**, 167-184.
- Mather JP & Roberts PE (1998). Introduction to Cell and Tissue Culture: Theory and Technique. *Plenum Press*. New York and London.
- McKinney PA (2004). Brain tumours: incidence, survival and aetiology. *J Neurosurg Psychiatry* **75**, ii12-ii17.
- McNamara JO, Andrechek ER, Wang Y, Viles KD, Rempel RE, Gilboa E, Sullenger BA, & Giangrande PH (2006). Cell type-specific delivery of siRNAs with aptamer-siRNA chimeras. *Nature Biotechnology* **24**, 1005-1015.
- Mencin N, Smuc T, Vranicar M, Marvi J, Hren M, Galesa K, Krkoc P, Ulrich H, & Solar B (2013). Optimisation of SELEX: Comparison of different methods for monitoring the progress of in vitro selection of aptamers. *Journal of pharmaceutical and biochemical analysis* **91**, 151-159.
- Meyer C, Eydeler K, Magbanua E, Zivkovic T, Piganeau N, Lorenzen I, Grotzinger J, Mayer G, John SR, & Hahn U (2012). Interleukin-6 receptor specific RNA aptamers for cargo delivery into target cells. *RNA Biology* **9**, 67-80.
- Meyer C, Hahn U, & Rentmeister A (2011). Cell-Specific Aptamers as Emerging Therapeutics. *J Nucleic acids* 2011, 904750.
- Mi J, Liu Y, Rabbani ZN, Yang Z, Urban JH, Sullenger BA, & Clary BM (2010). *In vivo* selection of tumor targeting RNA motifs. *Nat Chem Biol* **6**, 22-24.
- Mikuni N & Miyamoto S (2010). Surgical treatment for glioma: extent of resection applying functional neurosurgery. *Neurol Med Chir (Tokyo)* **50**, 720-726.
- Min K, Cho M, Han SY, Shim YB, Ku J, & Ban C (2008). A simple and direct electrochemical detection of interferon- $\gamma$  using its RNA and DNA aptamers. *Biosensors and Bioelectronics* **23**, 1819-1824.
- Mintz A, Gibo DM, Slagle-Webb B, Christensen ND, & Debinski W (2002). IL-13R $\alpha$ 2 is a glioma-restricted receptor for interleukin-13. *Neoplasia* **4**, 388-399.

- Mintz A & Debinski W (2000). Cancer genetics/epigenetics and the X chromosome possible new links for malignant glioma pathogenesis and immune-based therapies. *Crit Rev Oncog*, **11**, 77–95.
- Moncalero VL, Costanzo RV, Perandones C, & Radrizzani M (2011). Different Conformations of Phosphatase and Tensin Homolog, Deleted on Chromosome 10 (PTEN) protein within the Nucleus and Cytoplasm of Neurons. *PLoS ONE* **6**, e18857.
- Mrugala MM, Rudnick JD, Rockhill JK, & Recht LD (2009). Does bevacizumab increase the risk of leptomeningeal gliomatosis? *Neuro-Oncology* **11**, 634.
- Muller C, Paupert J, Monferran S, & Salles B (2005). The double life of the Ku protein: facing the DNA breaks and the extracellular environment. *Cell cycle* **4**, 438-441.
- Mullins CS, Schneider B, Stockhammer F, Krohn M, Classen CF, & Linnebacher M (2013) Establishment and Characterization of Primary Glioblastoma Cell Lines from Fresh and Frozen Material: A Detailed Comparison. *PLoS ONE* **8**, e71070.
- Nash KT, Thompson JP, & Debinski W (2001). Molecular targeting of malignant gliomas with novel multiply-mutated interleukin 13-based cytokins. *Critical Reviews in Oncology/Hematology* **39**, 87-98.
- Neff CP, Zhou J, Remling L, Kuruvilla J, Zhang J, Li H, Smith DD, Swiderski P, Rossi JJ, & Akkina R (2011). An aptamer siRNA chimera suppresses HIV-1 viral loads and protects from helper CD4<sup>(+)</sup> T cell decline in humanized mice. *Sci Transl Med* **3**, 66ra6.
- Nery AA, Wrenger C, & Ulrich H (2009). Recognition of biomarkers and cell-specific molecular signatures: aptamers as capture agents. *Journal of Separation Science* **32**, 1523-1530.
- Neuhoff S, Ungell AL, Zamora I, & Artursson P (2005). pH-dependent passive and active transport of acidic drugs across Caco-2 cell monolayers. *Eur J Pharm Sci* **25**, 211-220.
- Neuwelt EA, Bauer B, Fahlke C, Fricker G, Iadecola C, Janigro D, Leybaert L, Molnar Z, O'donnell ME, Povlishock JT, Saunders NR, Sharp F, Stanimirovic D, Watts RJ, & Drewes LR (2011). Engaging neuroscience to advance translational research in brain barrier biology. *Nat Rev Neurosci* **12**, 169-182.

- Nicol C, Cesur Ö, Forrest S, Belyaeva TA, Bunka DHJ, Blair GE, & Stonehouse NJ (2013). An RNA aptamer provides a novel approach for the induction of apoptosis by targeting the HPV16 E7 oncoprotein. *PLoS ONE* **8**, e64781.
- Nieuwlandt D, Wecker M, Gold L (1995). *In vitro* selection of RNA ligands to substance P. *Biochemistry* **24**, 5651–5659.
- Nitta T, Hata M, Gotoh S, Seo Y, Sasaki H, Hashimoto N, Furuse M, & Tsukita S (2003). Size-selective loosening of the blood-brain barrier in claudin-5-deficient mice. *J Cell Biol* **161**, 653-660.
- O'Donovan KJ, Diedler J, Couture GC, Fak JJ, & Darnell RB (2010). The onconeural antigen cdr2 is a novel APC/C target that acts in mitosis to regulate C-Myc target genes in mammalian tumor cells. *PLoS ONE* **5**, e10045.
- Ohgaki H & Kleihues P (2005). Epidemiology and etiology of glioma. *Acta neuropathol* **109**, 93-108.
- Ohgaki H & Kleihues P (2007). Genetic pathways to primary and secondary glioblastoma. *Am J Pathol* **170**, 1445-1453.
- Oka N, Soeda A, Inagaki A, Onodera M, Maruyama H, Hara A, Kunisada T, Mori H, & Iwama T (2007). VEGF promotes tumorigenesis and angiogenesis of human glioblastoma stem cells. *Biochem Biophys Res Commun* **360**, 553-559.
- Orava EW, Cicmil N, & Gariépy J (2010). Delivering cargoes into cancer cells using DNA aptamers targeting internalized surface portals. *Biochim Biophys Acta* **1798**, 2190-2200.
- Osborn AG, Salzman KL, Katzman G, Provenzale J, Castillo M, Hedlund G, Illner A, Harnsberger HR, Cooper J, Jones BV, & Hamilton B (2004). Diagnostic imaging: Brain. Salt lake city: Amirsys.
- Pan W & Clawson GA (2009). The shorter the better: reducing fixed primer regions of oligonucleotide libraries for aptamer selection. *Molecules* **14**, 1353-1369.
- Panciani PP, Fontanella M, Garbossa D, Agnoletti A, Ducati A, & Lanotte M (2012). 5-aminolevulinic acid and neuronavigation in high-grade glioma surgery: results of a combined approach. *Neurocirugia (Astur)* **23**, 23-28.
- Pang KS, Rodrigues AD, & Peter RM (2010). Enzyme and transporter-based drug-drug interactions. Progress and future challenges. *Springer* ISBN 978-1-4419-0839-1.

- Papadopoulos MC, Saadoun S, Woodrow CJ, Davies DC, Costa-Martins P, Moss RF, Krishna S, & Bell BA (2001). Occludin expression in microvessels of neoplastic and non-neoplastic human brain. *Neuropathol Appl Neurobiol* **27**, 384-395.
- Pardridge WM (2007). Drug targeting to the brain. *Pharm Res*, **24**, 1733-1744.
- Patil SD, Rhodes DG, & Burgess DJ (2005). DNA-based therapeutics and DNA delivery systems: A comprehensive review. *The AAPs Journal* **7**, E61-E77.
- Paul N, Springsteen G, & Joyce GF (2006). Conversion of a ribozyme to a deoxyribozyme through *in vitro* evolution. *Chem. Biol.* **13**, 329-338.
- Perez-Perez R, Lopez JA, Garcia-Santos E, Camafeita E, Gomez-Serrano M, Ortega-Delgado FJ, Ricart W, Fernandez- Real JM, & Peral B (2012). Uncovering suitable reference proteins for expression studies in human adipose tissue with relevance to obesity. *Plos one* **7**, e30326.
- Persson AI, Petritsch C, Swartling FJ, Itsara M, Sim FJ, Auvergne R, Goldenberg DD, Vandenberg SR, Nguyen KN, Yakovenko S, Ayers-Ringler J, Nishiyama A, Stallcup WB, Berger MS, Bergers G, McKnight TR, Goldman SA, & Weiss WA (2010). Non-stem cell origin for oligodendroglioma. *Cancer Cell* **18**, 669-682.
- Pestourie C, Tavitian B, & Duconge F (2005). Aptamers against extracellular targets for *in vivo* applications. *Biochimie* **87**, 921-930.
- Pieve C, Perkins A, & Missailidis S (2009). Anti-MUC1 aptamers: radiolabelling with (99m)Tc and biodistribution in MCF-7 tumour-bearing mice. *Nucl Med Biol* **36**, 703-710.
- Pittella F, Zhang M, Lee Y, Kim HJ, Tockary T, Osada K, Ishii T, Miyata K, Nishiyama N, & Kataoka K (2011). Enhanced endosomal escape of siRNA-incorporating hybrid nanoparticles from calcium phosphate and PEG-block charge-conversional polymer for efficient gene knockdown with negligible cytotoxicity. *Biomaterials* **32**, 3106-3114.
- Poirier A, Lave T, Portmann R, Brun ME, Senner F, Kansy M, Grimm HP, & Funk C (2008). Design, data analysis, and simulation of *in vitro* drug transport kinetic experiments using a mechanistic *in vitro* model. *Drug Metab Dispos* **36**, 2434-2444.

- Pollack IF, Randall MS, Kristofik MP, Kelly RH, Selker RG, & Vertosick FT (1990). Response of malignant glioma cell lines to epidermal growth factor and platelet-derived growth factor in serum-free medium. *J Neurosurg* **73**, 106-112.
- Poten J & Westermark B (1978). Properties of human malignant glioma cells *in vitro*. *Med Biol* **56**, 184-193.
- Preusser M, de Ribaupierre S, Wohrer A, Erridge SC, Hegi M, Weller M, & Stupp R (2011). Current concepts and management of glioblastoma. *Ann Neurol* **70**, 9-21.
- Provenzale JM, York G, Moya MG, Parks L, Choma M, Kealey S, Cole P, & Serajuddin H (2006). Correlation of relative permeability and relative cerebral blood volume in high-grade cerebral neoplasms. *AJR Am J Roentgenol* **187**, 1036-1042.
- Raaphorst GP, Yang DP, Li LF, & Malone S (2004). Comparison of human tumour cell response to cisplatin and ZD0473 with and without irradiation. *Anticancer research* **24**, 613-618.
- Ramao A, Gimenez M, Laure HJ, Izumi C, Santos Vida RC, Oba-Shinjo S, Marie SKN, & Rosa JC (2012). Changes in the expression of proteins associated with aerobic glycolysis and cell migration are involved in tumorigenic ability of two glioma cell lines. *Proteome Science* **10**, 53.
- Raudino G, Caffo M, Caruso G, Alafaci C, Raudino F, Marventano V, Romano A, Montemagno F, Belvedere M, Salpietro FM, Tomasello F, & Schillaci A (2013). From Gliomagenesis to Multimodal Therapeutic Approaches into High-Grade Glioma Treatment, Evolution of the Molecular Biology of Brain Tumors and the Therapeutic Implications. *Dr. Terry Lichtor (Ed.)*, ISBN: 978-953-51-0989-1, InTech, DOI: 10.5772/52782.
- Razali NM & Wah YB (2011). Power comparisons of Shapiro-Wilk, Kolmogorov-Smirnov, Lilliefors and Anderson-Darling tests. *Journal of statistical modeling and analytics* **2**, 21-33.
- Razis E, Selviaridis P, Labropoulos S, Norris JL, Zhu MJ, Song DD, Kalebic T, Torrens M, Kalogera-Fountzila A, Karkavelas G, Karanastasi S, Fletcher JA, & Fountzilas G (2009). Phase II study of neoadjuvant imatinib in glioblastoma: evaluation of clinical and molecular effects of the treatment. *Clin Cancer Res* **15**, 6258-6266.

- Reardon DA & Wen PY (2006). Therapeutic advances in the treatment of glioblastoma: rationale and potential role of targeted agents. *Oncologist* **11**,152-164.
- Reardon DA, Herndon JE, 2nd, Peters KB, Desjardins A, Coan A, Lou E, Sumrall AL, Turner S, Lipp ES, Sathornsumetee S, Rich JN, Sampson JH, Friedman AH, Boulton ST, Bigner DD, Friedman HS, & Vredenburgh JJ (2012). Bevacizumab continuation beyond initial bevacizumab progression among recurrent glioblastoma patients. *Br J Cancer* **107**, 1481-1487.
- Reyes-Reyes EM, Teng Y, & Bates PJ (2010). A new paradigm for aptamer therapeutic AS1411 action: Uptake by macropinocytosis and its stimulation by a nucleolin – dependent mechanism. *Cancer research* **70**, 8617-8629.
- Ricard D, Idbah A, Ducray F, Lahutte M, Hoang-Xuan K, & Delattre JY (2012). Primary brain tumours in adults. *The Lancet* **379**, 1984-1996.
- Rivlin N, Brosh R, Moshe O, & Rotter V (2011). Mutations in the p53 tumour suppressor gene. *Genes and cancer* **2**, 466-474.
- Roberts HC, Roberts TP, Brasch RC, & Dillon WP (2000). Quantitative measurement of microvascular permeability in human brain tumors achieved using dynamic contrast-enhanced MR imaging: correlation with histologic grade. *Am J Neuroradiol* **21**, 891-899.
- Rockey WM, Hernandez FJ, Huang SU, Cao S, Howell CA, Thomas GS, Liu XY, Lapteva N, Spencer DM, McNamara JO, Zou X, Chen SJ, & Giangrande PH (2011<sup>a</sup>). Rational truncation of an RNA aptamer to prostate-specific membrane antigen using computational structural modeling. *Nucleic Acid Ther.* **21**, 299-314.
- Rockey WM, Huang L, Kloepping KC, Baumhover NJ, Giangrande PH, & Schultz MK (2011). Synthesis and radiolabeling of chelator-RNA aptamer bioconjugates with copper-64 for targeted molecular imaging. *Bioorg. Med. Chem* **19**, 4080-4090.
- Rodriguez VJ, Vicente VO, & Canteras MJ (1997). Valor del ensayo colorimetrico con MTT en el estudio del crecimiento y citotoxicidad *in vitro* lineas de melanoma. *Pathologia* **30**, 18-27.
- Rosenberg JE, Bambury RM, van Allen EM, Drabkin HA, Lara PN Jr, Harzstark AL, Wagle N, Figlin RA, Smith GW, Garraway LA, Choueiri T, Erlandsson F, & Laber DA

- (2014) A phase II trial of AS1411 (a novel nucleolin-targeted DNA aptamer) in metastatic renal cell carcinoma. *Investigational new drugs* **32**, 178-187.
- Ruxton GD & Beauchamp G (2008). Time foe some a priori thinking about post hoc testing. *Behavioral ecology* **19**, 690-693.
- Sadones J, Michotte A, Veld P, Chaskis C, Sciot R, Menten J, Joossens EJ, Strauven T, D'Hondt LA, Sartenaer D, Califice SF, Bierau K, Svensson C, De Greve J, & Neyns B (2009). MGMT promoter hypermethylation correlates with a survival benefit from temozolomide in patients with recurrent anaplastic astrocytoma but not glioblastoma. *Eur J Cancer* **45**, 146–153.
- Sampson JH, Archer GE, Mitchell DA, Heimberger AB, Herndon JE 2nd, Lally-Goss D, Mcgehee-Norman S, Paolino A, Reardon DA, Friedman AH, Friedman HS, & Bigner DD (2009). An epidermal growth factor receptor variant III-targeted vaccine is safe and immunogenic in patients with glioblastoma multiforme. *Mol Cancer Ther* **8**, 2773-2779.
- Santisteban M, Buckner JC, Reid JM, Wu W, Scheithauer BW, Ames MM, Felten SJ, Nikcevich DA, Wiesenfeld M, Jaeckle KA, & Galanis E (2009). Phase II trial of two different irinotecan schedules with pharmacokinetic analysis in patients with recurrent glioma: North Central Cancer Treatment Group results. *J Neurooncol* **92**, 165-175.
- Savla R, Taratula O, Garbuzenko O, & Minko T (2011). Tumor targeted quantum dot-mucin 1 aptamer-doxorubicin conjugate for imaging and treatment of cancer. *J Control Release* **153**, 16–22.
- Schaap FG, French PJ, & Bovee JV (2013). Mutations in the isocitrate dehydrogenase genes IDH1 and IDH2 in tumours. *Adv anat pathol*, **20**, 32-38.
- Schindler R (1969). Use of cell culture in Pharmacology. *Annual Review of Pharmacology* **9**, 393-406.
- Schmidt F, Fischer J, Herrlinger U, Dietz K, Dichgans J, & Weller M (2006). PCV chemotherapy for recurrent glioblastoma. *Neurology* **66**, 587-589.
- Schneider SW, Ludwig T, Tatenhorst L, Braune S, Oberleithner H, Senner V, & Paulus W (2004). Glioblastoma cells release factors that disrupt blood-brain barrier features. *Acta Neuropathol* **107**, 272-276.

- Schwartzbaum JA, Fisher JL, Aldape KD, & Wrensch M (2006). Epidemiology and molecular pathology of glioma. *Nature clinical practice neurology* **2**, 494-503.
- Scott AM, Wolchok JD, & Old LJ (2012). Antibody therapy of cancer. *Nature reviews cancer* **12**, 278-287.
- Sedletska Y, Giraud-Panis MJ, & Malinge JM (2005). Cisplatin is a DNA-damaging antitumour compound triggering multifactorial biochemical responses in cancer cells: importance of apoptotic pathways. *Current Medicinal Chemistry: Anti-Cancer Agents* **5**, 251–265.
- Sefah K, Tang Z, Shangguan D, Chen H, Lopez-Colon D, Li Y, Parekh P, Martin J, Meng L, Phillips J, Kim YM, & Tan WH (2009). Molecular recognition of acute myeloid leukemia using aptamers. *Leukemia* **23**, 235-244.
- Seferos DS, Prigodich AE, Giljohann DA, Patel PC, & Mirkin CA (2009). Polyvalent DNA nanoparticle conjugates stabilize nucleic acids. *Nano Lett.* **9**, 308-311.
- Sehmer EAJ, Hall GJ, Greenberg DC, O’Hara C, Wallingford SC, & Wright KA (2014). Incidence of glioma in a northwestern region of England. *Neuro-oncology* **0**, 1-4.
- Seitz RJ & Wechsler W (1987). Immunohistochemical demonstration of serum proteins in human cerebral gliomas. *Acta Neuropathol* **73**, 145-152.
- Server A, Josefsen R, Kulle B, Maehlen J, Schellhorn T, Gadmar O, Kumar T, Haakonsen M, Langberg CW, & Nakstad PH (2010). Proton magnetic resonance spectroscopy in the distinction of high-grade cerebral gliomas from single metastatic brain tumors. *Acta Radiol* **51**, 316-325.
- Serwer LP & James CD (2012). Challenges in drug delivery to tumors of the central nervous system: an overview of pharmacological and surgical considerations. *Adv Drug Deliv Rev* **64**, 590-597.
- Shangguan D, Cao Z, Meng L, Mallikaratchy P, Sefah K, Wang H, Li Y & Tan W (2008). Cell-Specific Aptamer Probes for membrane protein elucidation in cancer cells. *J Proteome Res* **7**, 2133–2139.
- Shapiro SS & Wilk MB (1965). An analysis of variance test for normality (complete samples). *Biometrika* **52**, 591-611.

- Sharif TR & Sharif M (1999). A high throughput system for the evaluation of protein kinase C inhibitors based on Elk1 transcriptional activation in human astrocytoma cells. *Int J Oncol* **14**, 327-335.
- Shi H, Tang Z, Kim Y, Nie H, Huang YF, He X, Deng K, Wang K & Tan W (2010). *In vivo* fluorescence imaging of tumors using molecular aptamers generated by cell-SELEX. *Chem. Asian J* **5**, 2209-2213.
- Shigdar S, Macdonald J, O'Connor M, Wang T, Xiang D, Al.Shamaileh H, Qiao L, Wei M, Zhou SF, Zhu Y, Lingxue K, Bhattacharya S, Li ChunGuang Li, & Duan W (2013). Aptamers and theranostic agents: Modifications, serum stability and functionalization. *Sensors* **13**, 13624-13637.
- Singh SK, Clarke ID, Hide T, & Dirks PB (2004). Cancer stem cells in nervous system tumors. *Oncogene* **23**, 7267-7273.
- Sipayya V, Sharma I, Sharma KC, & Singh A (2012). Immunohistochemical expression of IDH1 in gliomas: a tissue microarray-based approach. *J Cancer Res Ther* **8**, 598-601.
- Sonabend AM, Yun J, Canoll P, & Bruce JN (2010). Novel strategies for diagnosis of glioblastoma multiforme. *European journal of clinical and medical oncology* **2**, 125-133.
- Song Y, Zhu Z, An Y, Zhang W, Zhang H, Liu D, Yu C, Duan W & Yang CJ (2013). Selection of DNA aptamers against epithelial cell adhesion molecule for cancer cell imaging and circulating tumor cell capture. *Anal. Chem* **85**, 4141-4149.
- Stoltenburg R, Reinemann C, & Strehlitz B (2007). SELEX- A (r)evolutionary method to generate high-affinity nucleic acid ligands. *Biomol. Eng* **24**, 381-403.
- Strik HM, Buhk JH, Wrede A, Hoffmann AL, Bock HC, Christmann M, & Kaina B (2008). Rechallenge with temozolomide with different scheduling is effective in recurrent malignant gliomas. *Mol Med Report* **1**, 863-867.
- Stuart RK, Stockerl-Goldstein K, Cooper M, Devetten M, Herzig R, Medeiros B, Schiller A, Wei A, Acton G, & Rizzieri D (2009). Randomized phase II trial of the nucleolin targeting aptamer AS1411 combined with high-dose cytarabine in relapsed/refractory acute myeloid leukemia (AML). *Journal of clinical oncology* **27**, 7019.

- Stummer W, Pichlmeier U, Meinel T, Wiestler OD, Zanella F, Reulen HJ, & ALA-glioma study group (2006). Fluorescence-guided surgery with 5-aminolevulinic acid for resection of malignant glioma: a randomised controlled multicentre phase III trial. *Lancet Oncol* **7**, 392-401.
- Stupp R, Hegi ME, Neyns B, Goldbrunner R, Schlegel U, Clement PM, Grabenbauer GG, Ochsenbein AF, Simon M, Dietrich PY, Pietsch T, Hicking C, Tonn JC, Diserens AC, Pica A, Hermisson M, Krueger S, Picard M, & Weller M (2010). Phase I/IIa study of cilengitide and temozolomide with concomitant radiotherapy followed by cilengitide and temozolomide maintenance therapy in patients with newly diagnosed glioblastoma. *J Clin Oncol* **28**, 2712-2718.
- Stupp R., Mason WP, van den Bent MJ, Weller M, Fisher B, Taphoorn MJ, Belanger K, Brandes AA, Marosi C, Bogdahn U, Curschmann J, Janzer RC, Ludwin SK, Gorlia T, Allgeier A, Lacombe D, Cairncross JG, Eisenhauer E, & Mirimanoff RO (2005) Radiotherapy plus concomitant and adjuvant temozolomide for glioblastoma. *N Engl J Med* **352**, 987–996.
- Stupp R, Hegi ME, Mason WP, van den Bent MJ, Taphoorn MJ, Janzer RC, Ludwin SK, Allgeier A, Fisher B, Belanger K, Hau P, Brandes AA, Gijtenbeek J, Marosi C, Vecht CJ, Mokhtari K, Wesseling P, Villa S, Eisenhauer E, Gorlia T, Weller M, Lacombe D, Cairncross JG, & Mirimanoff RO (2009). Effects of radiotherapy with concomitant and adjuvant temozolomide versus radiotherapy alone on survival in glioblastoma in a randomised phase III study: 5-year analysis of the EORTC-NCIC trial. *Lancet Oncol*, **10**, 459-466.
- Sultana S, Zhou R, Sadagopan MS, & Skalli O (1998). Effects of growth factors and basement membrane proteins on the phenotype of U-373 MG glioblastoma cells as determined by the expression of intermediate filament proteins. *Am J Pathol* **153**, 1157–1168.
- Sutradhar BC, Park J, Hong G, Choi SH, & Kim G (2010). Effects of trypsinisation on viability of equine chondrocytes in cell culture. *Pak Vet J* **30**, 232-238.
- Taal W, Segers-Van Rijn JM, Kros JM, Van Heuvel I, Van Der Rijt CC, Bromberg JE, Sillevius Smitt PA, & van den Bent MJ (2012). Dose dense 1 week on/1 week off temozolomide in recurrent glioma: a retrospective study. *J Neurooncol* **108**, 195-200.

- Taghavi MS, Akbarzadeh A, Mahdian R, Azadmanesh K, & Javadi G (2013). Cisplatin downregulates BCL2L12, a novel apoptosis- related gene, in glioblastoma cells. *In Vitro Cell Dev Boil Anim.* **49**, 465-472.
- Takano S, Tian W, Matsuda M, Yamamoto T, Ishikawa E, Kaneko MK, Yamazaki K, Kato Y, & Akira M (2011). Detection of IDH1 mutation in human gliomas: comparison of immunohistochemistry and sequencing. *Brain Tumour Pathol* **28**, 115-123.
- Takano S, Yamashita T, & Ohneda O (2010). Molecular therapeutic targets for glioma angiogenesis. *Journal of oncology*, doi:10.1155/2010/351908.
- Tan Y, Shi YS, Wu XD, Liang HY, Gao YB, Li SJ, Zhang XM, Wang F, & Gao TM (2013). DNA aptamers that target human glioblastoma multiforme cells overexpressing epidermal growth factor receptor variant III *in vitro*. *Acta Pharmacol Sin* **34**, 1491-1498.
- Tao F & Johns RA (2010). Tat-mediated peptide intervention in analgesia and anesthesia. *Drug Dev Res* **71**, 99-105.
- Thomas J, Wang L, Clark RE, & Pirmohammed M (2004). Active transport of imatinib into and out of cells: implications for drug resistant. *Blood* **104**, 3739-3745.
- Tombelli S, Minunni M, & Mascini M (2005). Analytical applications of aptamers,” *Biosensors and Bioelectronics* **20**, 2424-2434.
- Travascio P, Bennet AJ, Wang DJ, & Sen D (1999). A ribozyme and catalytic DNA with peroxidase activity: active site versus cofactor-binding sites. *Chem. Biol.* **6**, 779-787.
- Tsao MN, Mehta MP, Whelan TJ, Morris DE, Hayman JA, Flickinger JC, Mills M, Rogers CL, & Souhami L (2005). The American Society for Therapeutic Radiology and Oncology (ASTRO) evidence-based review of the role of radiosurgery for malignant glioma. *Int J Radiat Oncol Biol Phys* **63**, 47-55.
- Tyagi D, Sharma BS, Gupta SK, Kaul D, Vasishta RK, & Khosla VK (2002). Expression of Bcl2 proto-oncogene in primary tumours of the central nervous systems. *Neurol India* **50**, 290-294.
- Ulrich H, Martins AHB, & Pesquero JB (2004). RNA and DNA aptamers in cytomics analysis. *Cytometry* **59**, 220-231.

- van den Bent MJ (2010). Interobserver variation of the histopathological diagnosis in clinical trials on glioma: a clinician's perspective *Acta Neuropathol* **120**, 297-304.
- Van den Bent MJ, Carpentier AF, Brandes AA, Sanson M, Taphoorn MJ, Bernsen HJ, Frenay M, Tijssen CC, Grisold W, Sips L, Haaxma-Reiche H, Kros JM, van Kouwenhoven MC, Vecht CJ, Allgeier A, Lacombe D, & Gorlia T (2006). Adjuvant procarbazine, lomustine, and vincristine improves progression-free survival but not overall survival in newly diagnosed anaplastic oligodendrogliomas and oligoastrocytomas: a randomized European Organisation for Research and Treatment of Cancer phase III trial. *J Clin Oncol* **24**, 2715-2722.
- Van der Valk P, Lindeman J, & Kamphorst W (1997). Growth factor profiles of human gliomas. So non-tumour cells contribute to tumour growth in glioma. *Ann Oncol* **8**, 1023-1029.
- Van Meir EG, Hadjipanayis CG, Norden AD, Shu HK, Wen PY, & Olson JJ (2010). Exciting new advances in neuro-oncology. *CA Cancer J Clin* **60**, 166-193.
- Van Simaey D, López-Colón D, Sefah K, Sutphen R, Jimenez E, & Tan W (2010). Study of the Molecular Recognition of Aptamers Selected through Ovarian Cancer Cell-SELEX. *PLoS ONE* **5**, e13770.
- Vicens MC, Sen A, Vanderlaan A, Drake TJ, & Tan W (2005). Investigation of molecular beacon aptamer-based bioassay for platelet-derived growth factor detection. *Chembiochem* **6**, 900-907.
- Walsh R & DeRosa MC (2009). Retention of function in the DNA homolog of the RNA dopamine aptamer. *Biochem Biophys Res Commun* **388**, 732-735.
- Wang B, Siahaan B, Soltero TJ, & Richard A (2005). Drug delivery: Principles and Applications. *Am J Pharm Educ* **70**, 94.
- Wang RE, Wu H, Niu Y, & Cai J (2011). Improving the stability of aptamers by chemical modification. *Curr Med Chem* **18**, 4126-4138.
- Waters EK, R.J., Schaub RG, & Kurz JC (2009). Effect of NU172 and bivalirudin on ecarin clotting time in human plasma and whole blood. *J. Thromb. Haemost* (Supplement 2) Abstract PP-WE-168.
- Wen PY & Kesari S (2008) Malignant gliomas in adults. *New Engl J Med* **359**(5), 492-507.

- Wen PY, Yung WK, Lamborn KR, Dahia PL, Wang Y, Peng B, Abrey LE, Raizer J, Cloughesy TF, Fink K, Gilbert M, Chang S, Junck L, et al. (2006). Phase I/II study of imatinib mesylate for recurrent malignant gliomas: North American Brain Tumor Consortium Study 99-08. *Clin Cancer Res* **12**, 4899-4907.
- Westermarck B, Ponten J, & Hugosson R (1973). Determinants for the establishment of permanent tissue culture lines from human gliomas. *Acta Pathol Microbiol Scand Section A* **81**, 791-805.
- White SC, Lorigan P, Margison GP, Margison JM, Martin F, Thatcher N, Anderson H, & Ranson M (2006). Phase II study of SPI-77 (sterically stabilised liposomal cisplatin) in advanced non-small-cell lung cancer. *British Journal of Cancer* **95**, 822-828.
- Wick W, Puduvalli VK, Chamberlain MC, van den Bent MJ, Carpentier AF, Cher LM, Mason W, Weller M, Hong S, Musib L, Liepa AM, Thornton DE, & Fine HA (2010). Phase III study of enzastaurin compared with lomustine in the treatment of recurrent intracranial glioblastoma. *J Clin Oncol* **28**, 1168-1174.
- Wickstrand CJ, McLendon RE, Friedman AH, & Bigner DD (1995). Cell surface localization and density of the tumor-associated variant of the epidermal growth factor receptor, EGFRIII. *Cancer Res* **57**, 4130-4140.
- Wittrup A, Sandgren S, Lilja J, Bratt C, Gustavsson N, Morgelin M, & Belting M (2007). Identification of proteins released by mammalian cells that mediate DNA internalization through proteoglycan-dependent macropinocytosis. *J Biol Chem* **282**, 27897-27904.
- Wolburg H, Noell S, Fallier-Becker P, Mack AF, & Wolburg-Buchholz K (2012). The disturbed blood-brain barrier in human glioblastoma. *Mol Aspects Med* **33**, 579-589.
- Wolf AC, Hammond MEH, Schwartz JN, Hagerty KL, Allred DC, Cote RJ, Dowsett M, Fitzgibbons PL, Hanna WM, Langer A, Mcshane LM, Paik S, Pegram MD, Perez EA, Press MF, Rhodes A, Sturgeon C, Taube SE, Tubbs R, Vance GH, van de Vijver M, Wheeler TM, & Hayes DF (2007). American Society of Clinical Oncology/College of American Pathologists guideline recommendations for HER2 testing in breast cancer. *J Clin Oncol* **25**, 118-145.
- Wong JM, Panchmatia JR, Ziewacz JE, Bader AM, Dunn IF, Laws ER, & Gawande AA (2012). Patterns in neurosurgical adverse events: intracranial neoplasm surgery. *Neurosurgery focus* **33**,E16.

- Woo J, Chiu GNC, Karlsson G, Wasan E, Ickenstein L, Edwards K, Bally MB (2008). Use of passive equilibration methodology to encapsulate cisplatin into preformed thermosensitive liposomes. *International Journal of Pharmaceutics* **349**, 38-46.
- Wrensch M, Minn Y, Chew T, Bondy M, & Berger MS (2002). Epidemiology of primary brain tumours: current concepts and review of the literature. *Neuro Oncol* **4**, 278-299.
- Wu X, Liang H, Tan Y, Yuan C, Li S, Li X, Li G, Shi Y, & Zhang X (2014). Cell-SELEX Aptamer for highly specific radionuclide molecular imaging of glioblastoma *in vivo*. *PLoS ONE* **9**(3), e90752.
- Xin H, Jiang X, Ghu J, Sha X, Chen L, Law K, Chen Y, Wang X, Jiang Y, & Fang X (2011). Angiopep-conjugated poly (ethylene glycol)-co-poly (epsilon-caprolactone) nanoparticles as dual-targeting drug delivery system for brain glioma. *Biomaterials* **32**, 4293-4305.
- Xing H, Wong NY, Xiang Yu, & Lu Yi (2012). DNA Aptamer Functionalized Nanomaterials for Intracellular Analysis, Cancer Cell Imaging and Drug Delivery. *Curr Opin Chem Biol* **16**, 429-435.
- Xu C, Wu X, & Zhu J (2013). VEGF promotes proliferation of human glioblastoma multiforme stem-like cells through VEGF receptor 2. *The scientific world journal* **417413**, doi:10.1155/2013/417413.
- Yallapu MM, Gupta BK, Jaggi M, & Chauhan SC (2010). Fabrication of curcumin encapsulated PLGA nanoparticles for improved therapeutic effects in metastatic breast cancer cells. *J colloid interface SCI* **351**, 19-29.
- Yamanoto R, Baba T, & Kumar PK (2000). Molecular beacon aptamer fluoresces in the presence of Tat protein of HIV-1. *Genes cells* **5**, 389-396.
- Yan H, Wang L, Wang J, Weng X, Lei H, Wang X, Jiang L, Zhu J, Lu W, Wei X, & Li C (2012). Two-order targeted brain tumor imaging by using an optical/paramagnetic nanoprobe across the blood brain barrier. *ACS Nano* **6**(1), 410-420.
- Yang Y, Yan Z, Wei D, Zhong J, Liu L, Zhang L, Wang F, Wei X, Xie C, Lu W, & He D (2013). Tumor-penetrating peptide functionalization enhances the anti-glioblastoma effect of doxorubicin liposomes. *Nanotechnology* **24** (40), 405101.

- Yigit MV, Mazumdar D, & Lu Y (2008). MRI Detection of Thrombin with Aptamer Functionalized Superparamagnetic Iron Oxide Nanoparticles. *Bioconjugate Chem* **19**, 412-417.
- Yordanova YN, Moritz-Gasser S, & Duffau H (2011). Awake surgery for WHO Grade II gliomas within "noneloquent" areas in the left dominant hemisphere: toward a "supratotal" resection. Clinical article. *J Neurosurg* **115**, 232-239.
- Yu MK, Park J, & Jon S (2012). Targeting Strategies for Multifunctional Nanoparticles in Cancer Imaging and Therapy. *Theranostics* **2**, 3-44.
- Yu, C, Hu Y, Duan J, Yuan W, Wang C, Xu H, & Yang XD (2011). Novel aptamer-nanoparticle bioconjugates enhances delivery of anticancer drug to MUC1-positive cancer cells *in vitro*. *PLoS One* **6**, e24077.
- Zeng Z, Zhang P, Zhao N, Sheehan A, Tung C, Chang C, & Zu Y (2010). Using oligonucleotide aptamer probes for immunostaining of formalin-fixed and paraffin-embedded tissues. *Mod Pathol* **23**, 1553-1558.
- Zhang G, Huang S, & Wang Z (2012). A meta-analysis of bevacizumab alone and in combination with irinotecan in the treatment of patients with recurrent glioblastoma multiforme. *J Clin Neurosci* **19**, 1636-1640.
- Zhang H (2013). Thermally cross-linked superparamagnetic iron oxide nanoparticle-A10 RNA aptamer-doxorubicin conjugate. Aug 29 [Updated 2008 Oct 8]. In: Molecular Imaging and Contrast Agent Database (MICAD) [Internet]. Bethesda (MD): National Center for Biotechnology Information (US).
- Zhang K, Tang L, Sefah K, Zhao Z, Zhu G, Sun W, Goodison S, & Tan W (2012<sup>a</sup>). Novel aptamer developed for breast cancer cell internalisation. *ChemMedChem* **7**, 79-84.
- Zhang MZ, Yu RN, Chen J, Ma ZY, & Zhao YD (2012). Targeted quantum dots fluorescence probes functionalized with aptamer and peptide for transferrin receptor on tumour cells. *Nanotechnology* **23**, 485104.
- Zhao Z, Xu L, Shi X, Tan W, Fang X, & Shangguan D (2009). Recognition of subtype non-small cell lung cancer by DNA aptamers selected from living cells. *Analyst* **134**, 1808-1814.

- Zhou H, Luby-Phelps K, Mickey BE, Habib AA, Mason RP, & Zhao D (2009). Dynamic near-infrared optical imaging of 2-Deoxyglucose uptake by intracranial glioma of athymic mice. *PLoS ONE* **4**, e8051.
- Zhou R & Skalli O (2000). TGF- $\alpha$  Differentially Regulates GFAP, Vimentin, and Nestin Gene Expression in U-373 MG Glioblastoma Cells: Correlation with Cell Shape and Motility. *Experimental cell research* **254**, 269-278.
- Zhou W, Zhou Y, Wu J, Liu Z, Zhao H, Liu J, & Ding J (2014). Aptamer-nanoparticle bioconjugates enhance intracellular delivery of vinorelbine to breast cancer cells. *J Drug Target*, **22**, 57-66.
- Zueva E, Rubio LI, Ducongé F, & Tavitian B (2011). Metastasis-focused cell-based SELEX generates aptamers inhibiting cell migration and invasion. *Int. J. Cancer* **128**, 797-804.
- Zuker, M (2003). Mfold web server for nucleic acid folding and hybridization prediction. *Nucleic acids research*, **31**, 3406-3415.
- Zuker, M. The mfold Web Server. <http://mfold.rna.albany.edu/?q=mfold/DNA-Folding-Form> (accessed 7-22- 2011).
- Zulch KJ (1986). Brain Tumors: Their Biology and Pathology. *Berlin Heidelberg: Springer Verlag* 3<sup>rd</sup> edition, ISBN 978-0-387-10933-6.
- Zwang Y & Yarden Y (2009). Systems biology of growth factor-induced receptor endocytosis. *Traffic* **10**, 349-363.